AD-A052 797 WATER RESOURCES ENGINEERS INC AUSTIN TX F/G 8/8
COMPARISON OF NUMERICAL AND PHYSICAL HYDRAULIC MODELS, MASONBOR--ETC(U)
JUN 77 F D MASCH, R J BRANDES, J D REAGAN DACW72-72-C-0028
UNCLASSIFIED CERC-6ITI-6-APP-2-VOL-1 NL

1 OF 2
AD A052797

AD A052792

Comparison of Numerical and Physical Hydraulic Models, Masonboro Inlet, North Carolina

APPENDIX 2, VOLUME 1
Numerical Simulation of Hydrodynamics (WRE)

by

Frank D. Masch, Robert J. Brandes, and J. Dwight Reagan

GITI REPORT 6

June 1977

CERC GITI-6-APP-2-VOL-1

186p.

Prepared for

U.S. Army Coastal Engineering Research Center

under

Contract DACW72-72-C-0028

by

Water Resources Engineers, Inc.
8900 Shoal Creek Boulevard
Austin, Texas 78758

DDC
RECEIVED
APR 18 1978
A

AU NO.
DDC FILE COPY

GENERAL INVESTIGATION OF TIDAL INLETS

A Program of Research Conducted Jointly by
U.S. Army Coastal Engineering Research Center, Fort Belvoir, Virginia
U.S. Army Engineer Waterways Experiment Station, Vicksburg, Mississippi

Department of the Army
Corps of Engineers

APPROVED FOR PUBLIC RELEASE; DISTRIBUTION UNLIMITED

410642.

Reprint or republication of any of this material shall give appropriate credit to the U.S. Army Coastal Engineering Research Center.

Limited free distribution within the United States of single copies of this publication has been made by this Center. Additional copies are available from:

National Technical Information Service
ATTN: Operations Division
5285 Port Royal Road
Springfield, Virginia 22151

The findings in this report are not to be construed as an official Department of the Army position unless so designated by other authorized documents.

Cover Photo: Masonboro Inlet, North Carolina, 24 July 1974

Unclassified

SECURITY CLASSIFICATION OF THIS PAGE *(When Data Entered)*

REPORT DOCUMENTATION PAGE		READ INSTRUCTIONS BEFORE COMPLETING FORM
1. REPORT NUMBER GITI Report 6, Appendix 2	2. GOVT ACCESSION NO.	3. RECIPIENT'S CATALOG NUMBER
4. TITLE *(and Subtitle)* COMPARISON OF NUMERICAL AND PHYSICAL HYDRAULIC MODELS, MASONBORO INLET, NORTH CAROLINA; APPENDIX 2, NUMERICAL SIMULATION OF HYDRODYNAMICS (WRE)		5. TYPE OF REPORT & PERIOD COVERED Final report Appendix 2 (In 2 vols) 6. PERFORMING ORG. REPORT NUMBER
7. AUTHOR(s) Frank D. Masch Robert J. Brandes J. Dwight Reagan		8. CONTRACT OR GRANT NUMBER(s) DACW72-72-C-0028
9. PERFORMING ORGANIZATION NAME AND ADDRESS Department of the Army Coastal Engineering Research Center Kingman Building, Fort Belvoir, VA 22060		10. PROGRAM ELEMENT, PROJECT, TASK AREA & WORK UNIT NUMBERS F31019
11. CONTROLLING OFFICE NAME AND ADDRESS Department of the Army Coastal Engineering Research Center Kingman Building, Fort Belvoir, VA 22060		12. REPORT DATE June 1977 13. NUMBER OF PAGES 343
14. MONITORING AGENCY NAME & ADDRESS*(if different from Controlling Office)*		15. SECURITY CLASS. *(of this report)* Unclassified 15a. DECLASSIFICATION/DOWNGRADING SCHEDULE

16. DISTRIBUTION STATEMENT *(of this Report)*

Approved for public release; distribution unlimited.

17. DISTRIBUTION STATEMENT *(of the abstract entered in Block 20, if different from Report)*

18. SUPPLEMENTARY NOTES

This report has four appendices, published as four separate volumes.

19. KEY WORDS *(Continue on reverse side if necessary and identify by block number)*

Finite difference method	Masonboro Inlet, N. C.
Hydraulic models	Mathematical models
Hydrodynamics	Numerical simulation
	Tidal inlets

20. ABSTRACT *(Continue on reverse side if necessary and identify by block number)*

A two-dimensional finite difference tidal hydrodynamics model has been adapted to Masonboro Inlet, North Carolina. The model was initially calibrated to simulate prototype conditions of September and October 1969. Operational runs were then undertaken to simulate tides and currents corresponding to pre-project undeveloped inlet conditions of November 1964 and modified inlet and north jetty conditions of June 1967. For each case, the model was operated with mean and spring ocean tides. (Cont)

next page

DD FORM 1 JAN 73 1473 EDITION OF 1 NOV 65 IS OBSOLETE

Unclassified

SECURITY CLASSIFICATION OF THIS PAGE *(When Data Entered)*

20. ABSTRACT (Continued).

cont → The tidal hydrodynamics model applied at Masonboro Inlet uses an explicit numerical solution of the basic equations of motion and the continuity equation. As structured, the model includes bathymetric data for the inlet, bottom roughness, inundated areas and other features of the system. Because of the size and detail required in the simulations, a dual-model approach is employed. In this technique a coarse grid model is utilized to compute tidal flows which in turn are applied as boundary conditions to a finer sub-model of the immediate inlet area. Special requirements necessary for sequential operation of the two models are presented.

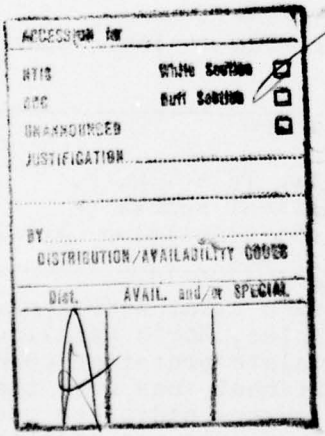

FOREWORD

This report was prepared by Water Resources Engineers, Inc., Austin, Texas, under Contract DACW72-72-C-0028 with the US Army Coastal Engineering Research Center as part of the General Investigation of Tidal Inlets (GITI). The GITI research program is under the technical surveillance of the US Army Coastal Engineering Research Center (CERC), and is conducted by CERC, the U.S. Army Waterways Experiment Station (WES), and other government agencies and private organizations. This report contains detailed results of a numerical model developed as part of an evaluation of physical and numerical models of a tidal inlet. Details of the evaluation are contained in the basic report "Comparison of Numerical and Physical Hydraulic Models, Masonboro Inlet, NC" to which this report is an Appendix.

This report is published, without change, as received from the contractor in 1973. Results and conclusions are those of the authors and are not necessarily accepted by CERC, WES, or the Corps of Engineers.

The report was prepared by F. D. Masch, R. J. Brandes, and J. D. Reagan of Water Resources Engineers, Inc. CERC contract monitors were B. R. Bodine and D. L. Harris. Technical Directors of CERC and WES were T. Saville, Jr. and F. R. Brown, respectively.

Comments on this publication are invited.

Approved for publication in accordance with Public Law 166, 79th Congress, approved 31 July 1945, as supplemented by Public Law 172, 88th Congress, approved 7 November 1963.

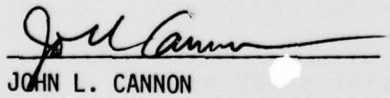

JOHN L. CANNON
Colonel, Corps of Engineers
Commander and Director
Waterways Experiment Station

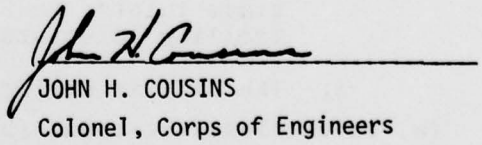

JOHN H. COUSINS
Colonel, Corps of Engineers
Commander and Director
Coastal Engineering Research Center

PREFACE

1. The Corps of Engineers, through its Civil Works program, has sponsored, over the past 23 years, research into the behavior and characteristics of tidal inlets. The Corps' interest in tidal inlet research stems from its responsibilities for navigation, beach erosion prevention and control, and flood control. Tasked with the creation and maintenance of navigable U. S. waterways, the Corps routinely dredges millions of cubic yards of material each year from tidal inlets that connect the ocean with bays, estuaries, and lagoons. Design and construction of navigation improvements to existing tidal inlets are an important part of the work of many Corps offices. In some cases, design and construction of new inlets are required. Development of information concerning the hydraulic characteristics of inlets is important not only for navigation and inlet stability, but also because inlets, by allowing for the ingress of storm surges and egress of flood waters, play an important role in the flushing of bays and lagoons.

2. A research program, General Investigation of Tidal Inlets (GITI), was developed to provide quantitative data for use in design of inlets and inlet improvements. It is designed to meet the following objectives:

> To determine the effects of wave action, tidal flow, and related phenomena on inlet stability and on the hydraulic, geometric, and sedimentary characteristics of tidal inlets; to develop the knowledge necessary to design effective navigation improvements, new inlets, and sand transfer systems at existing tidal inlets; to evaluate the water transfer and flushing capability of tidal inlets; and to define the processes controlling inlet stability.

3. The GITI is divided into three major study areas: (a) inlet classification, (b) inlet hydraulics, and (c) inlet dynamics.

a. The objectives of the inlet classification study are to classify inlets according to their geometry, hydraulics, and stability, and to determine the relationships that exist among the geometric and dynamic characteristics and the environmental factors that control these characteristics. The classification study keeps the general investigation closely related to real inlets and produces an important inlet data base useful in documenting the characteristics of inlets.

b. The objectives of the inlet hydraulics study are to define the tide-generated flow regime and water-level fluctuations in the vicinity of coastal inlets and to develop techniques for predicting these phenomena. The inlet hydraulics study is divided into three areas: idealized inlet model study, evaluation of state-of-the-art physical and numerical models, and prototype inlet hydraulics.

   (1) The idealized inlet model. The objectives of this model study are to determine the effect of inlet configurations and structures on discharge, head loss, and velocity distribution for a number of realistic inlet shapes and tide conditions. An initial set of tests in a trapezoidal inlet was conducted between 1967 and 1970. However, in order that subsequent inlet models are more representative of real inlets, a number of "idealized" models representing various inlet morphological classes are being developed and tested. The effects of jetties and wave action on the hydraulics are included in the study.

   (2) Evaluation of state-of-the-art modeling techniques. The objectives of this part of the inlet hydraulics study are to determine the usefulness and reliability of existing physical and numerical modeling techniques in predicting the hydraulic characteristics of inlet/bay systems, and to determine whether simple tests, performed rapidly and economically, are useful in the evaluation of proposed inlet improvements. Masonboro Inlet, North Carolina, was selected as the prototype inlet which would be used along with hydraulic and numerical models in the evaluation of existing techniques. In September 1969 a complete set of hydraulic and bathymetric data was collected at Masonboro Inlet. Construction of the fixed-bed physical model was initiated in 1969, and extensive

tests have been performed since then. In addition, three existing numerical models were applied to predict the inlet's hydraulics. Extensive field data were collected at Masonboro Inlet in August 1974 for use in evaluating the capabilities of the physical and numerical models.

(3) Prototype inlet hydraulics. Field studies at a number of inlets are providing information on prototype inlet/bay tidal hydraulic relationships and the effects of friction, waves, tides, and inlet morphology on these relationships.

c. The basic objective of the inlet dynamics study is to investigate the interactions of tidal flow, inlet configuration, and wave action at tidal inlets as a guide to improvement of inlet channels and nearby shore protection works. The study is subdivided into four specific areas: model materials evaluation, movable-bed modeling evaluation, reanalysis of a previous inlet model study, and prototype inlet studies.

(1) Model materials evaluation. This evaluation was initiated in 1969 to provide data on the response of movable-bed model materials to waves and flow to allow selection of the optimum bed materials for inlet models.

(2) Movable-bed model evaluation. The objective of this study is to evaluate the state-of-the-art modeling techniques, in this case movable-bed inlet modeling. Since, in many cases, movable-bed modeling is the only tool available for predicting the response of an inlet to improvements, the capabilities and limitations of these models must be established.

(3) Reanalysis of an earlier inlet model study. In 1957, a report entitled, "Preliminary Report: Laboratory Study of the Effect of an Uncontrolled Inlet on the Adjacent Beaches," was published by the Beach Erosion Board (now CERC). A reanalysis of the original data is being performed to aid in planning of additional GITI efforts.

(4) Prototype dynamics. Field and office studies of a number of inlets are providing information on the effects of physical forces and artificial improvements on inlet morphology. Of particular importance are studies to define the mechanisms of natural sand bypassing at inlets, the

response of inlet navigation channels to dredging and natural forces, and the effects of inlets on adjacent beaches.

4. This appendix discusses the calibration, base tests, and predictive test of a numerical model of Masonboro Inlet, N. C., conducted as part of the evaluation of the state-of-the-art inlet modeling techniques. It presents the data necessary for a comparison of results of the physical and numerical models discussed in the basic report and in the following appendixes:

a. Appendix 1. R. A. Sager and W. C. Seabergh, "Fixed-Bed Hydraulic Model Results."

b. Appendix 3. R. M. Chen and L. A. Hembree, "Numerical Simulation of Hydrodynamics (TRACOR)."

c. Appendix 4. C. J. Huval and G. L. Wintergerst, "Simplified Numerical (Lumped Parameter) Simulation."

ABSTRACT

A two-dimensional finite difference tidal hydrodynamics model has been adapted to Masonboro Inlet, North Carolina. The model was initially calibrated to simulate prototype conditions of September and October 1969. Operational runs were then undertaken to simulate tides and currents corresponding to pre-project undeveloped inlet conditions of November 1964 and modified inlet and north jetty conditions of June 1967. For each case, the model was operated with mean and spring ocean tides.

The tidal hydrodynamics model applied at Masonboro Inlet uses an explicit numerical solution of the basic equations of motion and the continuity equation. As structured, the model includes bathymetric data for the inlet, bottom roughness, inundated areas and other features of the system. Because of the size and detail required in the simulations, a dual-model approach is employed. In this technique a coarse grid model is utilized to compute tidal flows which in turn are applied as boundary conditions to a finer sub-model of the immediate inlet area. Special requirements necessary for sequential operation of the two models are presented.

TABLE OF CONTENTS

	Page
ABSTRACT	i
FOREWORD	ii
LIST OF FIGURES	v
LIST OF TABLES	ix
I. INTRODUCTION	1
Background	1
Objectives and Scope	2
Description of Study Area	3
II. FORMULATION AND SOLUTION TECHNIQUE	6
Tidal Hydrodynamic Equations	6
Solution Scheme	7
Basic Finite Difference Equations	11
Special Boundary Conditions	17
Water-Land Boundaries	18
Submerged Barrier Boundaries	18
Overtopping Barrier Boundaries	20
External Flow Boundaries	21
Artificial Offshore Tidal Boundaries	22
Artificial Tidal-Storage Boundaries	23
Inundation Boundaries	24
Choice of Time Step and Mesh Size	27
Implementation Procedure	27
III. MODEL APPLICATION AND VERIFICATION	29
Prototype Information	29
Model Resolution	32

Page

Dual-Model Procedure 39

Coarse Grid Model 41
Fine Grid Sub-Model 59

IV. PRE- AND POST-PROJECT SIMULATIONS 97

Model Modifications. 97

November 1964 Condition 100
June 1967 Condition 101

Tidal Excitation in Coarse Grid Model. 106

Operational Results. 113

V. SUMMARY AND RECOMMENDATIONS 120

LITERATURE CITED. 123

APPENDIX A - SIMULATED RESULTS FOR NOVEMBER 1964 INLET GEOMETRY 124

APPENDIX B - SIMULATED RESULTS FOR JUNE 1967 INLET GEOMETRY 142

LIST OF FIGURES

Figure	Title	Page
1	Location Map of Masonboro Inlet and Study Area	4
2	Discrete Element Variable Locations Used in HYDTID	10
3	Cell Flagging Scheme for Identifying Flow Boundary Conditions	25
4	Velocity Range and Tide Gage Locations	30
5	Typical Recorded Tide During Verification Period - Gage O.	31
6	Computer Time Requirements for HYDTID Model.	35
7	Areal Extent of Model Grids.	38
8	Coarse Grid Configuration Used to Describe September, 1969 Conditions	42
9	MSL Bottom and Ground Elevations Used in Verification of Coarse Grid Model.	44
10	Boundary Conditions Used for Verification of Coarse Grid Model.	45
11	Input Tides Used to Excite Coarse Grid Model for 12 September 1969 Conditions	48
12	Computational Cell Flags Used in Coarse Grid Model for 12 September 1969 Conditions	53
13	Convective Acceleration Cell Flags Used in Coarse Grid Model for 12 September 1969 Conditions	53
14	Channel Cross-Section at Velocity Ranges near Masonboro Inlet.	55
15	Comparison of Prototype and Simulated Flows from Coarse Grid Model	57

Figure	Title	Page
16	Tidal Verification at Gage 1	60
17	Tidal Verification at Gage 2	61
18	Tidal Verification at Gage 3	62
19	Tidal Verification at Gage 4	63
20	Tidal Verification at Gage 5	64
21	Tidal Verification at Gage 6	65
22	Fine Grid Configuration Used to Describe September 1969 Conditions	66
23	MSL Bottom and Ground Elevations Used in Verification of Fine Grid Sub-Model.	67
24	Boundary Condition Used for Verification of Fine Grid Model.	68
25	Computational Cell Flags Used in Fine Grid Sub-Model for 12 September 1969 Conditions	72
26	Convective Acceleration Cell Flags Used in Fine Grid Sub-Model for 12 September 1969 Conditions	73
27	Velocity Verification at Station 1-N	75
28	Velocity Verification at Station 1-C	76
29	Velocity Verification at Station 1-S	77
30	Velocity Verification at Station 2-N	78
31	Velocity Verification at Station 2-C	79
32	Velocity Verification at Station 2-S	80
33	Velocity Verification at Station 3-N	81
34	Velocity Verification at Station 3-C	82
35	Velocity Verification at Station 3-S	83

Figure	Title	Page
36	Velocity Verification at Station 4-E	84
37	Velocity Verification at Station 4-C	85
38	Velocity Verification at Station 4-W	86
39	Velocity Verification at Station 5-E	87
40	Velocity Verification at Station 5-C	88
41	Velocity Verification at Station 5-W	89
42	Simulated Velocity Pattern at Maximum Flood Flow Conditions, 12 September 1969.	92
43	Simulated Velocity Pattern at High Water Slack Tide Condition, 12 September 1969	93
44	Simulated Velocity Pattern at Maximum Ebb Flow Condition, 12 September 1969.	94
45	Simulated Velocity Pattern at Low Water Slack Tide Condition, 12 September 1969	95
46	Semi-Diurnal Mean and Spring Ocean Tides Used in Model Operation.	98
47	Areal Extent of Hydrographic Surveys	99
48	MSL Bottom and Ground Elevations Used in Coarse Grid Model for November 1964 Conditions	102
49	Computational Cell Flags Used in Coarse Grid Model for November 1964 Conditions	102
50	Convective Acceleration Cell Flags Used in Coarse Grid Model for November 1964 Conditions	102
51	MSL Bottom and Ground Elevations Used in Fine Grid Sub-Model for November 1964 Conditions	103
52	Computational Cell Flags Used in Fine Grid Sub-Model for November 1964 Conditions	104
53	Convective Acceleration Cell Flags Used in Fine Grid Sub-Model for November 1964 Conditions	105

Figure	Title	Page
54	MSL Bottom and Ground Elevations Used in Coarse Grid Model for June 1967 Conditions	107
55	Computational Cell Flags Used in Coarse Grid Model for June 1967 Conditions	107
56	Convective Acceleration Cell Flags Used in Coarse Grid Model for June 1967 Conditions	107
57	MSL Bottom and Ground Elevations Used in Fine Grid Sub-Model for June 1967 Conditions	108
58	Computational Cell Flags Used in Fine Grid Sub-Model for June 1967 Conditions	109
59	Convective Acceleration Cell Flags Used in Fine Grid Sub-Model for June 1967 Conditions	110
60	Mean Exciting Tides Used in Coarse Grid Model.	111
61	Spring Exciting Tides Used in Coarse Grid Model.	112
62	Simulated Velocity Pattern at Maximum Flood Flow Condition for Mean Tide, November 1964	113
63	Simulated Velocity Pattern at Maximum Flood Flow Condition for Spring Tide, November 1964	117
64	Simulated Velocity Pattern at Maximum Flood Flow Condition for Mean Tide, June 1967	118
65	Simulated Velocity Pattern at Maximum Flood Flow Condition for Spring Tide, June 1967	119

LIST OF TABLES

Table	Title	Page
1	Model Characteristics for Masonboro Inlet.	36
2	Characteristics of Barriers Used in Coarse Grid Model.	46
3	Assignment of Exciting Tides in Coarse Grid Model.	47
4	Tidal Constants Used in Verification of Coarse Grid Model. . .	51
5	Coarse Grid Cells Where Flows Were Compared.	58
6	Coarse Grid Cells Where Tides Were Compared.	58
7	Characteristics of Barriers Used in Fine Grid Sub-Model. . . .	69
8	Linkage Between Coarse Grid and Fine Grid Boundary Flows . . .	71
9	Cells Used in the Fine Grid Sub-Model for Velocity Verification	90
10	Linkage Between Additional Coarse Grid and Fine Grid Boundary Flows for November 1964 Conditions.	101
11	Bi-Modal Fourier Constants Used to Approximate the Mean and Spring Tides	113

I. INTRODUCTION

Background

This study was initiated by the U. S. Army Coastal Engineering Research Center to help evaluate the degree to which mathematical models can be used to predict quantitatively the hydrodynamics of flow through tidal inlets (exclusive of sediment transport). The project is a basic part of a more extensive investigation to determine the effectiveness of both mathematical and physical models for predicting tidal amplitudes and current velocities for selected prototype conditions. As a "typical" problem area, Masonboro Inlet, North Carolina, for which some actual tide and flow data are available, has been selected for comprehensive field and model investigations.

A specific requirement of this work was that prescribed tidal hydrodynamic simulations (including calibrations and applications) be undertaken using existing mathematical modeling procedures. For this purpose, HYDTID, a two-dimensional finite difference computational model was applied to Masonboro Inlet. HYDTID, with its genesis in the hurricane surge model of Reid and Bodine [1968], was formulated and programmed as a basic part of a comprehensive study for the development of estuarine transport models, Masch, et al [1969] and Masch and Brandes [1971], and has been developed to its present form through a series of application-improvement efforts. The basic outputs of this model are the time histories of tidal amplitudes and vertically integrated velocities (or flows per unit width) in each of two

areawise coordinate directions. The model utilizes as inputs excitation tides, inflows and wind stress, and accounts for irregular bathymetry, bottom roughness, islands, inundated areas and other physiographic features. Utilization of HYDTID in a variety of prototype applications by Brandes and Masch [1971a, 1971b, and 1972] has resulted in an expansion of the model's computational and output capabilities and improved programming efficiency.

Objectives and Scope

The primary objective of this project was to apply the two-dimensional tidal hydrodynamic modeling capabilities contained in HYDTID to Masonboro Inlet, North Carolina. More specifically, the project provided for:

1. *Adaptation of HYDTID to the geometric and bathymetric configuration of Masonboro Inlet in October 1969.*
2. *Calibration of HYDTID for prototype tides and currents of 12 September 1969.*
3. *Application of the calibrated model to predict tides, currents and tidal prisms at selected stations for:*
   a. *Pre-project undeveloped inlet conditions corresponding to November 1964 data, and*
   b. *Modified inlet and north jetty conditions corresponding to June 1967 survey data.*

   In each application, the model was operated with prescribed mean and spring ocean tides.

Additionally in this report the modeling capabilities in HYDTID are described and details of the basic equations, boundary conditions, numerical solution scheme and programming techniques are presented. This is followed by the application of HYDTID together with a discussion of the requirements imposed by Masonboro Inlet. Special attention is given to the resolution,

time steps and requirements for computer time and storage.

The HYDTID model as applied to Masonboro Inlet is programmed in FORTRAN IV source language at a level compatible with that on the UNIVAC 1108 computer system. The operating characteristics, the I/O data structures, support data management procedures and output report structures necessary to implement the model and evaluate the results are provided in the Appendix.

Description of Study Area

Masonboro Inlet and the surrounding area to which the model has been applied is shown in Figure 1. The topographic, physiographic and hydrographic details are contained in U. S. Geological Survey Topographic Map No. N3400-W7745/15 and U. S. Coast and Geodetic Survey Hydrographic Chart No. 1235. Supplemental information including hydrographic surveys for November 1964, June 1967, and October 1969, and pertinent details on the north jetty and its overflow section were provided by the Coastal Engineering Research Center.

The immediate study area shown in Figure 1 covers approximately nine square miles including an ocean approach section. It is characterized by a combination of inter-connected channels including the primary inlet, Masonboro Channel, Banks Channel, Shin Creek and the Atlantic Intracoastal Waterway. It is also seen that considerable area inshore of the inlet is subject to inundation above mean low water (MLW). This causes flows in some locations to be generally confined to the identified channels when tides are near MLW, whereas when tides are near mean high water (MHW), large areas are inundated and flows are less well defined.

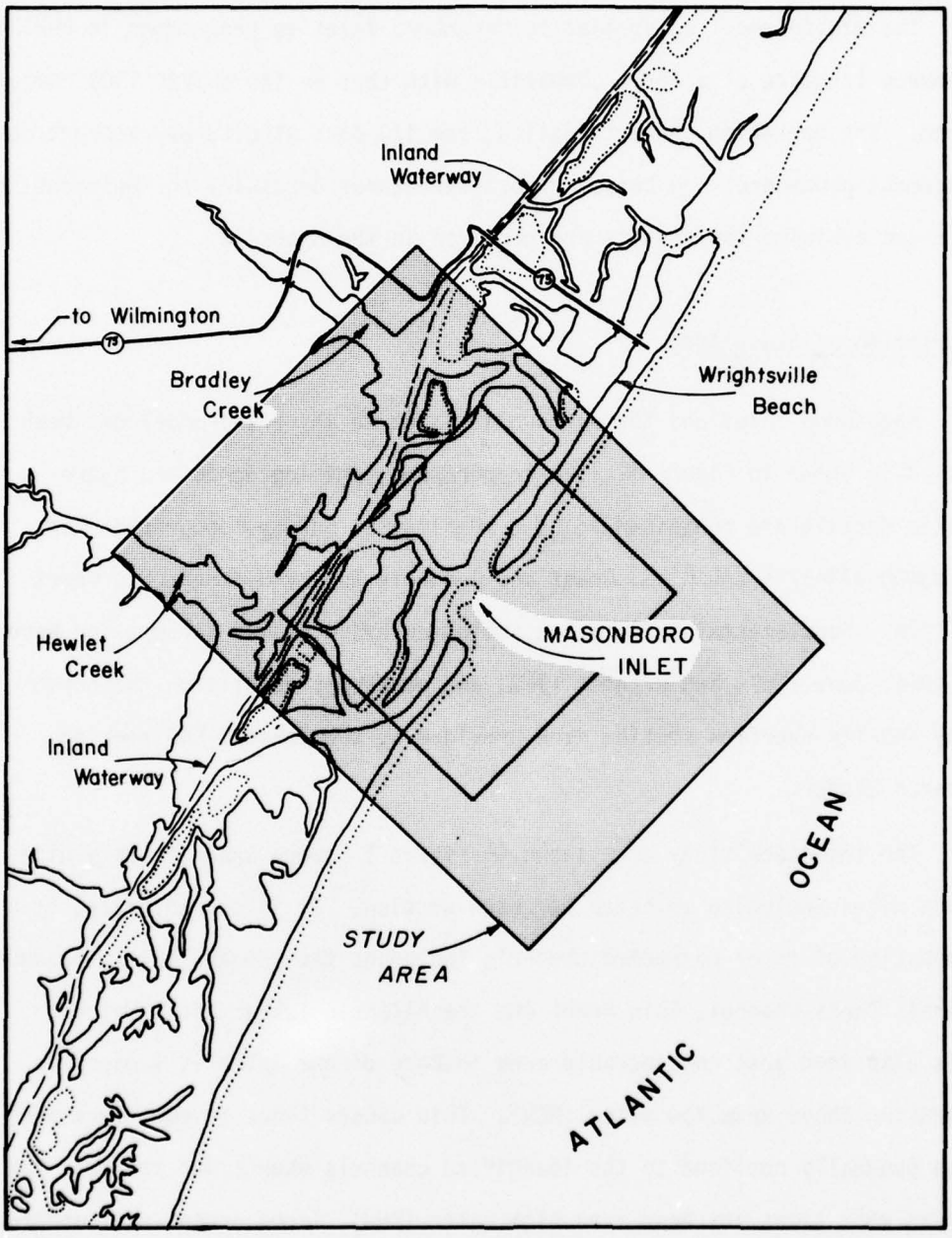

Figure 1

LOCATION MAP OF MASONBORO INLET AND STUDY AREA

Although not shown in Figure 1, the study area probably receives some local inland drainage and return flows through Bradley and Hewlet Creeks. However, no data on the magnitudes of these flows were available, nor is there any information on their distribution in the inland waterway and out through Masonboro Inlet.

II. FORMULATION AND SOLUTION TECHNIQUE

Tidal Hydrodynamic Equations

Mathematical characterization of the hydrodynamics in a tidal system requires the simultaneous solution of the dynamic equations of motion and the unsteady continuity equation. The theoretical basis for these equations has been dealt with in detail by Dronkers [1964] and will not be repeated here.

If it is assumed that vertical accelerations are negligible, pressures are hydrostatic over the depth and the fluid density is homogeneous, the equations of motion for a two-dimensional (areawise) tidal flow system can be written as:

$$\frac{\partial q_x}{\partial t} + \frac{q_x}{d}\frac{\partial q_x}{\partial x} + \frac{q_y}{d}\frac{\partial q_x}{\partial y} - \Omega q_y = - gd\frac{\partial h}{\partial x} - gdS_{ex} + K V_w^2 \cos \Psi \quad (1)$$

and

$$\frac{\partial q_y}{\partial t} + \frac{q_x}{d}\frac{\partial q_y}{\partial x} + \frac{q_y}{d}\frac{\partial q_y}{\partial y} + \Omega q_x = - gd\frac{\partial h}{\partial y} - gdS_{ey} + K V_w^2 \sin \Psi \quad (2)$$

The equation of continuity for the corresponding flow system can be expressed as:

$$\frac{\partial q_x}{\partial x} + \frac{\partial q_y}{\partial y} + \frac{\partial h}{\partial t} = r - e \quad (3)$$

In eqs. (1), (2), and (3), q_x and q_y are the vertically integrated flows per foot of width at time t in the x and y directions, respectively (x and y

taken in the plane of the surface area); h is the water surface elevation with respect to mean sea level (MSL) as datum; d is the depth of water at (x, y, t) and is equal to (h-z) where z is the bottom elevation with respect to MSL measured negatively downward; r is the rainfall intensity; e is the evaporation rate; V_w is the wind speed at a specified elevation above the water surface; Ψ is the angle between the wind velocity vector and the x-axis; and K is a nondimensional average wind stress coefficient taken as 1.8×10^{-6}, a value consistent with those suggested by Roll [1965] and Wilson [1960] for light winds. If it is further assumed in eqs. (1) and (2) that the dissipation of momentum due to bottom friction and turbulence can be expressed by the Manning Equation, then $S_{ex} = (n^2/2.21\ d^{10/3})\ q \cdot q_x$ and $S_{ey} = (n^2/2.21\ d^{10/3})\ q \cdot q_y$ where $q = (q_x^2 + q_y^2)^{1/2}$ and n is the Manning roughness coefficient estimated from formulas, tables or comparisons of measured and computed tide and velocity variations. The Coriolis parameter, Ω, is equal to $2\ \omega \sin \Phi$ where ω is the earth's angular velocity taken as 0.73×10^{-4} radians/second and Φ is the latitude equal to 34.2° at Masonboro Inlet.

Solution Scheme

The basic tidal hydrodynamic equations presented above are nonlinear partial differential equations in which there is also a dependence of d and q on the values of the three unknowns, q_x, q_y, and h. This difficulty, together with the complex geometry, various interior features and variable boundary conditions found in actual tidal systems, makes purely analytical approaches impractical. For these reasons, numerical schemes implemented on high speed, large capacity digital computers can be used to obtain approximate solutions to eqs. (1), (2), and (3).

The primary advantage of the numerical approach is that it permits discretization of a prototype system and facilitates prescribing in a more accurate manner the inputs necessary to describe the hydrodynamic behavior. A numerical model consists of a series of finite elements arranged in time and space so that the output from one element becomes the input to the next and so on. Each input to an element is operated on by a transfer function, and through an advancing series of spatial and time steps, the functional behavior of an entire prototype can be approximately determined. Thus, it becomes possible to evaluate the overall response of a total system by considering the interaction between individual elements satisfying common boundary conditions in succession.

It is important to recognize that the precision of the results obtained by numerical procedures depends in part upon the time interval and the element size selected for the calculations and the rate of change of the phenomena being studied. The greater the number of finite time intervals used over the total period of investigation and the greater the number of spatial elements used to describe physical detail, the greater also will be the accuracy of the expected results. Thus, solutions obtained may be refined within the basic assumptions to meet the demands of accuracy by decreasing the time interval and element size, although such reductions can be made only at the expense of increased operational costs. In addition to constraints imposed on the solution method by economics or by desired accuracy, there are also mathematical considerations involving stability, convergence and compatibility which limit the computational time interval and element size. It is only when a satisfactory compromise of all these factors is achieved that a potentially useful simulation tool results.

The computational scheme used in the model to solve the two equations of motion and the unsteady continuity equation involves a straight explicit formulation. In this method, eqs. (1), (2), and (3) are written in finite difference form and the three basic unknowns, q_x, q_y and h, are determined for each computational element at an advanced time level in terms of known conditions at the present time level. This solution scheme is similar to that used by Reid and Bodine [1968] in their hurricane surge model of Galveston Bay.

To facilitate application of this solution method, a computational grid composed of a mesh of square elements in two-dimensional Cartesian coordinates is used to represent the physical characteristics of the prototype system. The solution of the unknowns for each individual grid element proceeds spatially in a row by row manner over the entire array for a prescribed set of boundary conditions. Time is then advanced and the entire process repeated for a new set of initial and boundary conditions.

Variable definitions used in this explicit method are illustrated on the discrete element in Figure 2. Each element of this type is identified by the indices (i,j), i representing the x-direction, and j the y-direction, both coordinates being in the horizontal plane. The indices i and j increase with positive x and y, respectively. In the numerical analog, the discharges per unit width in the x and y directions are defined at the centers of the right and upper sides of each cell, respectively. The value of h is taken as the mean sea level water surface elevation and is defined at the center of the cell. Also defined at the center of each cell are the bottom elevation, the water depth, the Manning roughness coefficient, and the rainfall and evaporation rates.

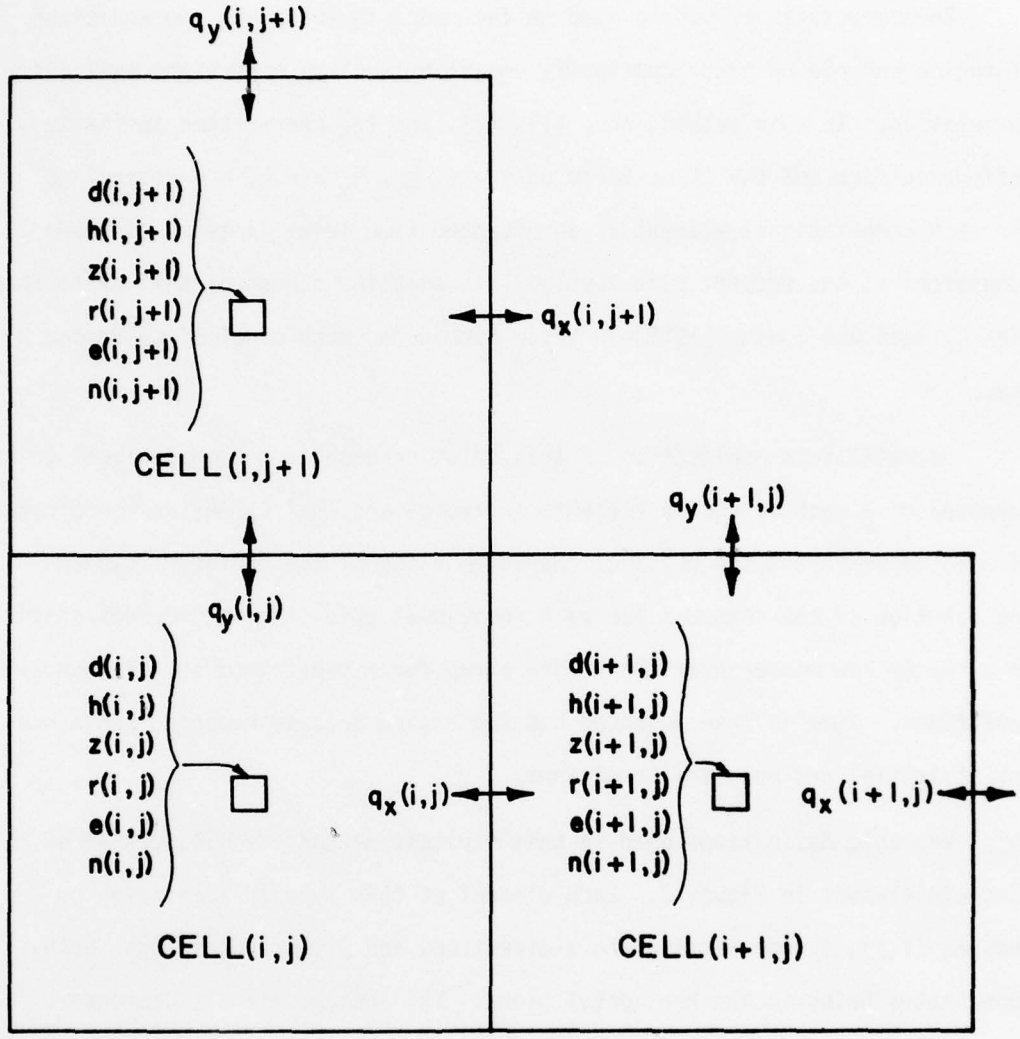

Figure 2

DISCRETE ELEMENT VARIABLE LOCATIONS USED IN *'HYDTID'*

The explicit solution method used is a time-centered difference scheme involving time operations of the "leap frog" type for computation of flows and water levels. For illustrative purposes, the following time notations are used to develop the recursion relations: $t-1 = (k-1/2)\,\Delta t$; $t = K\,\Delta t$; $t+1 = (k+1/2)\,\Delta t$; and $t+2 = (k+1)\,\Delta t$ where k is an integer. Time staggered computations are made for q_x and q_y at odd $(k\pm1/2)$ time levels and for h at even (k, k+1) time levels. The wind stresses are applied at spatial locations consistent with q_x and q_y but at even time levels. The selected time differencing scheme is such that the differences $(q_x^{t+1} - q_x^{t-1})$ and $(q_y^{t+1} - q_y^{t-1})$ are centered in time at the level of h^t and the difference $(h^{t+2} - h^t)$ is centered in time at the level of q_x^{t+1} or q_y^{t+1}.

Basic Finite Difference Equations

Using the above notations and writing the derivatives as centered differences, the terms in the equation of motion for the x direction, eq. (1), can be approximated as follows:

$$\frac{\partial q_x}{\partial t} = \frac{q_x^{t+1}(i,j) - q_x^{t-1}(i,j)}{\Delta t} \tag{4}$$

$$\frac{q_x}{d}\frac{\partial q_x}{\partial x} = \frac{q_x^{t+1}(i,j)}{d_x}\,\frac{q_x^{t-1}(i+1,\,j) - q_x^{t-1}(i-1,\,j)}{2\,\Delta x} \tag{5}$$

$$\text{where } d_x = \frac{d^t(i,j) + d^t(i+1,\,j)}{2}$$

$$\frac{q_y}{d}\frac{\partial q_x}{\partial y} = \frac{\bar{q}_y}{d_x}\,\frac{q_x^{t-1}(i,\,j+1) - q_x^{t-1}(i,\,j-1)}{2\,\Delta y} \tag{6}$$

$$\text{where } \bar{q}_y = \frac{1}{4}\left[q_y^{t-1}(i,j) + q_y^{t-1}(i+1, j) + q_y^{t-1}(i, j-1) + q_y^{t-1}(i+1, j-1)\right]$$

$$-\Omega q_y = -\Omega \bar{q}_y \tag{7}$$

$$-g d \frac{\partial h}{\partial x} = -g d_x \frac{h^t(i+1, j) - h^t(i,j)}{\Delta x} \tag{8}$$

$$gdS_{ex} = -\frac{g n^2 q_x \overline{q/d}}{2.21\, d^{4/3}} = -\frac{q n_x^2}{2.21\, d_x^{4/3}}\left[q_x^{t+1}(i,j) \cdot \overline{q/d}\right] \tag{9}$$

$$\text{where } n_x = \frac{n_{i,j} + n_{i+1, j}}{2}$$

$$\overline{q/d} = \frac{(q_x^{t-1}(i,j)^2 + \bar{q}_y^{\,2})^{1/2}}{d_x}$$

In these expanded terms, the only unknown quantity is q_x^{t+1}, the flow per unit width in the x direction at time level (k+1/2) Δt. Combining the terms according to eq. (1) and solving for q_x^{t+1}, a direct explicit expression for q_x can be written as follows:

$$q_x^{t+1}(i,j) = \left[q_x^{t-1}(i,j) - \Delta t \frac{\bar{q}_y}{d_x} \frac{q_x^{t-1}(i, j+1) - q_x^{t-1}(i, j-1)}{2\,\Delta y} + \Delta t\, \Omega\, \bar{q}_y - \Delta t\, g\, d_x \frac{h^t(i+1, j) - h^t(i,j)}{\Delta x} + \Delta t\, K\, W^2 \cos\Theta\right] / C_{fx} \tag{10}$$

$$\text{where, } C_{fx} = 1 + \frac{\Delta t}{d_x} \frac{q_x^{t-1}(i+1, j) - q_x^{t-1}(i-1, j)}{2\,\Delta x}$$

$$+ \frac{g\, n_x^2\, \Delta t}{2.21\, d_x^{4/3}} [\overline{q/d}] \qquad (11)$$

A similar expression for q_y at time level $(k+1/2)\,\Delta t$ can be developed from the equation of motion in the y direction, eq. (2), and written in difference form as follows:

$$q_y^{t+1}(i,j) = [q_y^{t-1}(i,j) - \Delta t \frac{\bar{q}_x}{d_y} \frac{q_y^{t-1}(i+1, j) - q_y^{t-1}(i-1, j)}{2\,\Delta x}$$

$$- \Delta t\, \Omega\, \bar{q}_x - \Delta t\, g\, d_y \frac{h^t(i, j+1) - h^t(i,j)}{\Delta y}$$

$$+ \Delta t\, K\, W^2\, \text{SIN}\, \Theta\,] / C_{fy} \qquad (12)$$

$$\text{where } C_{fy} = 1 + \frac{\Delta t}{d_y} \frac{q_y^{t-1}(i, j+1) - q_y^{t-1}(i, j-1)}{2\,\Delta y}$$

$$+ \frac{g\, n_y^2\, \Delta t}{2.21\, d_y^{4/3}} [\overline{q/d}] \qquad (13)$$

$$d_y = \frac{d^t(i,j) + d^t(i, j+1)}{2}$$

$$\bar{q}_x = \frac{1}{4} [q_x^{t-1}(i,j) + q_x^{t-1}(i, j+1) + q_x^{t-1}(i-1, j)$$

$$+ q_x^{t-1}(i-1, j+1)\,]$$

$$n_y = \frac{n_{i,j} + n_{i,j+1}}{2}$$

$$\overline{q/d} = \frac{(\bar{q}_x^2 + q_y^{t-1}(i,j)^2)^{1/2}}{d_y}$$

Similarly, the third unknown, the water level h, can be determined from the continuity equation, eq. (3) by approximating its derivatives with centered differences as follows:

$$\frac{\partial h}{\partial t} = \frac{h^{t+2}(i,j) - h^t(i,j)}{\Delta t} \tag{14}$$

$$\frac{\partial q_x}{\partial x} = \frac{q_x^{t+1}(i,j) - q_x^{t+1}(i-1,j)}{\Delta x} \tag{15}$$

$$\frac{\partial q_y}{\partial y} = \frac{q_y^{t+1}(i,j) - q_y^{t+1}(i,j-1)}{\Delta y} \tag{16}$$

Combining these difference terms and solving for h^{t+2}, the following expression for water level results,

$$h^{t+2}(i,j) = h^t(i,j) - \Delta t \frac{q_x^{t+1}(i,j) - q_x^{t+1}(i-1,j)}{\Delta x}$$

$$- \Delta t \frac{q_y^{t+1}(i,j) - q_y^{t+1}(i,j-1)}{\Delta y} + (r - e)\Delta t \tag{17}$$

It should be noted that in developing eq. (17), the previously determined flows per unit width at time level (t+1) are used to establish the spatial flow gradients. Thus in the solution process, the computed flows and the water levels are always determined one-half time step apart, although results are usually presented only at even time levels.

The difference formulations presented above for solution of the three basic unknowns are applicable to situations where grid elements can be considered as "open water" cells surrounded by free flowing water on all four sides. Usually the majority of the computational elements used to simulate a prototype system are of this type, however there are certain special cases where the cross-product terms associated with convective acceleration $\frac{q_y}{d}\frac{\partial q_x}{\partial y}$ and $\frac{q_x}{d}\frac{\partial q_y}{\partial x}$ must be formulated in a manner that is consistent with the conditions that exist in the prototype. For example, where an impermeable boundary such as an island or dike lies between two adjacent water cells as illustrated below by the heavy line, the flow gradient $\partial q_x/\partial y$ expressed as $[q_x(i, j+1) - q_x(i, j-1)]/2\ \Delta y$, eq. (6), has little meaning since the two flows used to approximate the gradients are not linked by a continuous water surface.

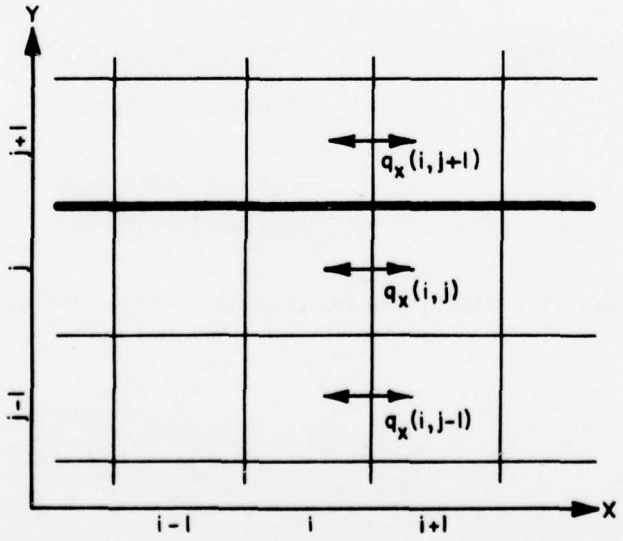

In this case, a more meaningful approximation of the gradient would be $[q_x(i,j) - q_x(i, j-1)]/\Delta y$. Similarly if the impermeable barrier were along the bottom of CELL (i,j), the quantity $[q_x(i, j+1) - q_x(i,j)]/\Delta y$ would define the flow gradient. For water cells lying between impermeable barriers, the lateral flow gradients are set equal to zero. These alterations to the finite difference approximations of the cross-product terms for both the x and y directions are made in the model for all possible combinations of impermeable barrier configurations.

To facilitate the use of the proper forms of the cross-product difference approximations in the model, a special cell flagging scheme has been devised. Each element in the grid is assigned a two digit number which designates the calculations that are to be performed in describing the flow gradients across the element in each of the two coordinate directions. The two digits may each range from one to four with the first digit applying to the x-direction and the second to the y-direction. Under this system, the following finite difference approximations to the two cross-product terms are made in the model according to the value of the individual digits.

DIGIT VALUE	TYPE OF APPROXIMATION
1	Centered Difference
2	Zero
3	Forward Difference
4	Backward Difference

For each of the two directions, the cross-product terms are expressed as follows:

X-DIRECTION

$$(1)\quad \frac{q_y}{d}\frac{\partial q_x}{\partial y} = \frac{\bar{q}_y}{d_x}\,\frac{q_x^{t-1}(i,\,j+1) - q_x^{t-1}(i,\,j-1)}{2\,\Delta y}$$

$$(2)\quad \frac{q_y}{d}\frac{\partial q_x}{\partial y} = 0$$

$$(3)\quad \frac{q_y}{d}\frac{\partial q_x}{\partial y} = \frac{\bar{q}_y}{d_x}\,\frac{q_x^{t-1}(i,\,j+1) - q_x^{t-1}(i,j)}{\Delta y}$$

$$(4)\quad \frac{q_y}{d}\frac{\partial q_x}{\partial y} = \frac{\bar{q}_y}{d_x}\,\frac{q_x^{t-1}(i,\,j) - q_x^{t-1}(i,\,j-1)}{\Delta y}$$

Y-DIRECTION

$$(1)\quad \frac{q_x}{d}\frac{\partial q_y}{\partial x} = \frac{\bar{q}_x}{d_y}\,\frac{q_y^{t-1}(i+1,\,j) - q_y^{t-1}(i-1,\,j)}{2\,\Delta x}$$

$$(2)\quad \frac{q_x}{d}\frac{\partial q_y}{\partial x} = 0$$

$$(3)\quad \frac{q_x}{d}\frac{\partial q_y}{\partial x} = \frac{\bar{q}_x}{d_y}\,\frac{q_y^{t-1}(i+1,\,j) - q_y^{t-1}(i,j)}{\Delta x}$$

$$(4)\quad \frac{q_x}{d}\frac{\partial q_y}{\partial x} = \frac{\bar{q}_x}{d_y}\,\frac{q_y^{t-1}(i,j) - q_y^{t-1}(i-1,\,j)}{\Delta x}$$

Special Boundary Conditions

Because of the complex geometry and flow behavior in most tidally influenced prototype systems, there are several different types of special flow boundaries that must be described to properly simulate prototype conditions with HYDTID. For the model application described herein, boundary

conditions can be grouped according to the following seven general classifications:

1. *Water-Land Boundaries*
2. *Submerged Barrier Boundaries*
3. *Overtopping Barrier Boundaries*
4. *External Flow Boundaries*
5. *Artificial Offshore Tidal Boundaries*
6. *Artificial Tidal-Storage Boundaries*
7. *Inundation Boundaries*

Water-Land Boundaries occur primarily around the perimeter of the system although other internal physical features such as islands, spoil banks, dikes and jetties can provide the equivalence of water-land boundaries. A necessary requirement for computation of tidal hydrodynamics adjacent to these boundaries is that the component of flow normal to the boundary be equal to zero, $q_n = 0$. In the model, this condition is handled by specifying the following equations for those elements where impermeable boundaries exist.

$$q_x^{t+1}(i,j) = 0 \tag{18}$$

$$q_y^{t+1}(i,j) = 0 \tag{19}$$

Submerged Barrier Boundaries are used in the model to describe interior flows across such barriers as submerged reefs, spoil banks, or pipe lines and to provide flow control through constrictions such as narrow channels and passes. An important characteristic of this type of flow boundary is that the water levels on each side of the barrier always exceed the barrier crest elevation. Under this situation, the flow across the barrier can be described

in a manner analogous to that used for submerged weirs, i.e.

$$q_n = \pm C_B d_B \sqrt{g|h_1 - h_2|} \tag{20}$$

where d_B is the depth of water over the crest of the weir, h_1 and h_2 are the water levels on each side of the weir, and C_B is an appropriate discharge coefficient.

Application of this boundary condition in the model is accomplished using the same set of finite difference equations previously developed for open water cells except that in place of a bottom resistance term involving the energy slope in eq. (9), a new term is substituted which incorporates the effect of weir control. With this substitution the only expressions affected are those for C_{fx} and C_{fy}, eqs. (11) and (13). For a typical barrier parallel to the y-axis and positioned at the right side of CELL (i,j), $q_x^{t+1}(i,j)$ can be determined using eq. (10) and the following,

$$C_{fx} = 1.0 + \frac{\Delta t}{d_x} \frac{q_x^{t-1}(i+1, j) - q_x^{t-1}(i-1, j)}{2\,\Delta x} + \frac{\Delta t\, d_x \left|q_x^{t-1}(i,j)\right|}{\Delta x \, (C_B\, d_B)^2} \tag{21}$$

in which

$$d_B = 1/2\,[h^t(i+1, j) + h^t(i,j)] - z_B$$

and z_B is the barrier crest elevation.

Similarly for a submerged barrier parallel to the x-axis at the top of CELL (i,j),

$$C_{fy} = 1.0 + \frac{\Delta t}{d_y} \frac{q_y^{t-1}(i, j+1) - q_y^{t-1}(i, j-1)}{2\,\Delta y} + \frac{\Delta t\, d_y \left| q_y^{t-1}(i,j) \right|}{\Delta y \, (C_B\, d_B)^2} \qquad (22)$$

$$\text{where } d_B = 1/2\,[h^t(i, j+1) + h^t(i,j)] - z_B$$

Again, the expressions for C_{fx} and C_{fy} are essentially the same as used by Reid and Bodine [1968] except that a term accounting for the convective acceleration has been added. This discharge coefficient C_B is also the same varying between 0.01 and 1.3 and is determined in part during the calibration process.

Overtopping Barrier Boundaries are included in the model to describe the flows which occur periodically over dikes, jetties, bridge embankments, levees, etc. as water levels rise and fall under the influence of tidal action, winds, flood waves, or other external forces. Normally the water level on only one side of these type boundaries exceeds the barrier crest elevation and under such conditions, flows are approximated in the model using an expression similar to the broad-crested weir formula,

$$q_n = \pm C_B' \, \Delta H \sqrt{g \Delta H} \qquad (23)$$

where C_B' is a discharge coefficient on the order of 0.5 and ΔH is the elevation of the upstream total energy line above the weir crest. For an overtopping barrier parallel to the y-axis and at the right side of CELL (i,j), eq. (23)

can be written as,

$$q_x^{t+1}(i,j) = \pm C_B' d_B \sqrt{g\, d_B} \tag{24}$$

where $d_B = h_{max} - z_B = \Delta H$

and $h_{max} = h^t(i,j)$ or $h^t(i+1, j)$, whichever is greater.

Similarly for a barrier at the top of CELL (i,j),

$$q_y^{t+1}(i,j) = \pm C_B' d_B \sqrt{g\, d_B} \tag{25}$$

where $d_B = h_{max} - z_B = \Delta H$

and $h_{max} = h^t(i,j)$ or $h^t(i, j+1)$, whichever is greater.

As the downstream water level rises due to an increasing flow across the barrier, it is possible that complete submergence of the barrier can occur. When this takes place, flow control for the barrier is transferred in the model to the appropriate submerged weir relation given by eq. (20) above. Therefore the overtopping barrier is subject to dynamic boundary conditions according to the water levels which exist on both sides of the barrier.

External Flow Boundaries are specified in the model where river inflows, diversions, and return flows enter or leave the perimeter of the system. These flows can be expressed quantitatively by the equation, $q_n = Q(t)$, which allows the external flows to be introduced or withdrawn in any time dependent manner or at a constant rate over a prescribed period of time at any boundary

location. Thus in the model,

$$q_x^{t+1}(i,j) = Q(t+1) \tag{26}$$

and

$$q_y^{t+1}(i,j) = Q(t+1) \tag{27}$$

where Q is the prescribed inflow.

Aside from being used to define inflows or withdrawals along the system perimeter, external flow boundaries are also necessary to describe flow conditions along the outer boundaries of fine-grid sub-models of localized areas. This, of course, assumes that such flows are known and can be prescribed with sufficient detail in both time and space to properly define prototype conditions. When this information is not available from field measurements, a coarse grid model of the entire system can be used to generate these internal flows, which upon interpolation, provide the necessary external inputs to the more detailed fine grid model.

Artificial Offshore Tidal Boundaries are used in the model to describe the tidal action which occurs immediately offshore of the prototype system. These boundaries must be accurately defined since they represent the boundary along which the major forcing function for excitation of the tidal hydrodynamics must be applied. In HYDTID, tidal boundaries are specified along an imaginary line offshore and generally parallel to the coastline. The tidal flow across this boundary corresponding to the excitation tide is computed according to the relationship,

$$q_n = C_T (H_g - h) \tag{28}$$

where C_T is an admittance coefficient taken approximately equal to the speed of a gravity wave ($\sqrt{g\ d}$), H_g is the forcing function or known water surface time history specified at the seaward boundary, and h is the actual water level at the outer boundary of the tidal system. This relation is consistent with that suggested by Reid and Bodine [1968].

For a typical computational element in the model with an ocean boundary on its right side, the tidal flow can be computed as follows,

$$q_x^{t+1}(i,j) = \pm C_T [H_g - h^t(i+1, j)] \quad (29)$$

Similarly for an ocean boundary at the top of an element,

$$q_y^{t+1}(i,j) = \pm C_T [H_g - h^t(i+1, j)] \quad (30)$$

In these equations, the sign is such that positive flow is into the tidal system.

Artificial Tidal-Storage Boundaries are specified in the model to provide the proper exchange of water across external model boundaries which lie inside the mouth of a tidal system where tidal flows occur. To eliminate the necessity to model the entire water area included in the tidal system, the storage provided by external water bodies adjacent to the modeled area can be simulated by using a relation similar to eq. (28) applied along the model perimeter. In this case, the forcing function, H_g, is the tide which occurs along the model perimeter in the prototype system. Since this tide is normally not available from measured data, it is often necessary to determine its shape and phasing during the verification of the model by comparing computed and measured flows inside the modeled area. Once these tidal conditions are established, cor-

relations can then be developed with other known tides which are always available from prototype records.

Inundation Boundaries are used in the model to account for flooding of areas with elevations between mean low and high water levels. Computations at this type of flow boundary are characterized by a check of the water levels in adjacent cells relative to the ground elevation to determine if inundation is possible. If not, the cell boundary remains a *Water-Land Boundary* and a condition of zero flow is specified. If flooding is possible, the boundary is treated as if it were an open water cell and the flows are computed according to eqs. (10) and (12).

Because of the variety of different boundary conditions that must be handled within HYDTID, it is both convenient in setting up the model and computationally expedient to define the different types of cells *a priori*. Each cell in the grid system is therefore identified or "flagged" according to the flow conditions along its top and right boundaries, Figure 3. (The designation of the cell flags in Figure 3 is completely independent of the two-digit flagging scheme used to handle the cross-product convective acceleration terms.)

Although the basic HYDTID model described herein accounts for forty-five combinations of different boundary conditions as defined along the top and right sides of the cells only twenty-eight were actually used in modeling Masonboro Inlet. The remaining unused cells result from permutations of the seven basic boundary conditions and experience with applications of HYDTID in other systems. It is probable that these additional flags will find use in other modeling efforts.

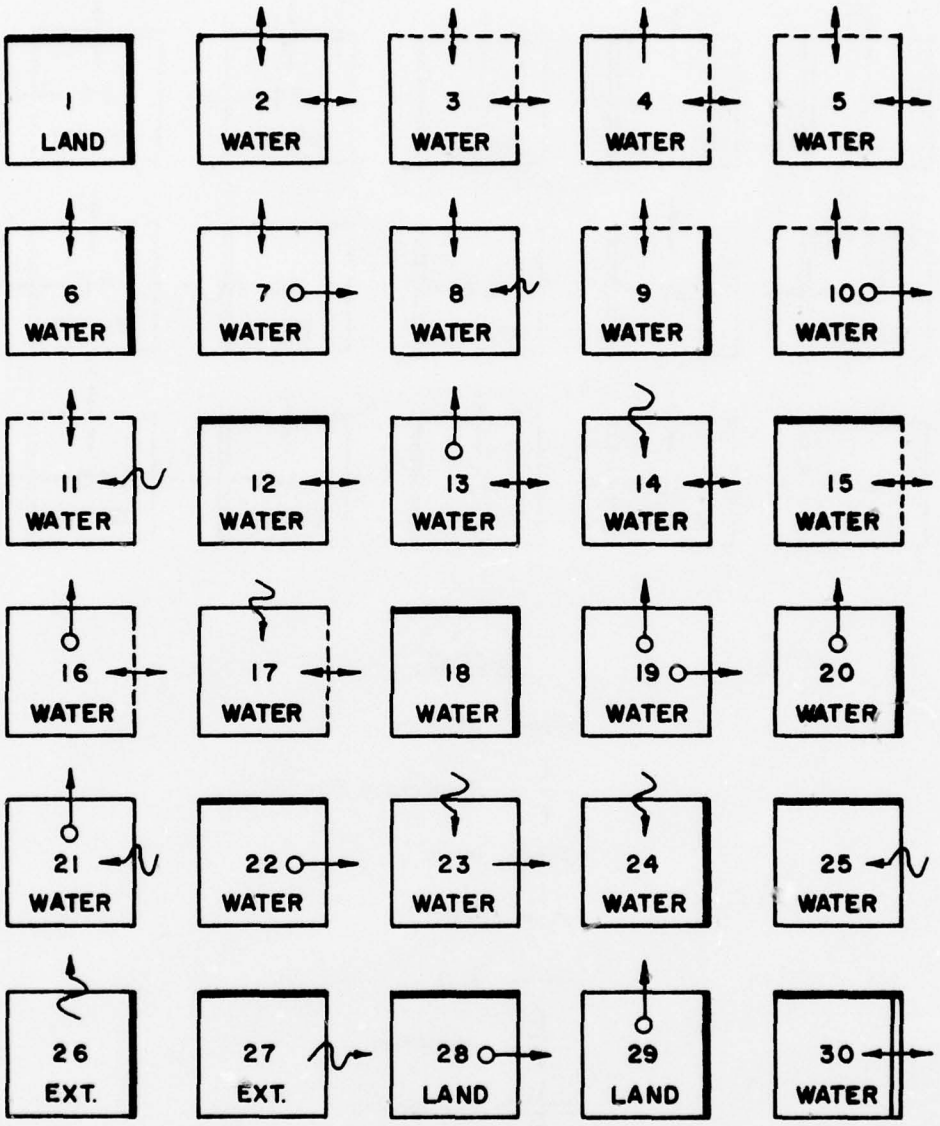

Figure 3

CELL FLAGGING SCHEME FOR IDENTIFYING FLOW BOUNDARY CONDITIONS

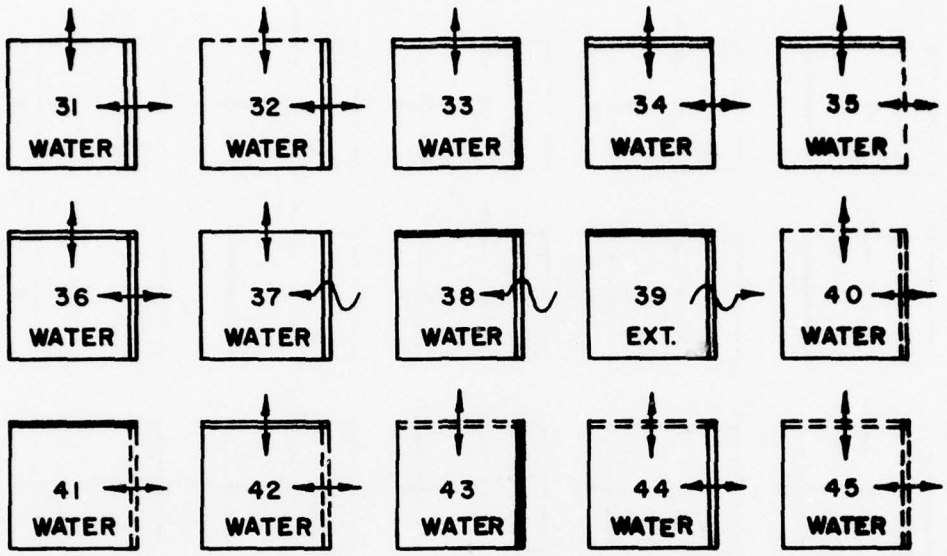

LEGEND

- No Flow
- Submerged Barrier
- Inflow
- Tidal
- Flow
- Inundation
- Overtopping

Figure 3, Cont.

CELL FLAGGING SCHEME FOR IDENTIFYING FLOW BOUNDARY CONDITIONS

Choice of Time Step and Mesh Size

In an explicit solution scheme, the mesh size and computational time step are related through mathematical considerations arising from stability, convergence and compatibility. Specifically, the following criterion must be maintained for a stable solution to eqs. (10), (12), and (17)

$$\Delta t \leq \frac{\Delta s}{\sqrt{2\, g\, d_{max}}} \tag{31}$$

where Δt is the time step; Δs is the mesh size; and d_{max} is the maximum water depth used in the model. Ideally, Δs (or Δx or Δy) is made as small as possible to provide maximum spatial resolution and detail. This, however, can only be done at the expense of computer storage and time. Thus, the selection of the mesh size must be based on available prototype data, required model detail, desired resolution of results, computer time and storage, as well as the mathematical constraint imposed by eq. (31).

Implementation Procedure

HYDTID is designed so that tidal computations begin at the seaward boundary and progress shoreward explicitly over the entire computational matrix. Time is advanced incrementally and the computations are repeated until the desired simulation period is completed. To apply and use HYDTID the following basic steps are required:

1. Define model resolution (in accordance with procedures outlined in the following Chapter).
2. Determine physical boundaries of the area to be modeled and superimpose a mesh of cells (scaled to provide the desired resolution) over the corresponding hydrographic chart of the model area.

3. Determine average MSL water depth (or land elevation) for each cell in the mesh.

4. Determine cell computational identification number (flag) according to Figure 3 for each element in the model. Consider only the top and right boundaries of individual cells when establishing flags.

5. Assign appropriate two-digit flag numbers to those cells where convective cross-product terms must be evaluated by expressions other than central difference approximations. (Flags "11" need not be specified.)

6. Assign discharge coefficients and crest elevations to all submerged and overtopping barriers in the model.

7. Estimate bottom friction in terms of Manning "n" coefficients for each water cell and for each land cell likely to be inundated.

8. Based on availability of tidal and hydraulic data, select periods for model calibration.

9. Assemble all model input data according to the order and formats specified in the Appendix.

10. Operate the model for the selected calibration period until repetitive conditions from one tidal cycle to the next are achieved and compare computed tides and velocities (as well as total exchange) against measured data at common sections.

11. Adjust and refine the model through bottom friction, discharge coefficients and elevations of submerged barriers used to control flow, and the admittance coefficients for excitation tides until desired agreement is obtained between computed and measured results.

12. Carry out operational runs using the verified model. Depending on the character of any proposed changes in the operational runs, it is usually necessary to change some cell flag identifications to account for the corresponding changes in the bathymetry or physical features in the system.

III. MODEL APPLICATION AND VERIFICATION

Prototype Information

For the 12 September 1969 verification period, physiographic and bathymetric information at Masonboro Inlet was obtained from a 1" = 500' hydrographic chart provided by CERC and based on data collected during September and October of 1969. The chart contained two-foot contours describing bottom topography below MLW and spot elevations for ground levels above MHW. The datum for all elevations was given as MLW. Also included on the chart were the jetty alignment and the locations of several recording tide gages and velocity stations where data were collected for the September verification period.

Seven tide gages were used to record continuous tidal information in the vicinity of Masonboro Inlet for most of the period 0300 to 2100 on 12 September 1969. The spatial coverage provided by the gages is illustrated in Figure 4 and is considered adequate for model development, particularly since tidal levels at these locations differ by only a few tenths of a foot and phase changes are generally less than an hour. For the verification period, tides were nearly sinusoidal in shape with a semi-diurnal period on the order of 12.5 hours. Representative of the tides measured at all of the gages is that for Gage 0 located on the ocean side of Wrightsville Beach north of the jetty. This offshore tide, shown in Figure 5, provides the primary tidal influence to the Masonboro Inlet area, and as such, is of major importance for providing tidal excitation in the model.

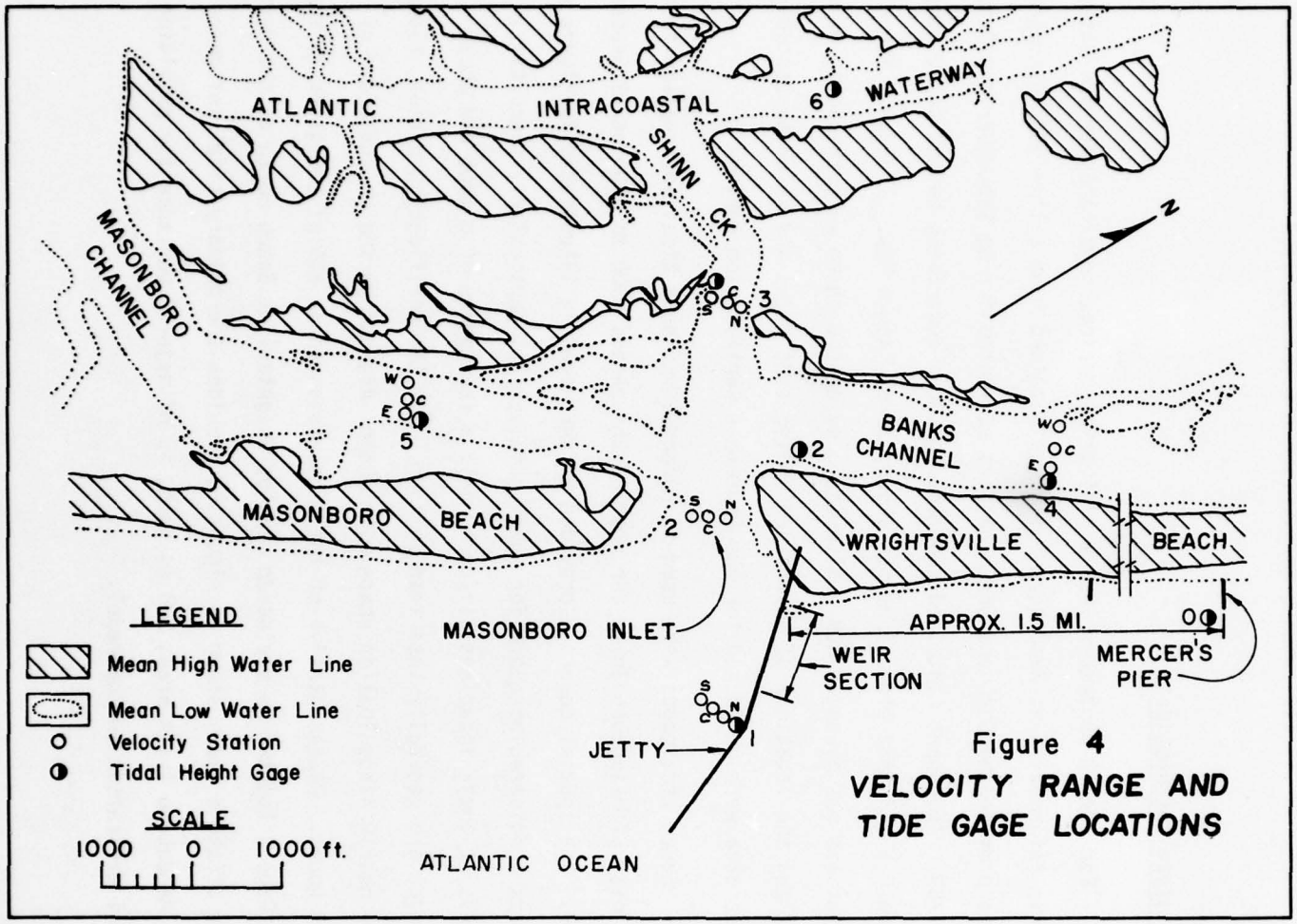

Figure 4

VELOCITY RANGE AND TIDE GAGE LOCATIONS

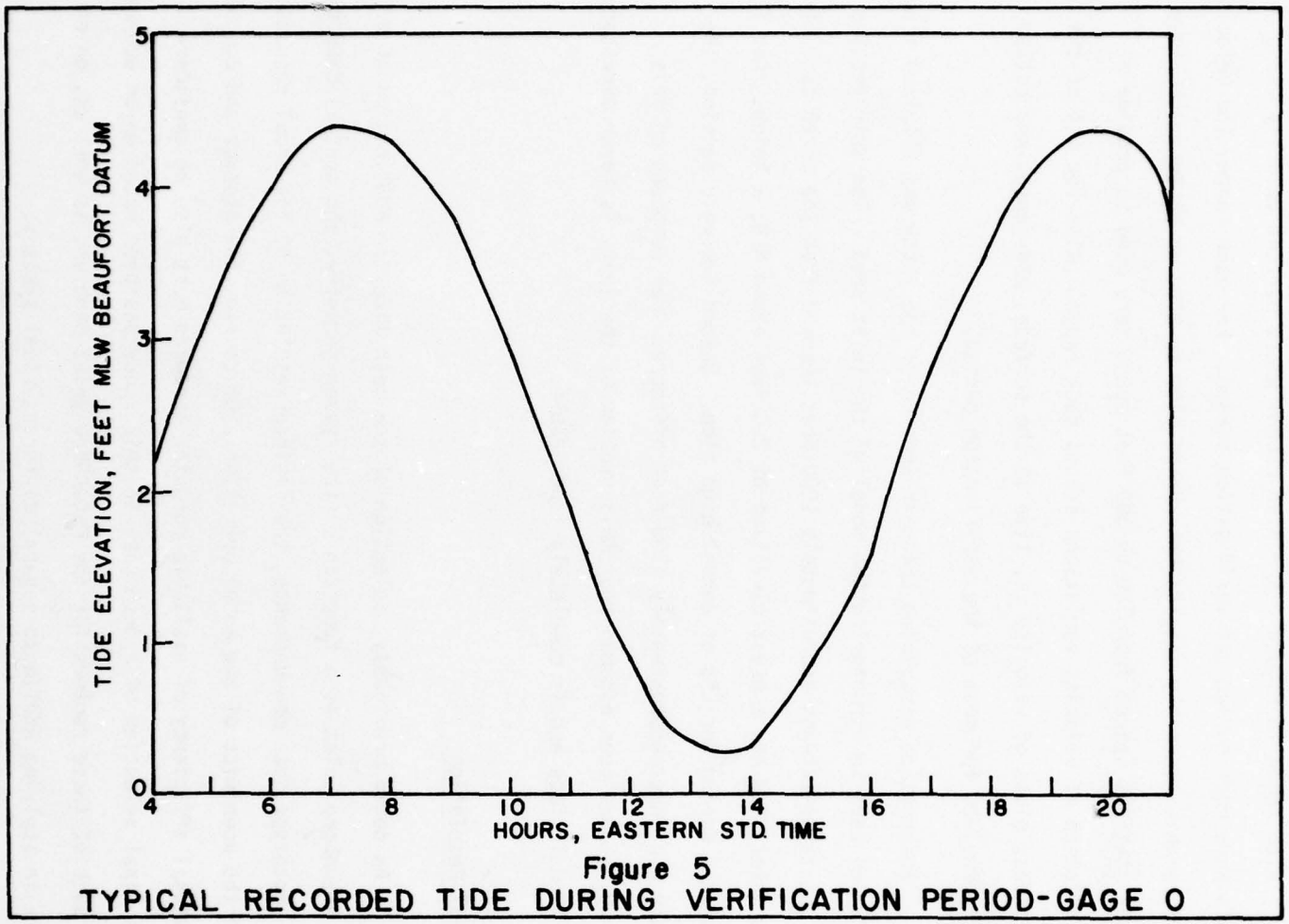

Figure 5
TYPICAL RECORDED TIDE DURING VERIFICATION PERIOD-GAGE O

Also shown in Figure 4 are five ranges where current velocity measurements were made during the verification period. For each range, the velocity measurements generably covered the period 0700 to 2100 on 12 September 1969. Three stations spaced from 150 to 300 feet apart were used to provide a description of velocity variations across each range. Also for all of the stations, plots of velocity vs. time at the surface, mid-depth, and bottom were provided for most of the verification period.

Information describing the weir section of the jetty was obtained from CERC and used in structuring the model of the inlet area. The weir section of the jetty extends approximately 1000 feet seaward from the north back of the inlet, and has a crest elevation of 2.0 feet above MLW, a height that is exceeded during periods of normal high tide. Beyond the weir section, the jetty continues approximately 1900 feet offshore. For purposes of this study, it has been assumed that this section of the jetty is never overtopped by normal tides and is completely impermeable.

Model Resolution

As noted previously, selection of the mesh size for application of HYDTID to Masonboro Inlet is a function of the system geometry, the spatial density of prototype data measurements, the desired resolution of the model results, and the economics of the model operation. Of course, the storage and computational efficiency of available computer hardware must also be considered. The final selection of a mesh size in this study has been based on an evaluation of each of these factors for the Masonboro Inlet problem, as well as, on experience in applying HYDTID to several different tidal systems.

A review of the Masonboro Inlet study area, Figures 1 and 4, including the configuration of islands, inter-connected channels, and inundated areas, suggests that a mesh size on the order of 1000 to 1200 feet would provide sufficient resolution for generally describing these features and allowing some simulation of tidal flows and water surface fluctuations. While this level of resolution would not permit the detailed description of flows and velocities within channels themselves, it would provide for reasonably accurate simulation of the gross flow distribution at the major channel junctures and through the main inlet.

However to be consistent with the spatial resolution of available prototype data, and in particular the velocity measurements, a mesh size of 100 to 300 feet more nearly conforms to the spacing between individual velocity stations. Additionally, this resolution would allow a better representation of the variable bottom topography in the inlet area, thereby permitting more accurate simulation of localized flows within the major branches of the system.

The advantages of using still finer resolution in the model of Masonboro Inlet are obvious, however as is often the case, it is the cost of operating the model that ultimately determines the fineness with which physical detail can be described. A reduction in the mesh size results not only in more computational elements to cover a given area, but also requires a reduction in the computational time step because of the stability criterion, eq. (31), imposed on the solution scheme. For example if the element size is reduced by half, the number of calculations required to simulate a specified period of real time is theoretically increased by a factor of eight, thus increasing the cost of operating the model also by a factor of about eight.

To aid in the selection of a near-optimal mesh size for the Masonboro Inlet model, the computer time required to operate models with different element sizes ranging from 200 to 1200 feet was estimated for simulation periods of one tidal cycle (12.5 hours). The study area identified in Figure 1 was used for structuring these hypothetical models, and experience with HYDTID in other systems was used to estimate the computer time requirements for each of the selected mesh sizes.

Figure 6 summarizes the UNIVAC 1108 CPU time requirements for HYDTID models of several different tidal systems with which WRE has had modeling experience. The abscissa in Figure 6 is equal to the product of the number of water cells included in the model where calculations must be performed and the number of time steps required to simulate 24 hours of real time. For example, if a model consisted of 100 water cells and used a time step of one minute, a total of (24 x 60)/1 = 1440 time steps would be required to simulate one day, and the abscissa value used in Figure 6 would be equal to 100 x 1440 = 144000. Thus, knowing the size of the prototype system, including its maximum depth, and selecting a trial mesh size, the allowable time step can be determined from eq. (31), and finally, the computer time and cost requirements for operating the model can be estimated from Figure 6. The magnitude of the error which might be expected in such a time estimate is indicated by the scatter of the points. Since not all tidal systems are exactly alike, model operation times also vary, not only because of mesh size and time step differences, but also because of the number and variety of boundary conditions required by models of different systems. It should also be noted that the UNIVAC 1108 CPU times used in developing Figure 6 were all determined based on

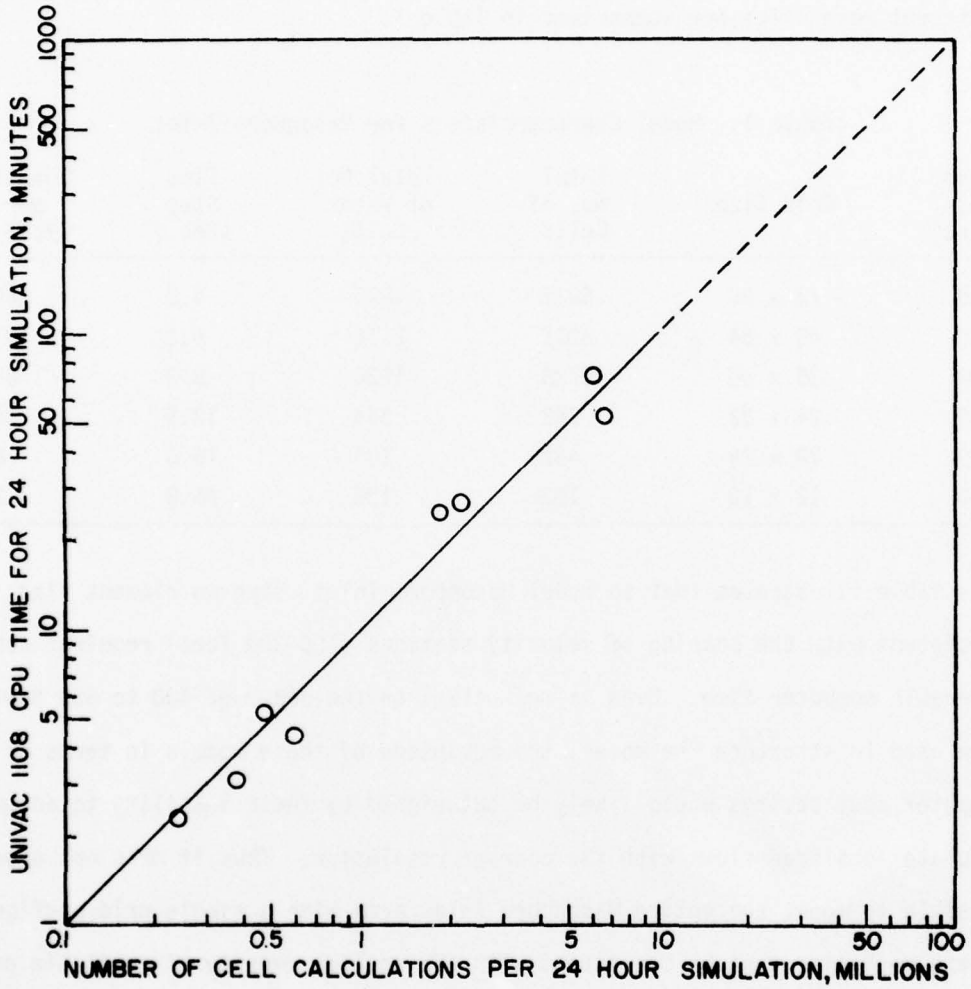

Figure 6

COMPUTER TIME REQUIREMENTS FOR *'HYDTID'* MODEL

the Tracor, Inc. computer system in Austin, Texas, and results from this figure may not be completely consistent with other UNIVAC 1108 systems.

For the Masonboro Inlet study area, the results of applying Figure 6 with different mesh sizes are summarized in Table 1.

Table 1. Model Characteristics for Masonboro Inlet

Mesh Size (feet)	Grid Size	Total No. of Cells	Total No. of Water Cells	Time Step (Sec.)	Computer Time per Tidal Cycle (min.)
200	72 x 96	6912	4896	4.2	544.0
300	48 x 64	3072	2176	6.3	161.6
400	36 x 48	1728	1224	8.3	68.0
600	24 x 32	768	544	12.5	20.2
800	18 x 24	432	306	16.6	8.5
1200	12 x 16	192	136	25.0	2.5

This table illustrates that to model Masonboro Inlet using an element size consistent with the spacing of velocity stations (100-300 feet) requires considerable computer time. Even if mesh sizes on the order of 400 to 600 feet were used to structure the model, the advantage of these models in terms of computer cost savings would likely be outweighed by their inability to adequately simulate localized flows with the coarser resolution. Thus it does not appear feasible to model the entire Masonboro Inlet area with a single grid configuration if the mesh size must be consistent with the spatial density of available prototype data.

An alternate procedure is to describe the hydrodynamics of the entire area on a large scale using a coarse grid model, and then use the simulated results

from this model to provide the external inputs to a fine grid sub-model of a localized area where more detail is desired. This dual-model approach results in a computer cost savings if the combined operation time of the two models is less than that of a single fine grid model of the entire area. For the Masonboro Inlet area, this can be shown to be the case by considering a coarse grid model of the entire area based on an element size of 1200 feet and a fine grid sub-model of only the inlet area using a mesh size of 300 feet. The extent of these models is shown in Figure 7 and covers the same area as that designated in Figure 1 as the study area.

From Table 1, the computer time required to simulate one tidal cycle with the 1200' coarse grid model should be about two to three minutes. Using a similar procedure, computer time for the fine grid sub-model can be estimated from Figure 6 as follows:

Mesh Size (feet)	Grid Size	Total No. of Cells	Total No. of Water Cells	Time Step (Sec.)	Computer Time per Tidal Cycle (min.)
300	33 x 30	990	360	5.0	33.6

Hence the combined computer time requirement of the two models is on the order of 36 minutes and less than the 162 minutes given in Table 1 for a single model covering the entire study area with a 300' mesh size. Based on these projections, the model of Masonboro Inlet has been developed using the dual-model approach with mesh sizes of 1200 and 300 feet.

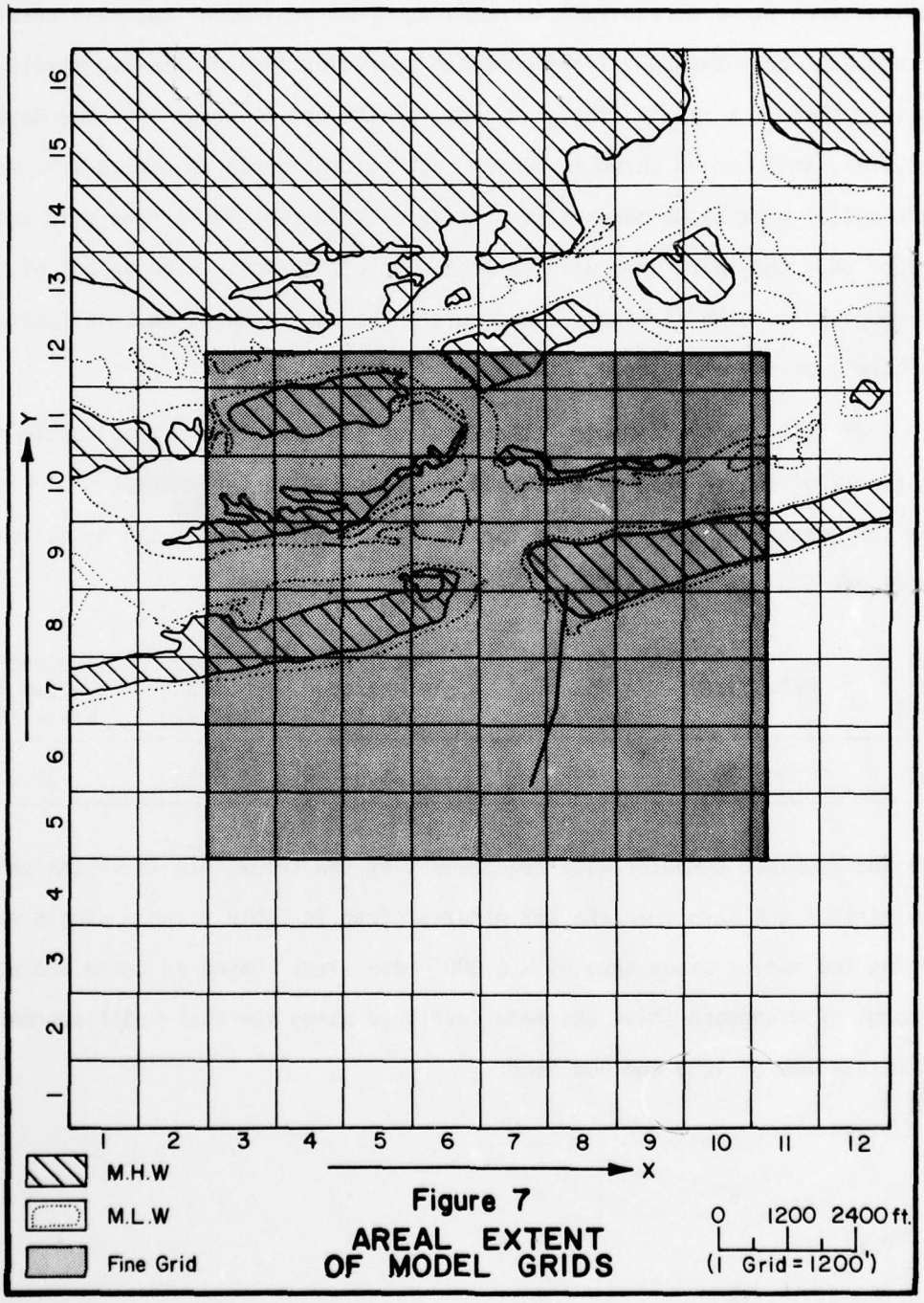

Figure 7

AREAL EXTENT OF MODEL GRIDS

Dual-Model Procedure

Implementation of the dual-model concept for verification of the 12 September 1969 conditions in Masonboro Inlet involved first the calibration of the coarse grid model for generalized flow simulation and reproduction of tidal amplitudes, and secondly, the calibration of the fine grid sub-model to describe localized flows and velocities. While the entire verification process required the development and tuning of two hydrodynamic models, calibration of the coarse grid model resulted in information directly usable in the fine grid sub-model. Linkage between the two models was provided by the flows computed in the coarse grid model across those cell boundaries which coincided with the external limits of the fine grid sub-model. Initial water levels in the fine grid sub-model were determined by interpolation of corresponding water levels computed with the coarse grid model.

An important consideration in implementing the dual-model concept is that the relation between depth and volume be the same in the two models for that portion of the prototype contained in both. Specifically, this means that ground elevations between MLW and MHW must be assigned to the individual cells in each of the models in a consistent manner so that for any water level above MLW, the amount of inundation is essentially the same, with both models providing equal quantities of water storage capacity. If the depth-volume relations are not the same, then computed tidal levels in the models will not agree when boundary flows to the two

systems are equal. The degree to which the depth-volume relations in the two models can be made to coincide depends on the relative difference between the grid mesh sizes and the variation of the topography between the MLW and MHW levels.

It should be pointed out that the differences in the computed hydrodynamics which result from not having compatible bottom depths and ground elevations in the two models are most discernible in the tidal levels rather than in the channel flows and velocities. The main reason for this is that simulated flows from the coarse grid model are used to excite the fine grid sub-model, and hence, flows within the fine grid system directly reflect these inputs. If the differences which occur in computed tidal levels due to inconsistent depth-volume relations are small compared to the total depths, the channel cross-sectional areas will not change significantly and consequently, the velocities will be only slightly affected.

To minimize the effects of inconsistent depth-volume relations in the two models, the bottom and ground elevations should first be established for each cell in the fine grid sub-model, and then, based on this information together with the inlet geometry, appropriate average elevations can be assigned to each cell in the coarse grid model. While the order of this procedure is the reverse of that normally used in model calibration and verification, it provides for better compatibility between the depth-volume relations even though a few small

depth adjustments may be necessary during subsequent calibration of the models. Aside from this variation, the development of the two models followed the general implementation procedure outlined in the previous chapter.

Coarse Grid Model. The coarse grid configuration used to describe the physiography of the Masonboro Inlet area is shown in Figure 8. Using a 1200' grid overlay with the 1" = 500' hydrographic chart, water-land boundaries were established to generally conform to the MHW line. Included in the grid network are 135 water cells covering an area of about seven square miles. The shaded cells in Figure 8 either represent dry land where inundation never occurs under normal tidal conditions or they denote "dead" cells where no calculations are required but are needed in the model to accommodate the two-dimensional indexing scheme and to facilitate the computations in certain boundary cells. It should be noted that an extra row and column of "dead" cells are included in the grid along the top and right sides, respectively. These additional cells permit definition of certain key variables that are used in the calculation process.

Bottom and ground elevations were assigned in the coarse grid model using the general procedure outlined above in an effort to minimize the differences in the depth-volume relations of the two models. Even using this procedure, inconsistencies reflected in the subsequent model results could not be avoided because of the coarse grid resolution. Using the 1" = 500' hydrographic chart, MLW elevations were first assigned to the

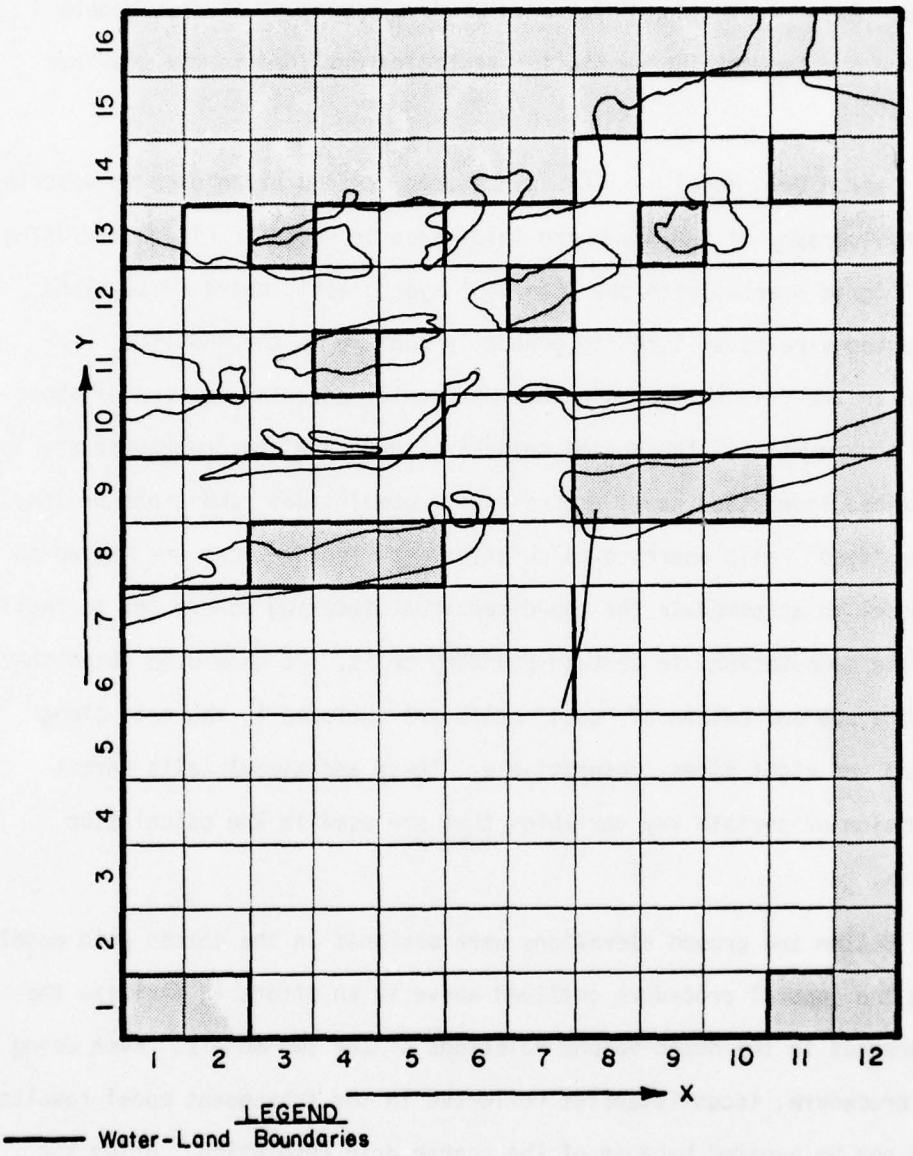

Figure 8

COARSE GRID CONFIGURATION USED
TO DESCRIBE SEPTEMBER, 1969 CONDITIONS

cells in the fine grid sub-model, and then appropriate averages were determined for the coarse grid cells. For coarse grid cells outside the external limits of the fine grid, MLW elevations were assigned directly from the hydrographic chart using a 1200' grid overlay. These MLW elevations were then converted to a MSL datum by applying a uniform vertical shift of 1.3 feet, the difference between MSL and MLW as reported by Tide Tables [1969] for the general coastal area in the vicinity of Masonboro Inlet. The field of MSL elevations used in the coarse grid model to simulate the 12 September 1969 conditions is given in Figure 9. Asterisks in Figure 9 denote land cells which are never inundated, and have a MSL elevation of +99 feet assigned to them in the model.

To adequately describe all of the physiographic features and flow controls included in the Masonboro Inlet area, several of the special boundary conditions discussed in the previous chapter were used. Figure 10 shows the locations of these boundaries at their respective cells in the coarse grid. Cell boundaries with no designation in Figure 10 are subject to the normal flow of water as described by the basic equations of motion, eqs. (1), (2), and (3).

The submerged and overtopping barrier boundaries identified in Figure 10 were used to provide flow control in the major channels and to describe flow constrictions which exist in the prototype such as the weir section of the jetty. Initial selection of barrier heights and discharge coefficients was based on physiographic detail in the vicinity of the barriers and experience using barriers in models of other tidal systems. Adjustments to these values were made during calibration of the model to provide better simulation of the

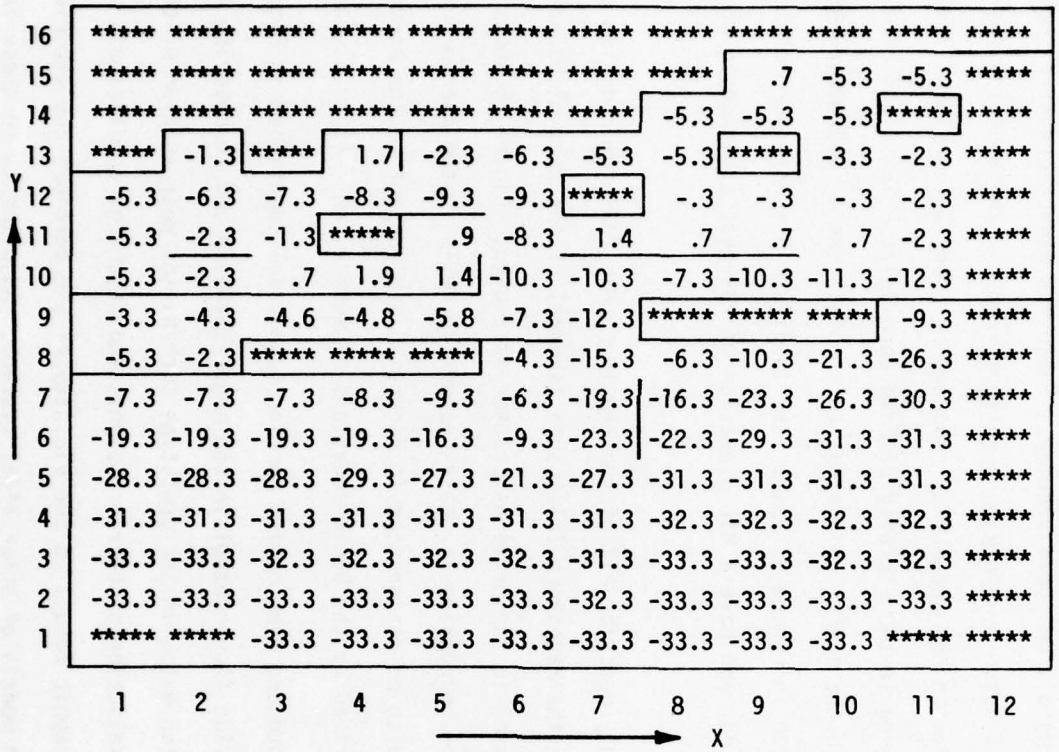

Figure 9

MSL BOTTOM AND GROUND ELEVATIONS USED IN VERIFICATION OF COARSE GRID MODEL

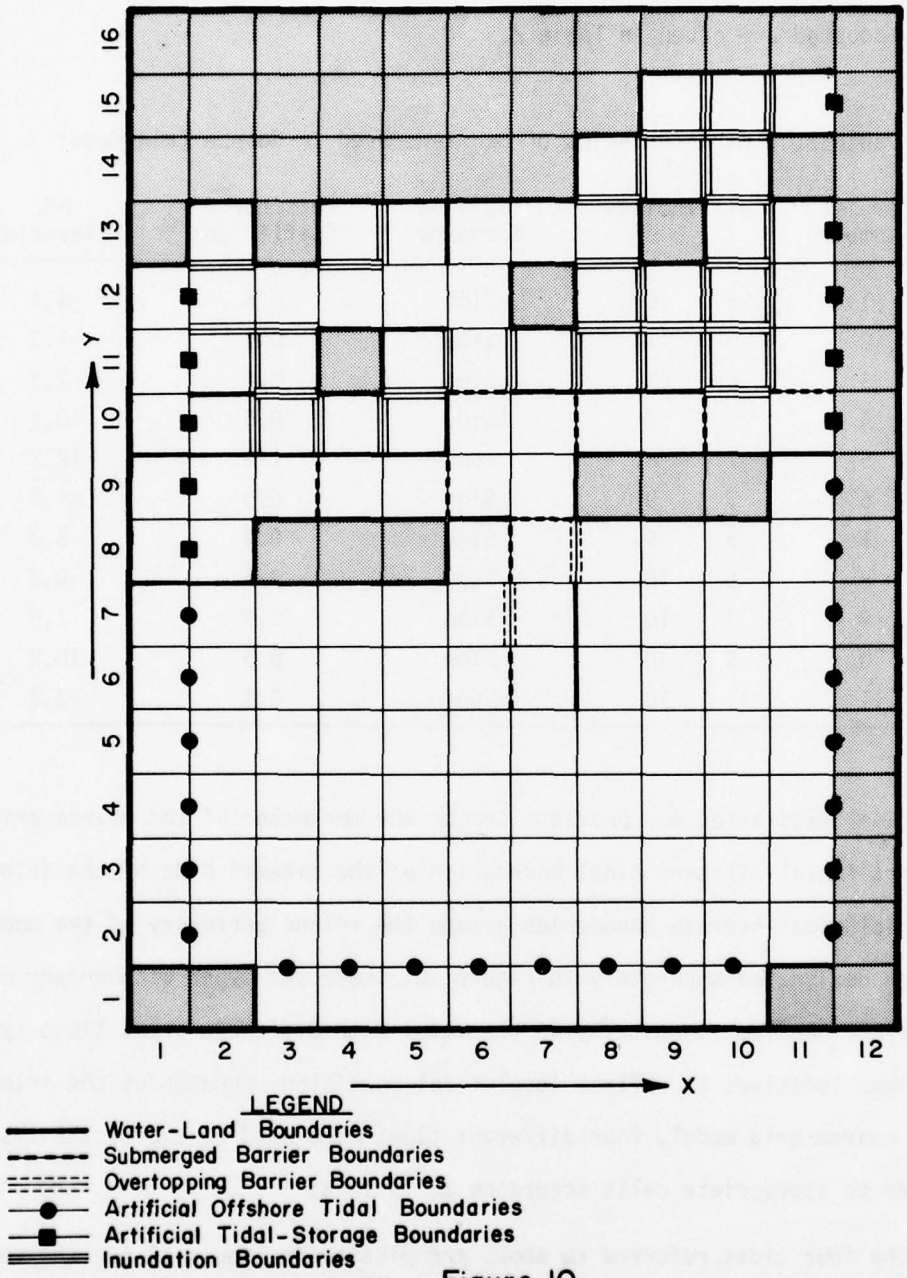

Figure 10
BOUNDARY CONDITIONS USED FOR
VERIFICATION OF COARSE GRID MODEL

flow distribution in the system. The barrier heights and discharge coefficients finally adopted are given in Table 2.

Table 2. Characteristics of Barriers Used in Coarse Grid Model

Barrier Number	Cell Indices I	J	Top/Side Boundary	Discharge Coefficient	MSL Elevation
1	6	6	Side	0.5	-6.3
2	6	7	Side	0.4	-1.3
3	6	8	Side	0.4	-2.3
4	7	8	Side	0.5	+0.7
5	7	8	Top	1.3	-12.2
6	3	9	Side	0.9	-4.5
7	5	9	Side	0.9	-5.7
8	6	10	Top	0.9	-8.2
9	7	10	Side	0.9	-7.2
10	9	10	Side	0.9	-10.2
11	11	10	Top	0.9	-3.2

Tidal excitation was provided around the perimeter of the coarse grid model using artificial offshore tidal boundaries on the seaward side of the inlet and artificial tidal-storage boundaries around the inland periphery of the model. Although designated separately in Figure 10, these two types of boundary conditions are handled identically in the model with different input tides specified at various locations to reflect local tidal conditions throughout the inlet area. In the coarse grid model, four different tides were used to excite the system and assigned to appropriate cells according to Table 3.

The four tides referred to above are plotted in Figure 11 for the verification period 0400 to 2100 on 12 September 1969. Tide No. 1 corresponds to

Table 3. Assignment of Exciting Tides in Coarse Grid Model

Tidal Cell Number	Cell Indices I	J	Top/Side Boundary	Tidal Identification No.
1	3	1	Top	1
2	4	1	Top	1
3	5	1	Top	1
4	6	1	Top	1
5	7	1	Top	1
6	8	1	Top	1
7	9	1	Top	1
8	10	1	Top	1
9	1	2	Side	1
10	11	2	Side	1
11	1	3	Side	1
12	11	3	Side	1
13	1	4	Side	1
14	11	4	Side	1
15	1	5	Side	1
16	11	5	Side	1
17	1	6	Side	1
18	11	6	Side	1
19	1	7	Side	1
20	11	7	Side	1
21	1	8	Side	2
22	11	8	Side	1
23	1	9	Side	2
24	11	9	Side	1
25	1	10	Side	4
26	11	10	Side	3
27	1	11	Side	4
28	11	11	Side	3
29	1	12	Side	4
30	11	12	Side	3
31	11	13	Side	3
32	11	15	Side	3

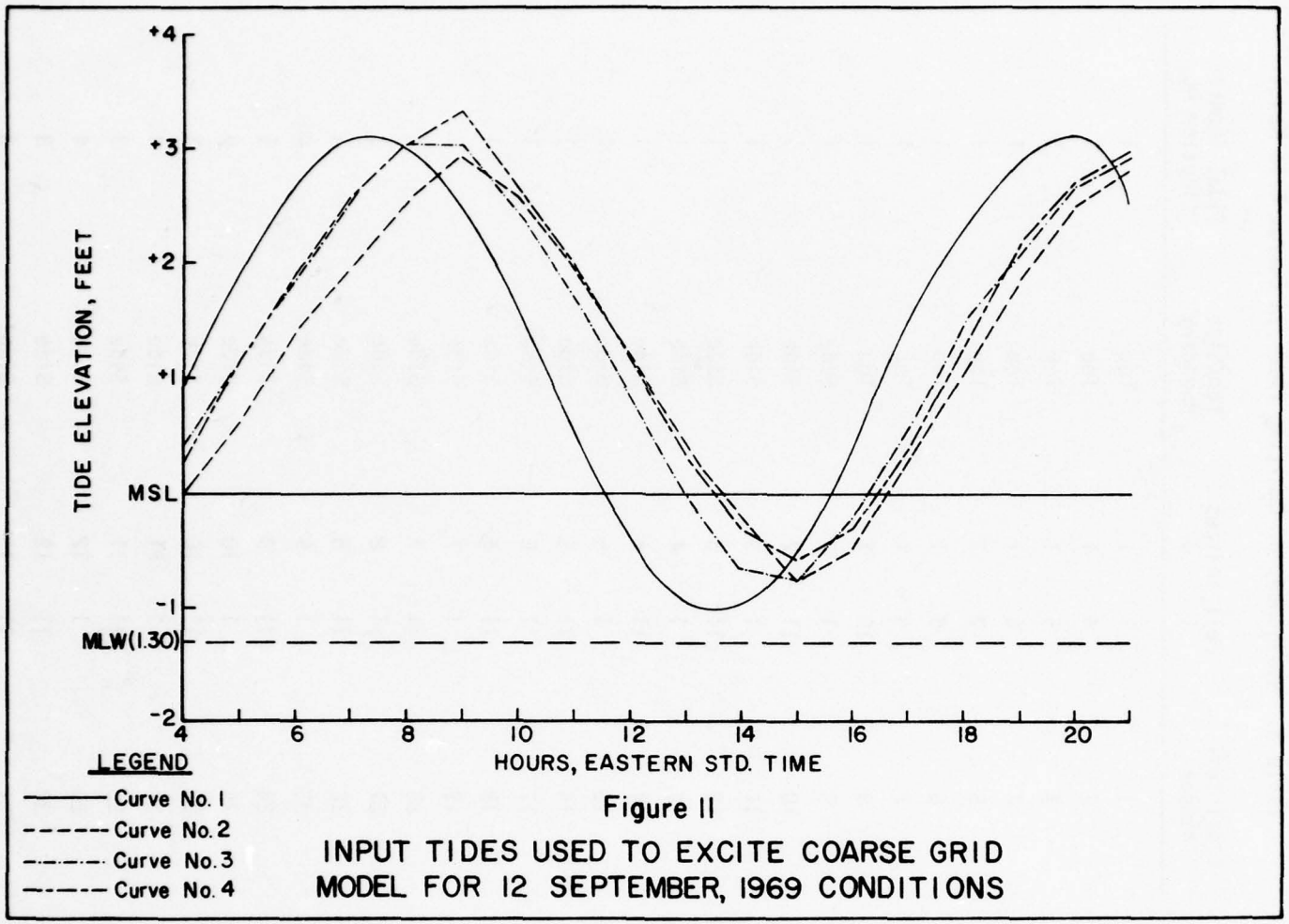

Figure 11

INPUT TIDES USED TO EXCITE COARSE GRID MODEL FOR 12 SEPTEMBER, 1969 CONDITIONS

the prototype tide measured at Gage 0 on the open coast, and it is specified in the model at each of the cells designated in Figure 10 as artificial offshore tidal boundaries. The other three tides were developed as part of the calibration process, and they represent the inputs necessary to simulate the general character of the flows in the major channels during the verification period. In the initial stages of model calibration, the Gage 5 tide was specified as Tide No. 2, the Gage 4 tide was used for Tide No. 3, and Tide No. 4 was set equal to the Gage 6 tide. During calibration of the model, these three interior input tides were adjusted in both phase and amplitude until the necessary flow simulation was obtained for input to the fine grid model.

Recognizing that future applications of the model to other conditions would require that all four of these input tides be known, a procedure has been devised whereby approximations of the three interior tides (Nos. 2, 3, and 4) can be obtained from the offshore tide at Gage 0 (Tide No. 1). In this analysis, it has been assumed that Gage 0 is a permanent installation, and that historical tidal records can always be obtained from this station. Using the calibrated input tides necessary for simulation of the 12 September 1969 conditions (Figure 11), correlations have been developed between each of the three interior tides and the Gage 0 tide. Because of the similarity between the tides, these correlations have been based on applying appropriate linear scaling factors to the Gage 0 tidal amplitudes lagged according to the phase differences determined in model calibration. To describe these tides, a bi-modal Fourier approximation of the following form has been used.

$$H_i = S_i \{A_o + C_{o1} \text{Sin}[(2\pi/T)\cdot(t + \Delta t_i) + \Phi_{o1}] + C_{o2} \text{Sin}[(4\pi/T)\cdot(t + \Delta t_i) + \Phi_{o2}]\} + HS_i \quad (32)$$

In this expression, the subscript i refers to the identification number of the input tide used in the coarse grid model ($1 \leq i \leq 4$), H_i is the MLW tidal elevation, A_o is the Gage O mean tide level with respect to MLW averaged over one tidal cycle having a duration of T hours, t is the time in hours after the beginning of the tidal cycle when H_i occurs, C_{o1} and C_{o2} are Fourier coefficients determined for approximation of the tide at Gage O, Φ_{o1} and Φ_{o2} are the corresponding Fourier phase angles for the Gage O tide, Δt_i is the phase difference between the i^{th} tide and the Gage O tide, S_i is an appropriate linear scaling factor for the i^{th} tide, and HS_i is the corresponding vertical tidal adjustment for the i^{th} tide.

For the period 0400 to 1650 on 12 September 1969, the following Fourier constants have been determined for the Gage O tide.

$$A_o = 2.38920$$
$$C_{o1} = 2.08673$$
$$\Phi_{o1} = -0.10846$$
$$C_{o2} = 0.04220$$
$$\Phi_{o2} = 1.31290$$

To determine hourly values of the four input tides used for final verification of the coarse grid model, the constants given in Table 4 were applied to eq. (32).

Table 4. Tidal Constants Used in Verification of Coarse Grid Model

Tidal Identification No.	S_i	HS_i	Δt_i
1	1.000	0.00	0.00
2	0.802	0.53	-1.70
3	0.888	0.40	-1.05
4	0.878	0.60	-1.45

It should be pointed out that the general use of input tides determined for other simulation periods by eq. (32) and the constants in Table 4 are limited somewhat by the degree to which these tidal conditions agree with those of the 12 September 1969 verification period. The constants in Table 4 were determined through analysis of only one tidal period using the tidal records which were readily available. Hence a certain amount of caution should be exercised when applying them to other periods to assure that at least general similarity exists between the new tides and those of 12 September 1969. Should additional prototype data be available for Masonboro Inlet during other periods, it would be advantageous to test these constants through operation of the model, and possibly develop other correlations more applicable to different tidal conditions. For purposes of this study, it is believed that these constants provide adequate descriptions of the tidal inputs because of the similarities in the actual measured tides.

The specification of boundary conditions for each cell in the model was handled using the cell flagging scheme described in Figure 3. Using

these cell identification numbers and the boundary conditions identified in Figure 10, flags were assigned to each cell in the coarse grid model as illustrated in Figure 12. In a similar manner those cells which required special finite difference formulations of the convective acceleration cross-product terms were identified using the two-digit flagging scheme described earlier. Only those cells which required flags other than "11" were identified and input into the model as data since the initialization of program variables in the model includes assigning "11" to all cells. The field of two-digit convective acceleration cell flags is shown in Figure 13.

Manning's "n" values were assigned to each cell in the coarse grid model and input into the program as part of the basic cell data. Although slight adjustments were made to the Manning's "n" field during calibration of the model, initial values were determined using the following relationships which have been developed through experience with modeling other tidal systems.

$$n = 0.0377 + 0.00667\,z, \quad z \leq -4$$
$$n = 0.0550 + 0.00500\,z, \quad -4 \leq z \leq 0$$
$$n = 0.0550 + 0.00500\,z, \quad z > 0$$

In these relations, z is the MSL bottom or ground elevation measured negatively downwards as defined in the basic equations of motion. Values obtained from these relations range from 0.0177 for water depths of 30 feet to 0.0500 for water depths of one foot.

Calibration of the coarse grid model involved the successive operation of the model under the prescribed input conditions of 12 September 1969, including an average northeast wind with a velocity of four knots, and

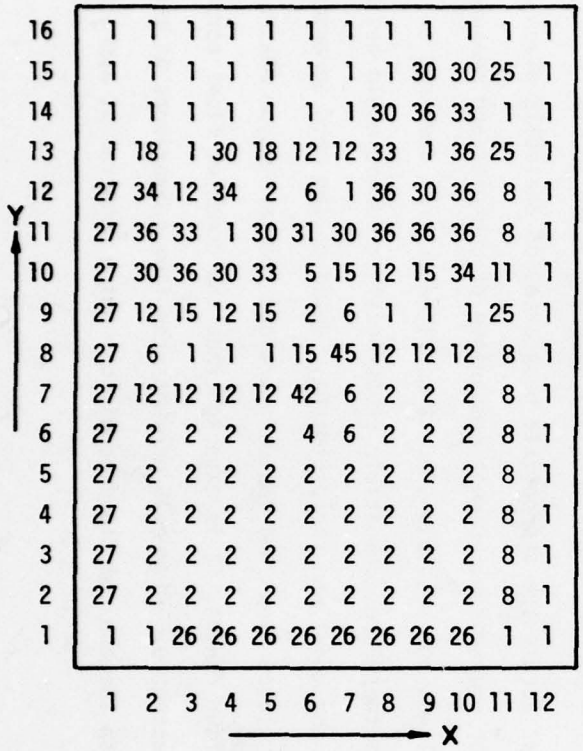

Figure 12

COMPUTATIONAL CELL FLAGS USED IN COARSE GRID MODEL FOR 12 SEPTEMBER 1969 CONDITIONS

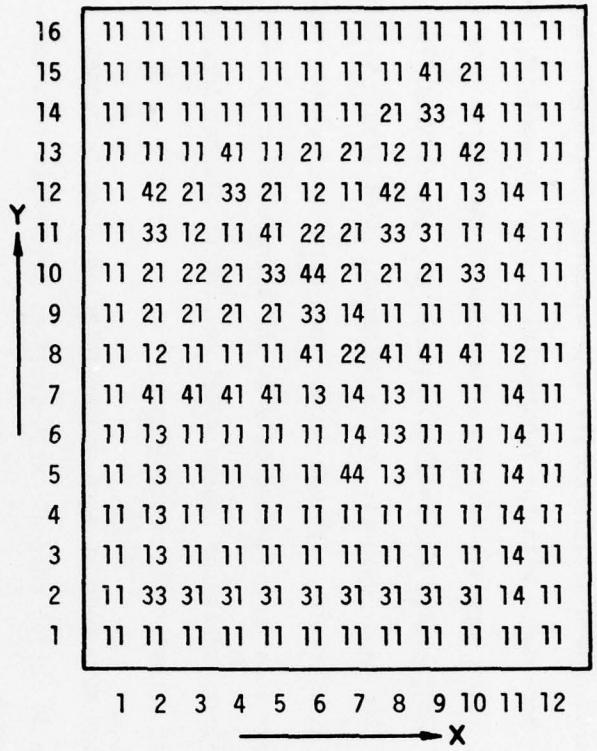

Figure 13

CONVECTIVE ACCELERATION CELL FLAGS USED IN COARSE GRID MODEL FOR 12 SEPTEMBER 1969 CONDITIONS

the appropriate adjustment of input tides, barrier elevations and coefficients, bottom and ground elevations, bottom friction, and tidal discharge coefficients until simulated results agreed satisfactorily with measured prototype tide and flow conditions. In accordance with the fundamental concept of applying the dual-model approach, major emphasis during calibration of the coarse grid model was placed on tidal verification and on simulation of the generalized flow distribution between the major channels in the Masonboro Inlet area. Velocity verification was a consideration although comparisons between simulated results and measured prototype data were limited only to the average velocity condition across each of the ranges since the coarse model resolution did not provide for direct comparisons of actual field measurements.

Flow comparisons were made at each of the interior velocity ranges identified in Figure 4. Using channel cross-sections determined from the 1" = 500' hydrographic chart, maximum ebb and flood flows in the prototype were computed based on the detailed velocity measurements at the three stations across each range. The plotted cross-sections used are shown in Figure 14. From the model, flows across the appropriate boundaries of the cells given in Table 5 were used for comparison. Direct comparison of computed and measured flows across Range 1 was not possible since a confined channel does not exist at this location and therefore, compatible cross-sectional areas could not be determined for both the model and the prototype. Based on the good agreement, however, between simulated flows and those determined from prototype measurements at the other four ranges, it is expected that the computed flows across Range 1 are also reasonable. Figure 15 presents the flow comparisons at these other ranges for both the ebb and flood conditions which occurred at approxi-

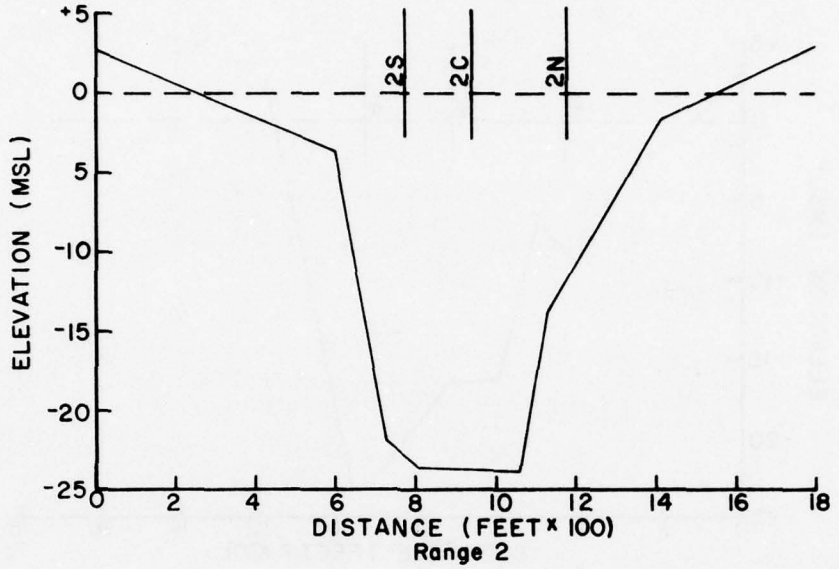

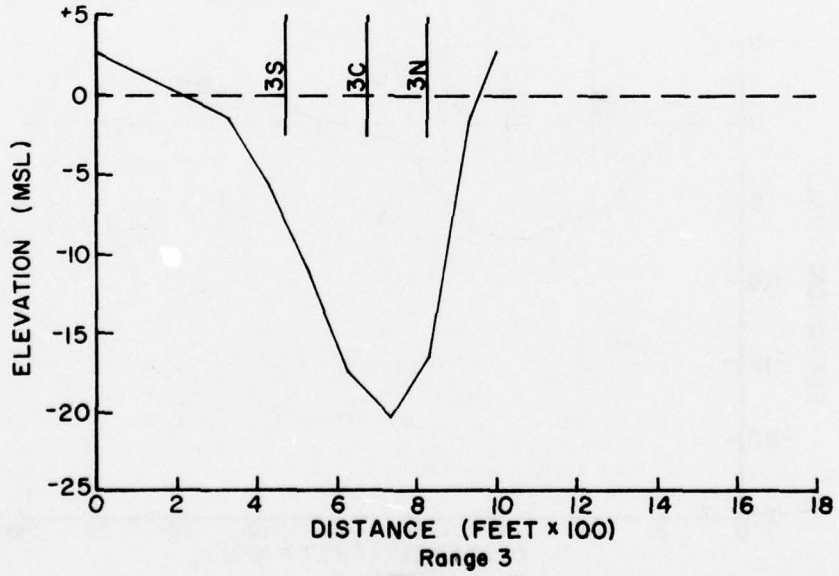

Figure 14

CHANNEL CROSS-SECTIONS AT VELOCITY RANGES NEAR MASONBORO INLET

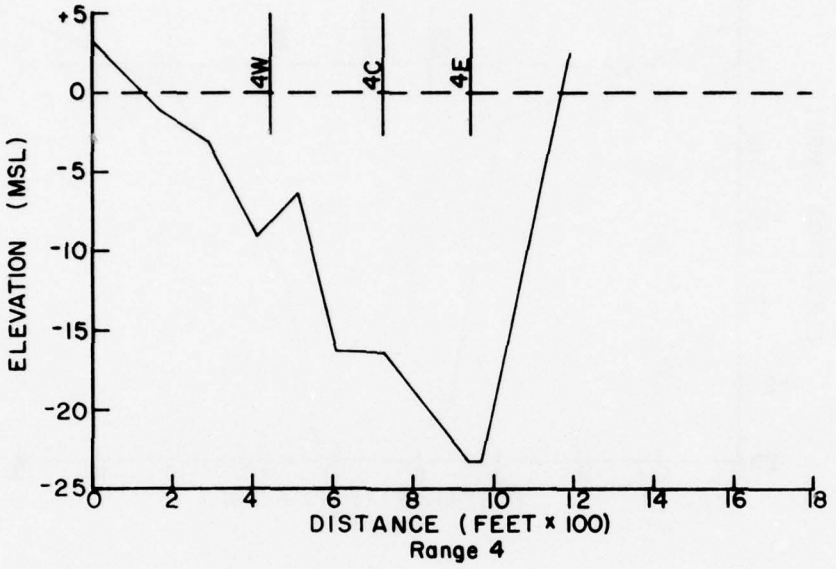

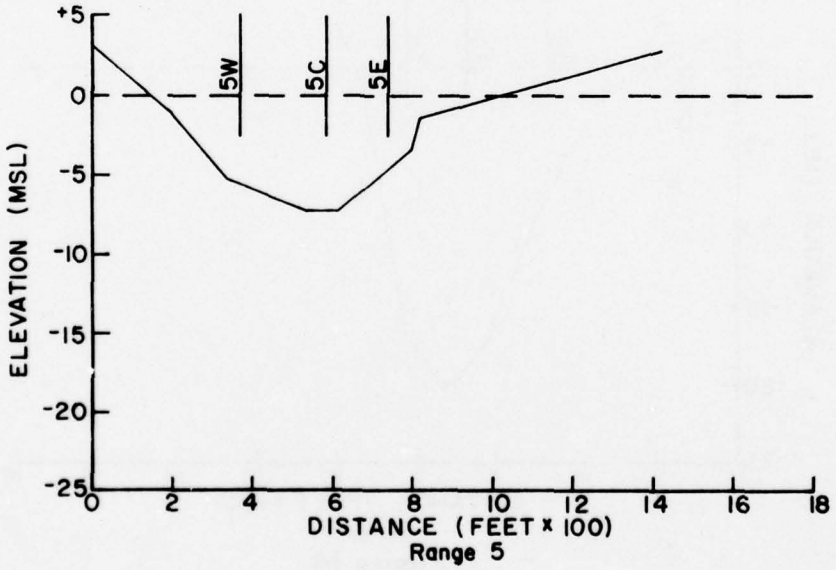

Figure 14, Cont.

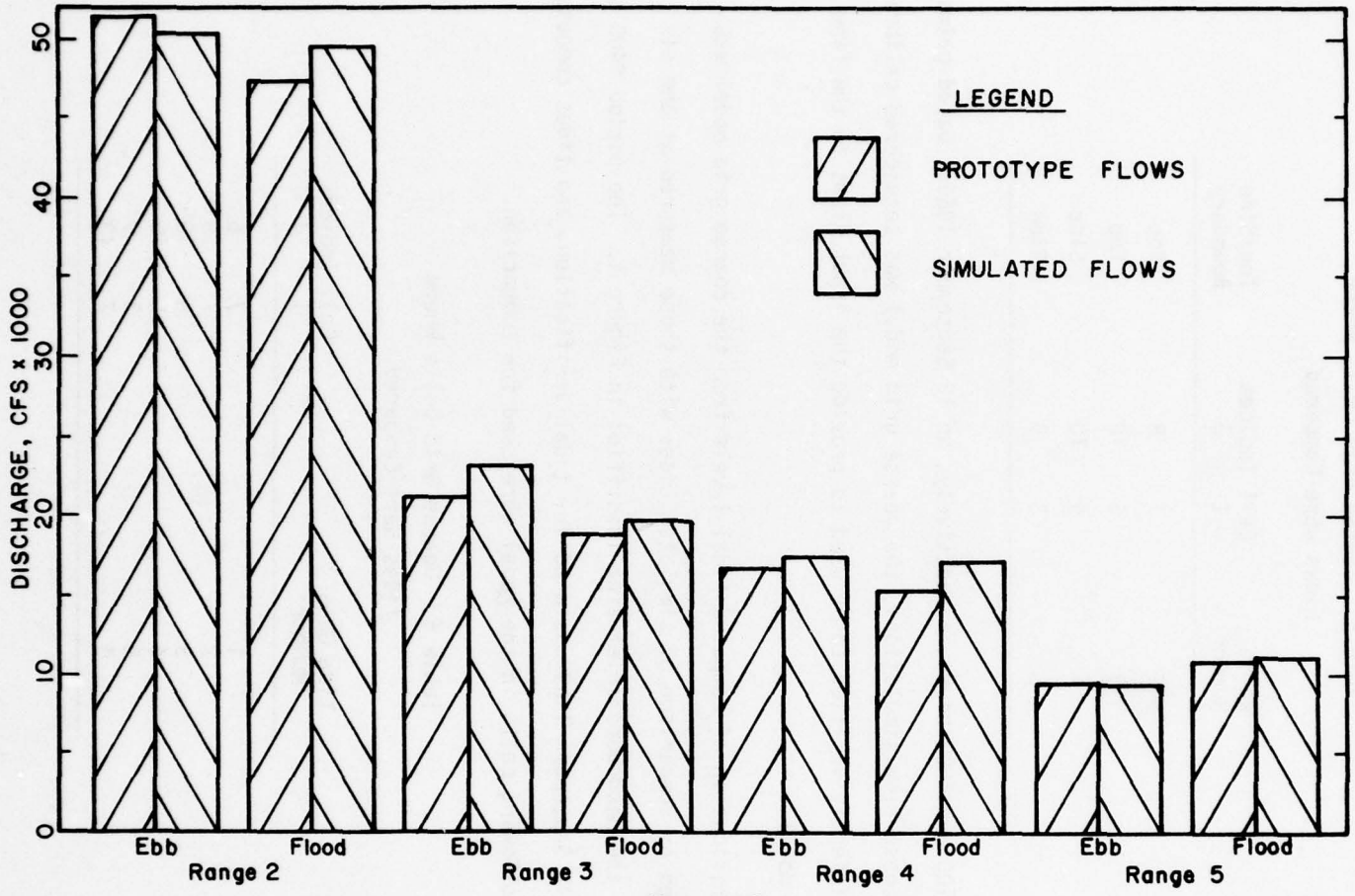

Figure 15

COMPARISON OF PROTOTYPE AND SIMULATED FLOWS FROM COARSE GRID MODEL

Table 5. Coarse Grid Cells Where Flows Were Compared

Range Number	Cell Indices I	J	Top/Side Boundary
2	7	8	Top
3	6	10	Top
4	9	10	Side
5	3	9	Side

mately 1100 and 1800 hours, respectively, on 12 September 1969. Based primarily on these flow simulations, the coarse grid model was considered calibrated and sufficiently verified to be used to provide the input flows to the fine grid sub-model.

Verification of computed tidal levels from the coarse grid model was determined by comparison of simulated tides with those measured at the six gages in the Masonboro Inlet area identified in Figure 4. The period 0400 to 2100 on 12 September 1969 was used for tidal verification, and tides computed at the following cells in the model were used for comparison.

Table 6. Coarse Grid Cells Where Tides Were Compared

Tide Gage Number	Cell Indices I	J
1	7	6
2	7	8
3	6	10
4	9	10
5	3	9
6	7	13

Selection of these cell locations for comparison of tides facilitated not only tidal verification but also flow verification since computed results for several of these cells were used in both verification processes. Because only a limited number of cells could be identified in the model for output of hourly hydrodynamics, some of the above cells may not fall directly on tide gage locations, however the error in using these slightly shifted tides is not appreciable. Tidal simulations using results from the calibrated coarse grid model are presented in Figures 16 through 21 for the six tide gages, and they are considered adequate for purposes of this study.

Fine Grid Sub-Model. The areal extent of the fine grid sub-model covers the immediate inlet area and is generally bounded on the inland side by the three interior velocity ranges (3, 4, and 5) and on the seaward side by the jetty and a portion of the ocean. Figure 7 shows the relation of the fine grid area to the coarse grid area. Again using the 1" = 500' hydrographic chart and a 300' grid overlay, water-land boundaries were established in the fine grid model, and the computational grid network was set up according to that shown in Figure 22. Included in the model are approximately 360 water cells covering slightly over one square mile of surface area. The field of MSL bottom and ground elevations assigned to each cell in the grid is presented in Figure 23. Again, asterisks denote "dead" cells where computations are not required and where ground elevations are set equal to +99 feet.

The special boundary conditions used in the fine grid sub-model are shown in Figure 24. To be compatible with the coarse grid model, several submerged barrier boundaries were specified in the fine grid sub-model at the locations shown. Barrier elevations and discharge coefficients were

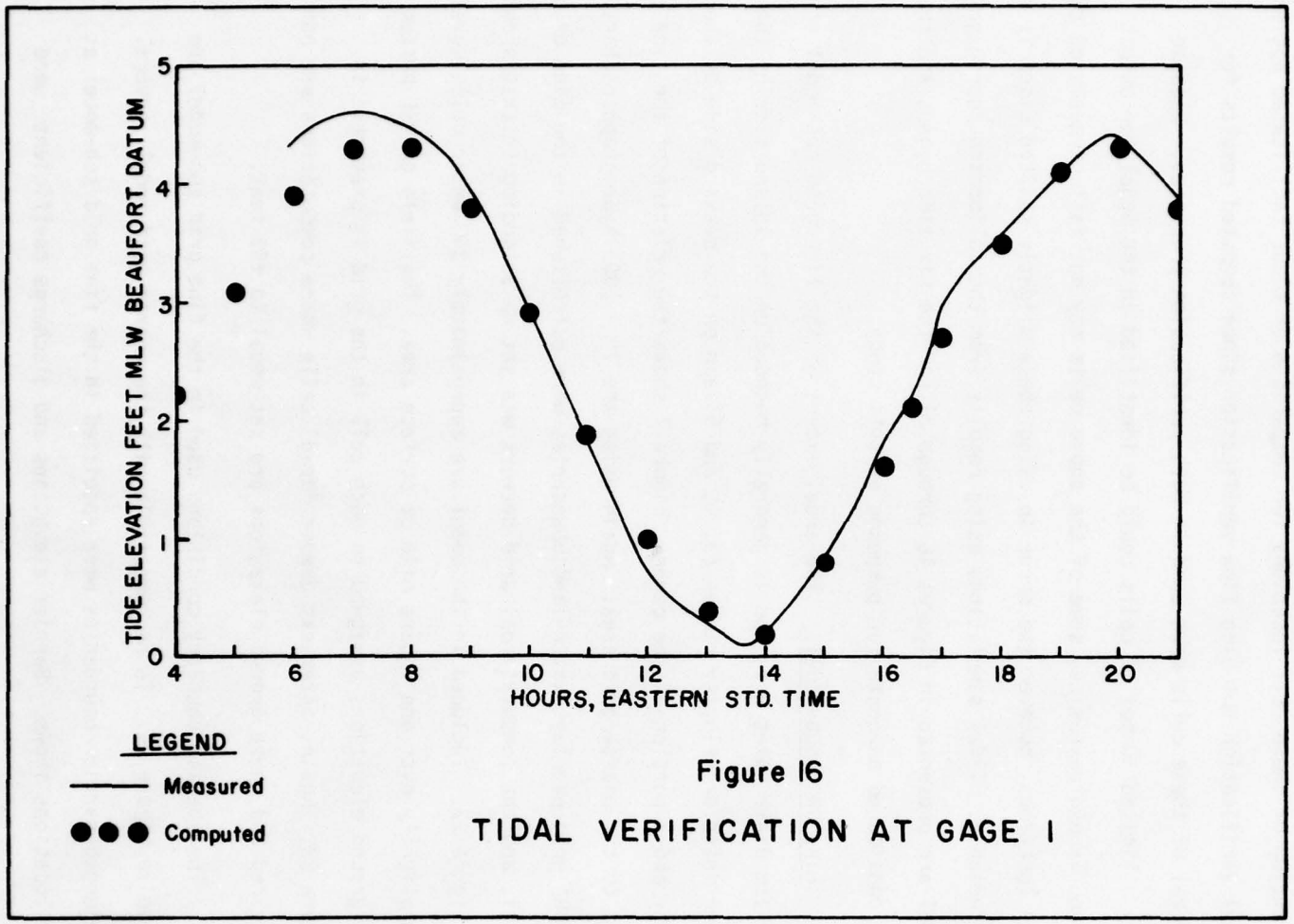

Figure 16

TIDAL VERIFICATION AT GAGE 1

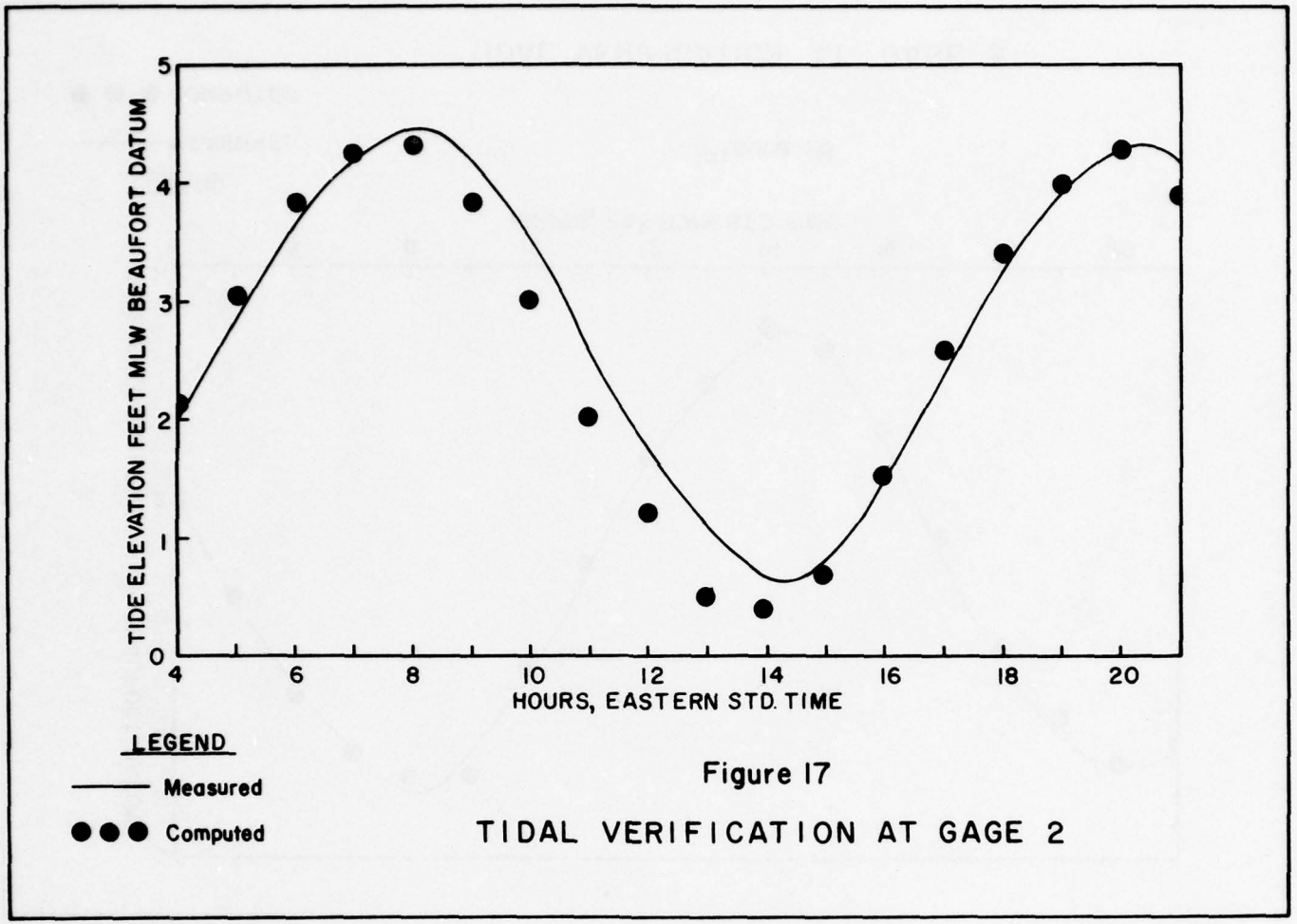

Figure 17

TIDAL VERIFICATION AT GAGE 2

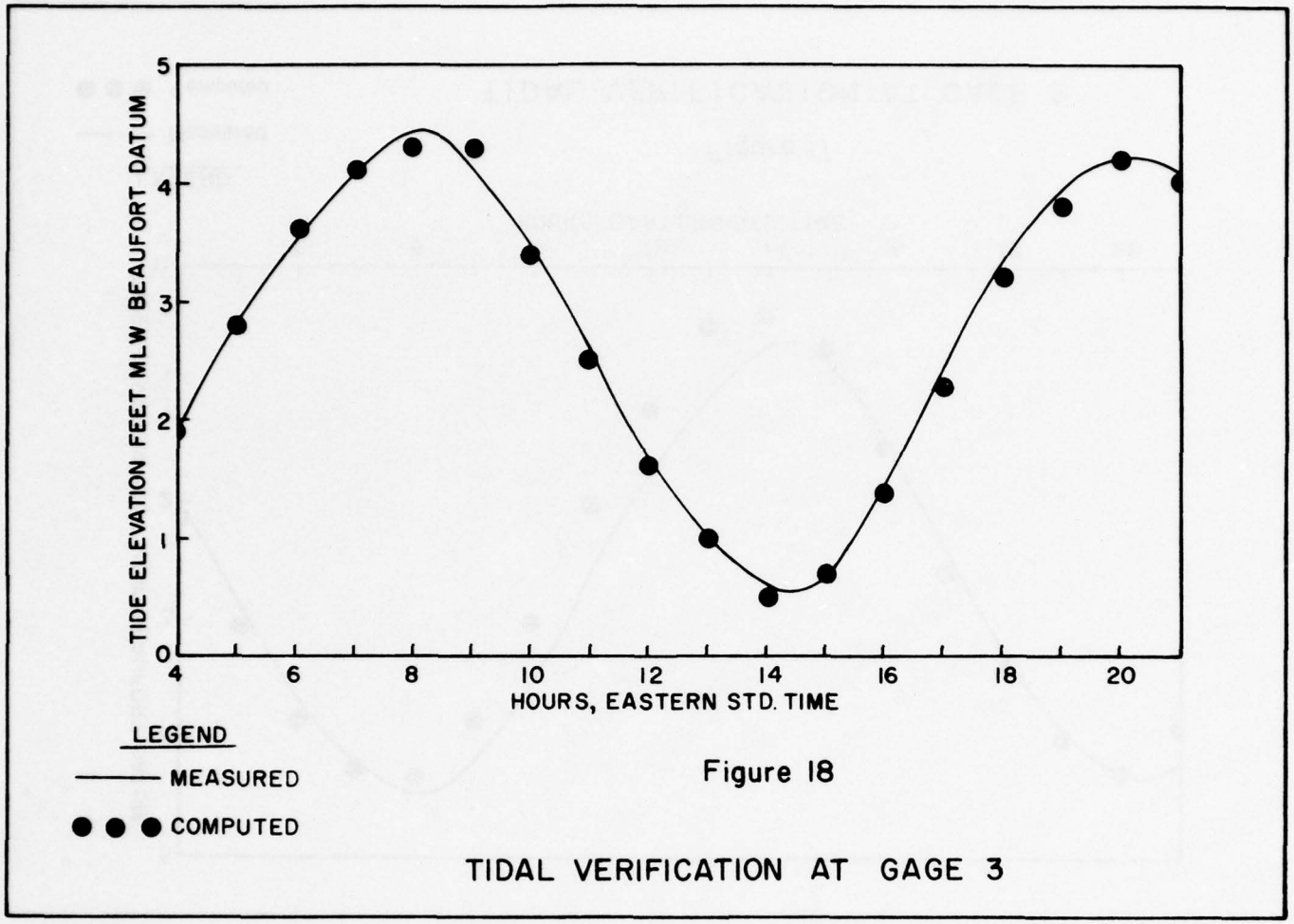

Figure 18

TIDAL VERIFICATION AT GAGE 3

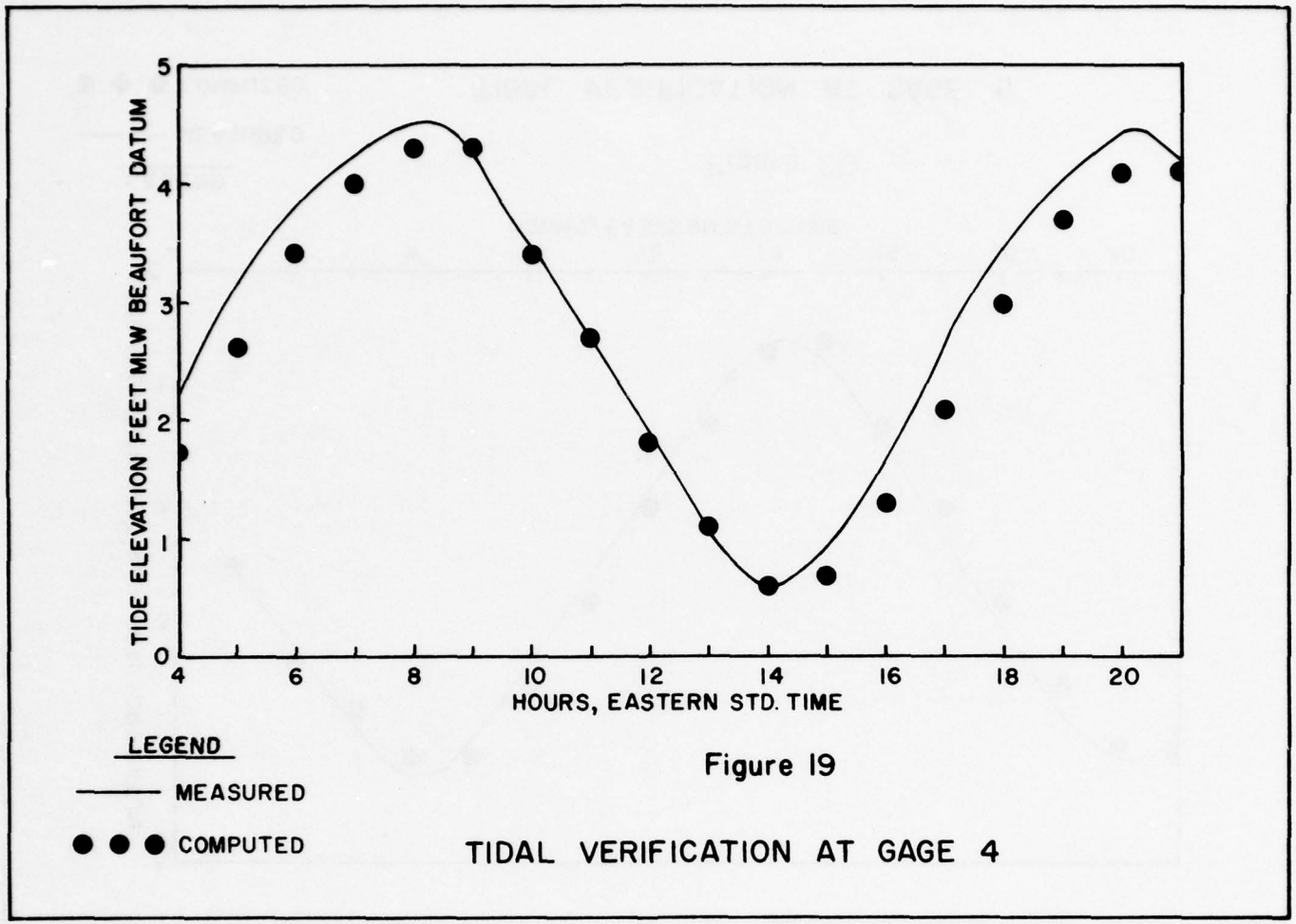

Figure 19

TIDAL VERIFICATION AT GAGE 4

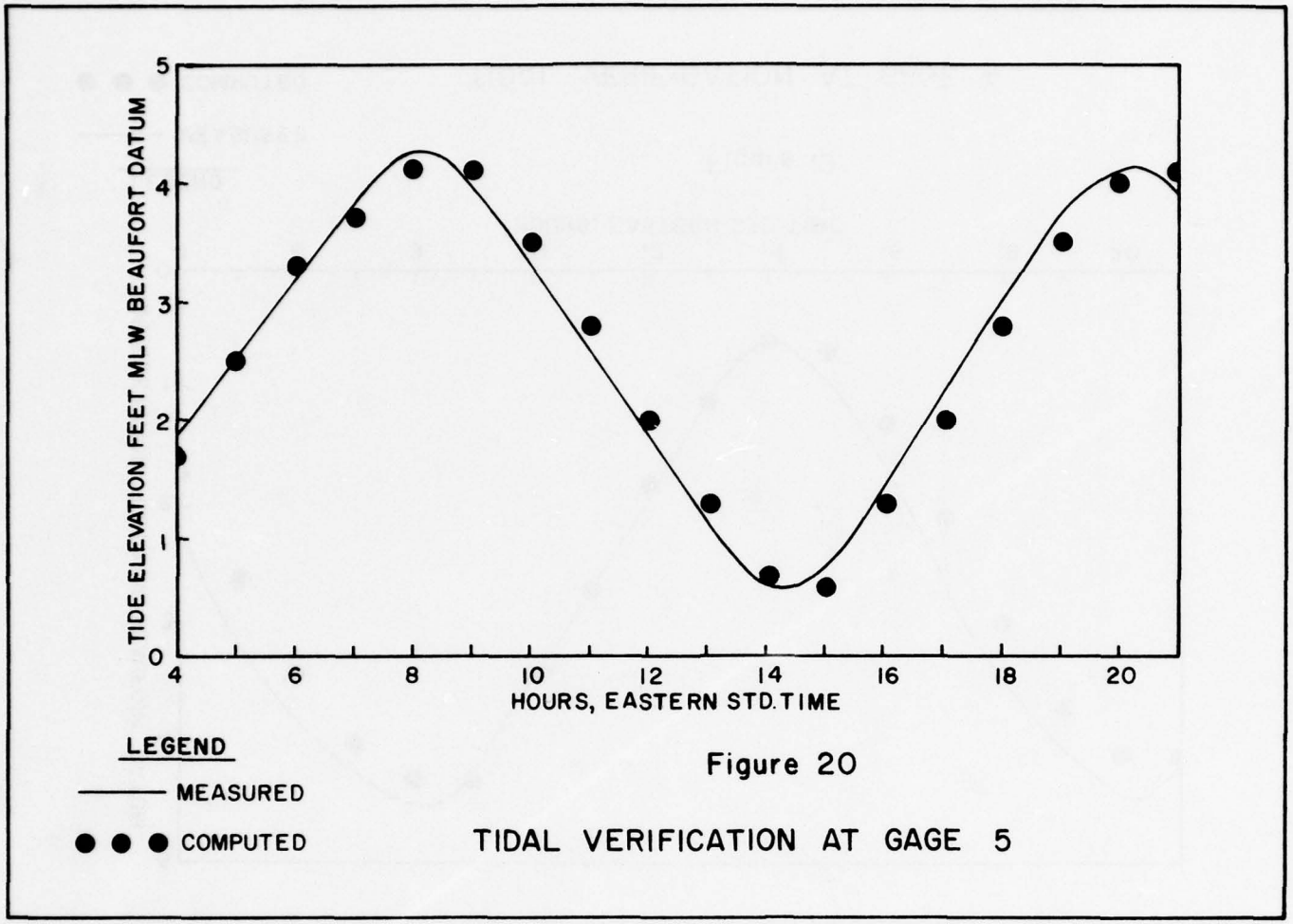

Figure 20

TIDAL VERIFICATION AT GAGE 5

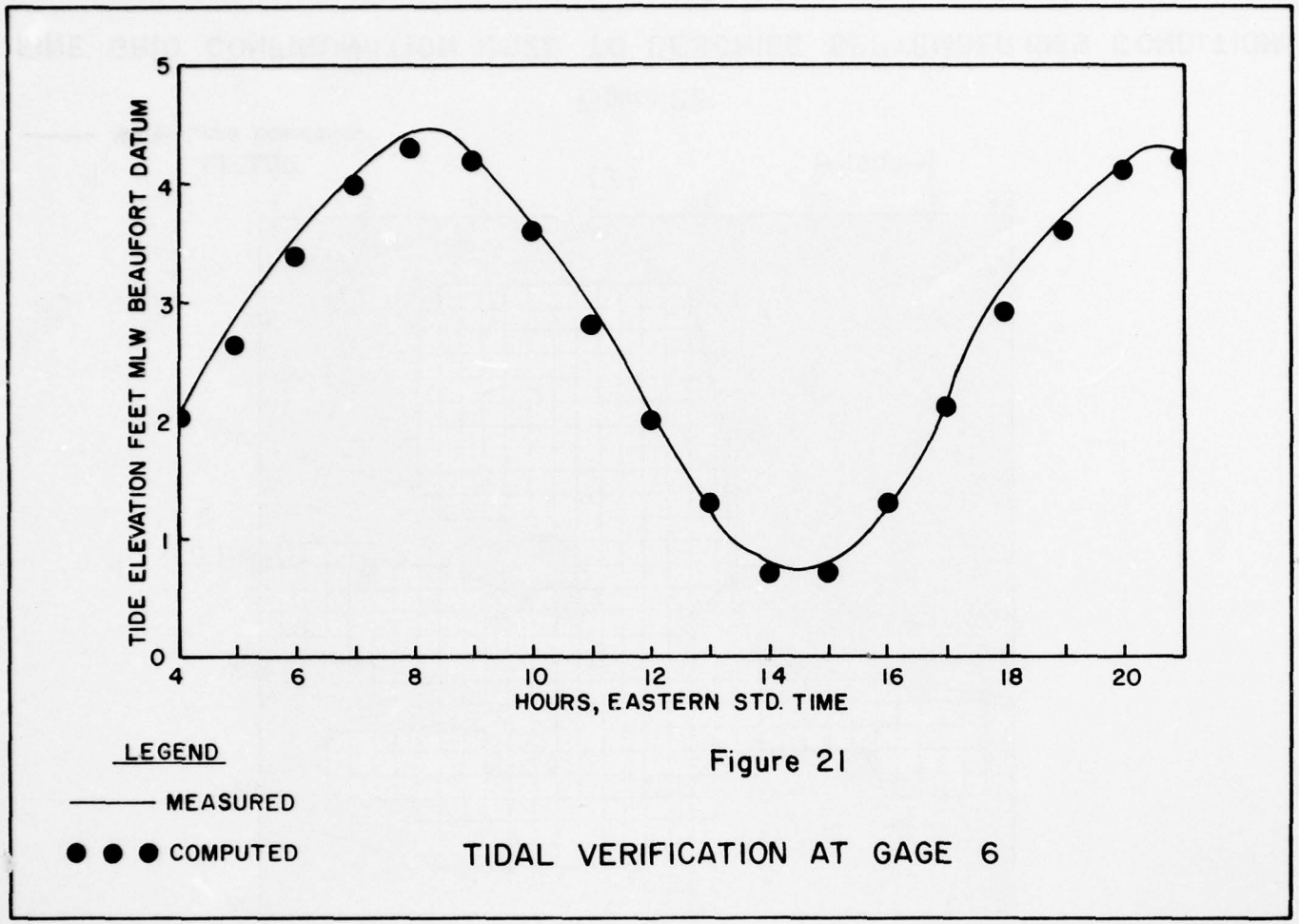

Figure 21

TIDAL VERIFICATION AT GAGE 6

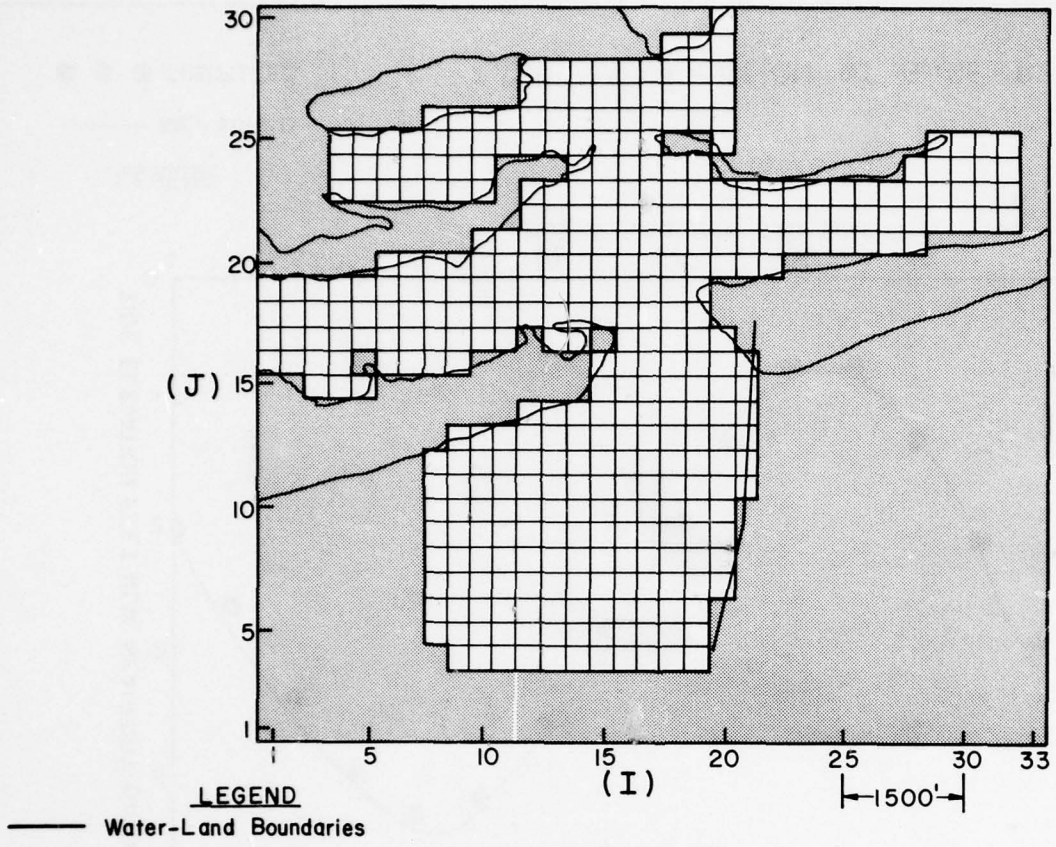

Figure 22

FINE GRID CONFIGURATION USED TO DESCRIBE SEPTEMBER 1969 CONDITIONS

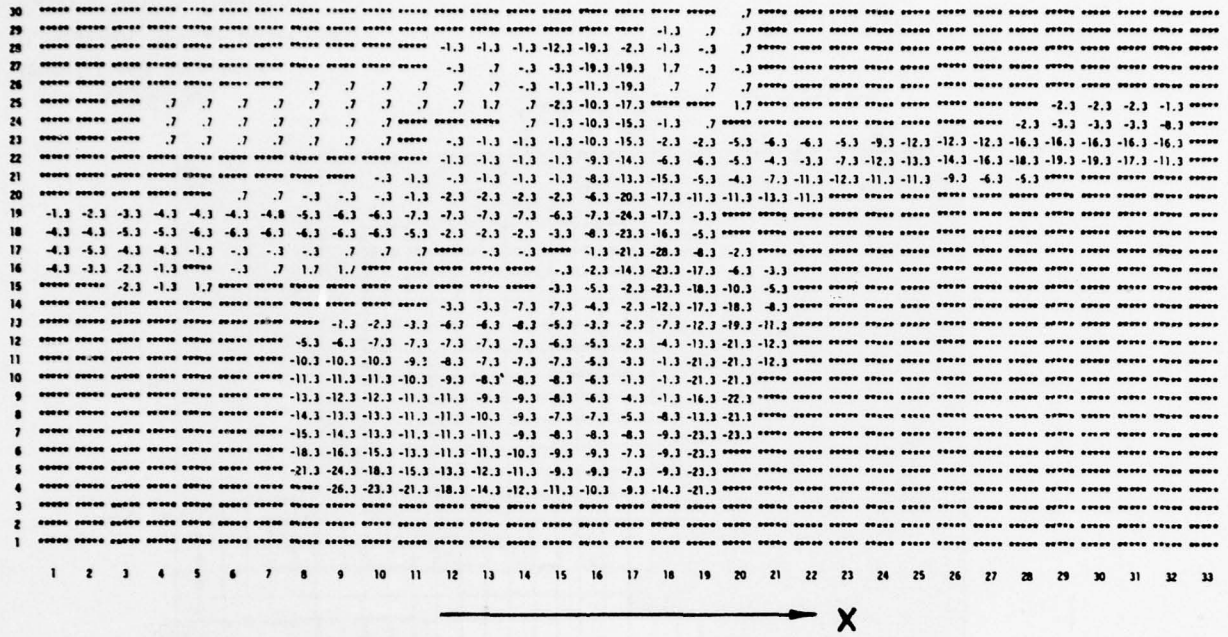

Figure 23

MSL BOTTOM AND GROUND ELEVATIONS USED
IN VERIFICATION OF FINE GRID SUB-MODEL

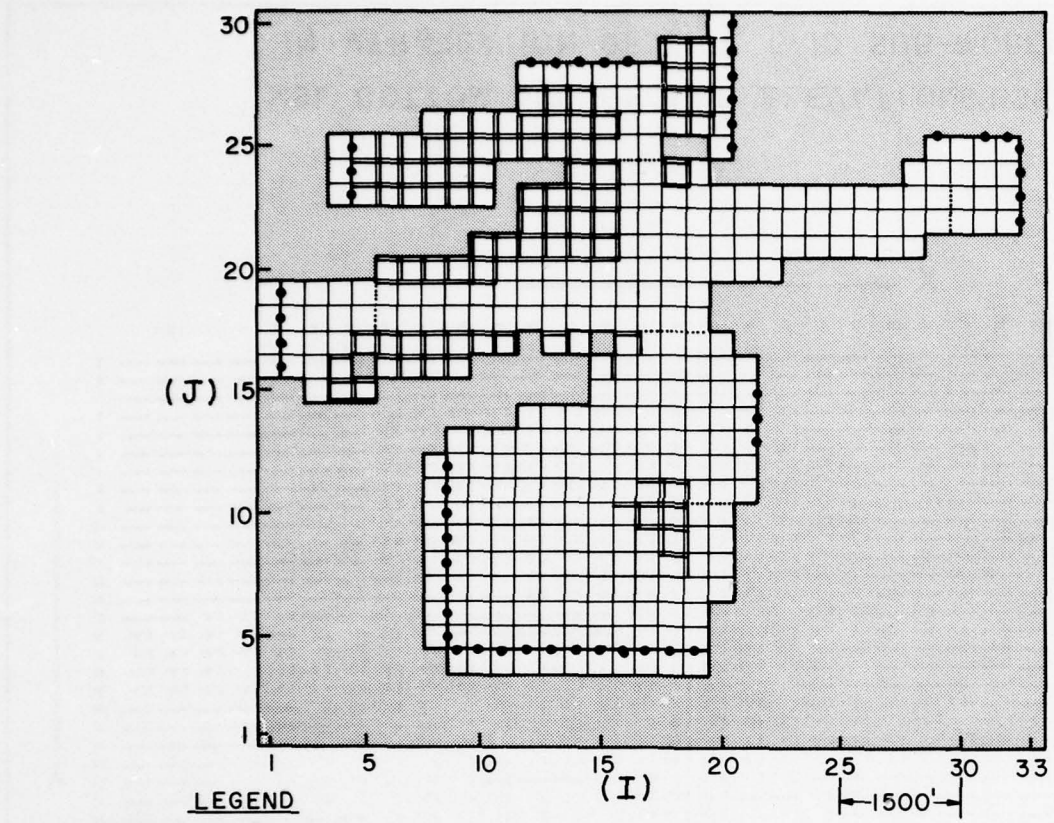

Figure 24

BOUNDARY CONDITIONS USED FOR VERIFICATION OF FINE GRID MODEL

initially prescribed in a manner consistent with those used in the coarse grid model, and then adjusted during model calibration. Table 7 summarizes the barrier characteristics.

Table 7. Characteristics of Barriers Used in Fine Grid Sub-Model

Barrier Number	Cell Indices I	J	Top/Side Boundary	Discharge Coefficient	MSL Elevation
1	19	10	Top	0.90	-21.2
2	20	10	Top	0.90	-16.3
3	17	17	Top	1.00	-21.2
4	18	17	Top	1.00	-16.2
5	19	17	Top	0.90	-5.2
6	5	18	Side	0.90	-6.2
7	5	19	Side	0.90	-4.2
8	29	22	Side	0.90	-19.2
9	29	23	Side	0.90	-16.2
10	16	24	Top	0.90	-10.2
11	17	24	Top	0.90	-15.2

As stated earlier, tidal flows determined from the coarse grid model are used to excite the fine grid sub-model. These flows are prescribed around the perimeter of the fine grid sub-model at appropriate locations where the external boundaries of the model intersect the various channels and passes in the inlet area. These locations are identified in Figure 24 as external inflow boundaries.

The determination of the input flows for each of these external inflow boundaries in the fine grid sub-model requires both temporal and spatial adjust-

ments to the coarse grid flows. First of all, since the computational time steps used in the two models are not the same (Δt = 20 seconds in the coarse grid model and Δt = 5 seconds in the fine grid sub-model), the coarse grid flows must be interpolated to obtain the intermediate values required by the fine grid sub-model. Also because of the different mesh sizes used in the models, coarse grid flows must be proportioned and distributed to the appropriate fine grid cells in order for flow continuity to be maintained. Flow distribution from the coarse grid to the fine grid system is made on the basis of the relative depths of the fine grid cells where a particular coarse grid flow is to be specified. For example if the flow Q_c from one coarse grid cell is to be input to the fine grid sub-model through four cells having water depths of d_1 = 1, d_2 =1, d_3 = 2 and d_4 = 2, then the corresponding individual fine grid flows would be determined as $Q_1 = Q_2 = (1/6)\ Q_c$ and $Q_3 = Q_4 = (2/6)\ Q_c$. Both the temporal interpolation and the spatial distribution of coarse grid flows are carried out during operation of the coarse grid model with the input flows to the fine grid sub-model stored on magnetic tape at the end of each run. Table 8 summarizes the linkage between the two sets of flows in the models.

Again to reflect the special boundary conditions identified in Figure 24 in the model, the computational cell flagging scheme shown in Figure 3 was used. The assigned flags used in the fine grid sub-model for the verification conditions are presented in Figure 25. The two-digit cell flags which specify in the model appropriate formulations of the convective acceleration cross-product terms are shown in Figure 26. The values of Manning's "n" bottom roughness coefficients used in the fine grid sub-model were determined in a manner consistent with that described earlier for the coarse grid model.

Table 8. Linkage Between Coarse Grid and Fine Grid Boundary Flows

Flow Number	*FINE GRID INPUT FLOWS* Cell Indices I	J	X/Y Component	*COARSE GRID SOURCE FLOWS* Cell Indices I	J	X/Y Component
1	9	4	Y	5	5	Y
2	10	4	Y	5	5	Y
3	11	4	Y	5	5	Y
4	12	4	Y	5	5	Y
5	13	4	Y	6	5	Y
6	14	4	Y	6	5	Y
7	15	4	Y	6	5	Y
8	16	4	Y	6	5	Y
9	17	4	Y	7	5	Y
10	18	4	Y	7	5	Y
11	19	4	Y	7	5	Y
12	8	5	X	4	6	X
13	8	6	X	4	6	X
14	8	7	X	4	6	X
15	8	8	X	4	6	X
16	8	9	X	4	7	X
17	8	10	X	4	7	X
18	8	11	X	4	7	X
19	8	12	X	4	7	X
20	21	13	X	7	8	X
21	21	14	X	7	8	X
22	21	15	X	7	8	X
23	1	16	X	2	9	X
24	1	17	X	2	9	X
25	1	18	X	2	9	X
26	1	19	X	2	9	X
27	32	22	X	10	10	X
28	4	23	X	3	10	X
29	32	23	X	10	10	X
30	4	24	X	3	10	X
31	32	24	X	10	10	X
32	4	25	X	3	10	X
33	20	25	X	7	11	X
34	29	25	Y	10	10	Y
35	31	25	Y	10	10	Y
36	32	25	X	10	10	X
37	32	25	Y	10	10	Y
38	20	26	X	7	11	X
39	20	27	X	7	11	X
40	12	28	Y	6	11	Y
41	13	28	Y	6	11	Y
42	14	28	Y	6	11	Y
43	15	28	Y	6	11	Y
44	16	28	Y	6	11	Y
45	20	28	X	7	11	X
46	20	29	X	7	11	X
47	20	30	X	7	11	X

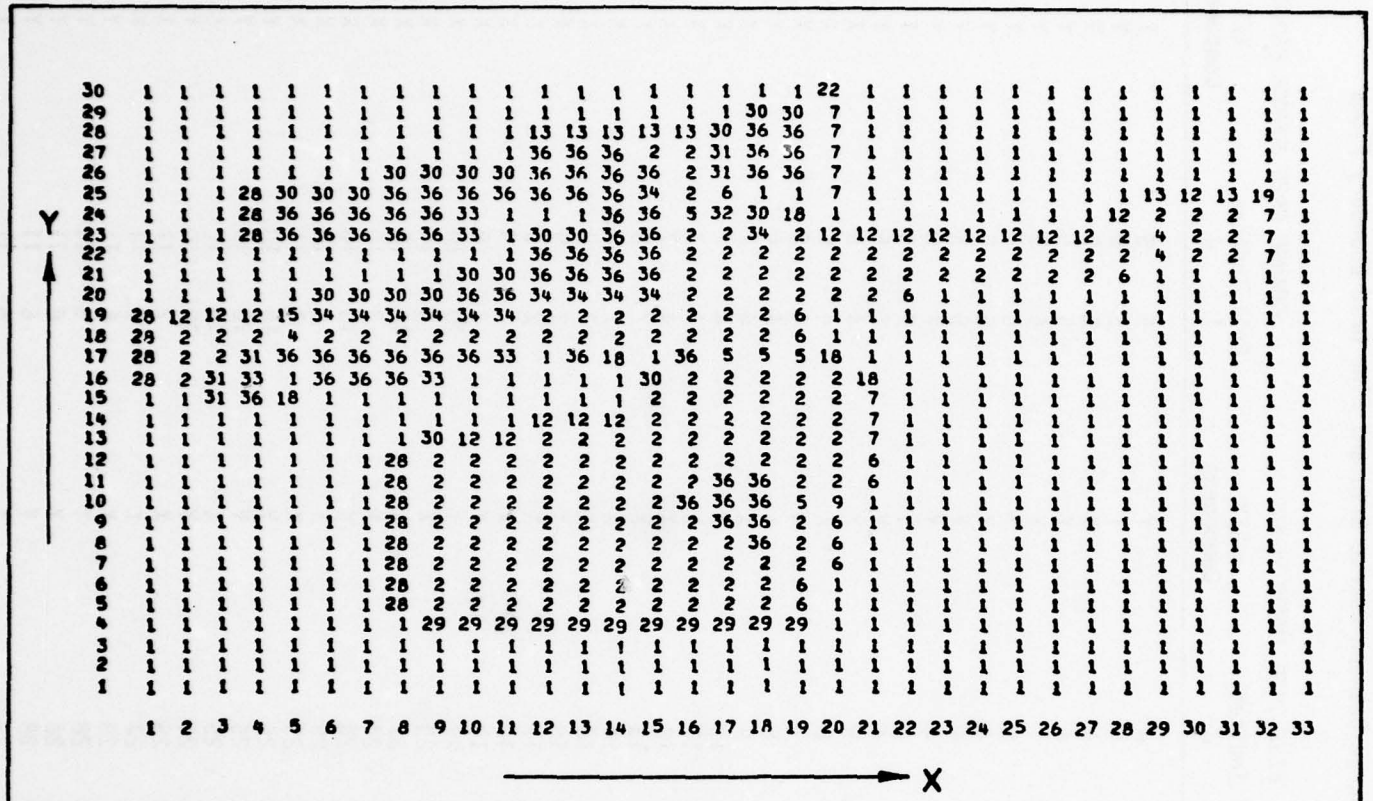

Figure 25

COMPUTATIONAL CELL FLAGS USED IN FINE GRID SUB-MODEL FOR 12 SEPTEMBER 1969 CONDITIONS

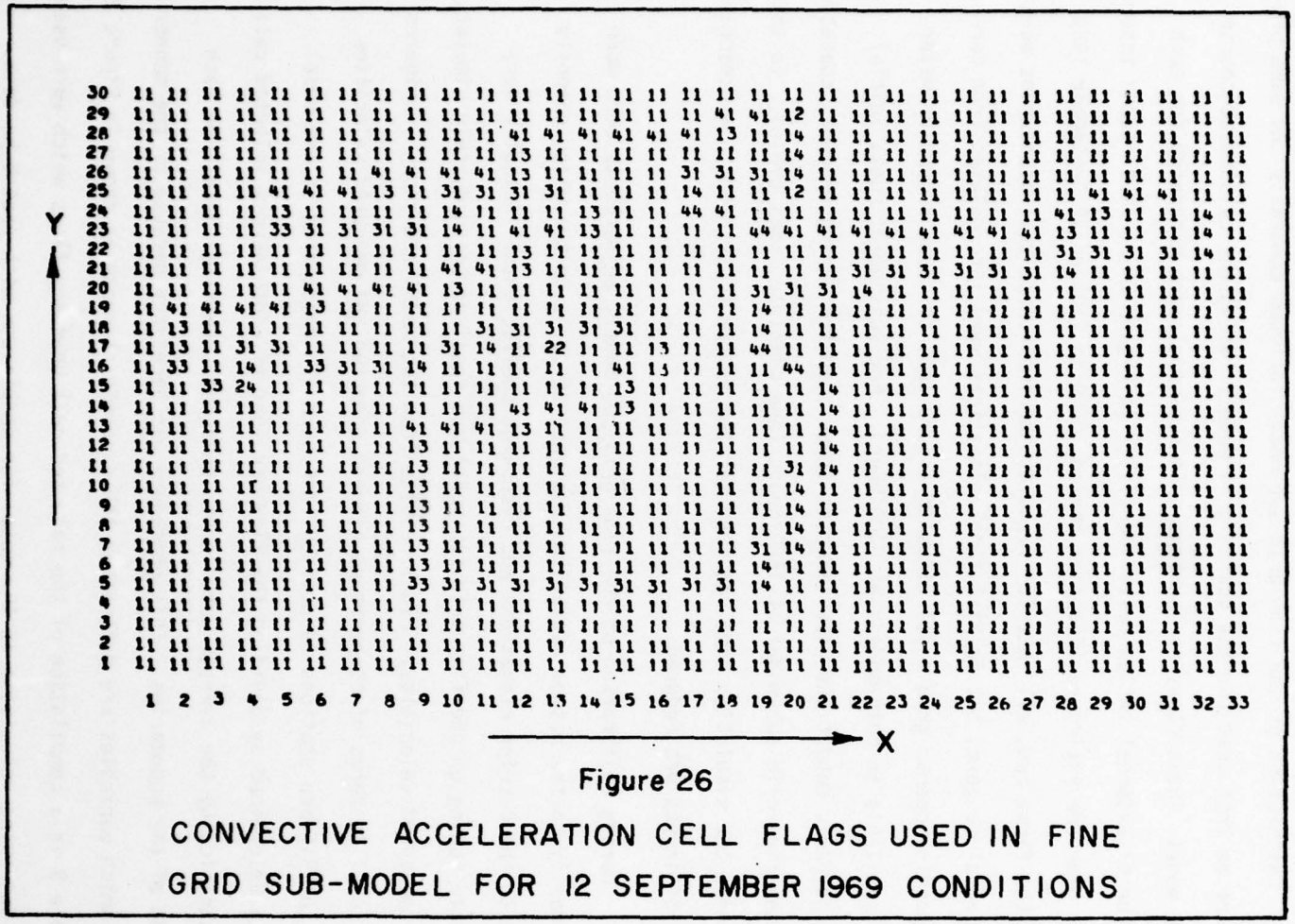

Figure 26

CONVECTIVE ACCELERATION CELL FLAGS USED IN FINE GRID SUB-MODEL FOR 12 SEPTEMBER 1969 CONDITIONS

Calibration of the fine grid sub-model followed generally the same procedure as that used for the coarse grid model. Using the calibrated coarse grid model, input flows to the fine grid sub-model were generated for each of the 47 external inflow cells identified in Figure 24 at five second intervals over the entire verification period, 0400 to 2100 on 12 September 1969. For the first run, all interior flows at the individual cell boundaries were set equal to zero, but initial tidal elevations were interpolated from corresponding coarse grid model tides to assure that the same volume of water was available in both models at 0400 hours. For subsequent runs, initial hydrodynamic conditions were taken as those computed during previous operations of the fine grid sub-model at 1650 hours (one complete tidal cycle). In this manner, the simulation time required for the system to respond to a prescribed set of inputs was reduced.

During calibration of the fine grid sub-model, adjustments were made primarily to the bottom elevations assigned to cells in the major channels and to the barrier elevations and discharge coefficients. Actually very little tuning of the fine grid sub-model was required to adequately simulate the measured velocities. Final results from the model are shown in Figures 27 to 41 in terms of comparisons between computed and measured velocities at the fifteen stations identified in Figure 4. Velocities in the model were determined by dividing the flow per foot of width across selected cell boundaries by the average water depth computed from water levels on each side of the boundaries. This procedure was necessary because of the manner in which variables are defined on the discrete elements as shown in Figure 2. Table 9 is a compilation of the selected cell boundary flows which were used to determine velocities in the model for comparison with prototype data.

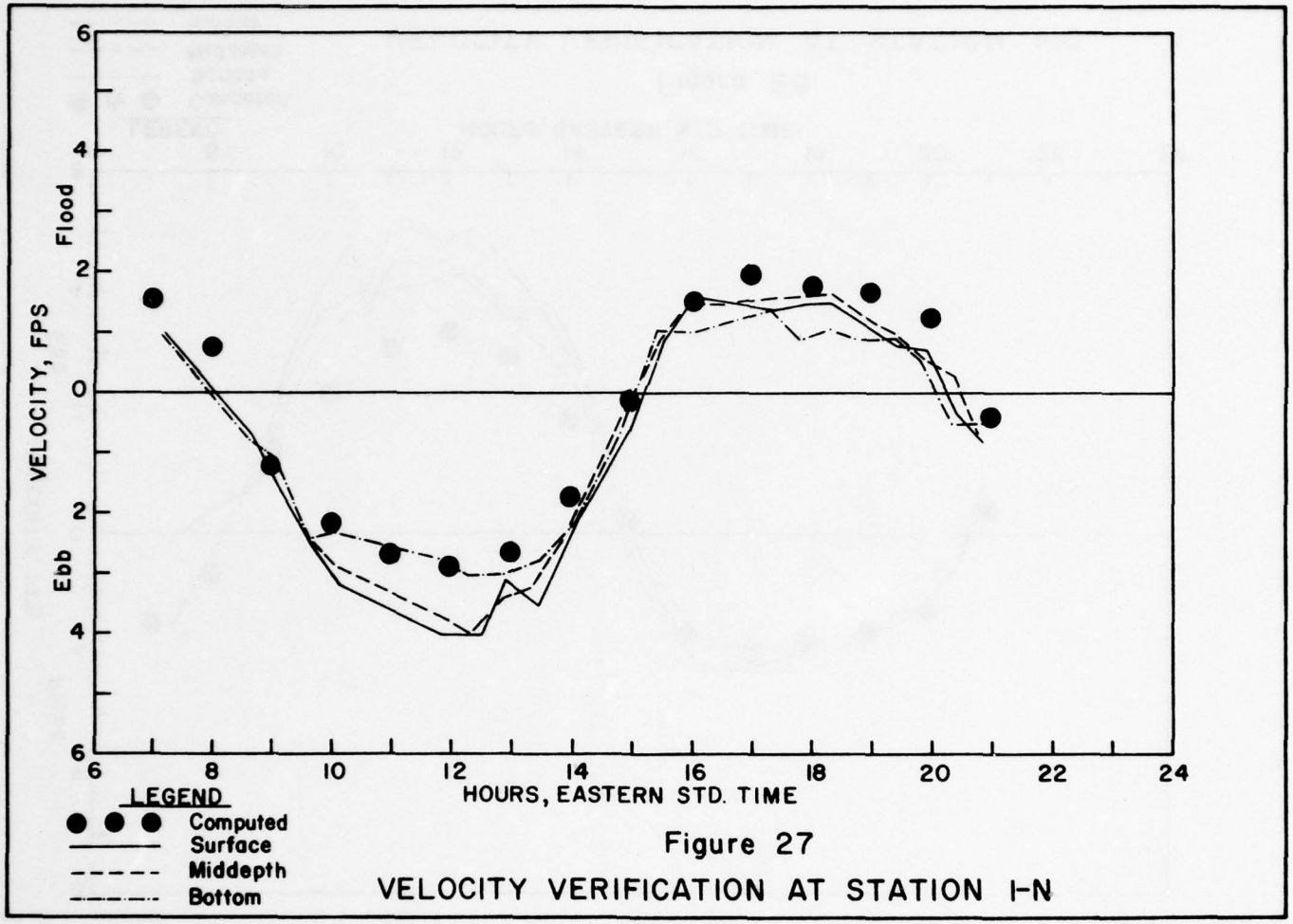

Figure 27

VELOCITY VERIFICATION AT STATION I-N

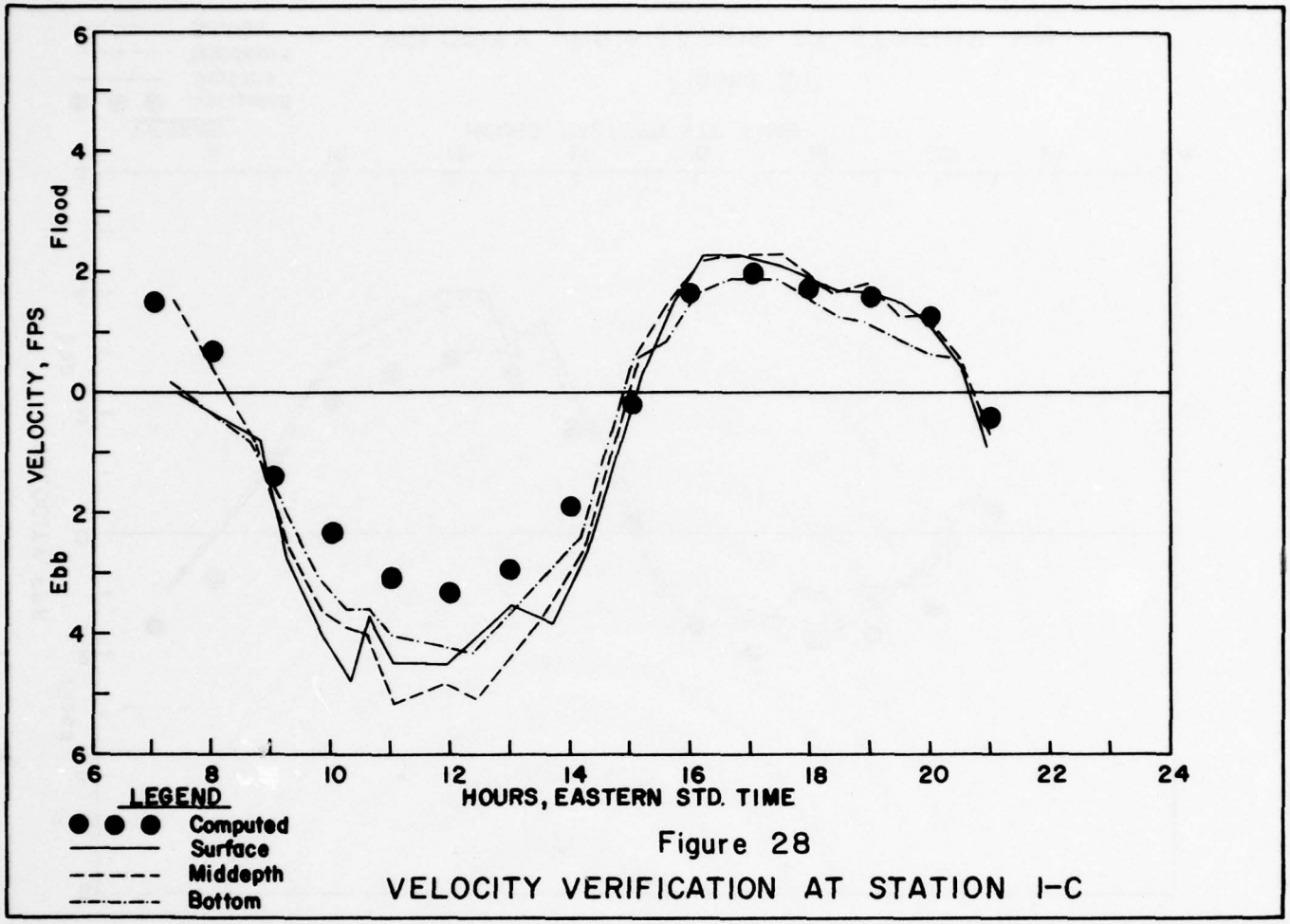

Figure 28

VELOCITY VERIFICATION AT STATION I-C

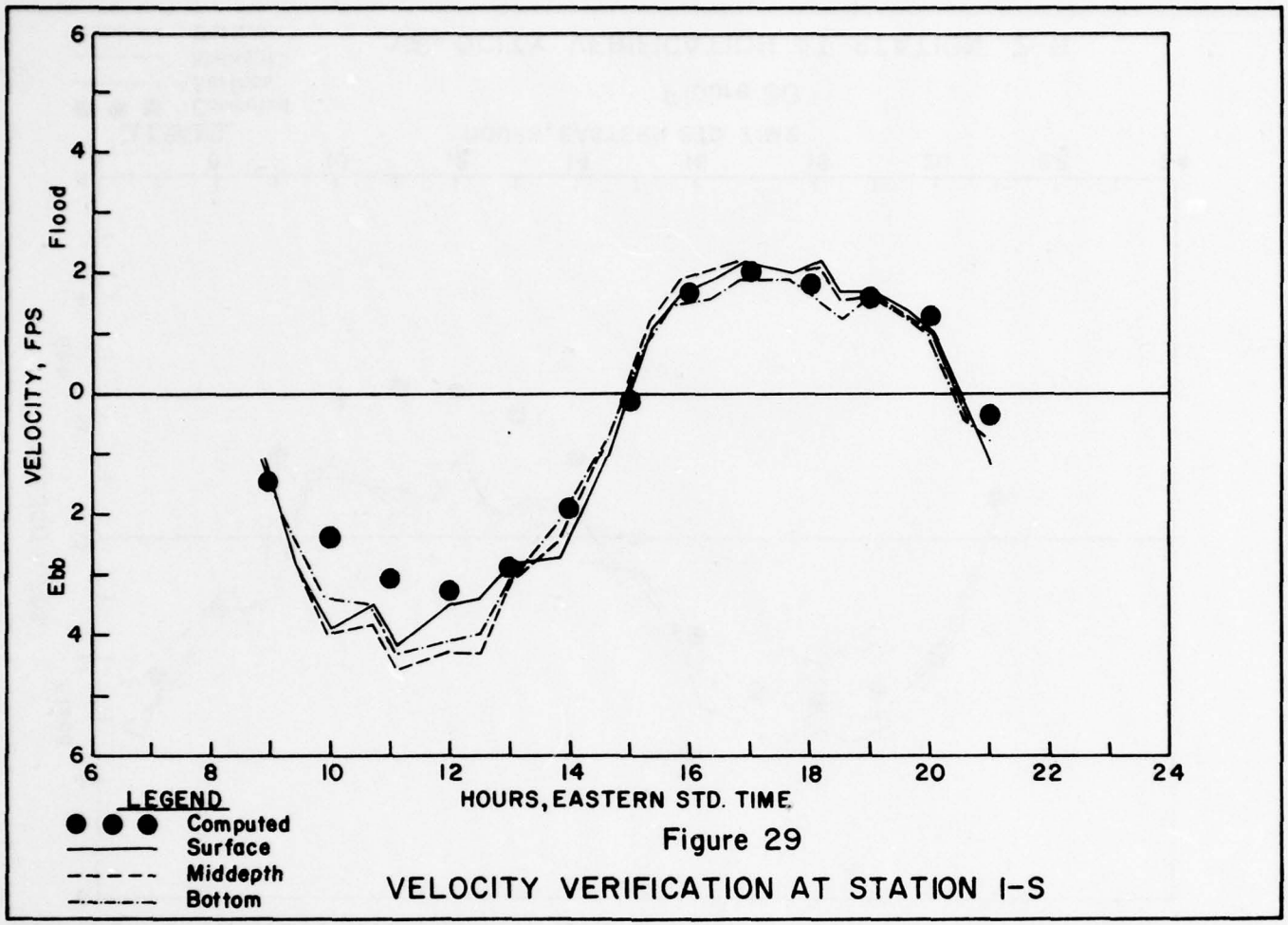

Figure 29

VELOCITY VERIFICATION AT STATION I-S

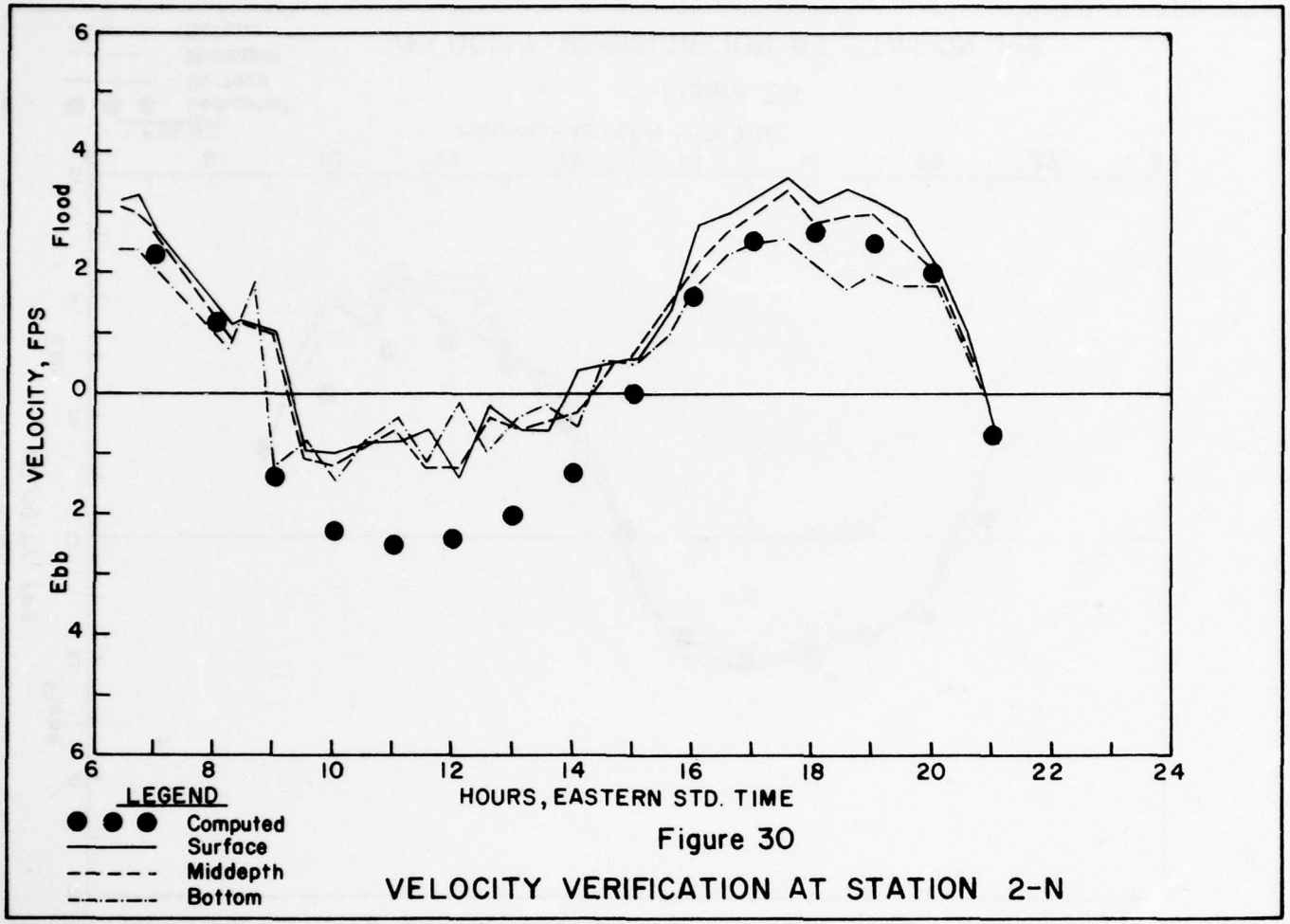

Figure 30

VELOCITY VERIFICATION AT STATION 2-N

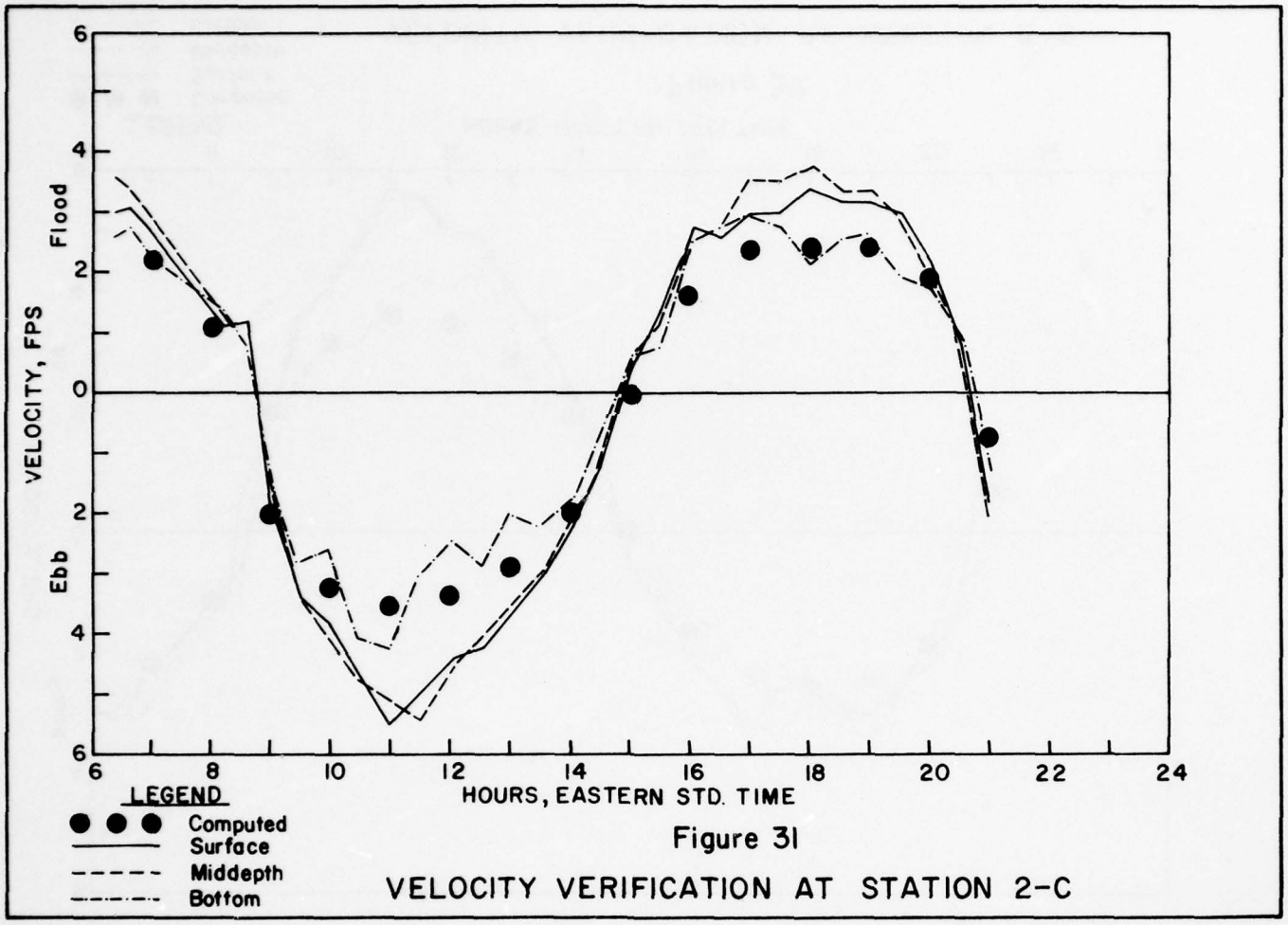

Figure 31

VELOCITY VERIFICATION AT STATION 2-C

AD-A052 797 WATER RESOURCES ENGINEERS INC AUSTIN TX F/G 8/8
COMPARISON OF NUMERICAL AND PHYSICAL HYDRAULIC MODELS, MASONBOR--ETC(U)
JUN 77 F D MASCH, R J BRANDES, J D REAGAN DACW72-72-C-0028
UNCLASSIFIED CERC-6ITI-6-APP-2-VOL-1 NL

2 OF 2
AD A052797

END
DATE FILMED
5-78
DDC

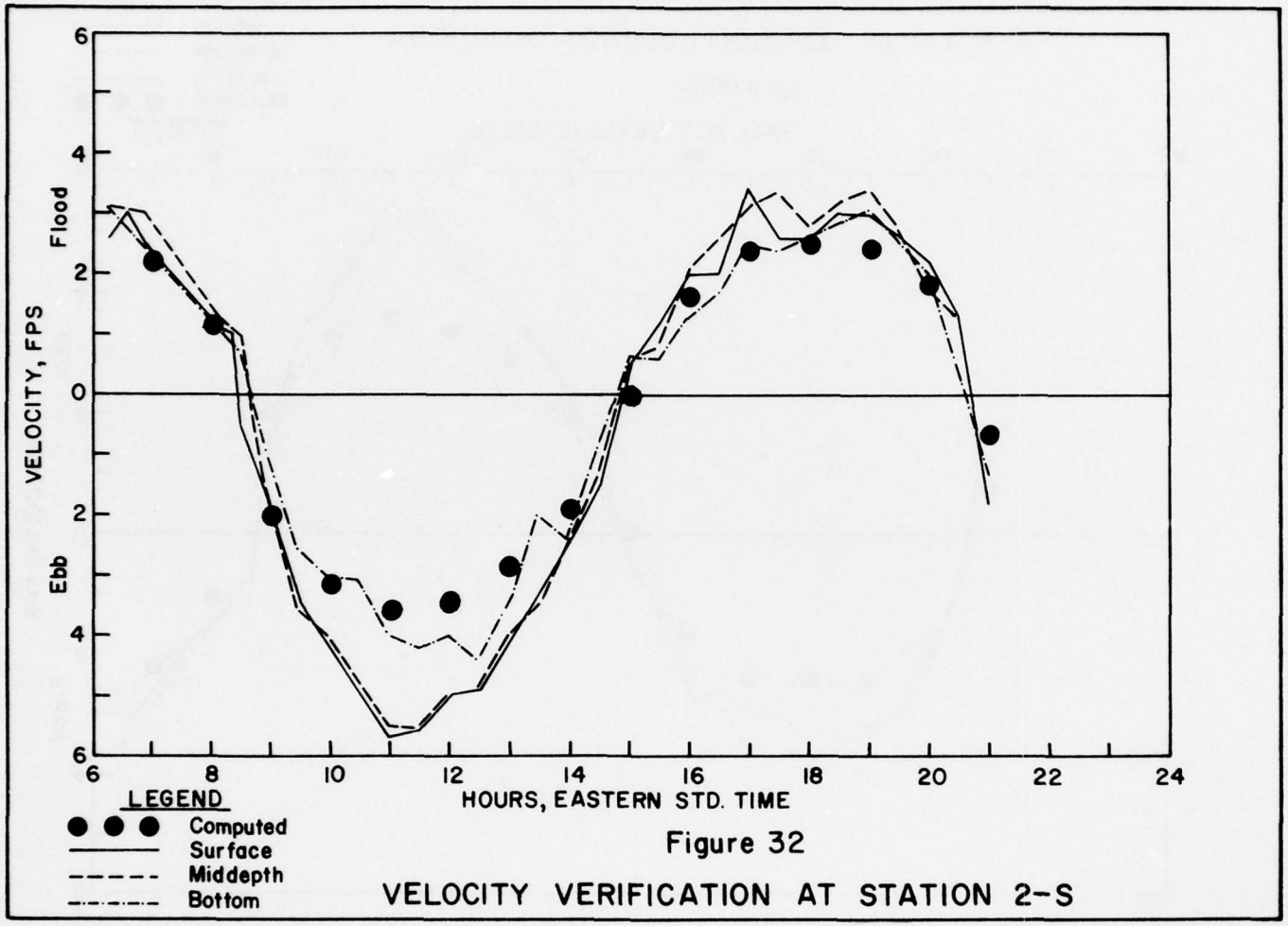

Figure 32

VELOCITY VERIFICATION AT STATION 2-S

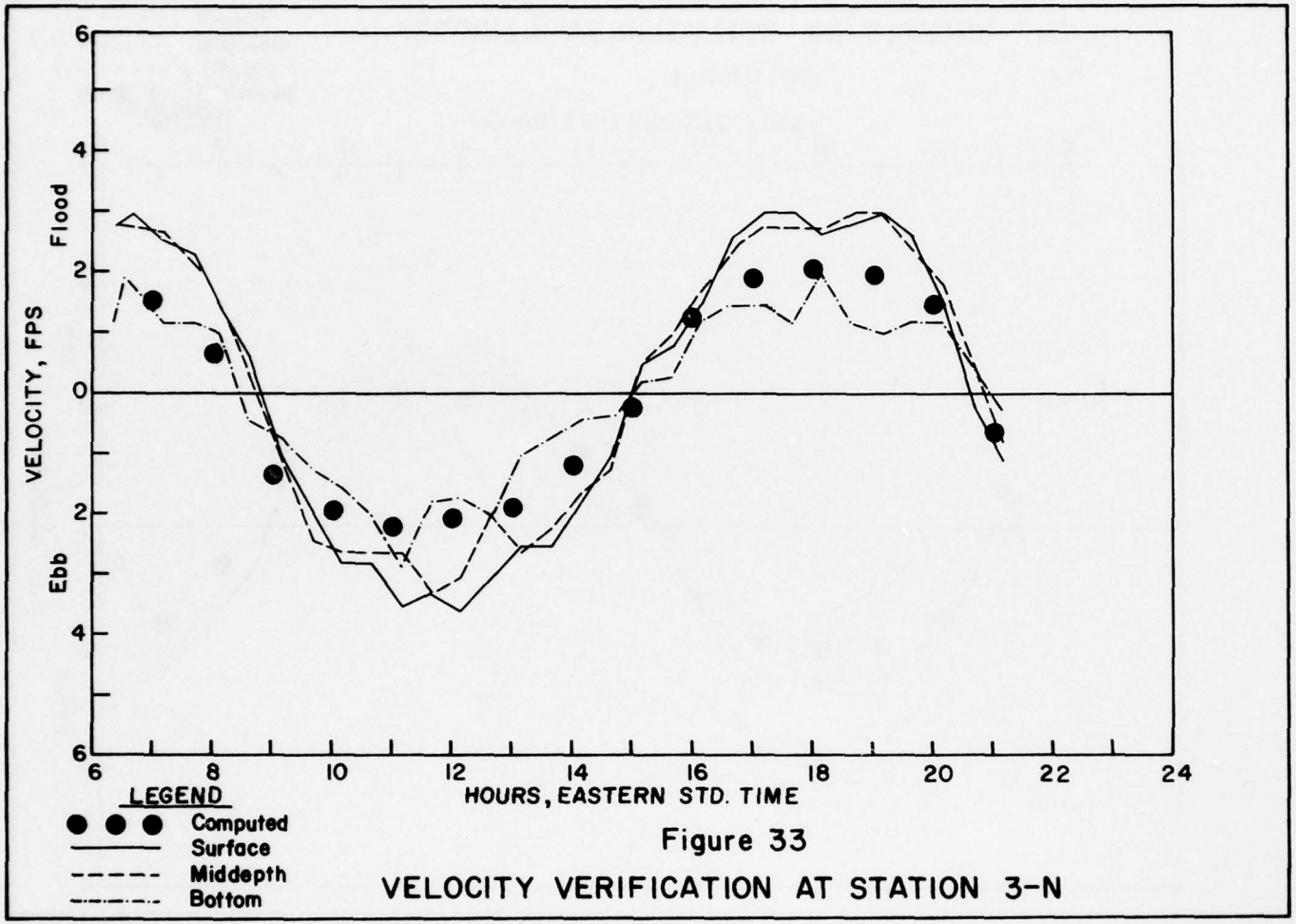

Figure 33

VELOCITY VERIFICATION AT STATION 3-N

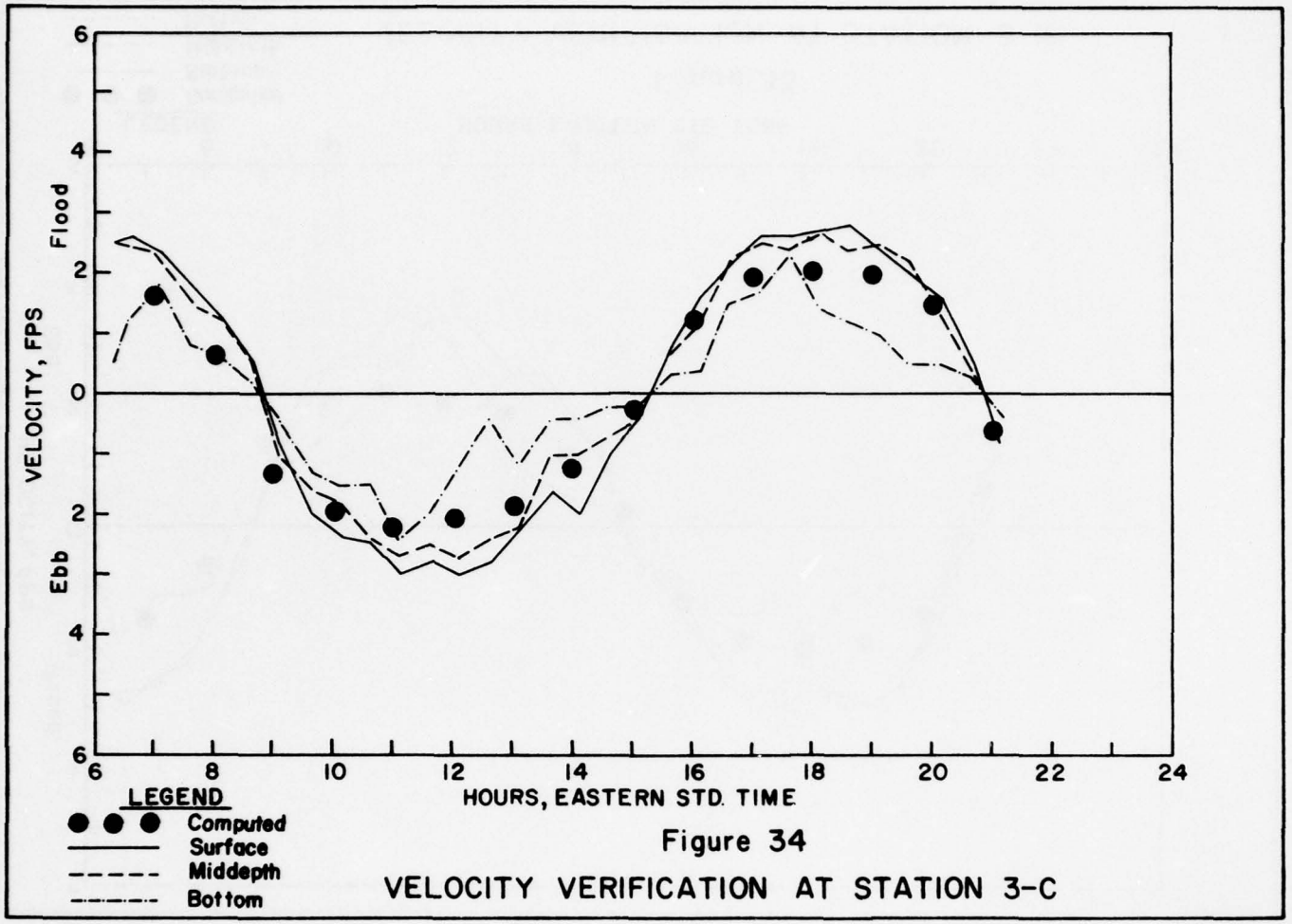

Figure 34

VELOCITY VERIFICATION AT STATION 3-C

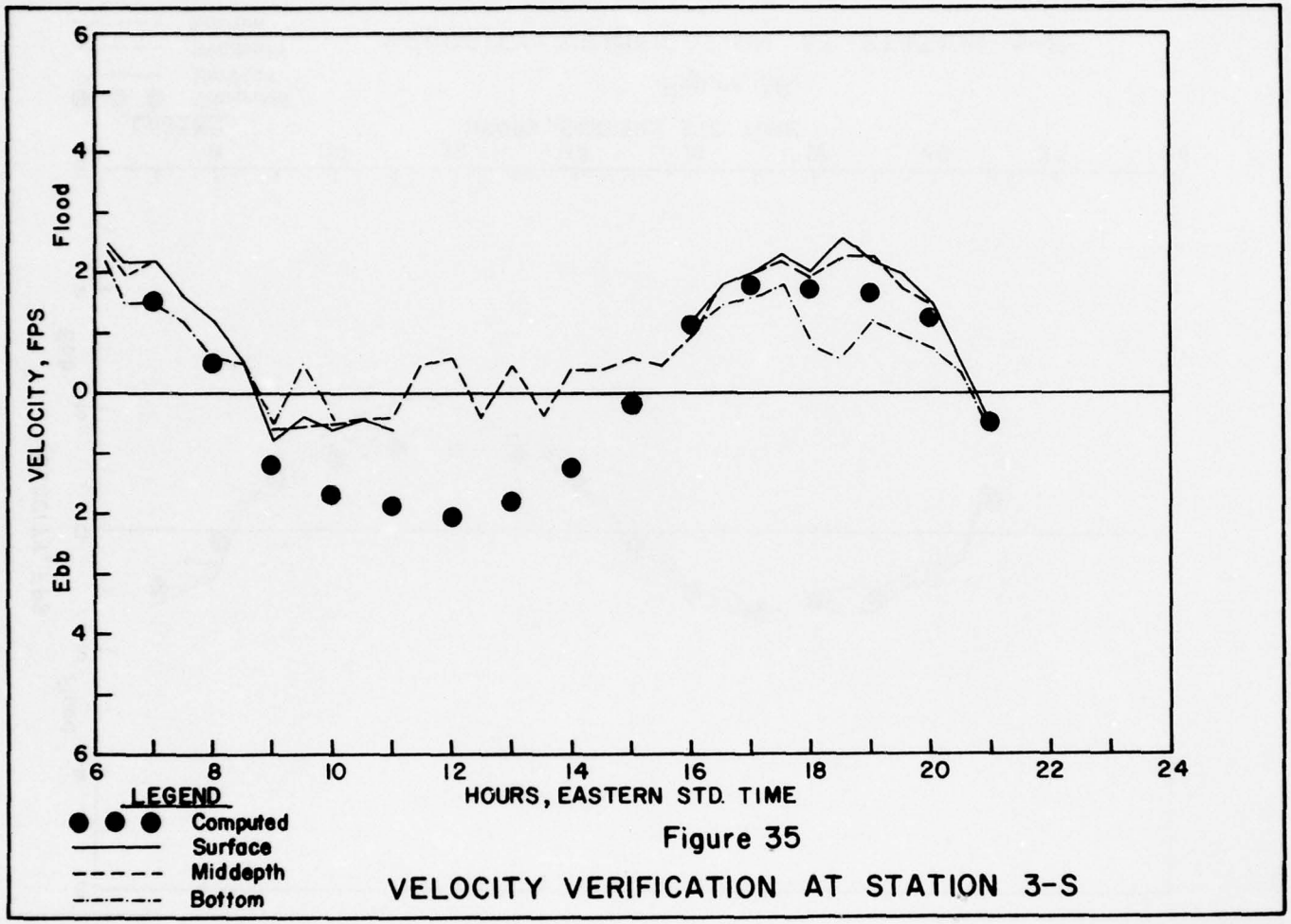

Figure 35

VELOCITY VERIFICATION AT STATION 3-S

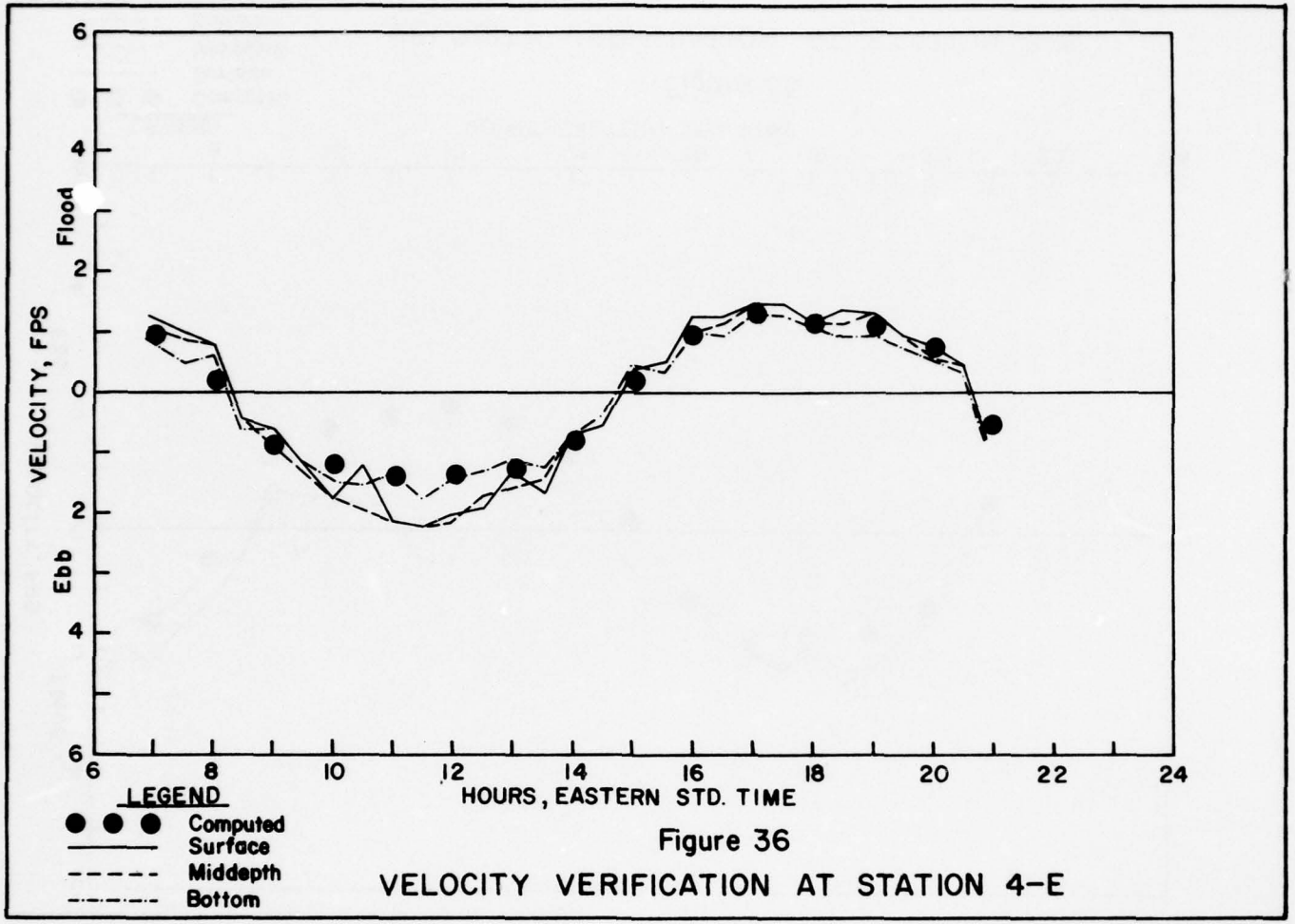

Figure 36

VELOCITY VERIFICATION AT STATION 4-E

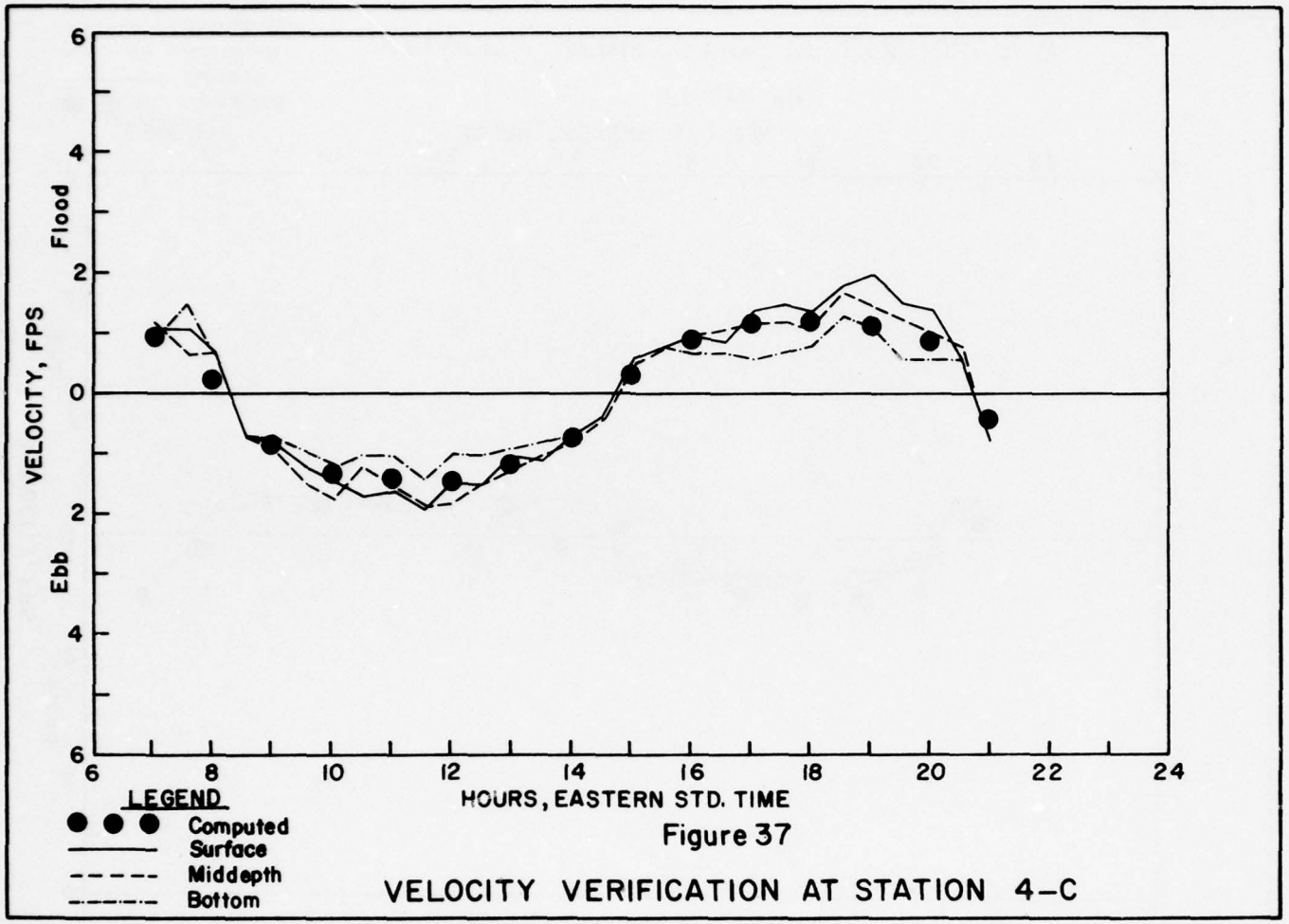

Figure 37

VELOCITY VERIFICATION AT STATION 4-C

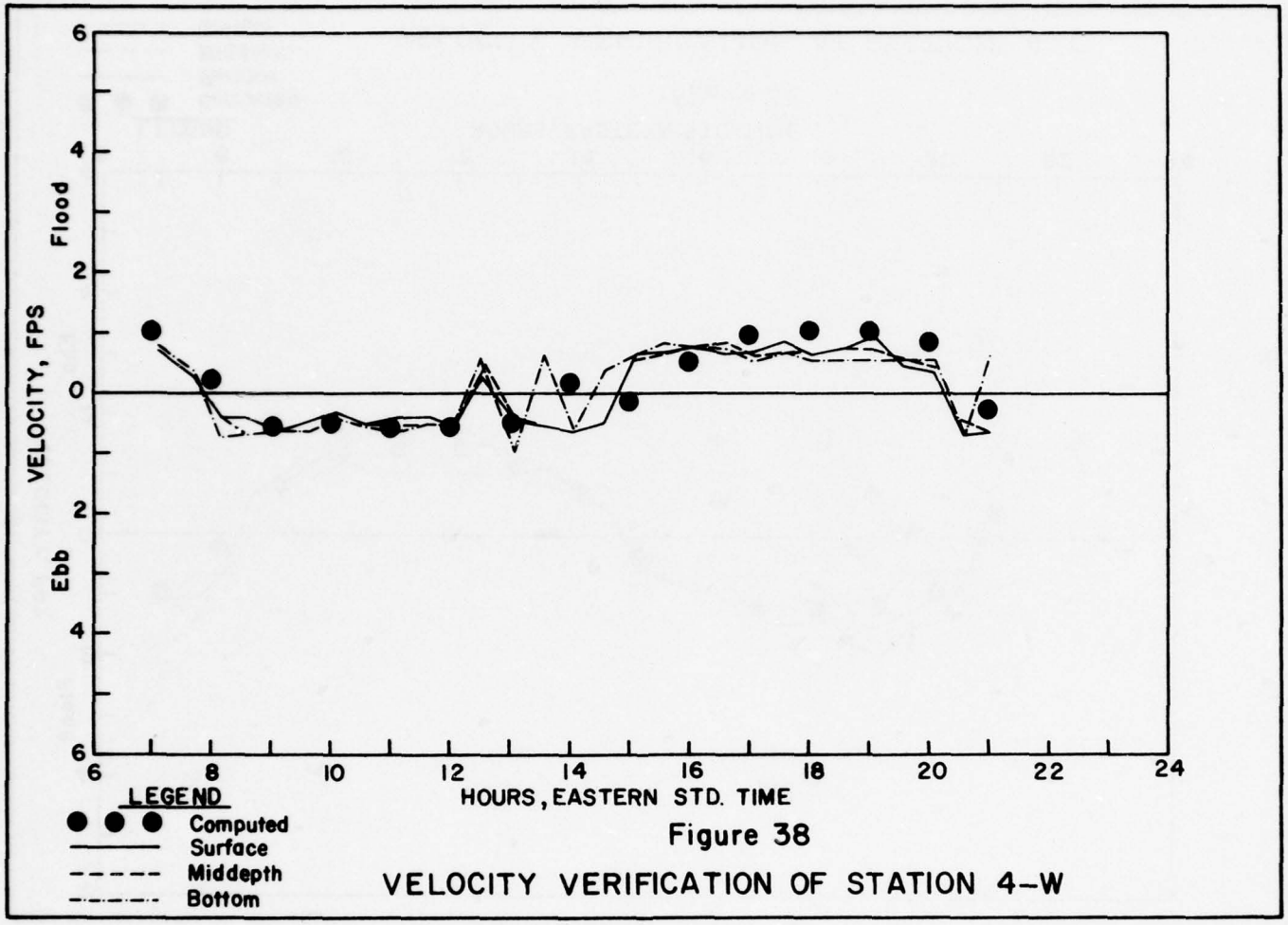

Figure 38

VELOCITY VERIFICATION OF STATION 4–W

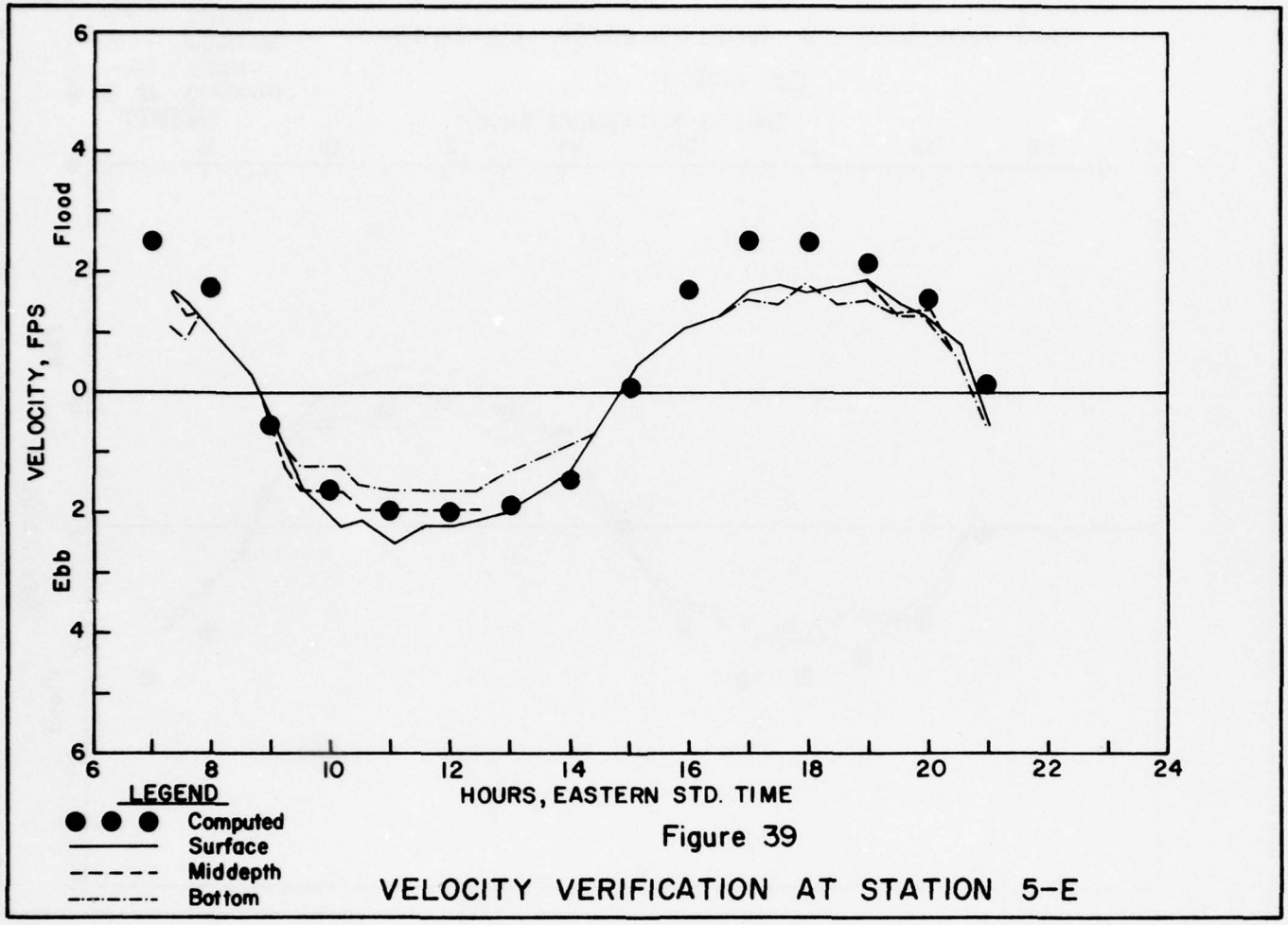

Figure 39

VELOCITY VERIFICATION AT STATION 5-E

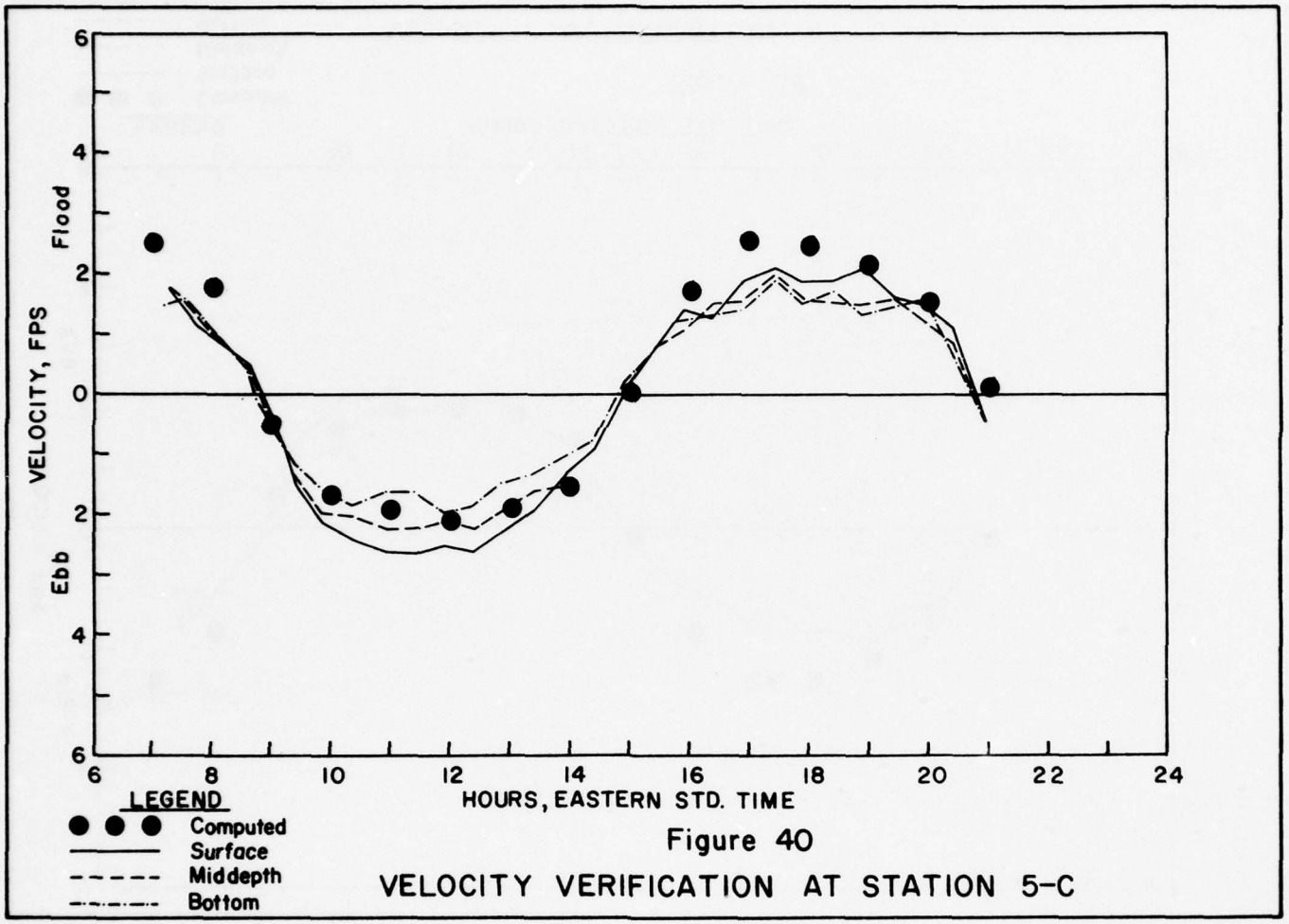

Figure 40

VELOCITY VERIFICATION AT STATION 5-C

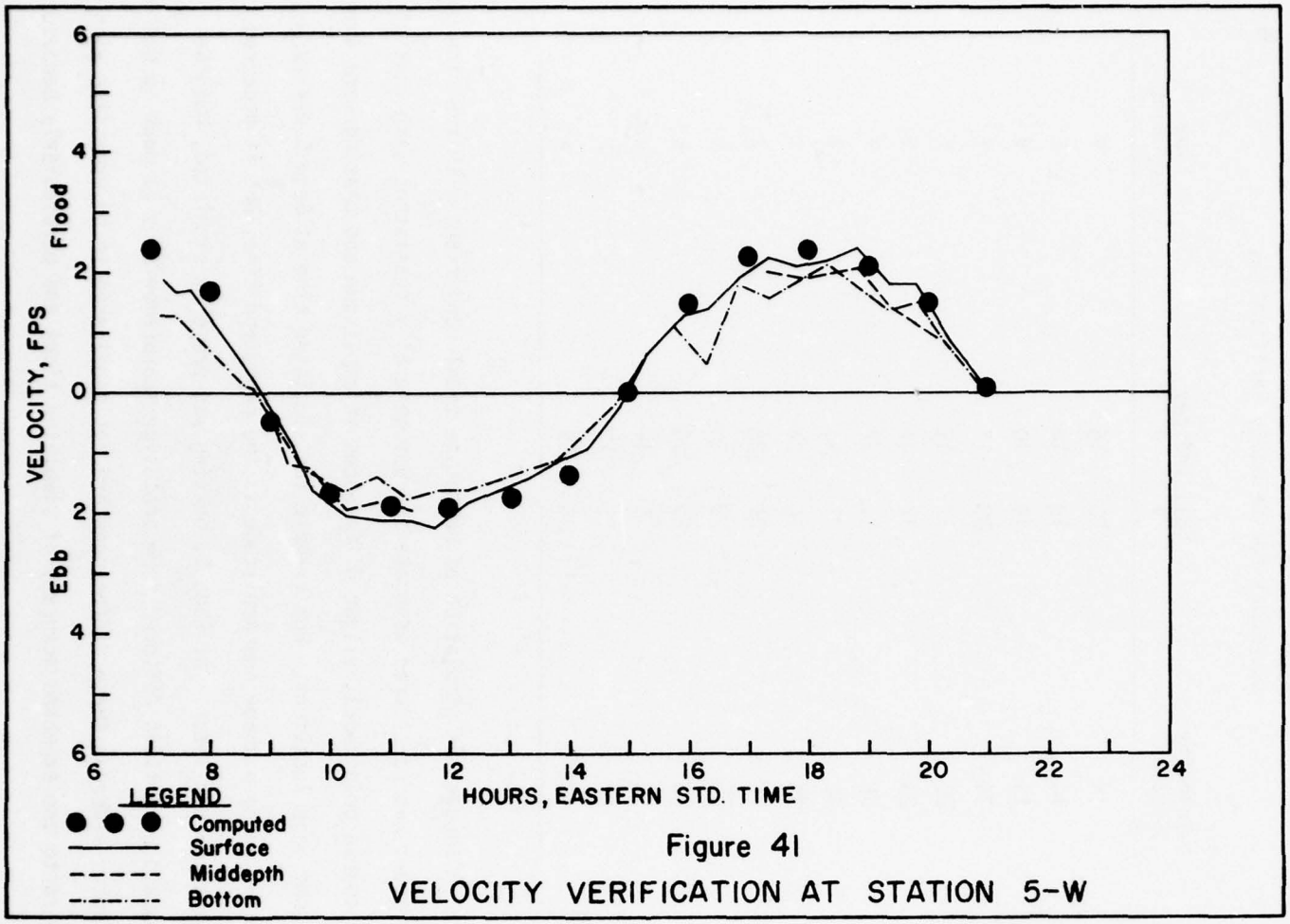

Figure 41

VELOCITY VERIFICATION AT STATION 5-W

Table 9. Cells Used in the Fine Grid Sub-Model for Velocity Verification

Velocity Station	Cell Indices I	J	Flow Component
1N	20	10	Y
1C	19	10	Y
1S	19	10	Y
2N	18	17	Y
2C	17	17	Y
2S	17	17	Y
3N	17	24	Y
3C	17	24	Y
3S	16	24	Y
4E	29	22	X
4C	29	23	X
4W	29	24	X
5E	5	18	X
5C	5	18	X
5W	5	19	X

Although the simulation of prototype tidal conditions with the fine grid sub-model was considered adequate and was generally consistent with that of the coarse grid model, slight differences in amplitude and phasing were noted at some gage locations. For example the simulated tide at Gage 5 was very similar in both shape and amplitude to the prototype tide, but it occurred almost an hour later. At Gage 1, phasing was properly simulated, but the computed peak tides differed from prototype measurements by as much as 0.4 of a foot. Although these differences are not considered to be excessive with regard to the expected accuracy of simulated tides and particularly because

of the good agreement between computed and measured velocities, it is nevertheless important to recognize their probable causes so that model results can be interpreted accordingly. The primary reason for these discrepancies lies in the fact that the coarse grid resolution was not detailed enough to adequately describe all of the inundated areas as they exist in the prototype. At some locations such as in the vicinity of Gage 5, the inundated areas could not be accounted for at all with the 1200' mesh size, even though the ground elevation at other inundated cells in the grid were adjusted slightly by appropriate amounts to reflect this inundation and to maintain the proper relation between depth and volume in the model. Even with these adjusted elevations, the depth-volume relations in the two models could not be made exactly the same because of the coarse grid resolution. In light of these considerations, plus the fact that all of the tide gage locations are not included within the boundaries of the fine grid sub-model, it is felt that tidal simulations with the coarse grid model better reflect prototype conditions.

An idea of the general velocity pattern in the immediate vicinity of the inlet can be determined from the array of velocity vectors plotted in Figures 42, 43, 44 and 45. These velocity patterns correspond to the maximum flood condition, the high water slack condition, the maximum ebb condition, and the low water slack condition, respectively, and they cover an area bounded by rows 5 and 24 and columns 12 and 21 in the fine grid. Although no prototype measurements are available with which to verify these velocity patterns, they do agree with anticipated results, particularly with regard to the flow directions.

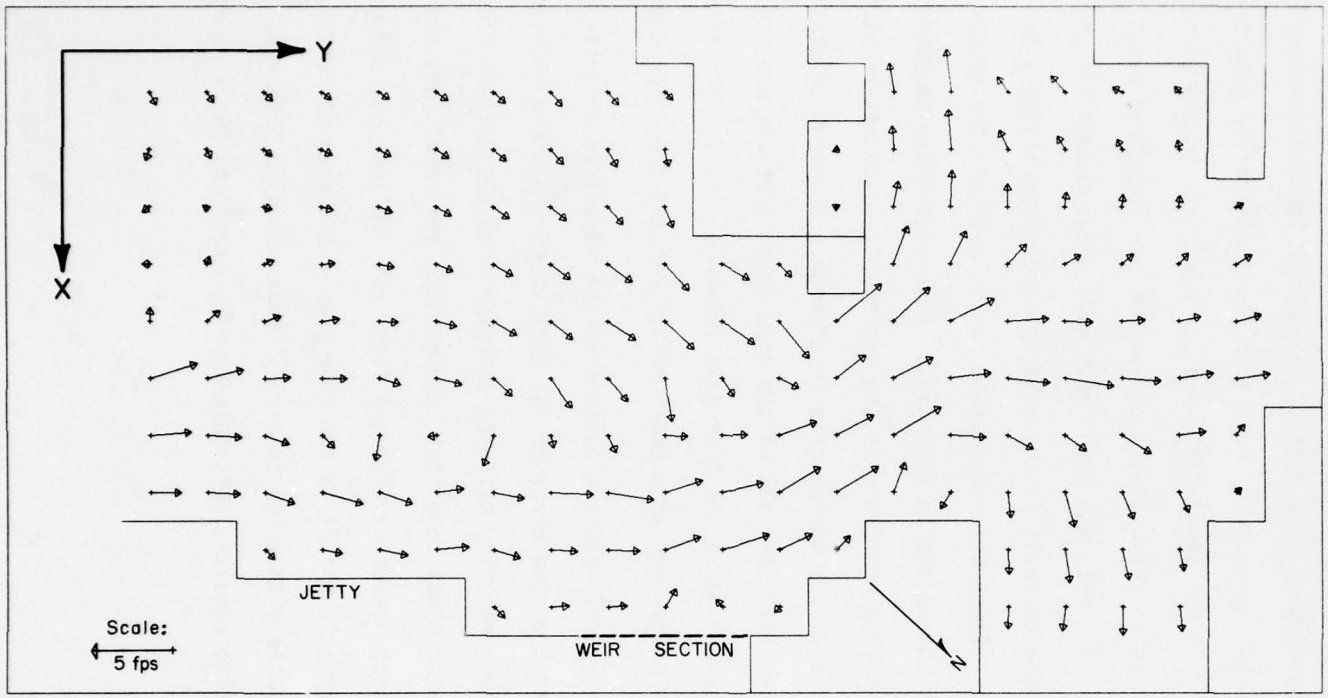

Figure 42

SIMULATED VELOCITY PATTERN AT MAXIMUM FLOOD FLOW CONDITIONS, 12 SEPTEMBER 1969

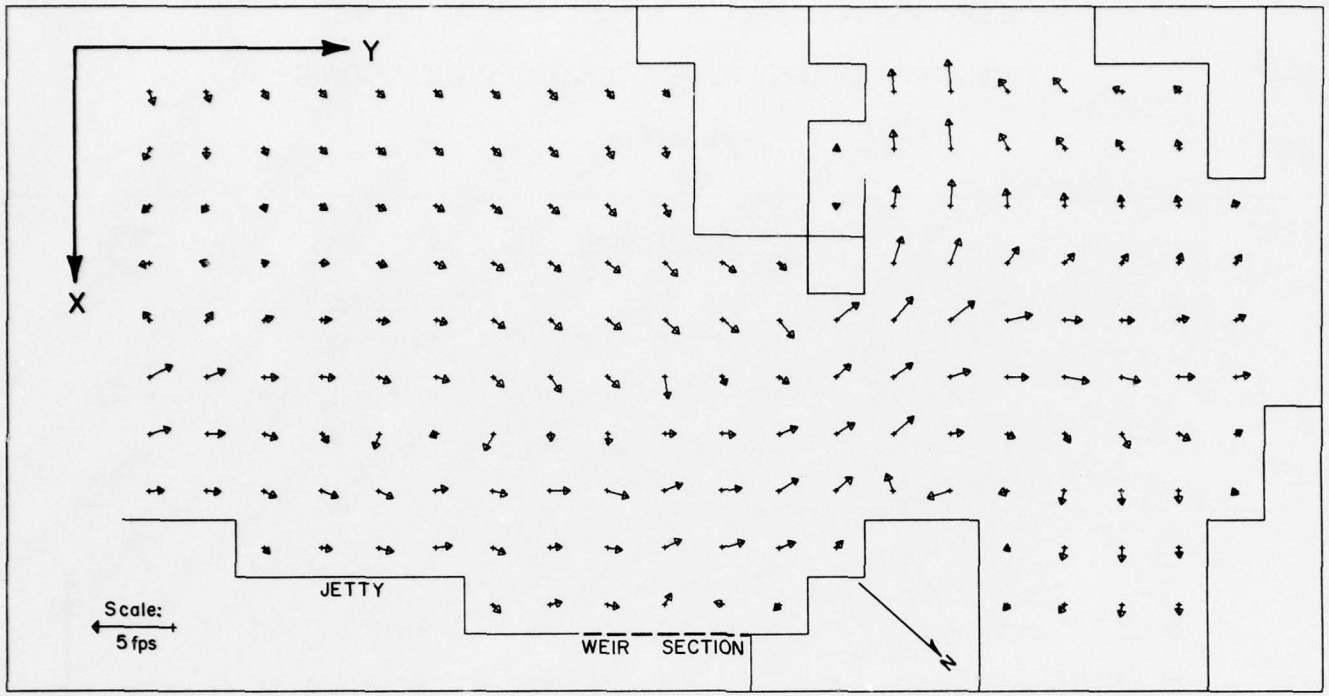

Figure 43

SIMULATED VELOCITY PATTERN AT HIGH WATER

SLACK TIDE CONDITION, 12 SEPTEMBER 1969

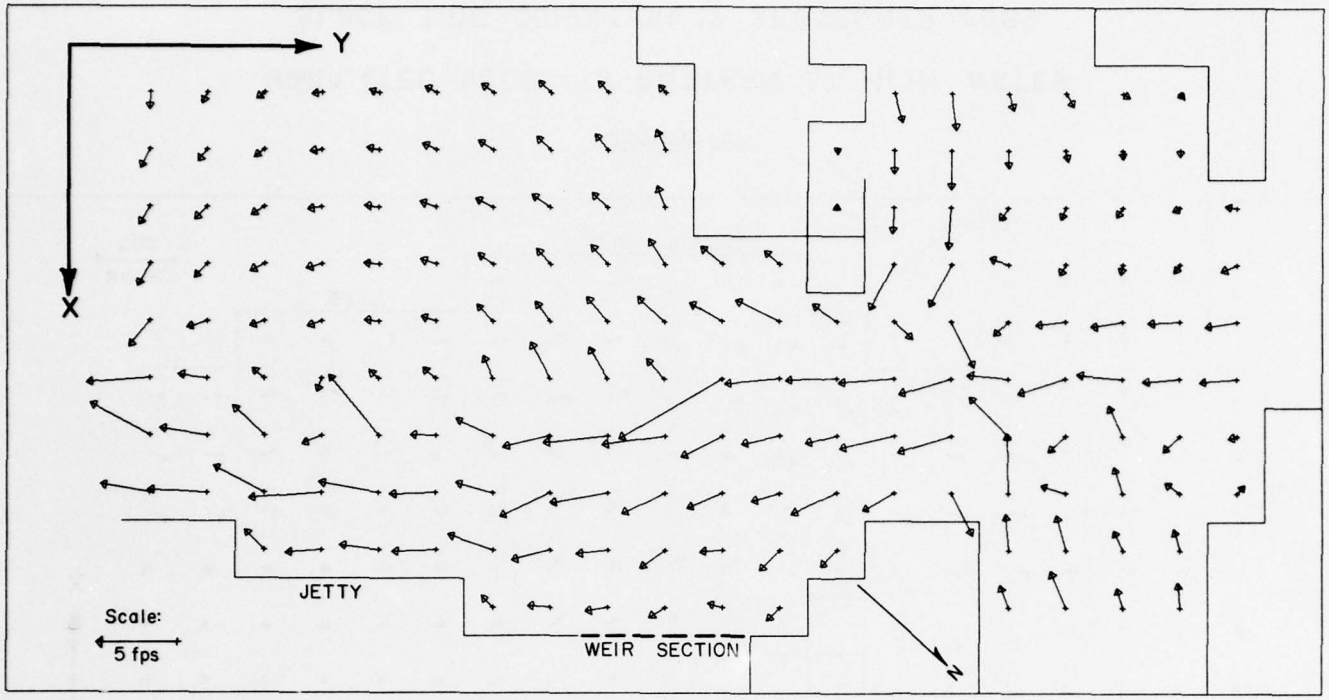

Figure 44

SIMULATED VELOCITY PATTERN AT MAXIMUM

EBB FLOW CONDITION, 12 SEPTEMBER 1969

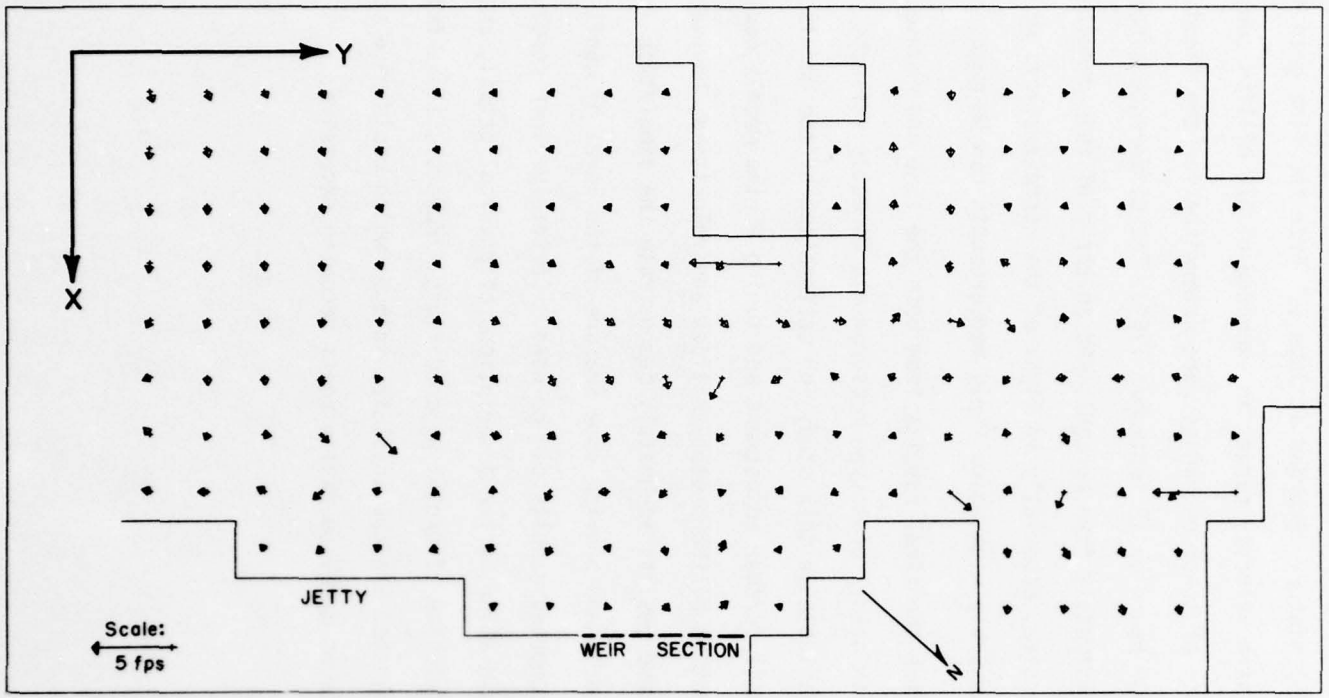

Figure 45

SIMULATED VELOCITY PATTERN AT LOW WATER

SLACK TIDE CONDITION, 12 SEPTEMBER 1969

For the verification period, the tidal exchange in the prototype was determined to be 641 million cubic feet from the velocity measurements made at Range 2 and the tidal history recorded at Gage 1. From the fine grid submodel results at this same velocity range, an exchange of 678 million cubic feet was computed. Both of these exchanges were determined for the flood flow period 1400 to 2100 hours on 12 September 1969. The difference between the two values is approximately five percent, and an error of this magnitude is not considered excessive, especially in light of the approximations made in the model and the accuracy with which field measurements can be made.

The degree to which the final results from both the fine and coarse grid models compare with actual prototype measurements directly reflects the level of effort available in this study for calibration of the models. It is possible that still further adjustment and tuning of the models could provide better reproduction of the prototype tides and velocities, however, it is believed that these results adequately demonstrate the simulation capabilities of the models and provide some measure of the level of confidence with which the computed results can be used. Certainly finer resolution in both the models would allow better descriptions of physical detail, and undoubtably better simulation of prototype conditions. However, it is felt that the mesh sizes selected are the absolute minimums which could have been used in this study without model operation costs becoming excessive.

IV. PRE- AND POST-PROJECT SIMULATIONS

Model Modifications

With the calibration and verification of the models for the 12 September 1969 conditions satisfactorily completed, operation of the models was undertaken to simulate the inlet hydrodynamics for the following two conditions:

1. *Pre-project conditions (without jetty) as of November 1964, and*
2. *Post-project conditions (with jetty) as of June 1967.*

Each of these inlet configurations was investigated using both mean and spring tides to excite the models. Figure 46 illustrates these tides for one semi-diurnal tidal cycle.

Physiographic information for each condition was provided by means of 1" = 500' hydrographic surveys covering the immediate inlet area. The spatial limit of these surveys is shown in Figure 47 relative to the model grids. The information provided did not extend over either of the entire grid areas, and therefore, for simulation of both June 1967 and November 1964 conditions, the bottom and ground elevations and water-land boundaries outside of the survey limits were not changed in the models from those used in the verification process. Alterations were made only to interior cells.

Five-foot bottom contours were provided for each of the operational conditions on the hydrographic surveys together with MLW and MHW lines.

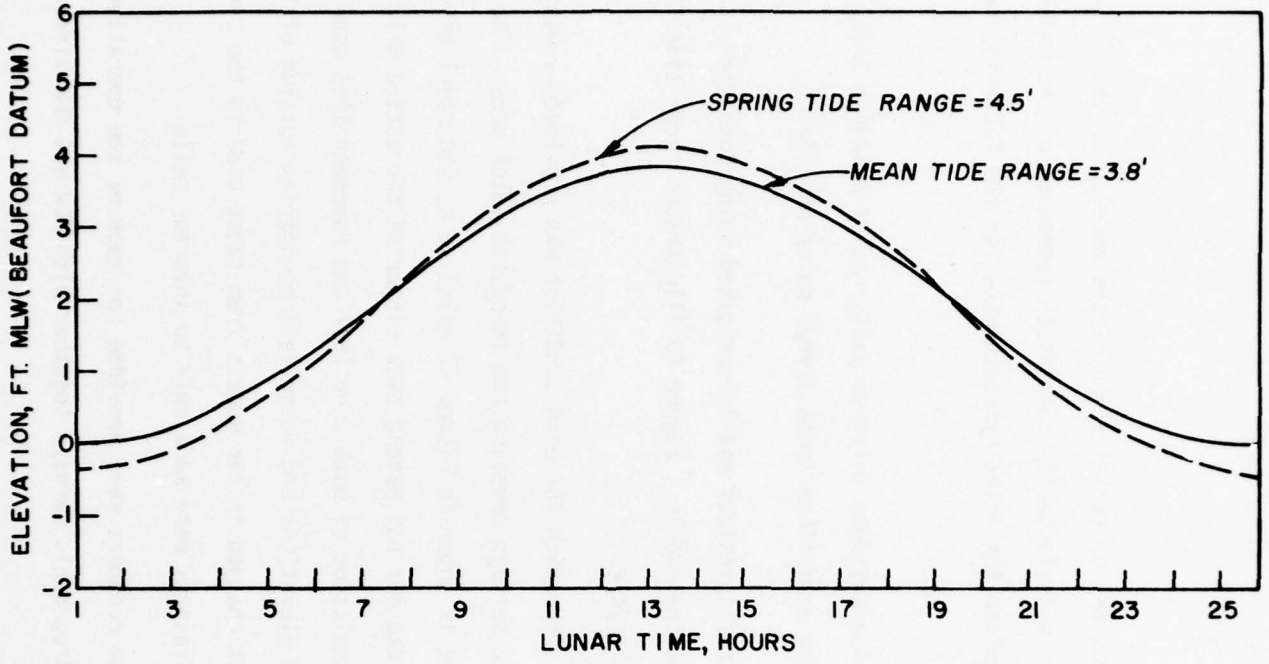

Figure 46

SEMI-DIURNAL MEAN AND SPRING OCEAN TIDES USED IN MODEL OPERATION

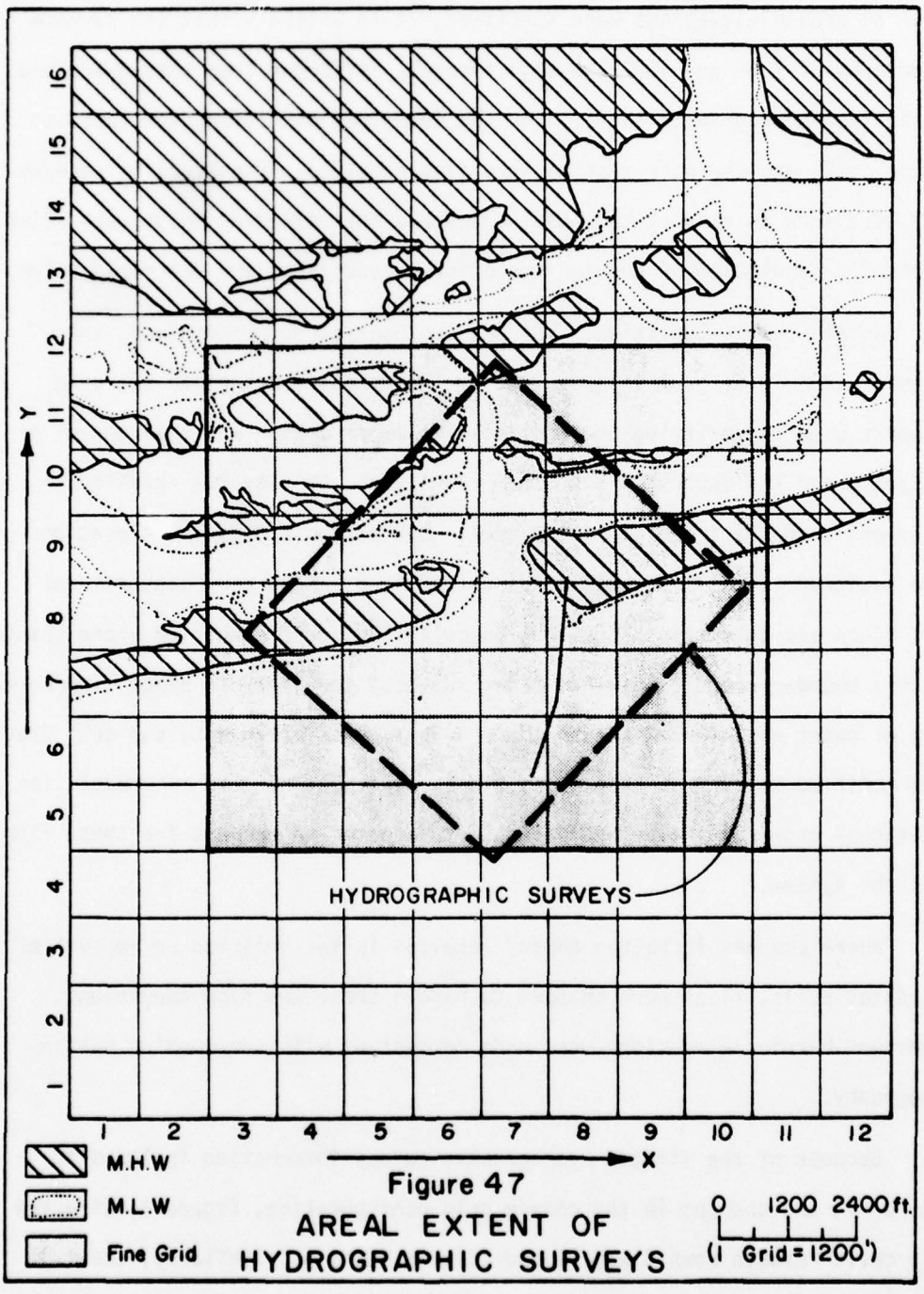

Figure 47

AREAL EXTENT OF HYDROGRAPHIC SURVEYS

While no ground elevations were specified, it is unlikely that the surface topography of 1964 and 1967 was significantly different from that described on the 1969 hydrographic chart. For the June 1967 condition, the location of the jetty and the weir section were also provided. The specific changes that were made to each of the model grids and the attendent input data alterations for simulation of the two operational conditions are described below.

November 1964 Condition. Of the two operational conditions, the November 1964 inlet geometry required the most modifications to the grid networks used in verifying the models. The major change was the removal of the jetty and the inclusion in the fine grid of several additional water cells in the immediate jetty area. New bottom and ground elevations were assigned to cells in both grids as required. Also new computational cell flags and convective acceleration cell flags were specified where changes in cell boundary conditions were made. Without the jetty in place, the normal flow of water was allowed across the original jetty alignment, and cell flags were modified to reflect these conditions. In the fine grid sub-model, ten additional external inflow boundaries were created to account for these flows into the system.

Where changes in bottom depths resulted in the creation or removal of inundated cells, flags were changed to handle these new flow conditions. Submerged barrier elevations were made consistent with surrounding bottom topography.

Because of the limited hydrographic survey information included in Figure 47, the changes in the coarse grid configuration, Figure 8, affected only cells between rows 5 and 11 and columns 4 and 8. Similarly, the fine

grid changes were made only to cells between rows 4 and 24 and columns 9 and 22, Figure 22. The new arrays of bottom and ground elevations, computational cell flags, and convective cell flags for both models are presented in Figures 48 through 53 for the November 1964 conditions. Table 10 describes the linkage between the two models for the ten additional external inflow boundary cells created in the fine grid sub-model.

Table 10. Linkage Between Additional Coarse Grid and Fine Grid Boundary Flows for November 1964 Conditions

	FINE GRID INPUT FLOWS			*COARSE GRID SOURCE FLOWS*		
Flow Number	Cell Indices I	J	X/Y Component	Cell Indices I	J	X/Y Component
12	20	4	Y	7	5	Y
13	21	4	Y	7	5	Y
15	21	5	X	7	6	X
17	21	6	X	7	6	X
19	21	7	X	7	6	X
21	21	8	X	7	6	X
23	21	9	X	7	7	X
25	21	10	X	7	7	X
27	21	11	X	7	7	X
29	21	12	X	7	7	X

June 1967 Condition. Because the inlet geometry during this period was quite similar to that used for calibration of the models, only a few modifications were required to describe the physiography of this condition. Of the changes made all were required because of the different bottom topography, and consequently external boundary conditions in both the coarse and the fine grid models

Y \ X	4	5	6	7	8
11	*****	1.0	-8.3	1.2	.7
10	1.4	1.2	-10.3	-7.3	-7.3
9	-4.8	-5.8	-5.3	-16.3	*****
8	*****	*****	-4.3	-11.3	-5.3
7	-8.3	-3.3	-4.3	-11.3	-11.3
6	-19.3	-16.3	-8.3	-15.3	-21.3
5	-29.3	-27.3	-21.3	-21.3	-31.3

Figure 48
MSL BOTTOM AND GROUND ELEVATIONS USED IN COARSE GRID MODEL FOR NOVEMBER 1964 CONDITIONS

Y \ X	4	5	6	7	8
11	1	30	31	30	36
10	30	33	5	12	12
9	12	15	2	6	1
8	1	1	12	2	12
7	12	12	2	2	2
6	2	2	2	2	2
5	2	2	2	2	2

Figure 49
COMPUTATIONAL CELL FLAGS USED IN COARSE GRID MODEL FOR NOVEMBER 1964 CONDITIONS

Y \ X	4	5	6	7	8
11	11	41	22	21	33
10	21	33	44	21	21
9	21	21	33	14	11
8	11	11	41	42	41
7	41	41	13	11	11
6	11	11	11	11	11
5	11	11	11	11	11

Figure 50
CONVECTIVE ACCELERATION CELL FLAGS USED IN COARSE GRID MODEL FOR NOVEMBER 1964 CONDITIONS

Y	9	10	11	12	13	14	15	16	17	18	19	20	21	22
24	.7	.7	*****	*****	*****	.7	-2.5	-12.5	-7.5	-2.5	.7	*****	*****	*****
23	.7	.7	*****	-1.5	-2.5	-2.5	-2.5	-11.5	-10.5	-2.5	-2.5	-3.5	-7.5	-7.5
22	*****	*****	*****	-2.5	-2.5	-2.5	-2.5	-10.5	-12.5	-6.5	-6.5	-7.5	-11.5	-4.5
21	*****	-1.5	-2.5	-1.5	-2.5	-2.5	-2.5	-9.5	-12.5	-7.5	-8.5	-9.5	-12.5	-12.5
20	-1.5	-1.5	-2.5	-3.5	-2.5	-2.5	-2.5	-7.5	-14.5	-20.5	-12.5	-9.5	-5.5	-4.5
19	-7.5	-7.5	-8.5	-8.5	-2.5	-2.5	-2.5	-6.5	-20.5	-20.5	-2.5	*****	*****	*****
18	-7.5	-7.5	-6.5	-3.5	-2.5	-2.5	-2.5	-2.5	-20.5	-20.5	-2.5	*****	*****	*****
17	.7	.7	.7	*****	.7	-2.5	-2.5	-2.5	-14.5	-20.5	-2.5	-2.5	*****	*****
16	1.7	*****	*****	*****	*****	-2.5	-2.5	-5.5	-19.5	-18.5	-5.5	-2.5	-3.5	*****
15	*****	*****	*****	*****	*****	-2.5	-2.5	-6.5	-14.5	-16.5	-7.5	-5.5	-3.5	*****
14	*****	*****	*****	-4.5	-2.5	-2.5	-3.5	-7.5	-13.5	-13.5	-9.5	-5.5	-4.5	*****
13	-2.5	-3.5	-4.5	-7.5	-2.5	-2.5	-5.5	-7.5	-12.5	-12.5	-9.5	-6.5	-5.5	*****
12	-3.5	-2.5	-2.5	-2.5	-2.5	-4.5	-5.5	-7.5	-11.5	-12.5	-10.5	-7.5	-5.5	*****
11	-3.5	-2.5	-2.5	-2.5	-3.5	-4.5	-4.5	-6.5	-9.5	-12.5	-9.5	-7.5	-6.5	*****
10	-3.5	-3.5	-5.5	-7.5	-6.5	-4.5	-2.5	-6.5	-8.5	-12.5	-10.5	-8.5	-7.5	*****
9	-6.5	-7.5	-7.5	-7.5	-6.5	-6.5	-4.5	-7.5	-9.5	-12.5	-11.5	-10.5	-9.5	*****
8	-14.5	-14.5	-12.5	-12.5	-8.5	-8.5	-6.5	-7.5	-10.5	-12.5	-12.5	-12.5	-12.5	*****
7	-15.5	-14.5	-12.5	-12.5	-14.5	-12.5	-9.5	-7.5	-9.5	-12.5	-12.5	-12.4	-14.5	*****
6	-17.5	-16.5	-14.5	-12.5	-8.5	-14.5	-13.5	-10.5	-8.5	-9.5	-11.5	-13.5	-19.5	*****
5	-25.5	-19.5	-16.5	-14.5	-11.5	-17.5	-17.5	-16.5	-13.5	-13.5	-17.5	-22.5	-22.5	*****
4	-27.5	-24.5	-22.5	-19.5	-15.5	-13.5	-12.5	-11.5	-10.5	-15.5	-22.5	-22.5	-22.5	*****

X

Figure 51

MSL BOTTOM AND GROUND ELEVATIONS USED IN FINE GRID SUB-MODEL FOR NOVEMBER 1964 CONDITIONS

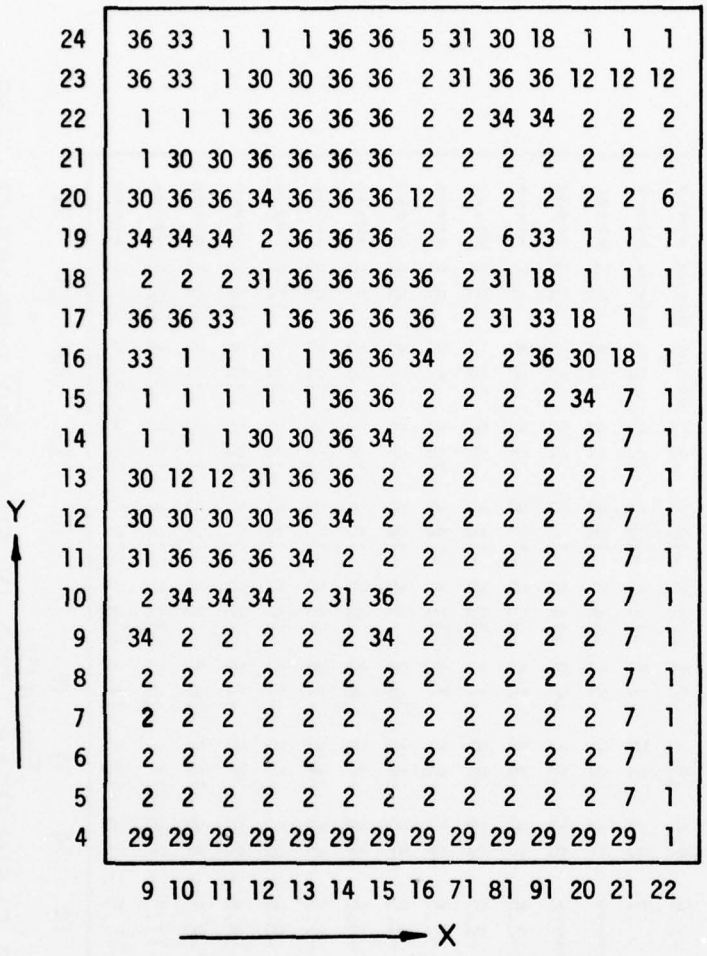

Figure 52

COMPUTATIONAL CELL FLAGS USED IN FINE GRID SUB-MODEL FOR NOVEMBER 1964 CONDITIONS

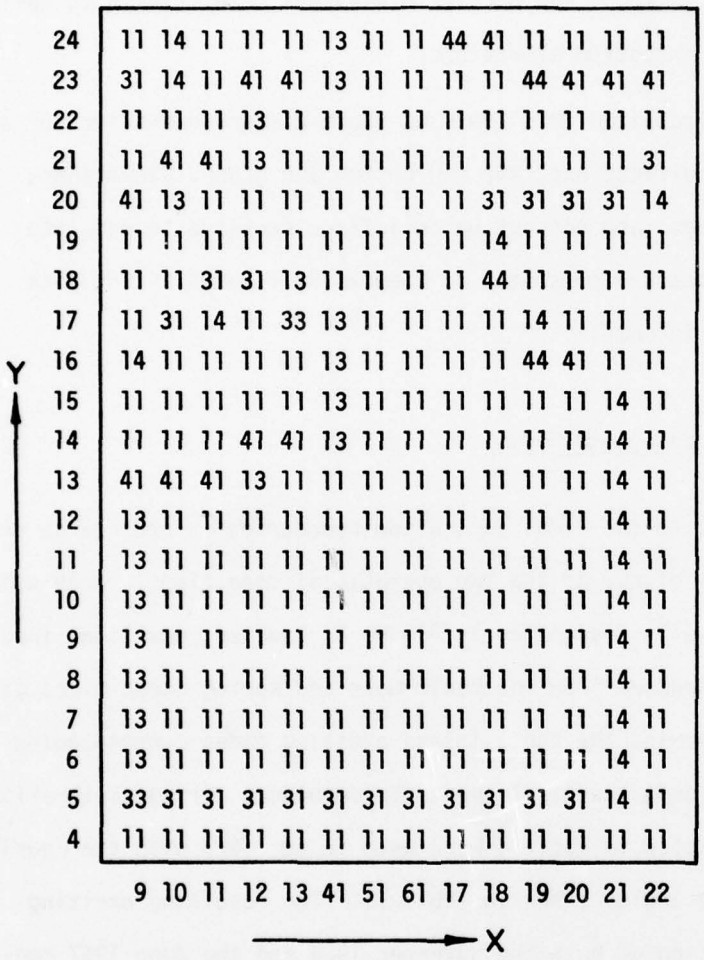

Figure 53

CONVECTIVE ACCELERATION CELL FLAGS USED IN FINE GRID SUB-MODEL FOR NOVEMBER 1964 CONDITIONS

remained the same. Because bottom elevation changes caused some cells in the models to become periodically inundated, computational cell flags had to be modified accordingly. Also, a few barrier elevations were changed to reflect corresponding changes in bottom elevations.

Using the same localized grid areas as those described earlier for the November 1964 model modifications, the new bottom and ground elevations, computational cell flags, and convective cell flags required to simulate the June 1967 conditions are presented in Figures 54 through 59 for both the coarse and fine grid models.

Tidal Excitation in Coarse Grid Model

No modifications to the tidal excitation boundaries in the coarse grid model were required by either of the two operational conditions. Both utilized the same tidal input cells designated in Figure 4; however, new tidal input curves had to be constructed from the basic mean and spring ocean tides given in Figure 46. To determine the three inland exciting tides corresponding to the mean and spring tides, the tidal constants developed during calibration of the model and presented in Table 4 were used in eq. (32) with the Fourier coefficients and phase angles shown in Table 11. The resulting exciting tides used for simulation of both the November 1964 and the June 1967 conditions are presented in Figures 60 and 61 for the mean and spring tides, respectively. These tides were assigned to appropriate boundary cells according to the tidal identification numbers given in Table 3.

Y						
	11	*****	1.1	-8.3	1.4	.7
	10	1.7	1.4	-6.3	-6.3	-7.3
	9	-4.8	-5.8	-3.3	-11.3	*****
	8	*****	*****	-1.3	-11.3	-6.3
	7	-8.3	-9.3	-6.3	-9.3	-16.3
	6	-19.3	-16.3	-10.3	-10.3	-22.3
	5	-29.3	-27.3	-21.3	-27.3	-31.3
		4	5	6	7	8

X

Figure 54
MSL BOTTOM AND GROUND ELEVATIONS USED IN COARSE GRID MODEL FOR JUNE 1967 CONDITIONS

Y						
	11	1	30	31	30	36
	10	30	33	2	12	12
	9	12	15	2	6	1
	8	1	1	30	42	12
	7	12	12	34	6	2
	6	2	2	2	6	2
	5	2	2	2	2	2
		4	5	6	7	8

X

Figure 55
COMPUTATIONAL CELL FLAGS USED IN COARSE GRID MODEL FOR JUNE 1967 CONDITIONS

Y						
	11	11	41	22	21	33
	10	21	33	44	21	21
	9	21	21	33	14	11
	8	11	11	41	12	41
	7	41	41	13	14	13
	6	11	11	11	14	13
	5	11	11	11	44	13
		4	5	6	7	8

X

Figure 56
CONVECTIVE ACCELERATION CELL FLAGS USED IN COARSE GRID MODEL FOR JUNE 1967 CONDITIONS

Y	9	10	11	12	13	14	15	16	17	18	19	20	21	22
24	.7	.7	*****	*****	*****	.7	-1.3	-11.3	-10.3	-1.3	-1.3	*****	*****	*****
23	.7	.7	*****	-.3	-1.3	-1.3	-1.3	-10.3	-9.3	-2.3	-3.3	-4.3	-6.3	-6.3
22	*****	*****	*****	-1.3	-1.3	-1.3	-1.3	-9.3	-11.3	-7.3	-8.3	-8.3	-10.3	-3.3
21	*****	-.3	-1.3	-.3	-1.3	-1.3	-1.3	-8.3	-14.3	-13.3	-10-3	-11.3	-11.3	-11.3
20	-.3	-.3	-1.3	-2.3	-2.3	-2.3	-2.3	-6.3	-15.3	-15.3	-10.3	-5.3	-4.3	-3.3
19	-6.3	-6.3	-7.3	-7.3	-7.3	-7.3	-6.3	-5.3	-15.3	-15.3	-1.3	*****	*****	*****
18	-6.3	-6.3	-5.3	-2.3	-1.3	-1.3	-2.3	-6.3	-14.3	-14.3	-4.3	*****	*****	*****
17	.7	.7	.7	*****	.7	-.3	-.3	-2.3	-13.3	-16.3	-9.3	-1.3	*****	*****
16	1.7	*****	*****	*****	*****	.7	-.3	-2.3	-11.3	-16.3	-12.3	-7.3	-2.3	*****
15	*****	*****	*****	*****	*****	.7	-.3	-6.3	-2.3	-16.3	-13.3	-9.3	-4.3	*****
14	*****	*****	*****	-3.3	.7	-.3	-3.3	-4.3	-1.3	-14.3	-12.3	-10.3	-7.3	*****
13	-1.3	-2.3	-3.3	-6.3	-1.3	-3.3	-6.3	-1.3	-5.3	-11.3	-11.3	-10.3	-8.3	*****
12	-6.3	-7.3	-7.3	-7.3	-6.3	-6.3	-2.3	-3.3	-9.3	-11.3	-10.3	-9.3	-7.3	*****
11	-10.3	-10.3	-9.3	-8.3	-6.3	-6.3	-4.3	-5.3	-11.3	-10.3	-9.3	-8.3	-6.3	*****
10	-11.3	-11.3	-10.3	-9.3	-5.3	-5.3	-5.3	-7.3	-11.3	-10.3	-8.3	-7.3	*****	*****
9	-12.3	-12.3	-11.3	-11.3	-6.3	-6.3	-6.3	-9.3	-12.3	-9.3	-7.3	-6.3	*****	*****
8	-13.3	-13.3	-11.3	-11.3	-6.3	-6.3	-6.3	-11.3	-12.3	-8.3	-7.3	-6.3	*****	*****
7	-14.3	-13.3	-11.3	-11.3	-6.3	-7.3	-9.3	-13.3	-13.3	-10.3	-8.3	-7.3	*****	*****
6	-16.3	-15.3	-13.3	-11.3	-7.3	-8.3	-11.3	-14.3	-16.3	-10.3	-10.3	*****	*****	*****
5	-24.3	-18.3	-15.3	-13.3	-10.3	-9.3	-11.3	-15.3	-16.3	-11.3	-13.3	*****	*****	*****
4	-26.3	-23.3	-21.2	-18.3	-14.3	-12.3	-11.3	-10.3	-9.3	-14.3	-21.3	*****	*****	*****

X

Figure 57

MSL BOTTOM AND GROUND ELEVATIONS USED IN FINE GRID SUB-MODEL FOR JUNE 1967 CONDITIONS

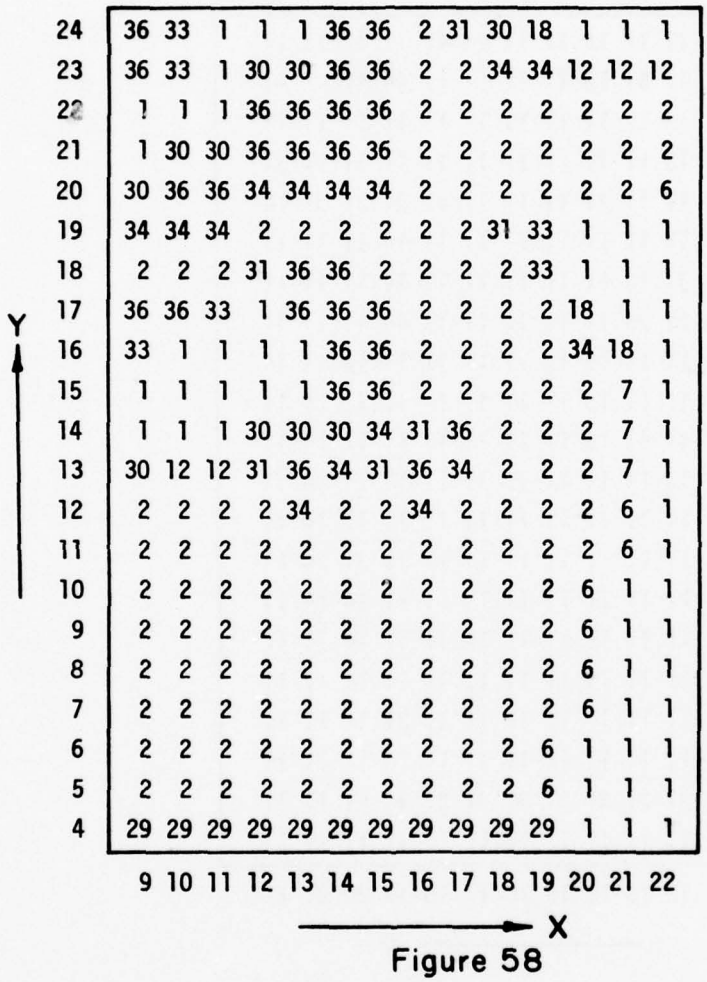

Figure 58

COMPUTATIONAL CELL FLAGS USED IN FINE GRID SUB-MODEL FOR JUNE 1967 CONDITIONS

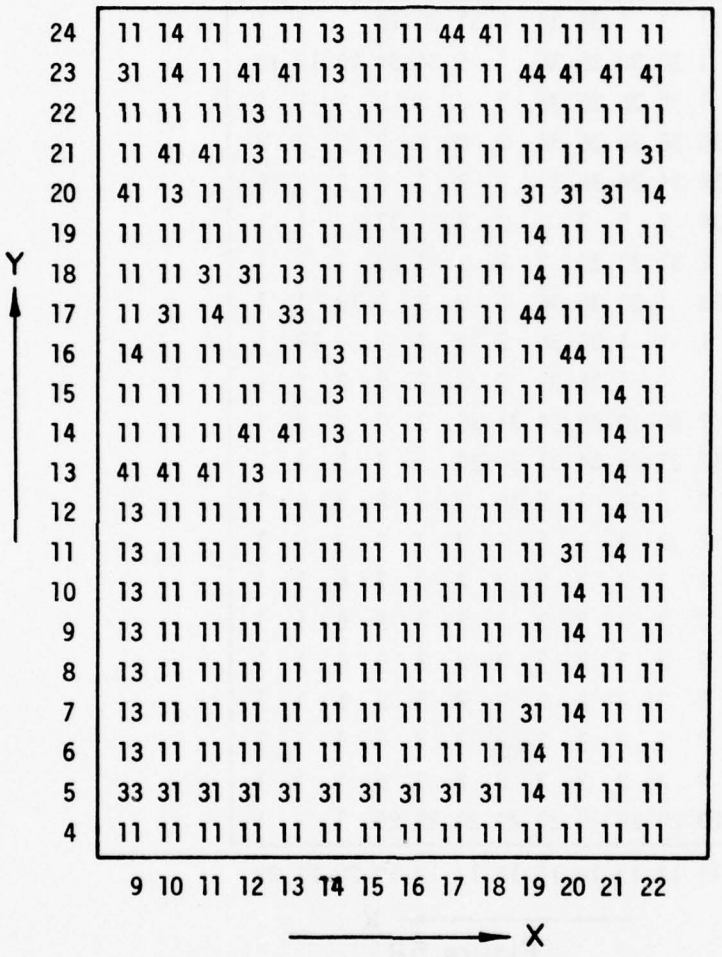

Figure 59

CONVECTIVE ACCELERATION CELL FLAGS USED IN FINE GRID SUB-MODEL FOR JUNE 1967 CONDITIONS

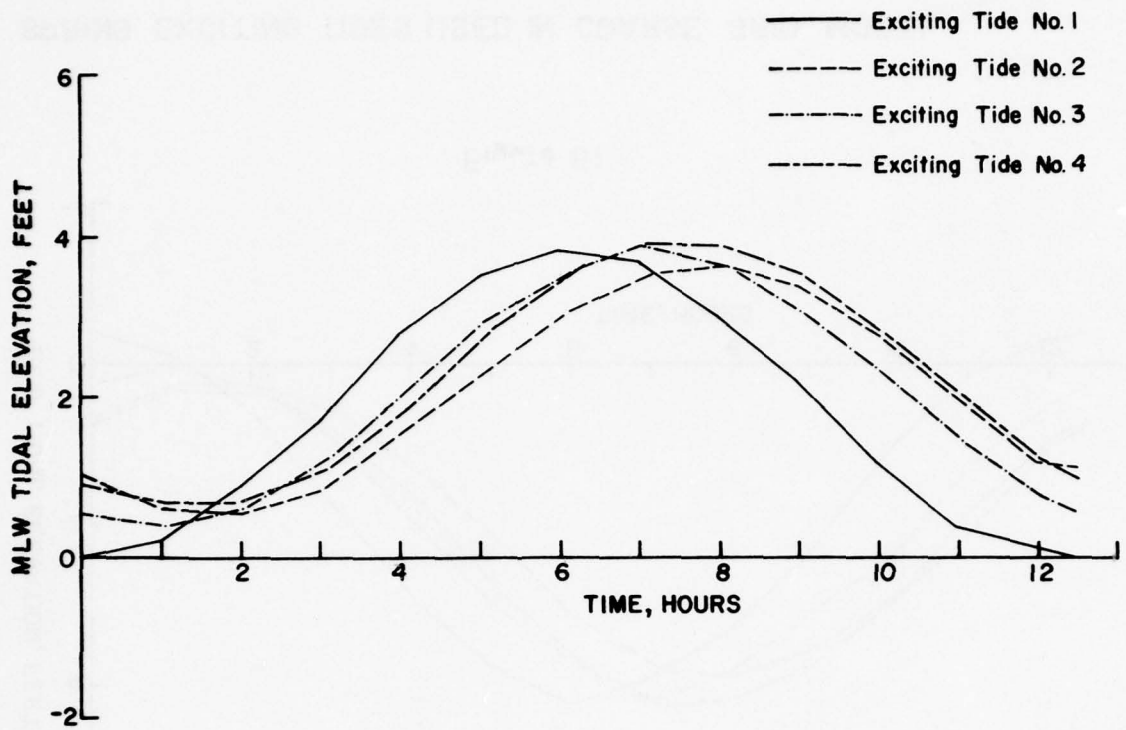

Figure 60

MEAN EXCITING TIDES USED IN COARSE GRID MODEL

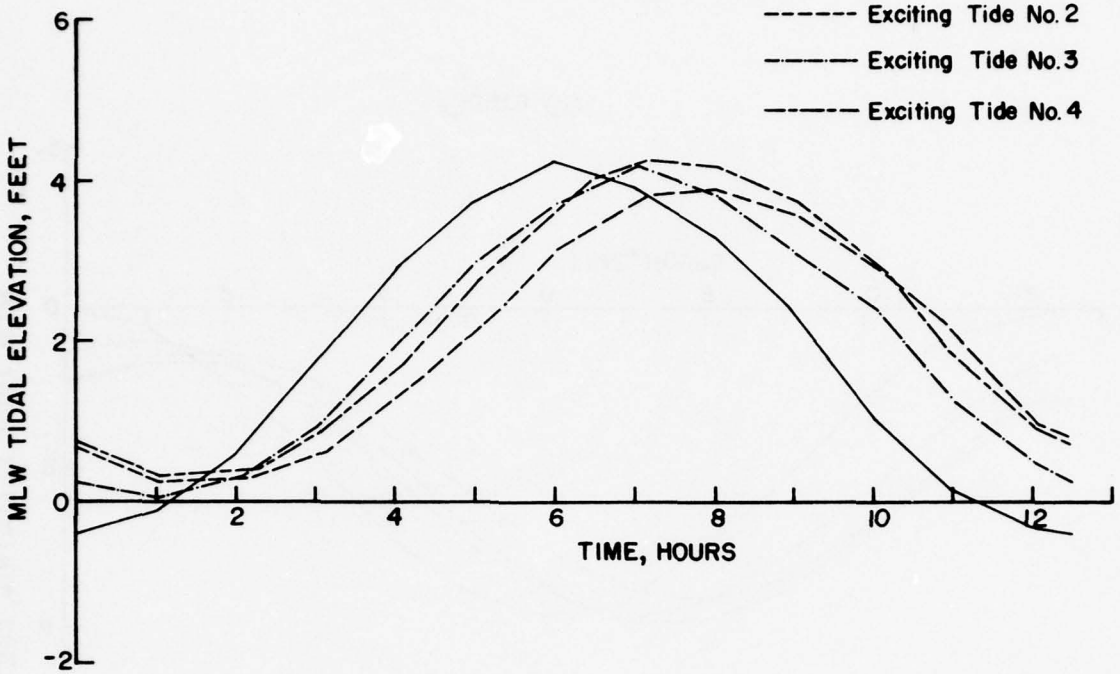

Figure 61

SPRING EXCITING TIDES USED IN COARSE GRID MODEL

Table 11. Bi-Modal Fourier Constants
Used to Approximate the Mean and Spring Tides

Parameter	Mean Tide	Spring Tide
A_o	1.88200	1.85040
C_{01}	1.93147	2.28753
Φ_{01}	-1.54206	-1.54514
C_{02}	0.03943	0.03028
Φ_{02}	-1.17606	-1.38140

Operational Results

Once the necessary changes had been made in the models to accommodate the physiographic conditions of the 1964 and 1967 operational periods, simulation of the hydrodynamics was carried out using the same procedure as that employed in the verification simulations. For each inlet geometry and prescribed exciting tide, the coarse grid model was operated to obtain the necessary boundary input flows for the fine grid sub-model. With the initial hydrodynamics set equal to zero, two complete tidal cycles (≈25 hours) were simulated with the flows and tides from the second cycle used to determine the inputs to the fine grid sub-model. Again the coarse grid flows were interpolated temporally and distributed spatially to provide the proper linkage with the fine grid flows. Time steps in both models were the same as those used in verification. With the fine grid exciting flows stored on magnetic tape, the fine grid sub-model was operated for two tidal cycles beginning with initial hydrodynamics set equal to zero. Results from the second cycle were used for presentation.

For both of the operational periods, the average wind condition for each of the months was included in the models for all of the simulations. The wind data was obtained from the NOAA Environmental Data Service Division in Asheville, North Carolina, and the wind conditions measured at the Wilmington, North Carolina, first order station were used in the models. The wind speed and direction were held constant throughout the entire simulation period.

The results from the simulations for each of the two inlet conditions with the mean and spring exciting tides are presented in the Appendix. Tidal elevations computed with the models are shown for each of the six tide gage locations in the inlet area. The same coarse grid cells identified in Table 6 were used to obtain the computed tides at the gage locations. Gage 0 results are not presented since it has been assumed that the prescribed offshore exciting tides (Figure 46) correspond to those which would occur at the Gage 0 location. The computed velocities are also shown at the same stations identified in Figure 4 which were used for model verification. Because the three stations at several of the velocity ranges were too closely spaced to allow each to be described with a separate cell in the fine grid, the velocity simulated for a single grid cell in some instances had to be used as the velocity which occurs at two adjacent stations. For this reason, some of the velocity plots in the Appendix correspond to two velocity stations, and they are labeled accordingly.

Using the mean and spring tidal flows computed across Range 2 in the fine grid sub-model, CELLS (17,17), (18,17), and (19,17), the total exchange during the flood period was determined for both the November 1964 and June 1967 inlet geometries. For the 1964 condition, the mean tidal exchange was

determined to be 489 million cubic feet and the spring tidal exchange was computed as 565 million cubic feet. Similarly for the 1967 inlet geometry with the jetty in place, mean and spring tidal exchanges were calculated to be 400 and 451 million cubic feet, respectively. These smaller values are consistent with those anticipated, and they reflect the changes made to ground elevations in each of the models for the two operational conditions, as well as the reduced influence of ocean exciting tides with the jetty in place.

Generalized velocity patterns at the maximum flood flow condition for both the mean and spring tides are shown in Figures 62 through 65 for each of the inlet geometries. Only slight differences are discernible between the mean and spring tidal conditions for the same inlet geometry, however as would be expected, there are very pronounced changes in the velocities for the simulations with and without the jetty in place. For the pre-project November 1964 condition, long-shore velocities are, of course, somewhat higher than those computed with the jetty and the result of these higher velocities is directly reflected in the exchange values presented above for the two inlet configurations.

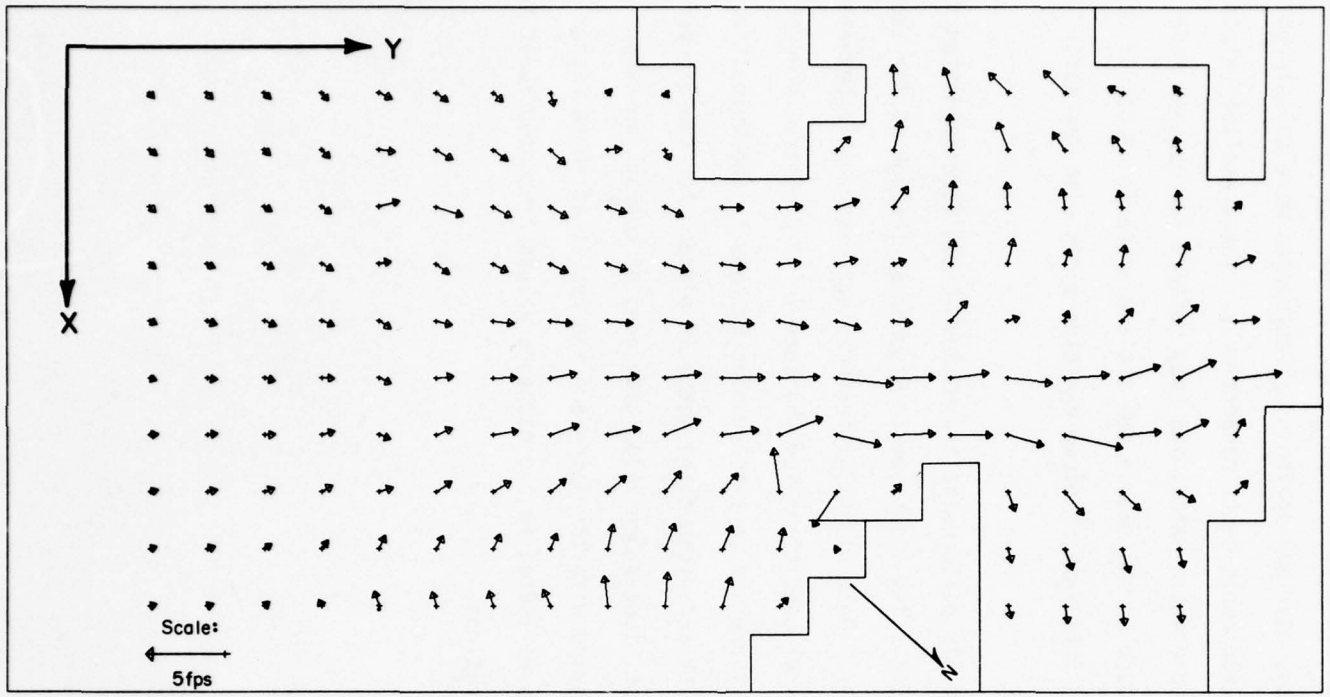

Figure 62

SIMULATED VELOCITY PATTERN AT MAXIMUM FLOOD FLOW CONDITION FOR MEAN TIDE, NOVEMBER 1964

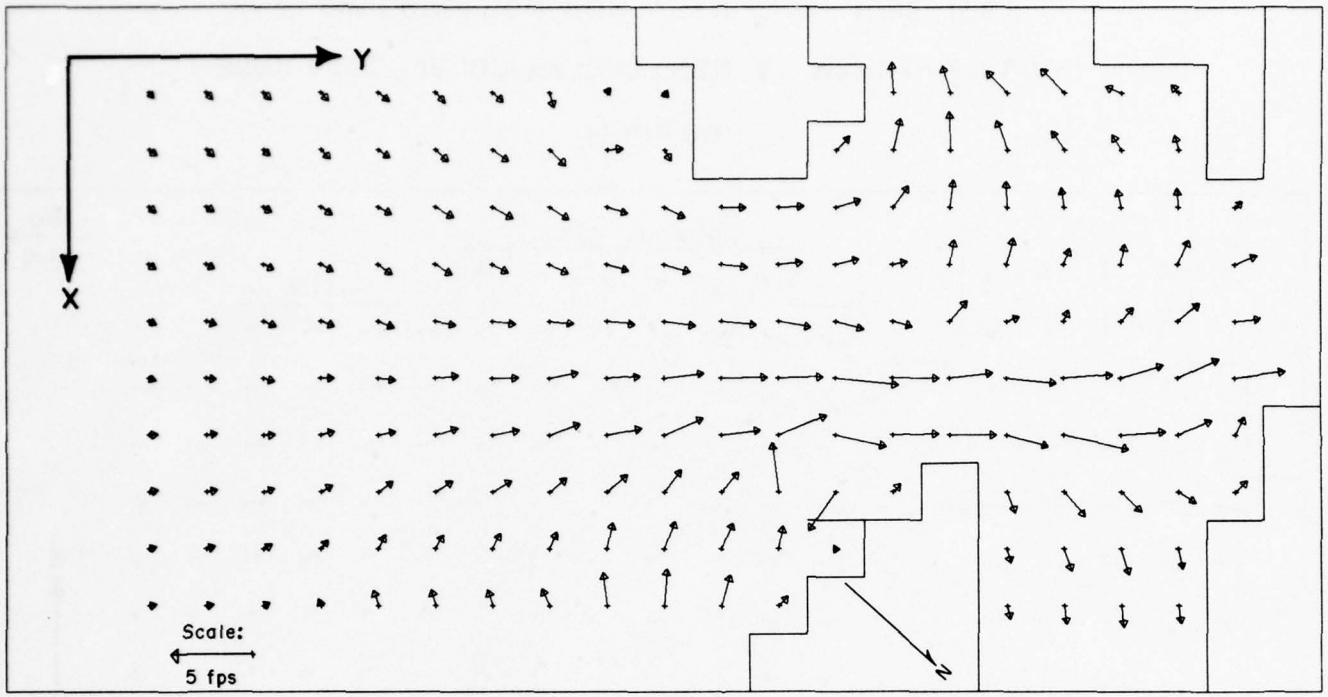

Figure 63

SIMULATED VELOCITY PATTERN AT MAXIMUM FLOOD FLOW CONDITION FOR SPRING TIDE, NOVEMBER 1964

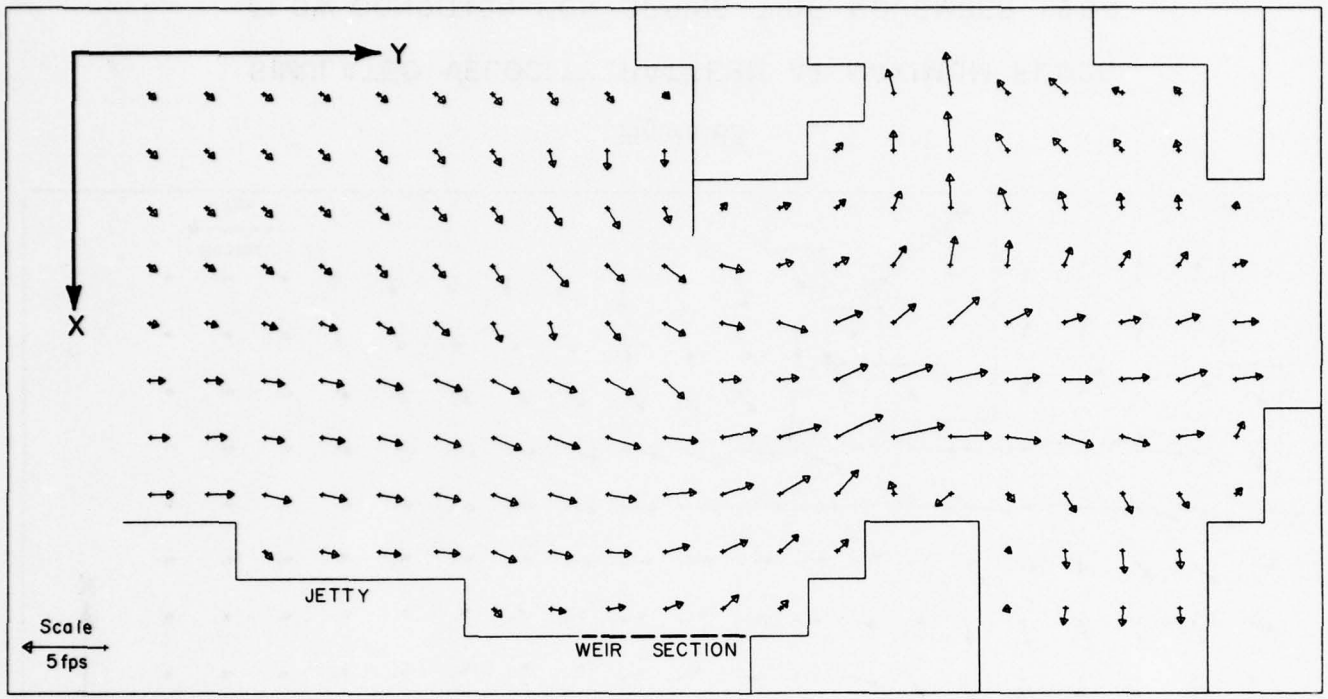

Figure 64

SIMULATED VELOCITY PATTERN AT MAXIMUM FLOOD FLOW CONDITION FOR MEAN TIDE, JUNE 1967

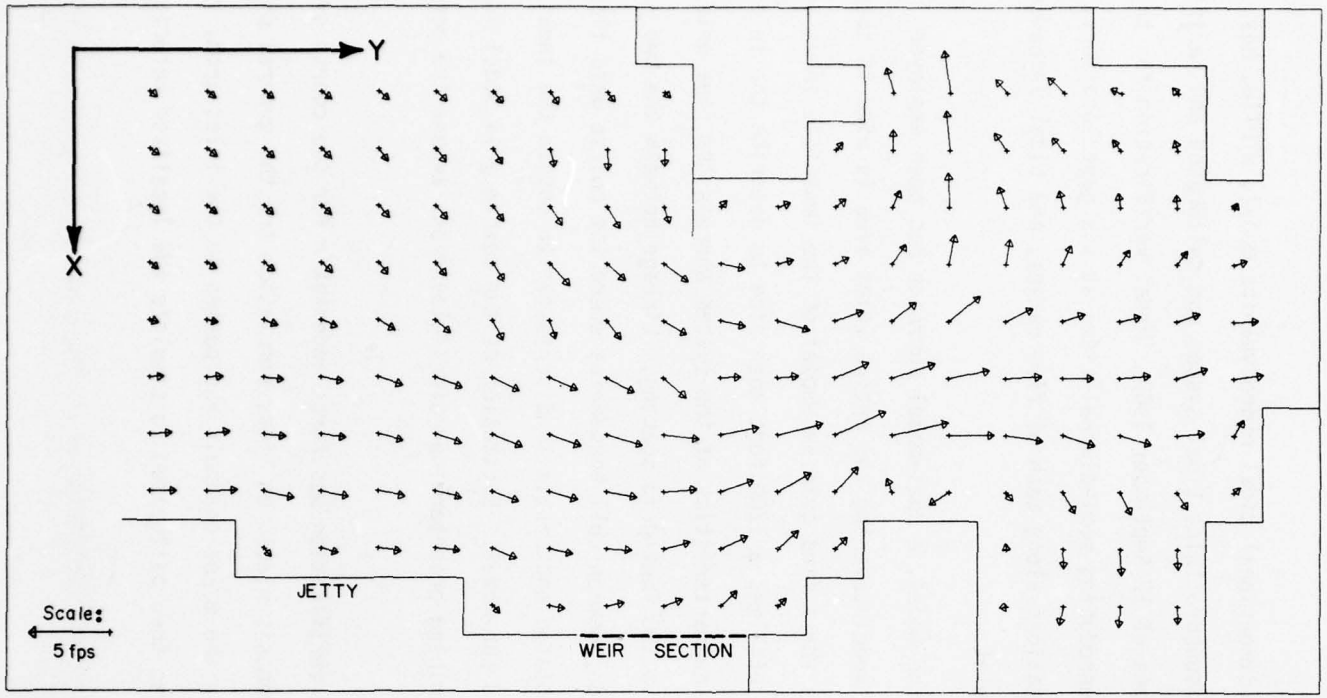

Figure 65

SIMULATED VELOCITY PATTERN AT MAXIMUM FLOW CONDITION FOR SPRING TIDE, JUNE 1967

V. SUMMARY AND RECOMMENDATIONS

A spatially two-dimensional tidal hydrodynamics model, HYDTID, has been applied to the Masonboro Inlet tidal system and calibrated and verified for prototype conditions of 12 September 1969. Model verification for this period consisted of reproducing semi-diurnal tides at six gage locations, velocities at three stations along each of five ranges, and tidal exchange at the mouth of the inlet.

In structuring the model, a dual-model approach has been employed whereby a coarse grid model covering the entire inlet area is used to generate the exciting flows for a fine grid sub-model of the immediate inlet area. The course grid model utilizes a 1200 foot mesh size to describe the inlet geometry and physical characteristics of the system whereas the fine grid sub-model is based on a 300 foot grid spacing. Linkage between the two models is provided along common cell boundaries where the coarse grid flows are temporally interpolated and spatially distributed to obtain the input flows to the fine grid sub-model. Excitation of the coarse grid model is accomplished by prescribing predetermined tidal elevations around the periphery of the model.

Calibration and verification was first undertaken for the coarse grid model with primary emphasis placed on tidal simulation and the general distribution of flows within the major channels and passes in the inlet area. The fine grid sub-model was then calibrated to simulate the localized velocities

at each of the stations along the velocity ranges. An important consideration in calibrating each of the models was that the relation between water depth and volume be the same in both of the models for that portion of the prototype included in the fine grid sub-model.

With both of the models satisfactorily calibrated and verified, operational runs were carried out to simulate the inlet hydrodynamics under mean and spring tidal conditions for two different inlet geometries. One series of runs corresponded to the November 1964 pre-project condition without the jetty, and the other was for the modified inlet configuration of June 1967 with the jetty in place. Alterations were made to each of the models to reflect the new inlet conditions and simulations were made for two complete tidal cycles. Results were compared at the same tide gage locations and velocity stations used for verifying the models.

It is believed that the conformity of the simulations obtained in this study are consistent with the numerical techniques employed in the model and the accuracy with which field measurements can be made. While it is possible to obtain even better agreement between the computed and measured values by making further model adjustments, small incremental improvements can be achieved only at the expense of additional calibration runs. Such extended verification may not be justified without at least some supplemental flow information at some other locations near the inlet. Also it would be desirable to extend the model verification to other tidal conditions. With respect to operation of the Masonboro Inlet models, the following specific recommendations should be considered.

1. *As additional prototype information becomes available the models should be applied and adjusted as required to extend their range of verification.*

2. *The correlations between the offshore tide and those prescribed at the inland artificial tidal-storage boundaries should be tested for other tidal conditions.*

3. *Although the coarse and fine grid models in their present form use time steps of twenty and five seconds, respectively, it is suggested that increments of twenty-four and six seconds be used if it is desired to reduce computational run time.*

For future applications of HYDTID to other tidal inlets, consideration should be given to the following.

1. *In order to facilitate the application of HYDTID, concerted effort should be made to collect the information necessary to establish model boundary conditions rather to develop them in the calibration process.*

2. *When employing the dual-model approach it would be desirable to incorporate in the program an internal check on the depth-volume relations of the two models.*

3. *The HYDTID program could be refined by:*

   a. *Elimination of those subroutines not required for a specific simulation of inlet hydrodynamics, and*

   b. *Further generalization of the program to provide for direct input of all required model data.*

The Masonboro Inlet problem is certainly one of the more complex applications of HYDTID. The major difficulty encountered was providing the necessary spatial resolution to describe the local detail in a cost-effective manner. While the methodology employed proved workable, it is probable that a more efficient procedure could be developed within the HYDTID framework. Such procedure might involve a variable grid or a series of non-overlapping sub-models with different mesh sizes systematically linked through the hydrodynamics.

LITERATURE CITED

[1] Brandes, R. J. and Masch, F. D., "Tidal Hydrodynamic and Salinity Models for San Antonio and Matagorda Bays, Texas", Report to the Texas Water Development Board, June 1971a, Frank D. Masch and Associates, Austin, Texas.

[2] Brandes, R. J. and Masch, F. D., "Analysis of Tidal Hydrodynamics and Salinity - Estuario del Cano Macareo, Venezuela", Report to Konstantin Zagustin, Ingeniero Consultor, Caracas, November 1971b, Frank D. Masch and Associates, Austin, Texas.

[3] Brandes, R. J. and Masch, F. D., "Hurricane Tides in Cayo del Oso", Report to the City of Corpus Christi, Texas, March 1972, Water Resources Engineers, Inc., Austin, Texas.

[4] Dronkers, J. J., *Tidal Computations in Rivers and Coastal Waters*, North Holland Publishing Co., Amsterdam, Publishers: John Wiley and Sons Inc., New York, 1964.

[5] Masch, F. D., Shankar, N. J., Jeffrey, M., Brandes, R. J. and White, W. A., "A Numerical Model for the Simulation of Tidal Hydrodynamics in Shallow Irregular Estuaries", Tech. Rep. HYD 12-6901 to the Office of Water Resources Research, February 1969, Hydraulic Engineering Laboratory, The University of Texas at Austin.

[6] Masch, F. D. and Brandes, R. J., "Tidal Hydrodynamic Simulation in Shallow Estuaries", Tech. Rep. HYD 12-7102 to the Office of Water Resources Research, August 1971, Hydraulic Engineering Laboratory, The University of Texas at Austin.

[7] Reid, R. O. and Bodine, B. R., "Numerical Model for Storm Surges in Galveston Bay", Journal of Waterways and Harbors Division, Proceedings, ASCE, Vol. 94, No. WW1, February 1968, pp. 33-57.

[8] Roll, H. V., *Physics of the Marine Atmosphere*, International Geophysics Series, Vol. 7, Academic Press, New York and London, 1965, pp. 158-159.

[9] *Tide Tables, East Coast, North and South America, 1969*, U. S. Department of Commerce, Coast and Geodetic Survey, Washington, D. C.

[10] Wilson, B. W., "Note on Surface Wind Stress over Water at Low and High Speeds", Journal of Geophysical Research, Vol. 65, No. 10, October 1960, pp. 3377-3382.

Appendix A

SIMULATED RESULTS FOR NOVEMBER 1964 INLET GEOMETRY

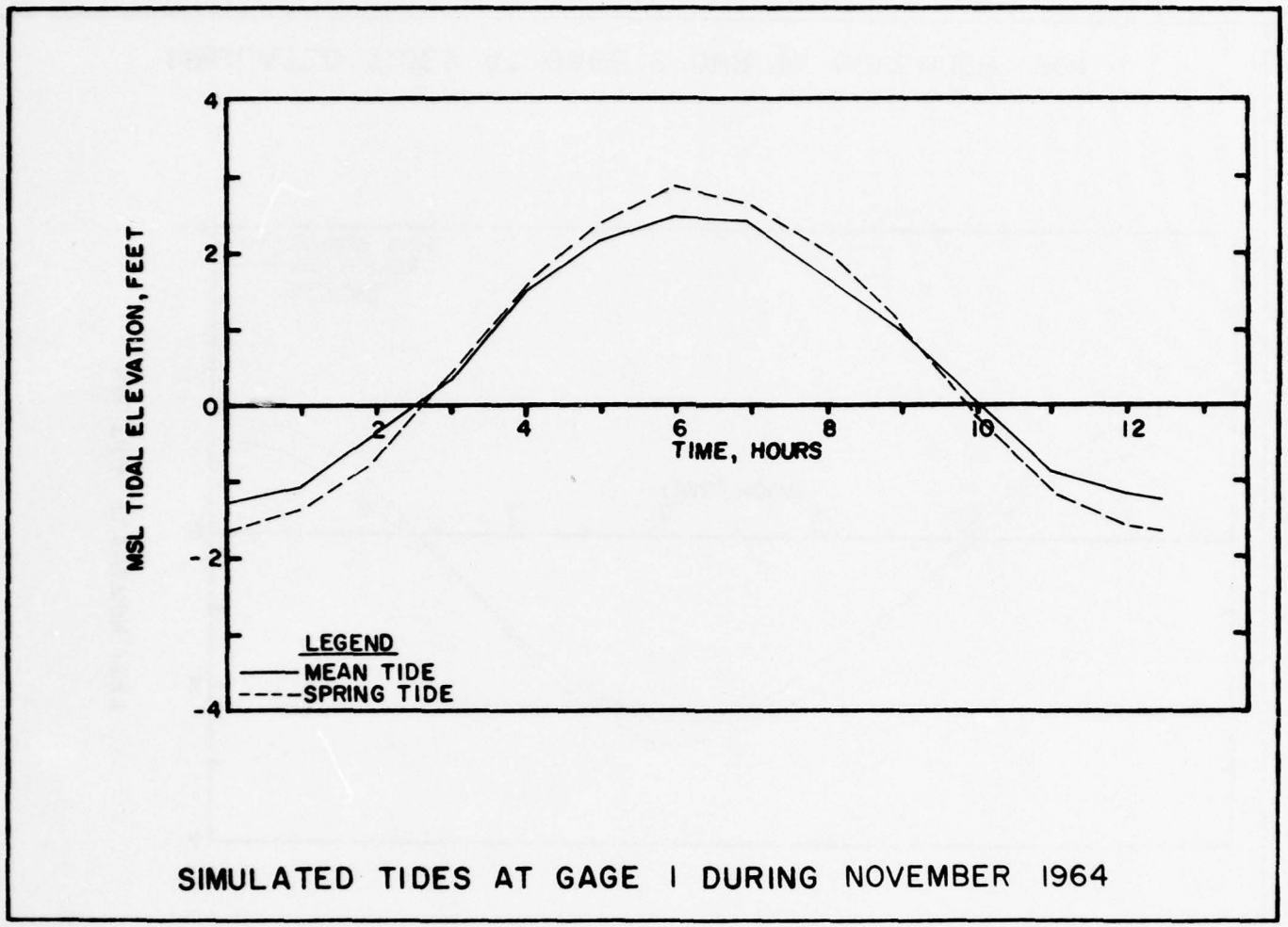

SIMULATED TIDES AT GAGE I DURING NOVEMBER 1964

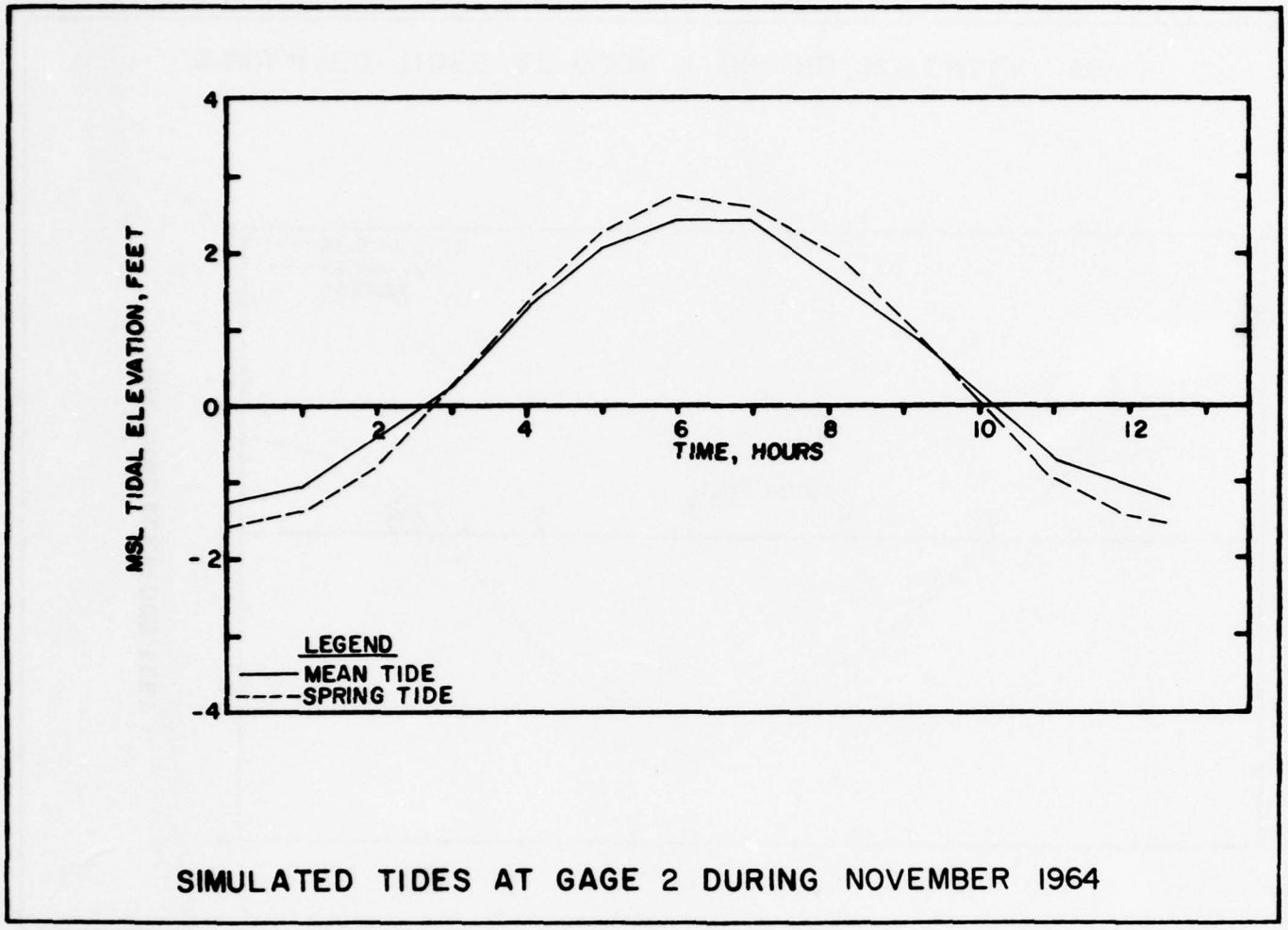

SIMULATED TIDES AT GAGE 2 DURING NOVEMBER 1964

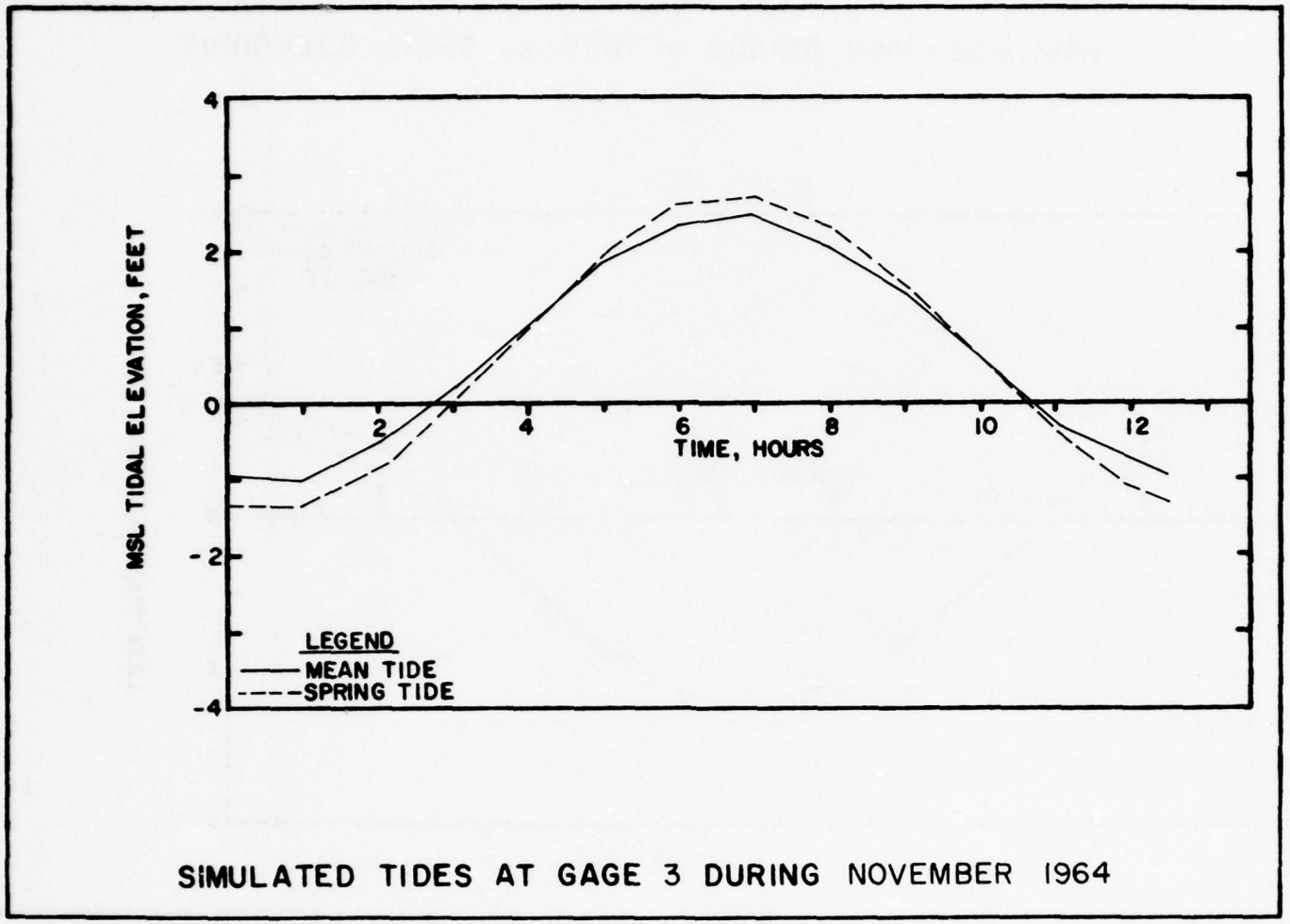

SIMULATED TIDES AT GAGE 3 DURING NOVEMBER 1964

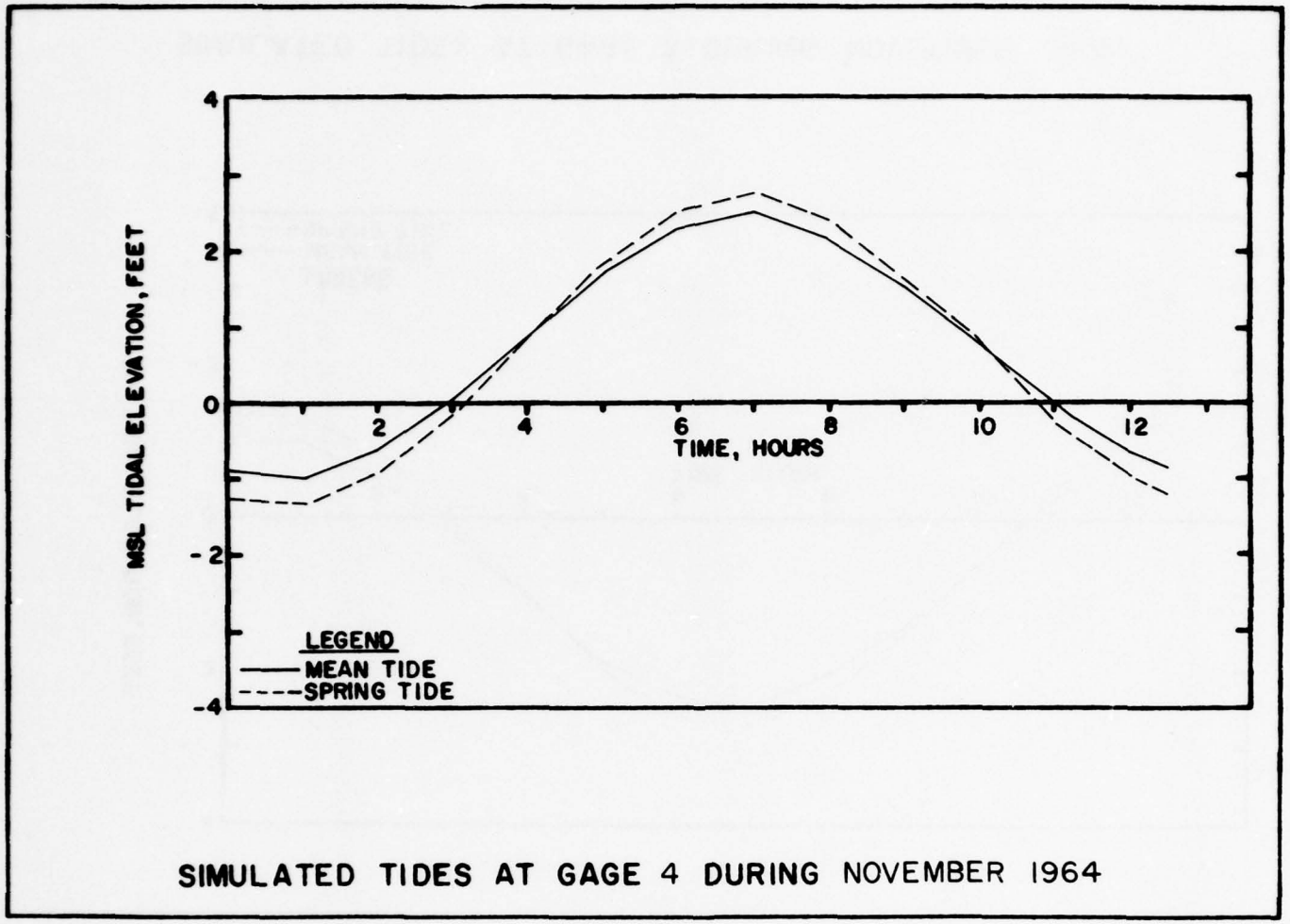

SIMULATED TIDES AT GAGE 4 DURING NOVEMBER 1964

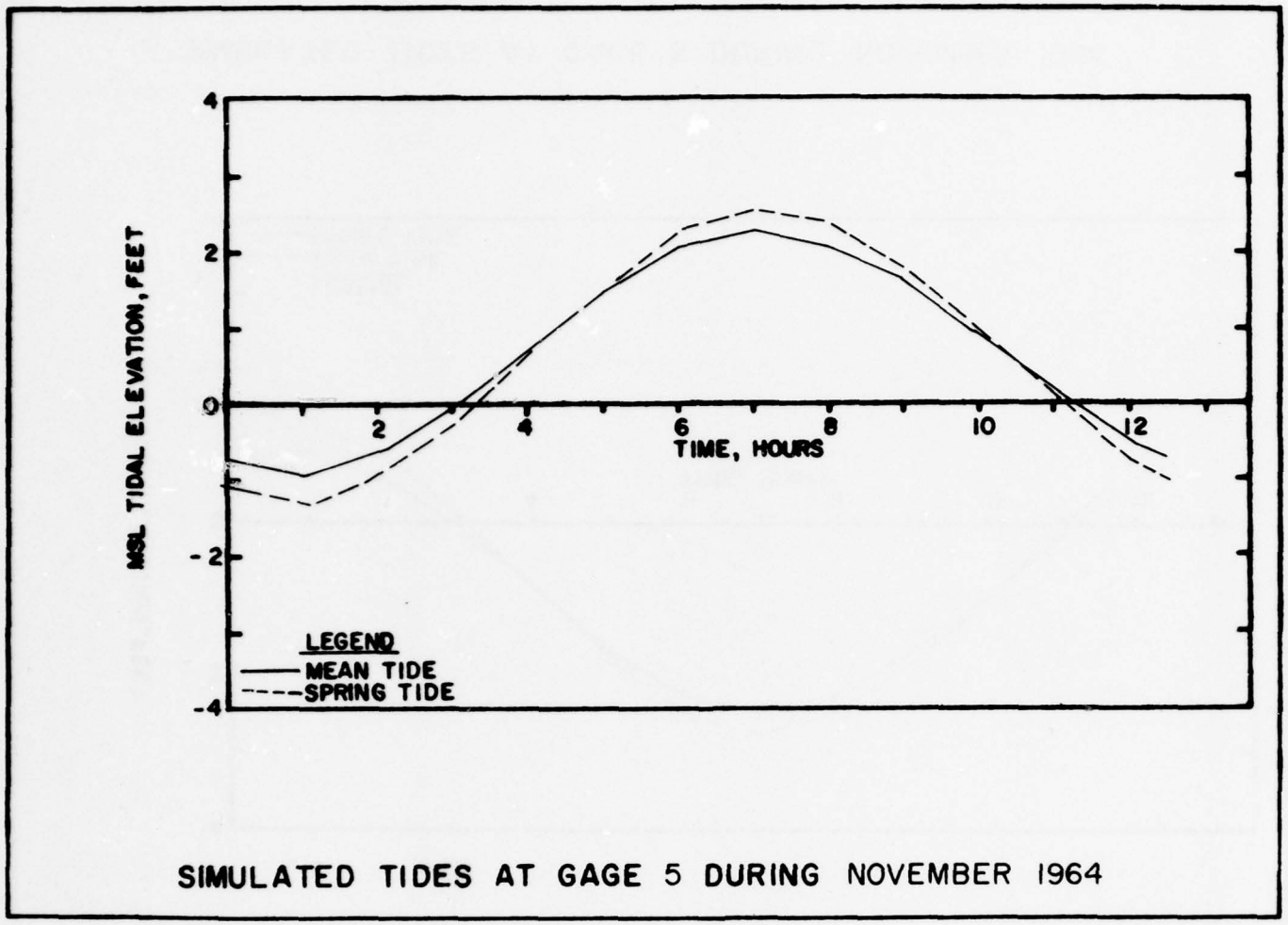

SIMULATED TIDES AT GAGE 5 DURING NOVEMBER 1964

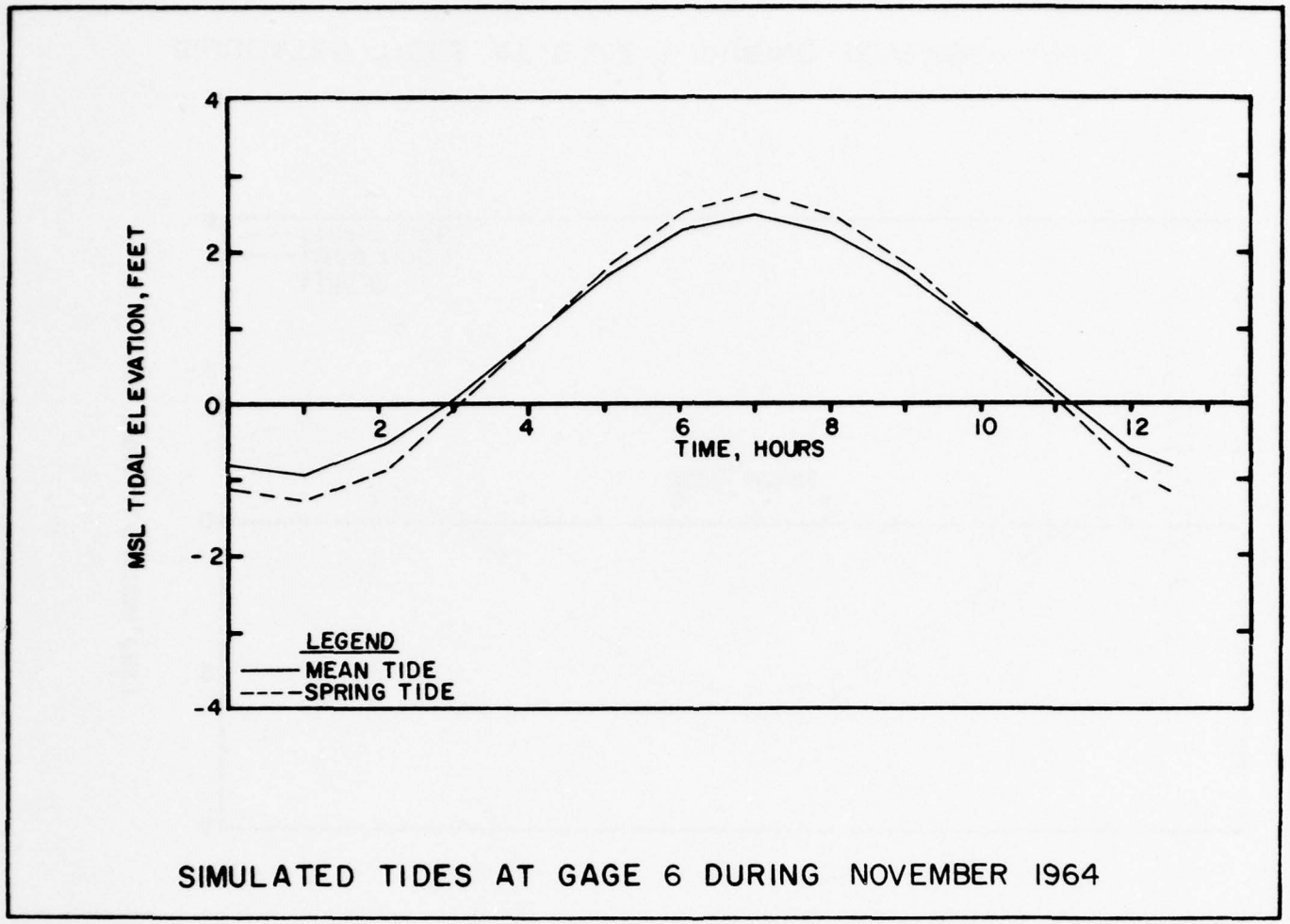

SIMULATED TIDES AT GAGE 6 DURING NOVEMBER 1964

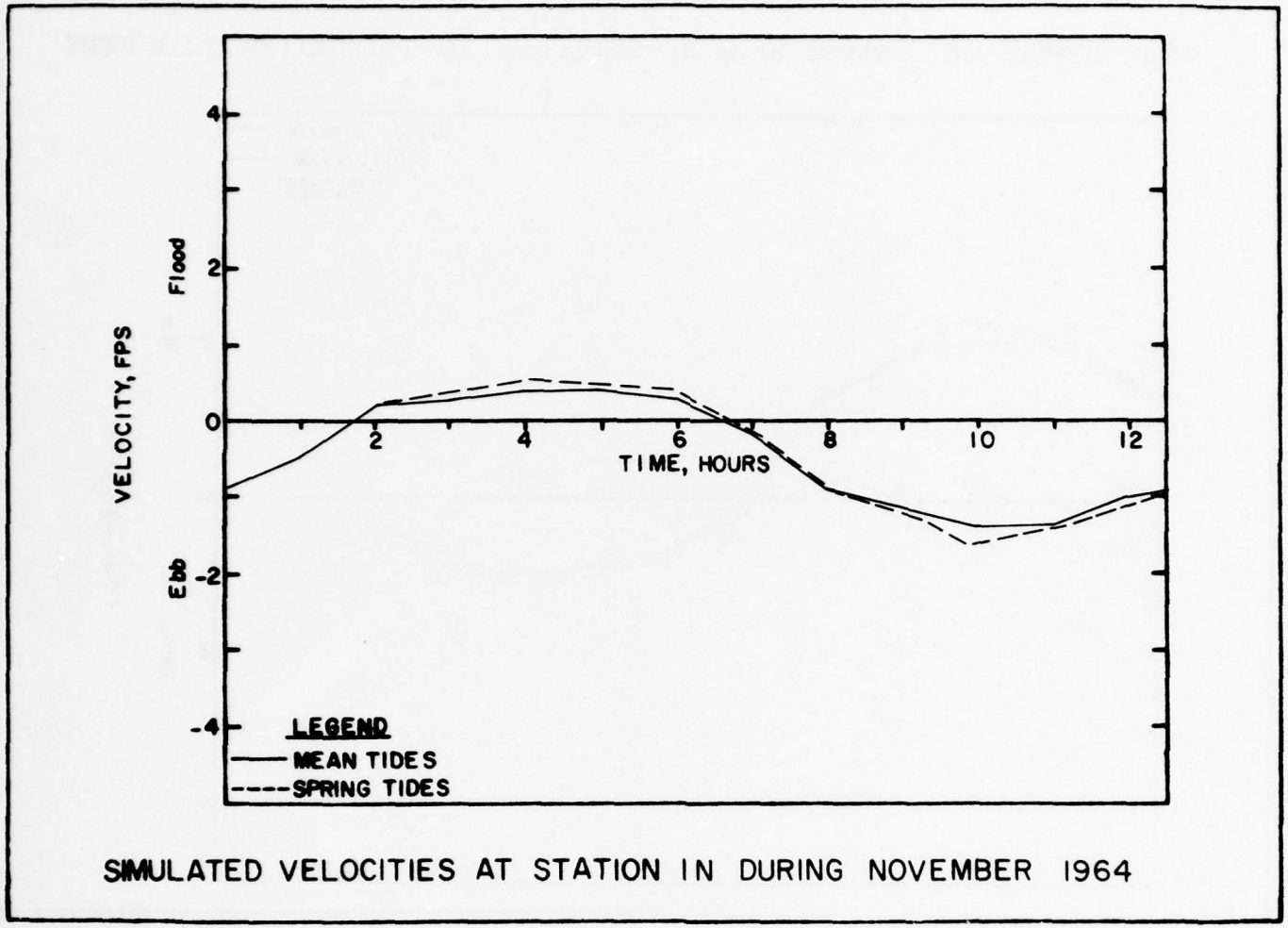

SIMULATED VELOCITIES AT STATION IN DURING NOVEMBER 1964

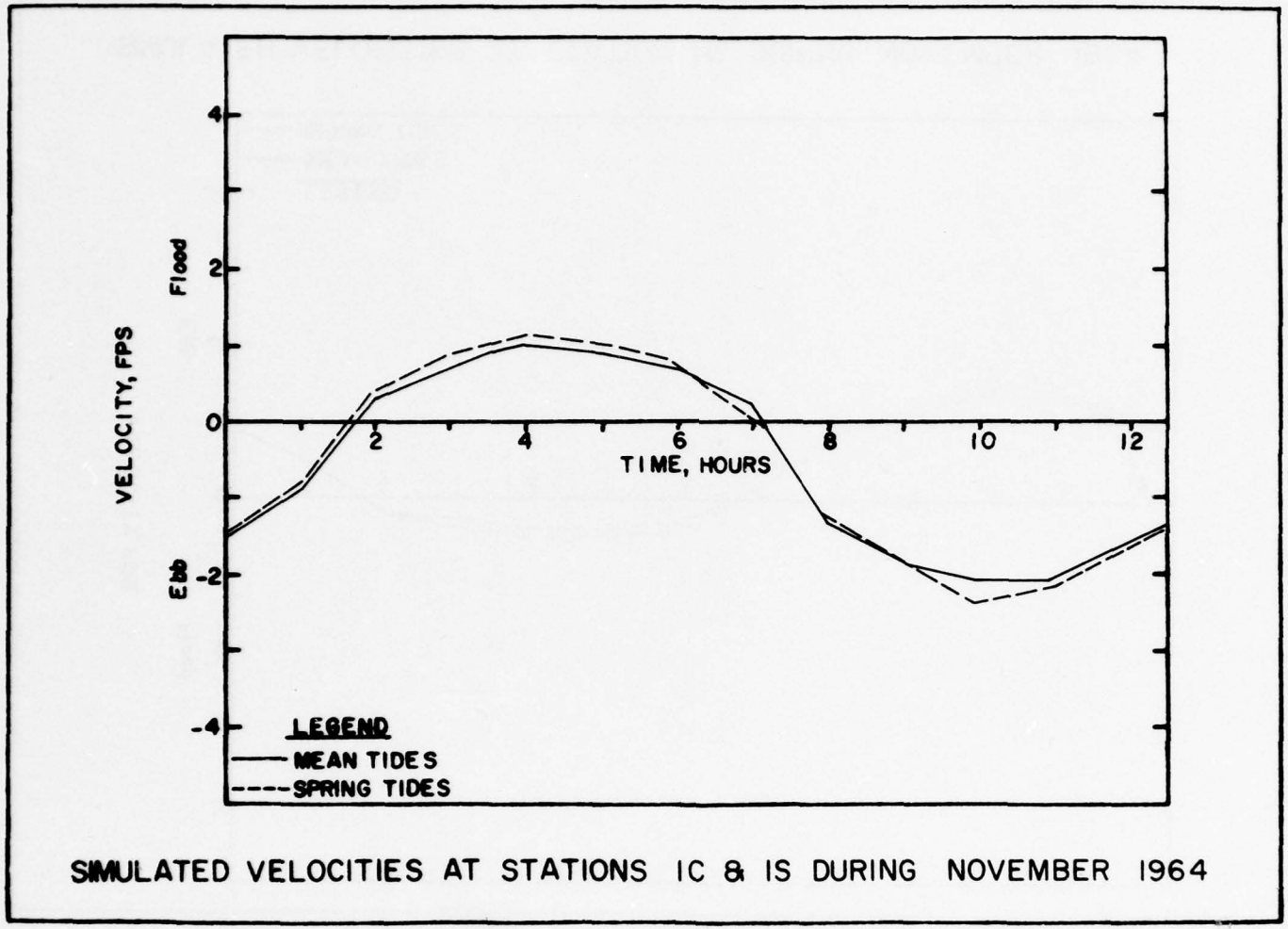

SIMULATED VELOCITIES AT STATIONS IC & IS DURING NOVEMBER 1964

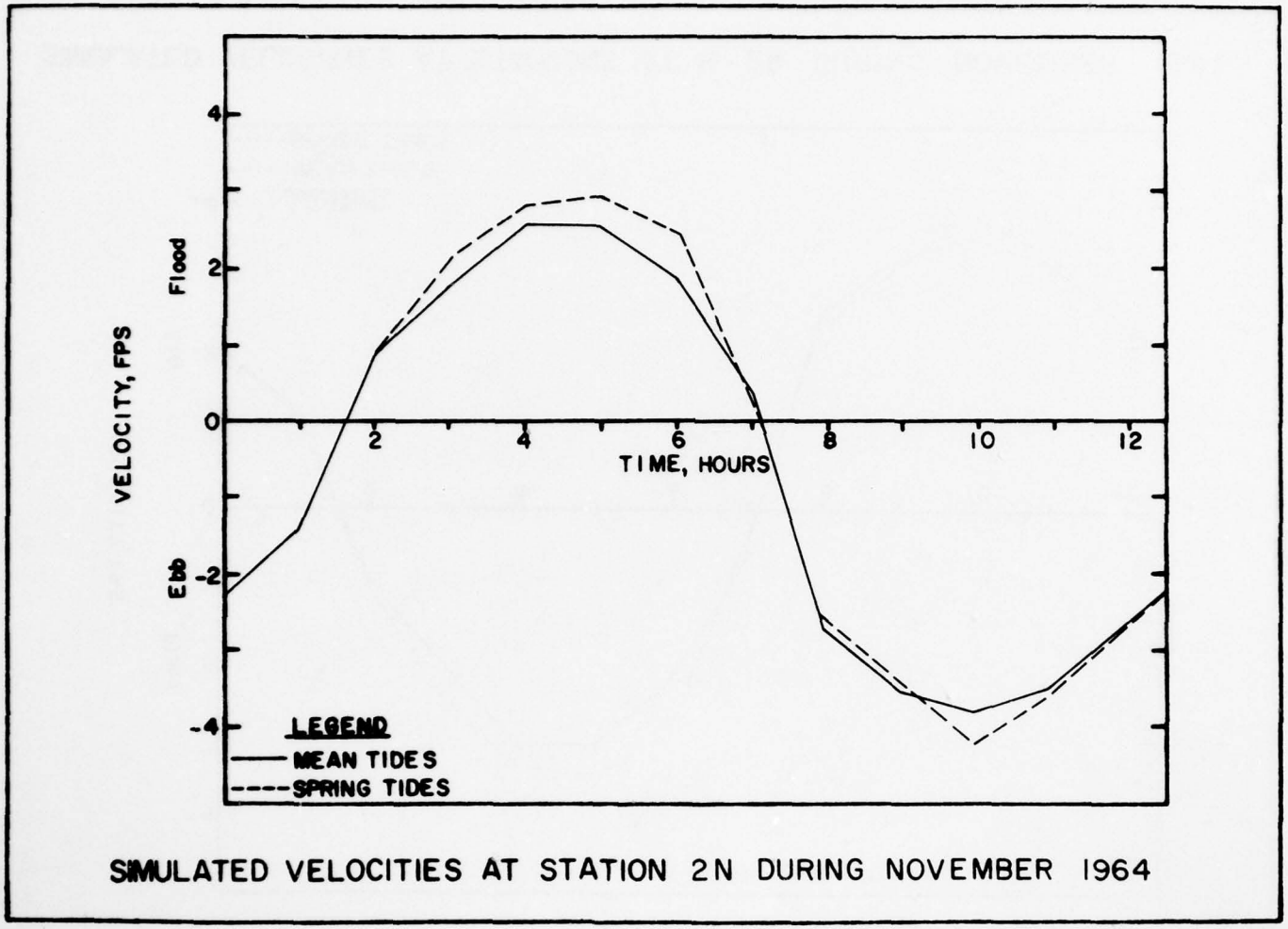

SIMULATED VELOCITIES AT STATION 2N DURING NOVEMBER 1964

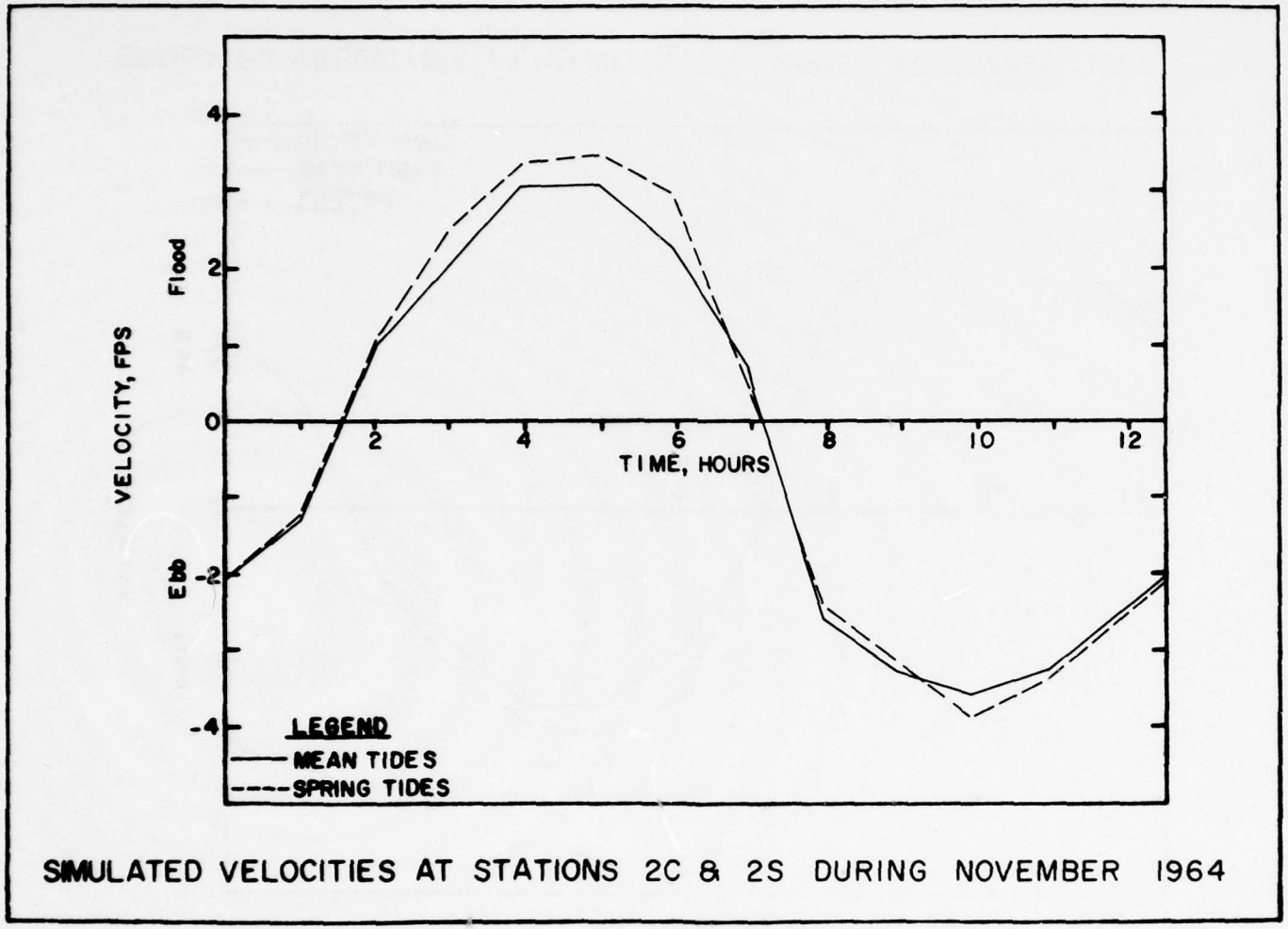

SIMULATED VELOCITIES AT STATIONS 2C & 2S DURING NOVEMBER 1964

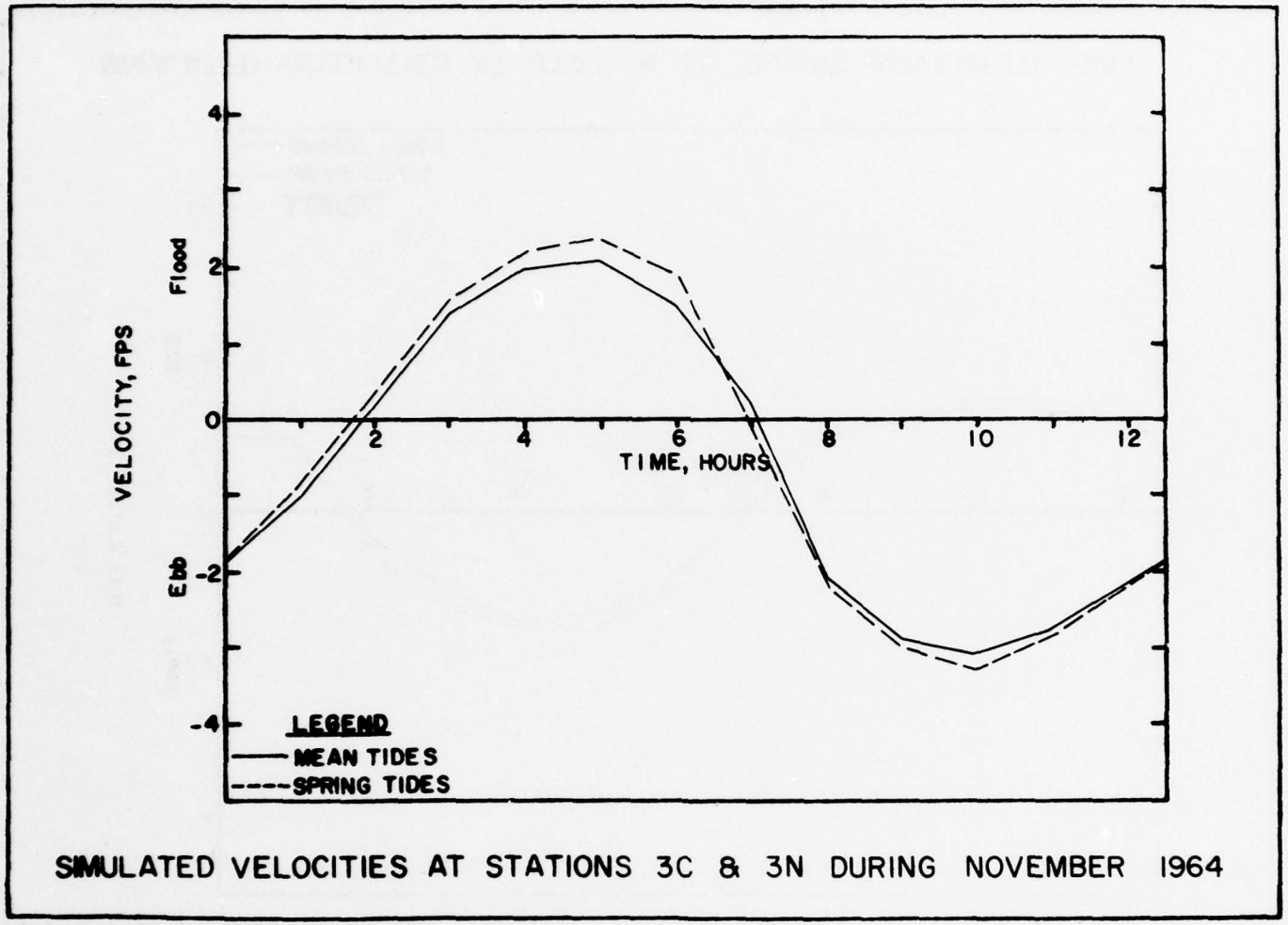

SIMULATED VELOCITIES AT STATIONS 3C & 3N DURING NOVEMBER 1964

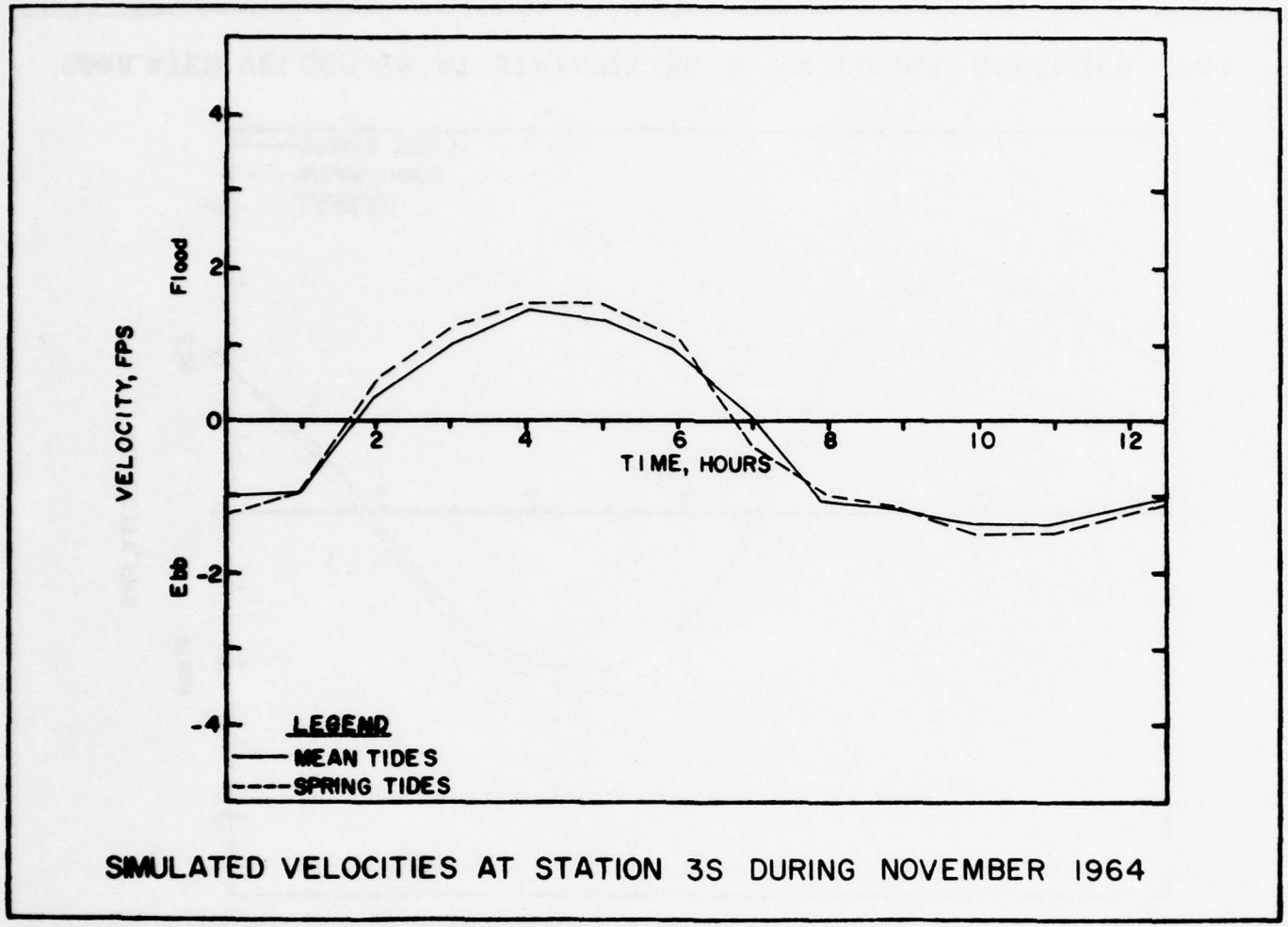

SIMULATED VELOCITIES AT STATION 3S DURING NOVEMBER 1964

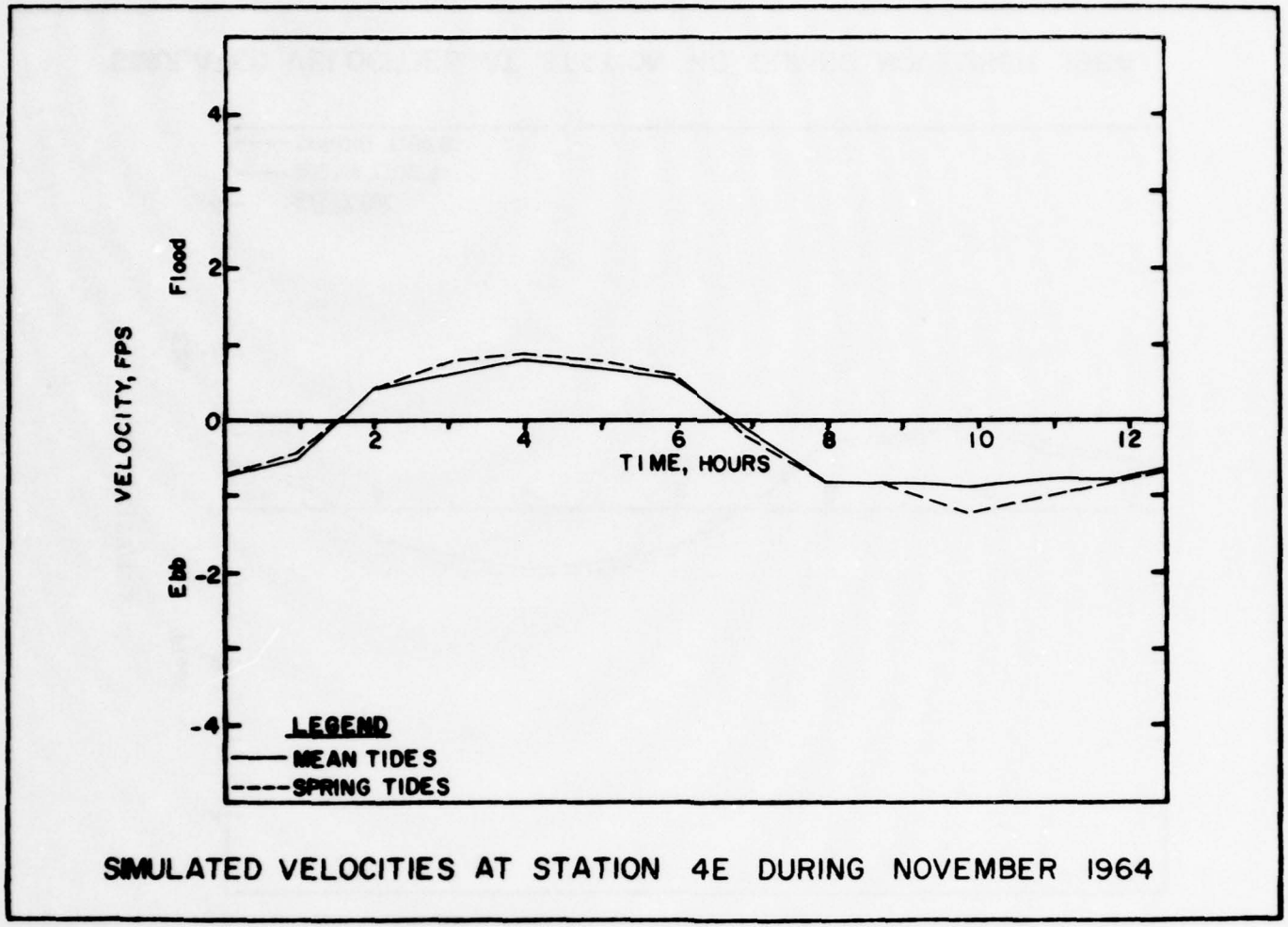

SIMULATED VELOCITIES AT STATION 4E DURING NOVEMBER 1964

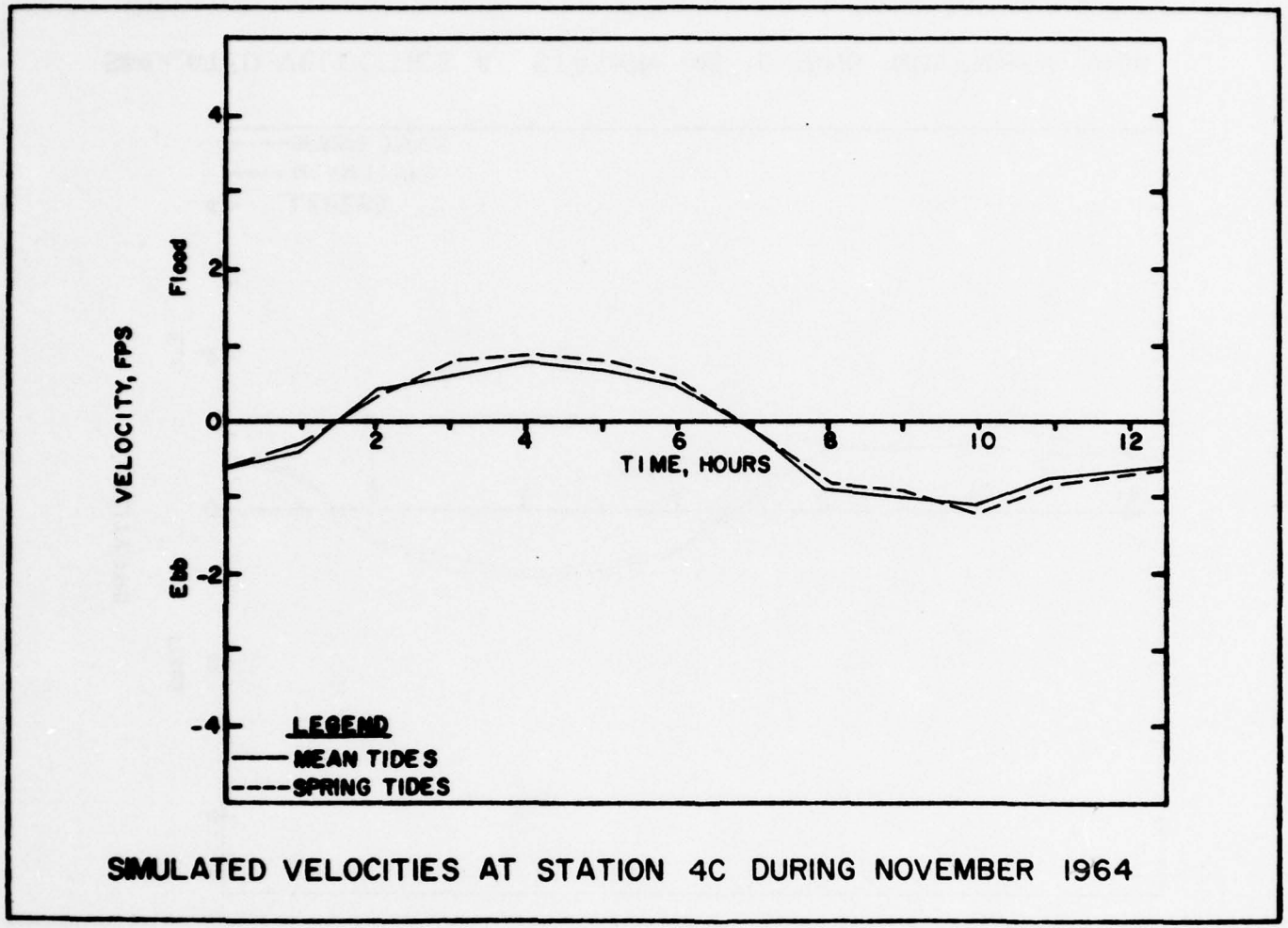

SIMULATED VELOCITIES AT STATION 4C DURING NOVEMBER 1964

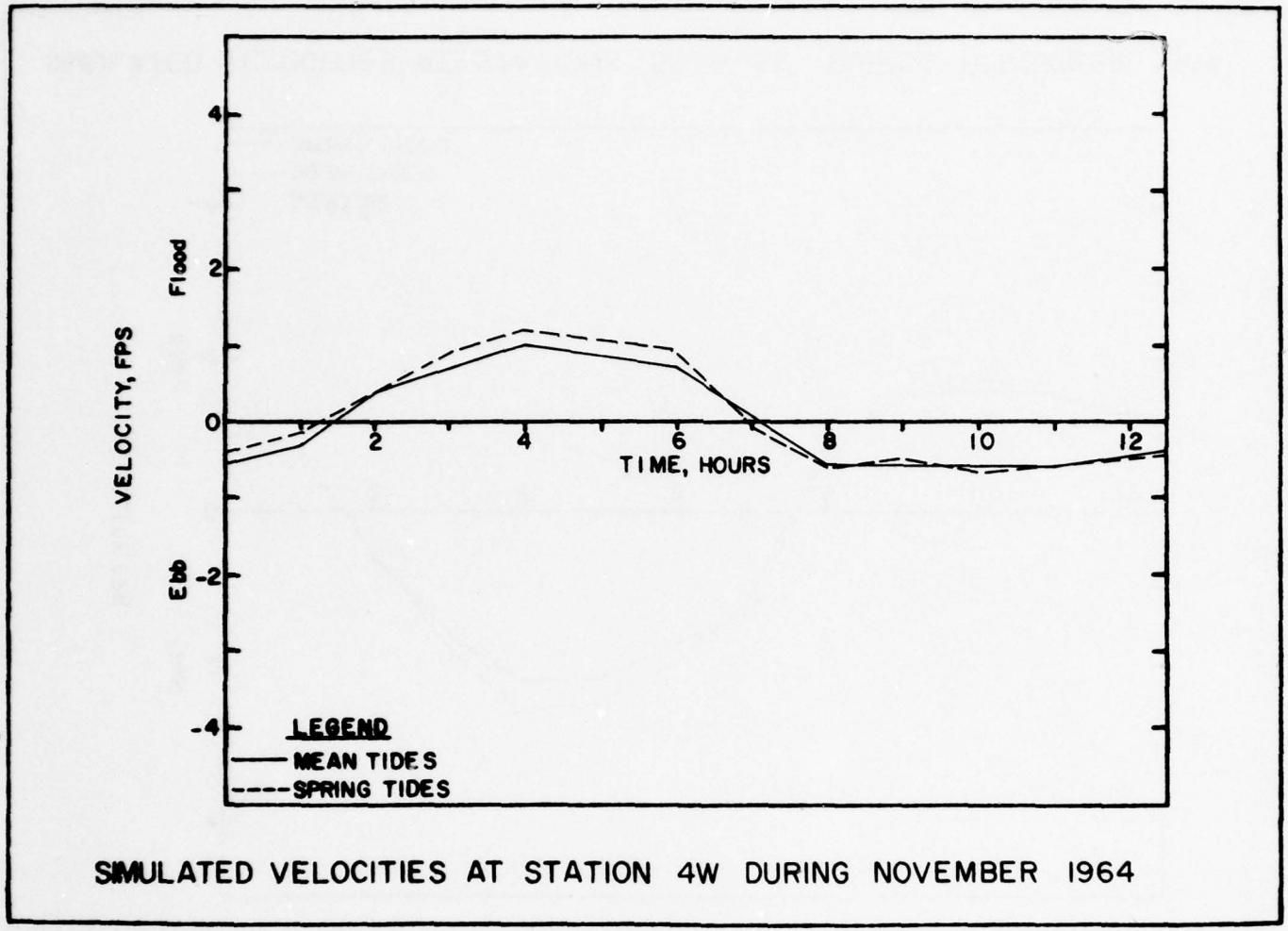

SIMULATED VELOCITIES AT STATION 4W DURING NOVEMBER 1964

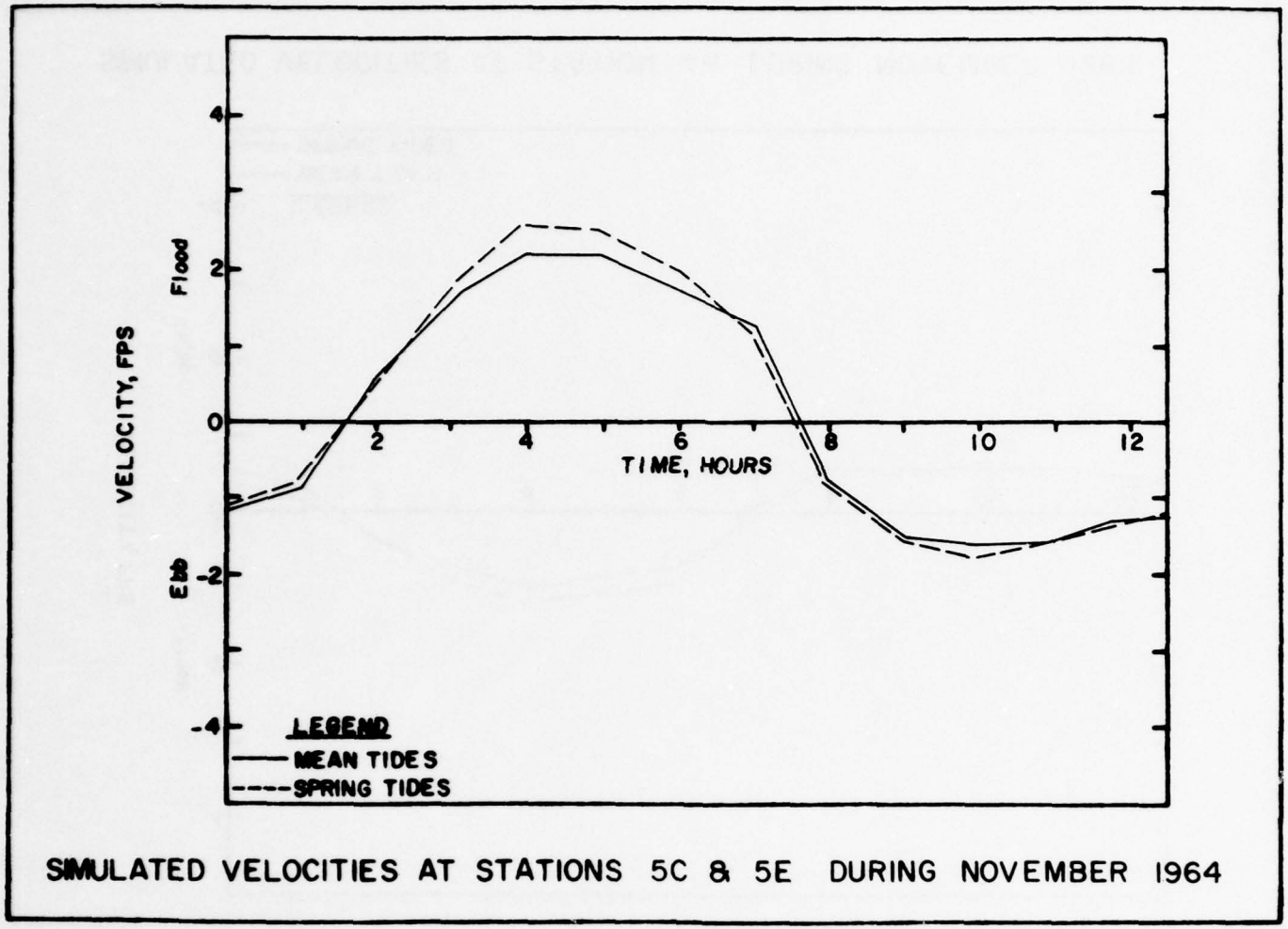

SIMULATED VELOCITIES AT STATIONS 5C & 5E DURING NOVEMBER 1964

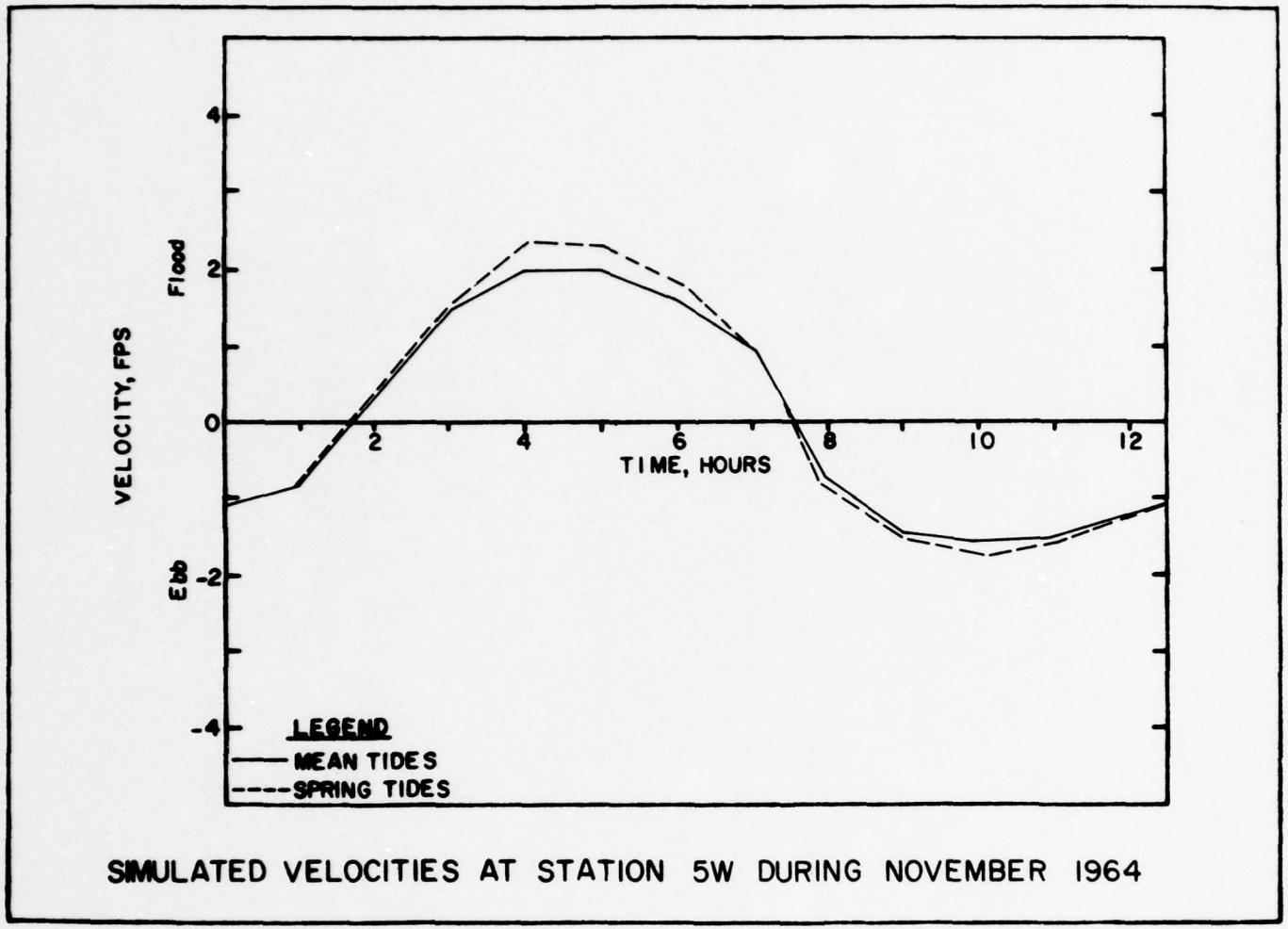

SIMULATED VELOCITIES AT STATION 5W DURING NOVEMBER 1964

Appendix B

SIMULATED RESULTS FOR JUNE 1967 INLET GEOMETRY

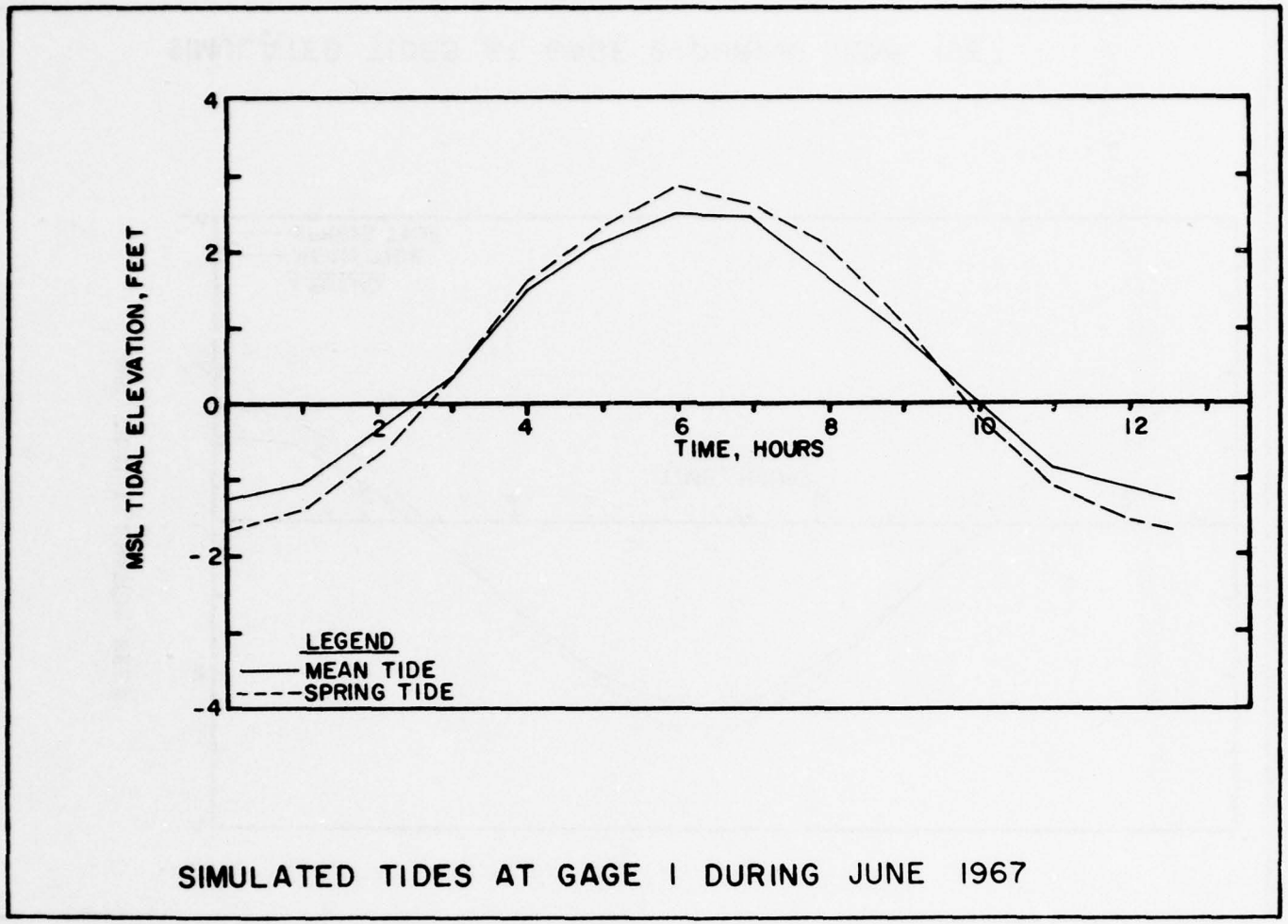

SIMULATED TIDES AT GAGE I DURING JUNE 1967

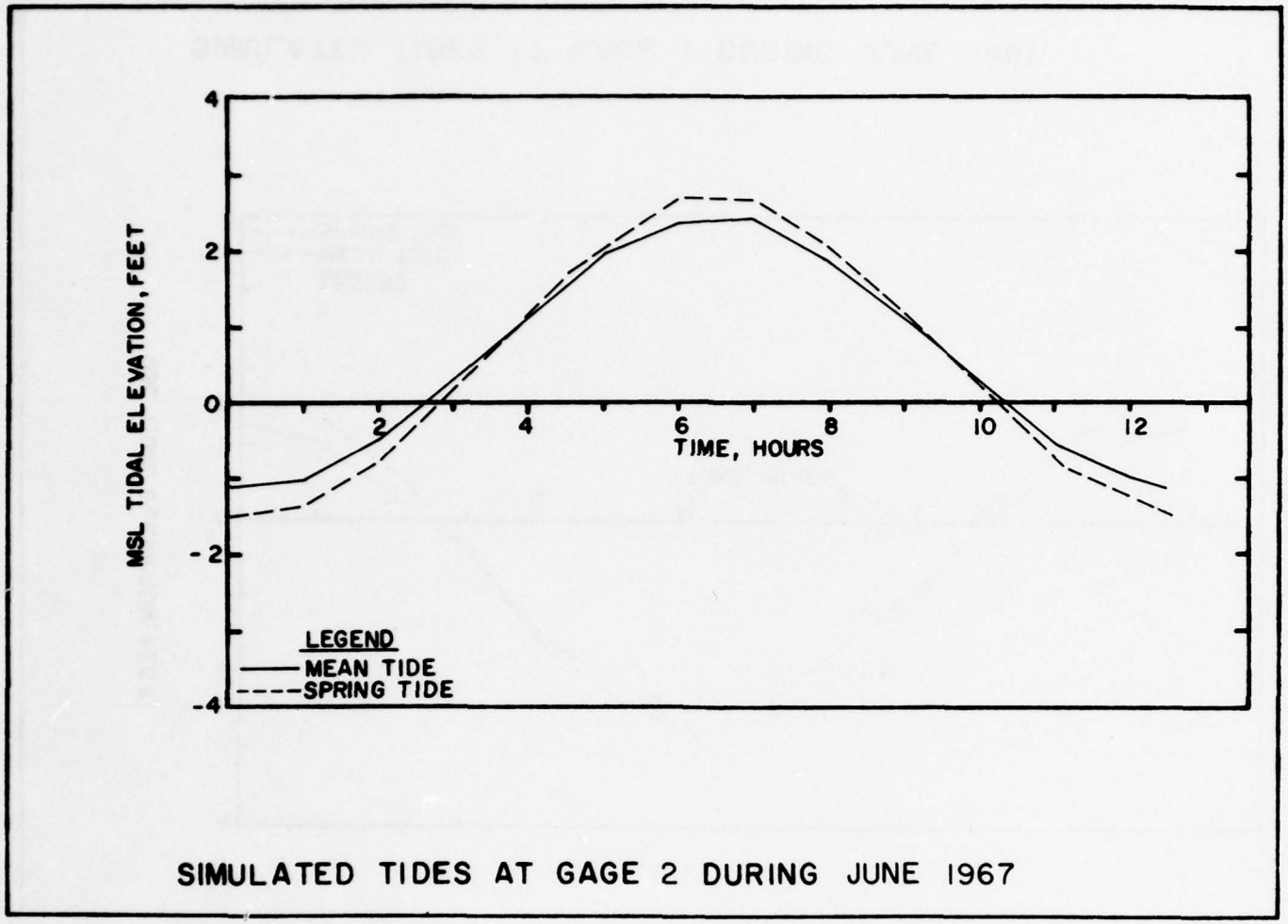

SIMULATED TIDES AT GAGE 2 DURING JUNE 1967

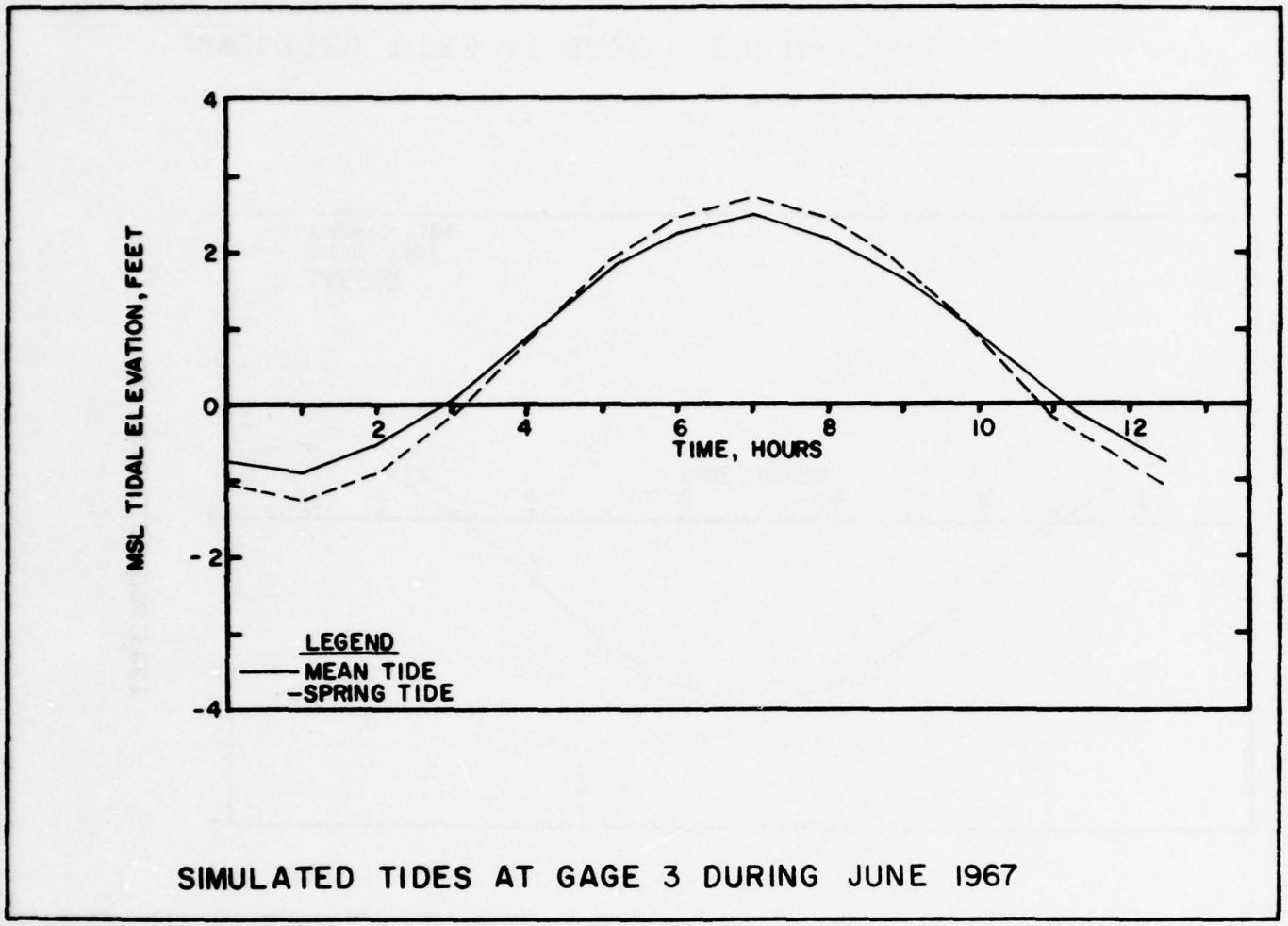

SIMULATED TIDES AT GAGE 3 DURING JUNE 1967

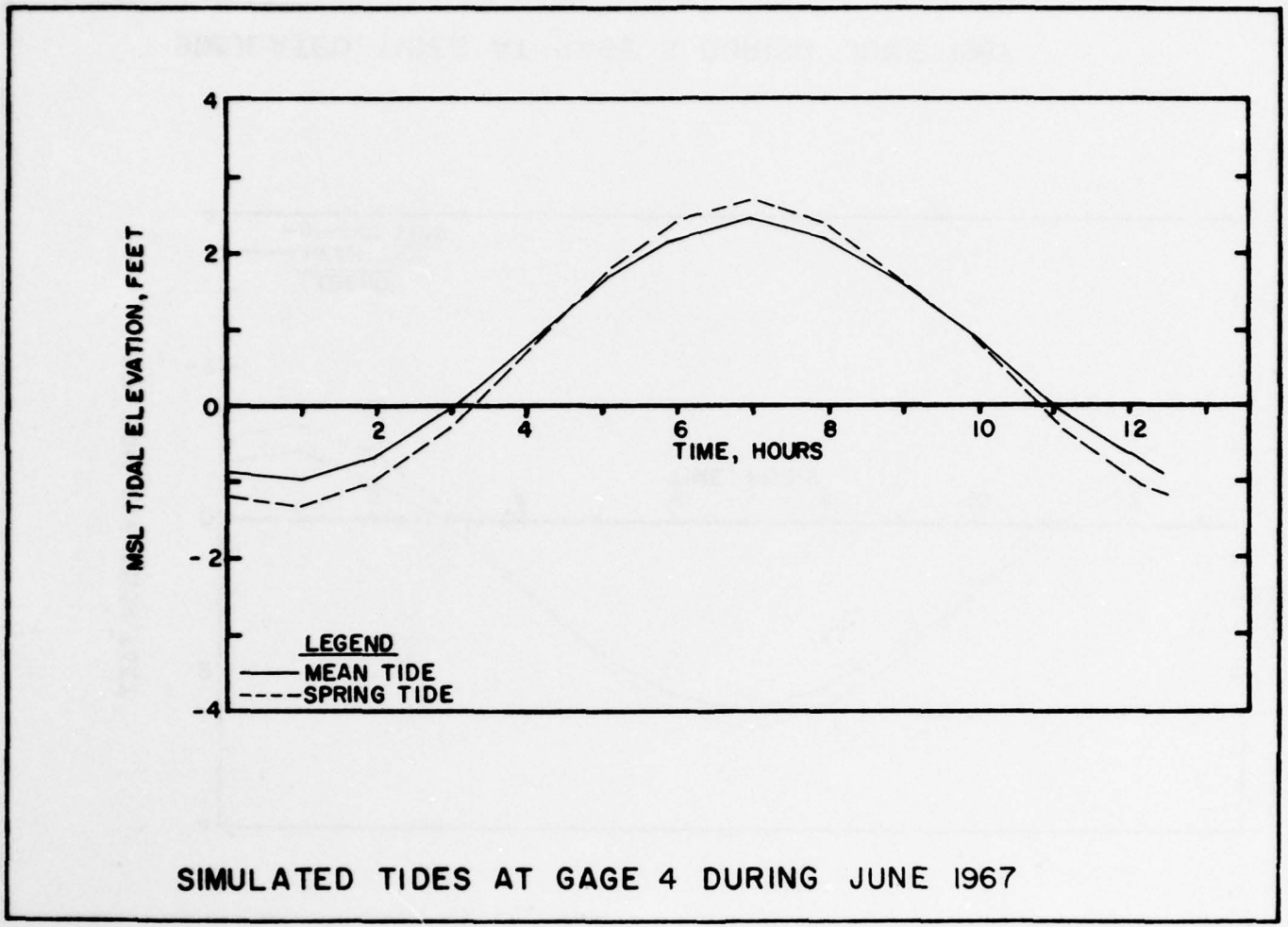

SIMULATED TIDES AT GAGE 4 DURING JUNE 1967

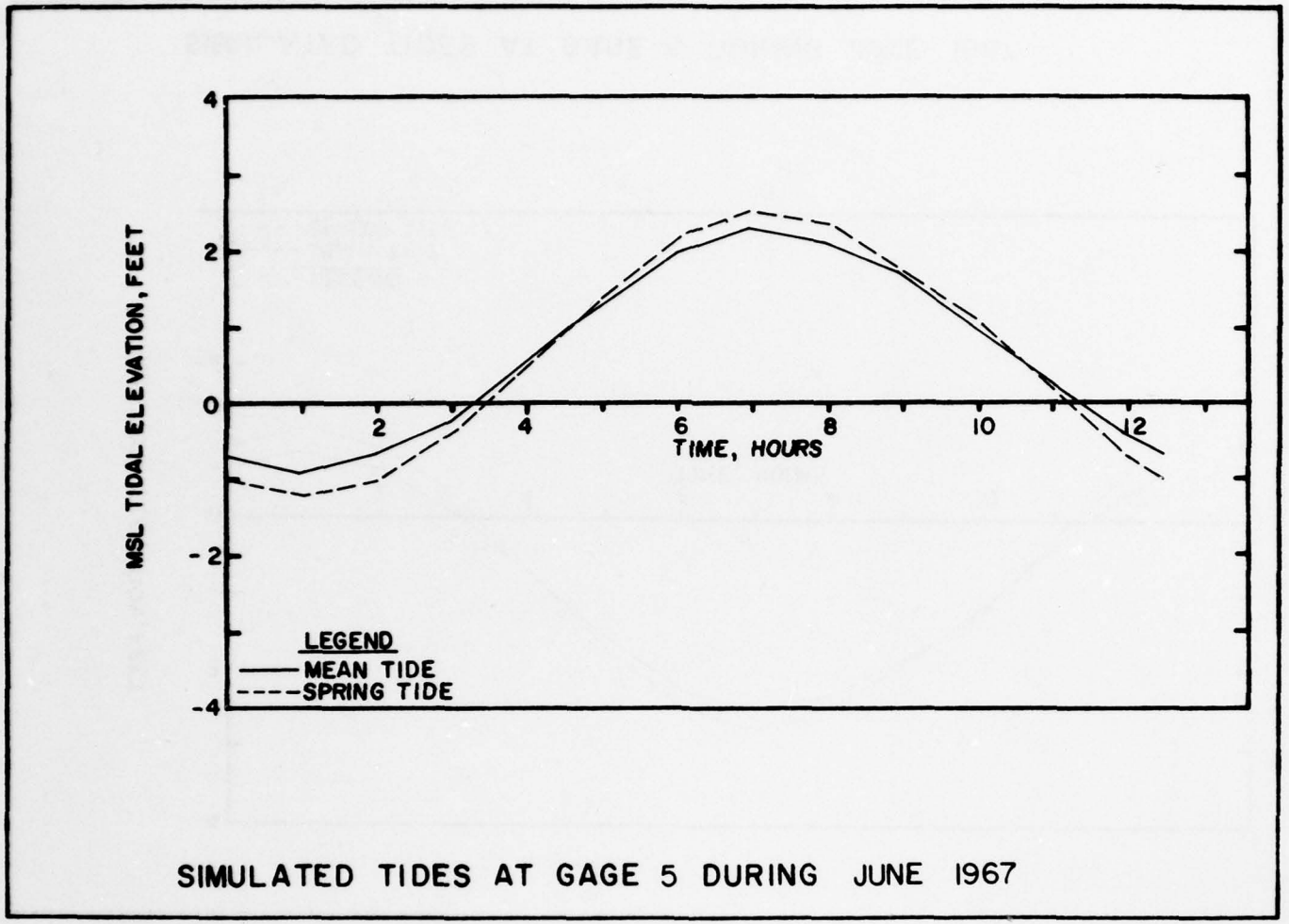

SIMULATED TIDES AT GAGE 5 DURING JUNE 1967

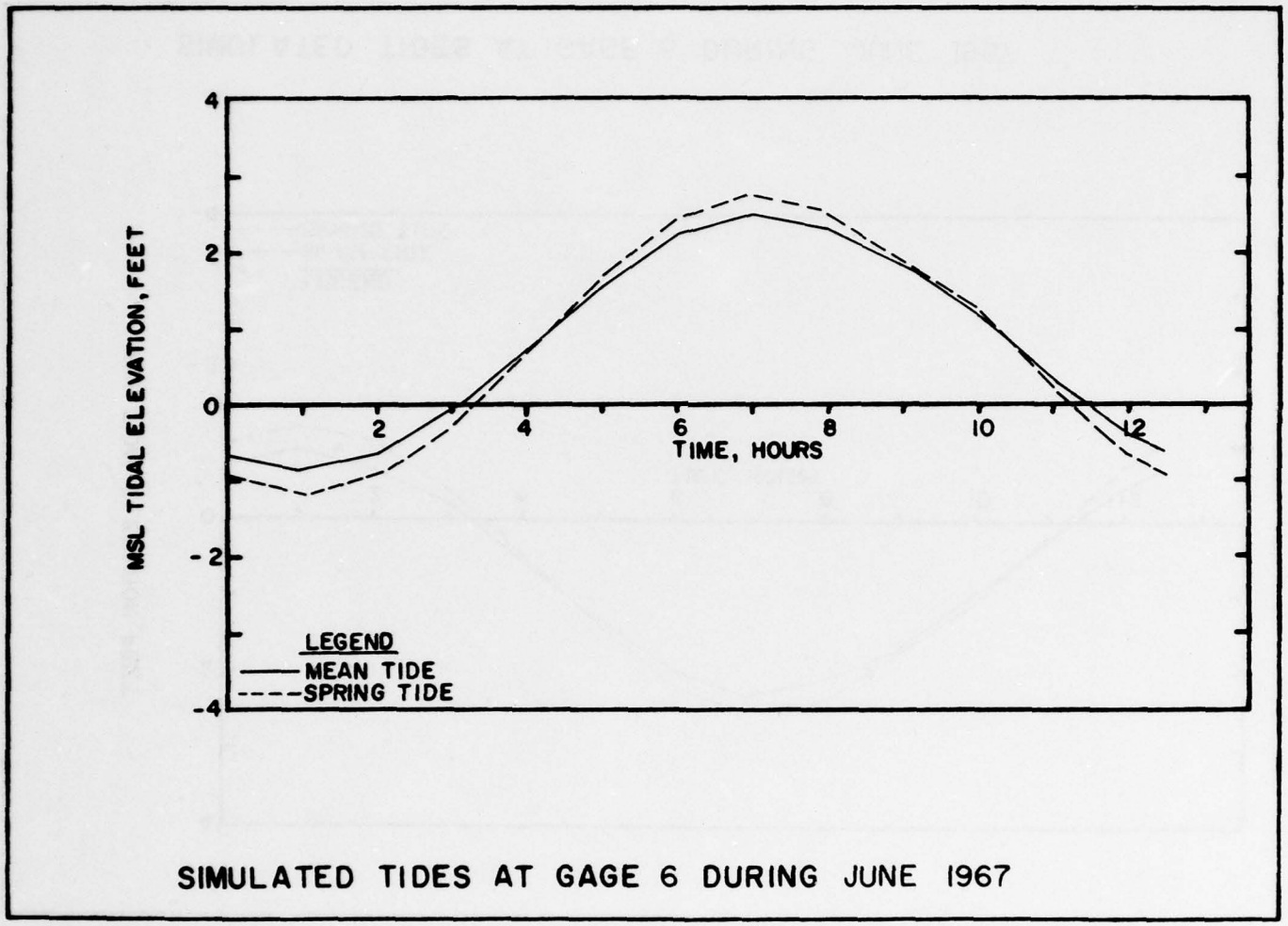

SIMULATED TIDES AT GAGE 6 DURING JUNE 1967

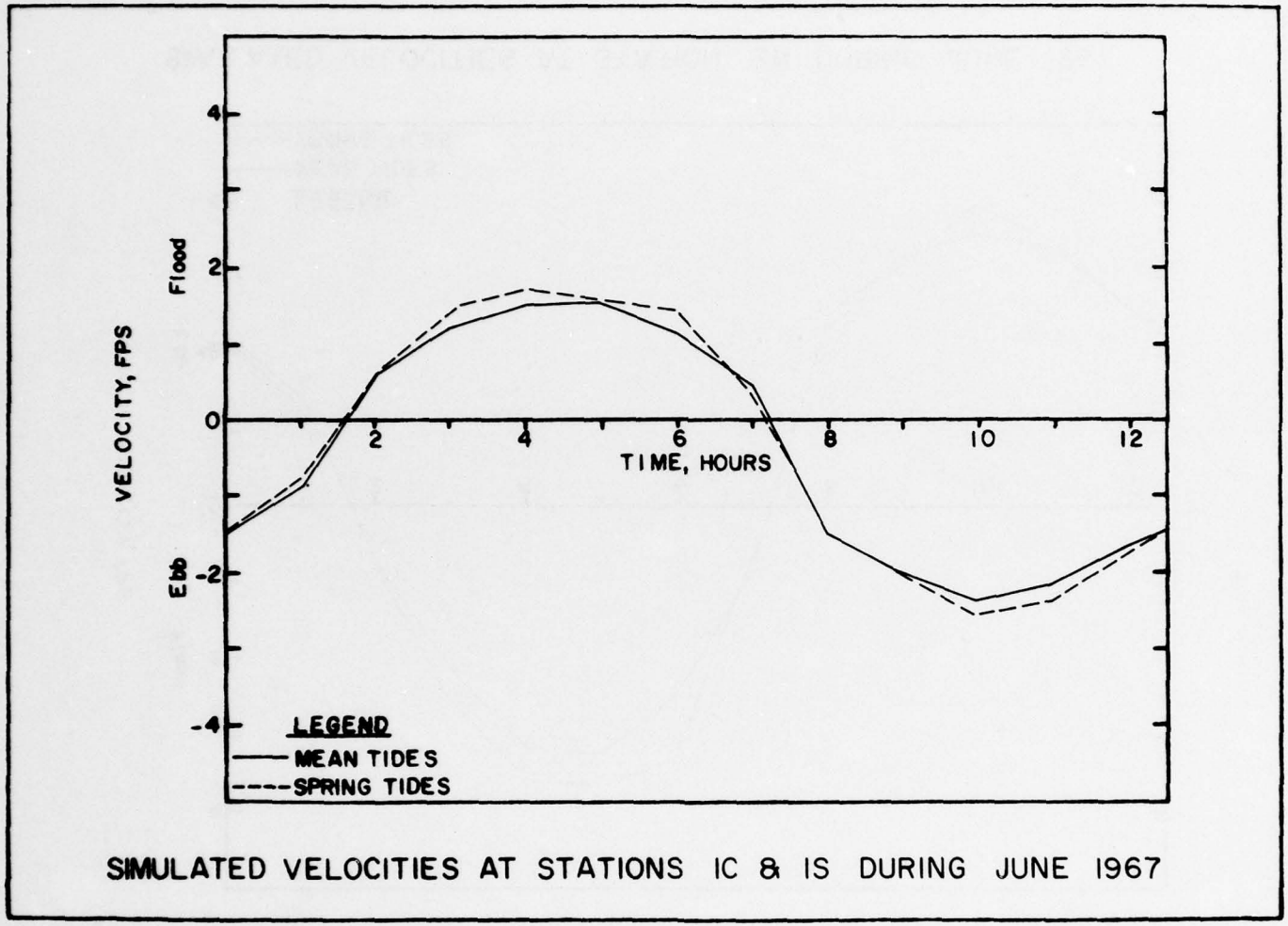

SIMULATED VELOCITIES AT STATIONS IC & IS DURING JUNE 1967

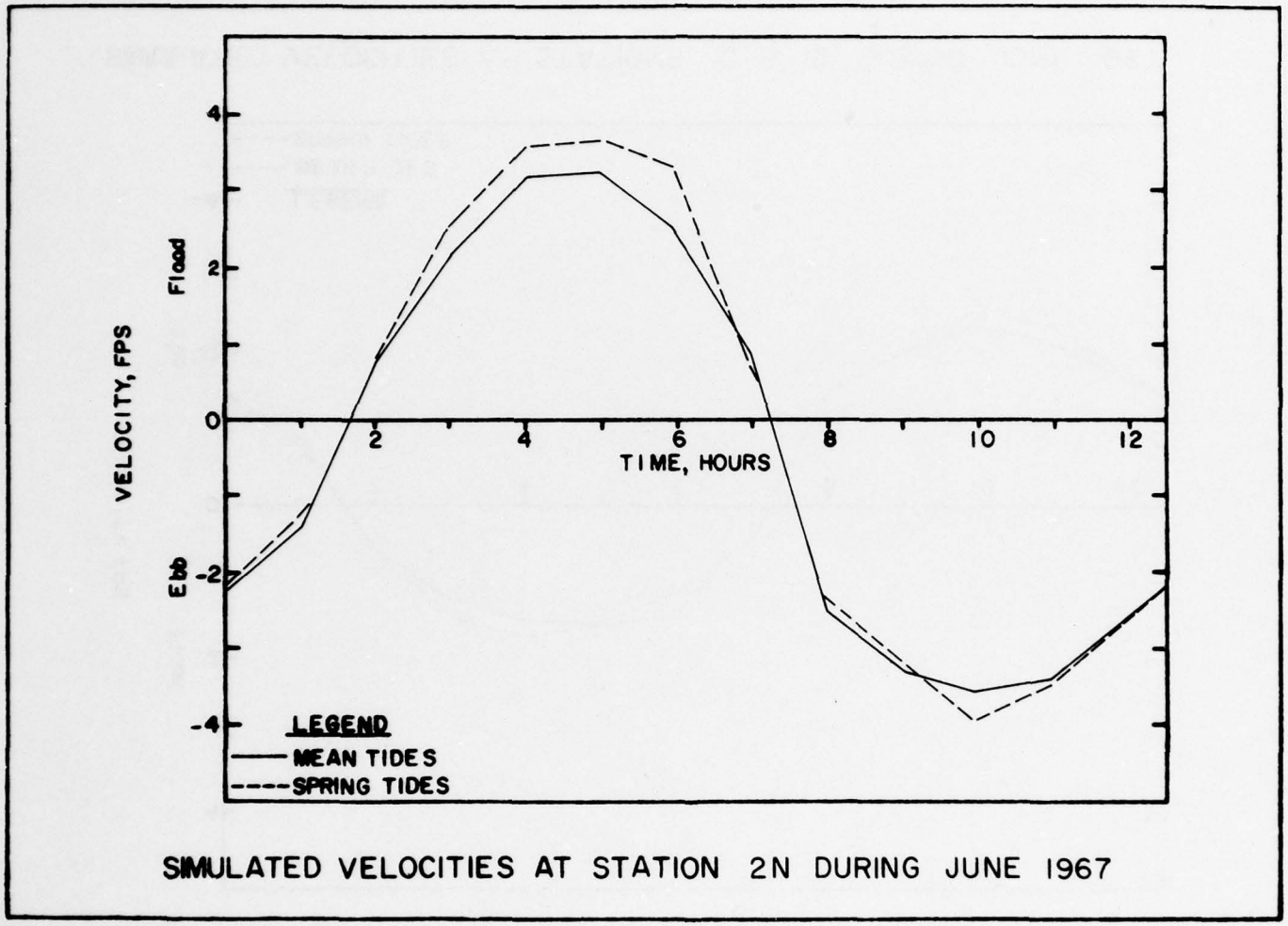

SIMULATED VELOCITIES AT STATION 2N DURING JUNE 1967

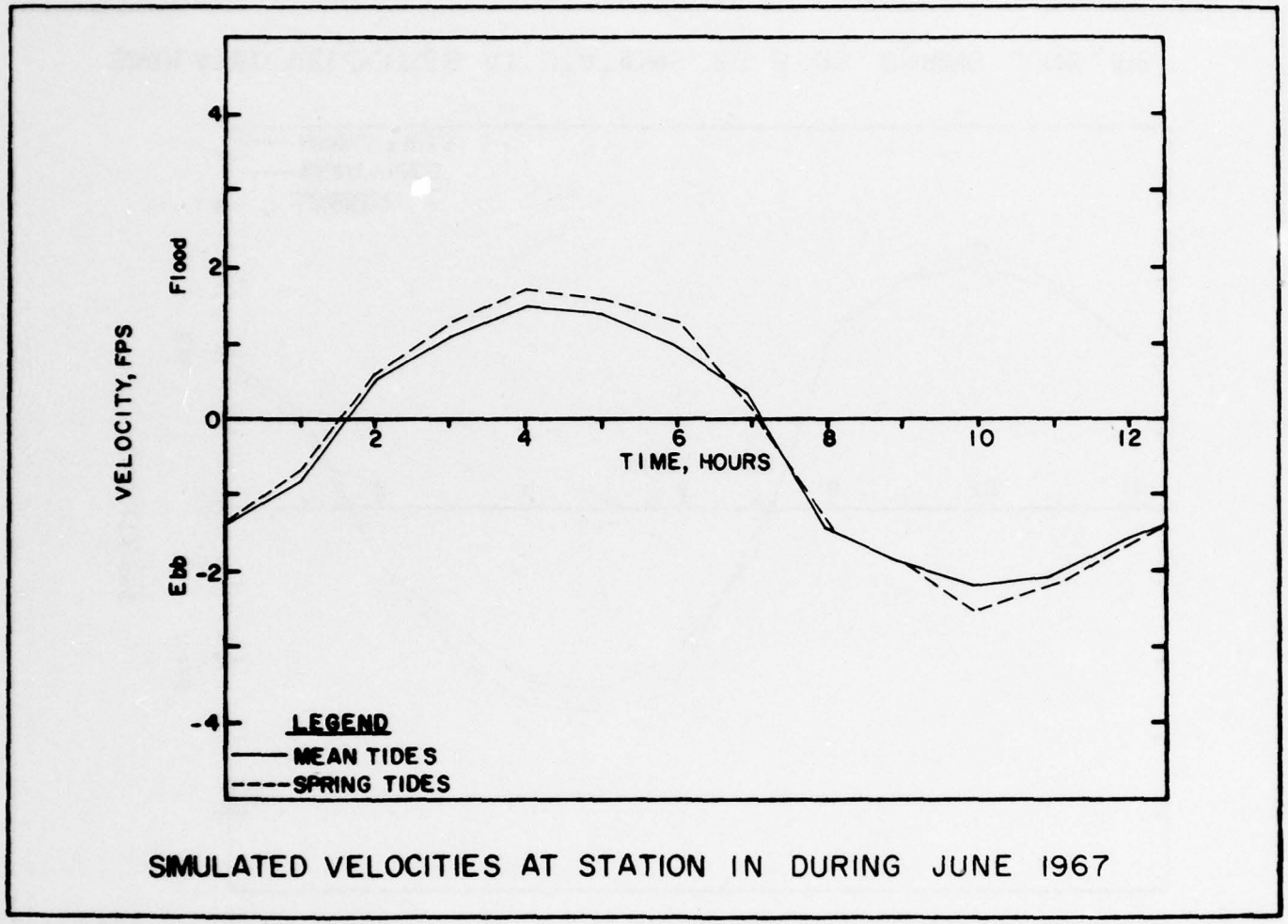

SIMULATED VELOCITIES AT STATION IN DURING JUNE 1967

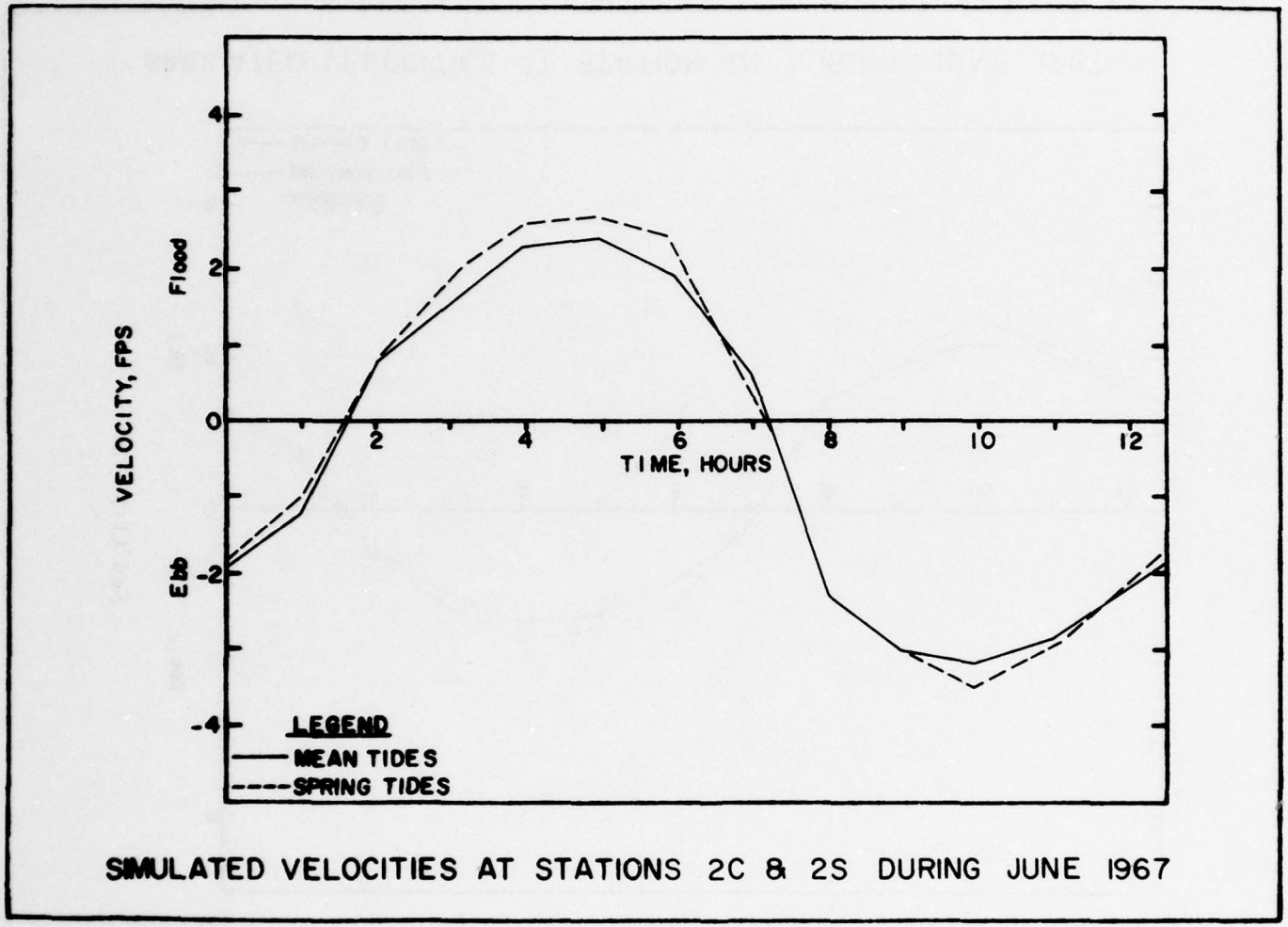

SIMULATED VELOCITIES AT STATIONS 2C & 2S DURING JUNE 1967

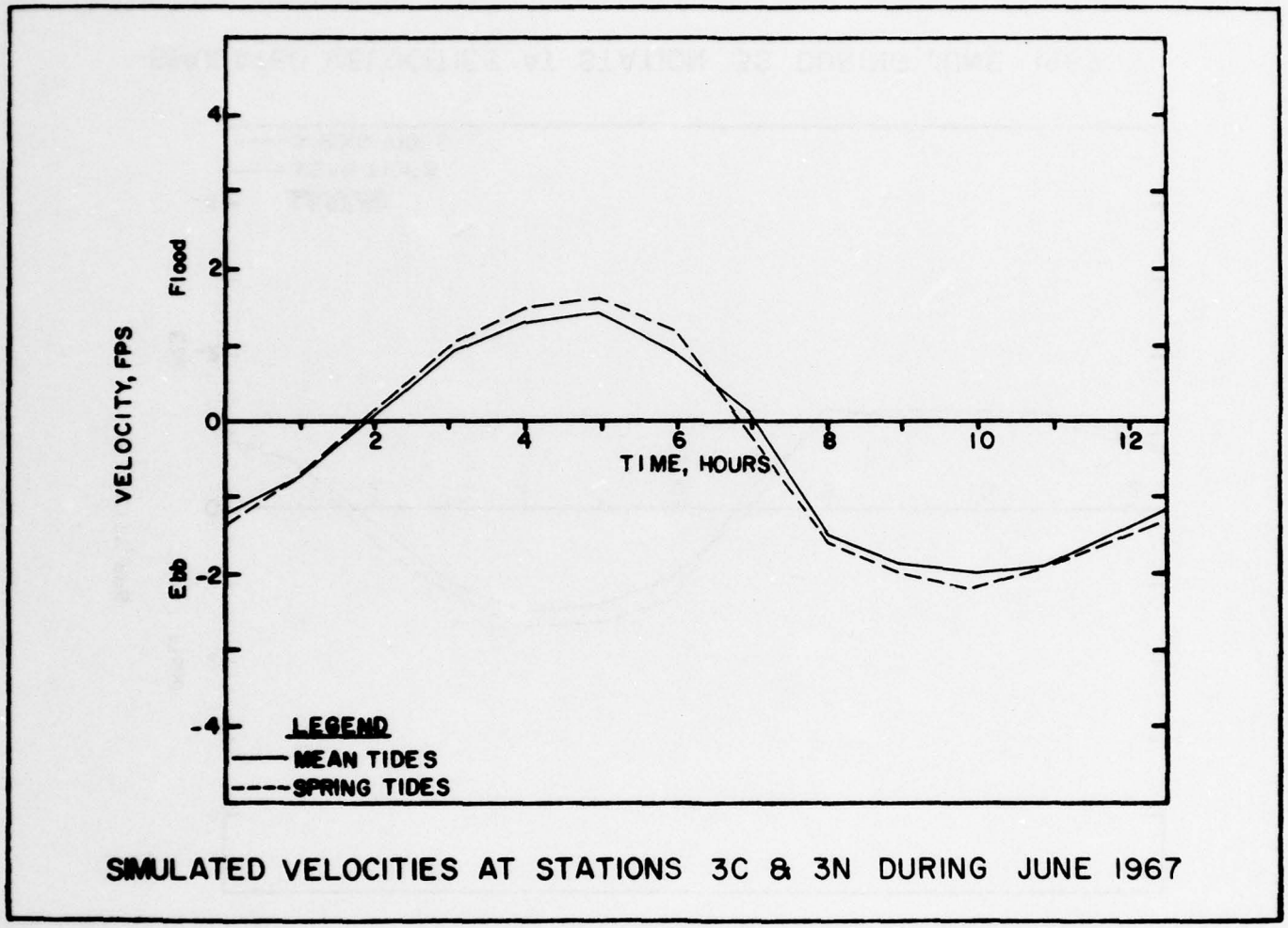

SIMULATED VELOCITIES AT STATIONS 3C & 3N DURING JUNE 1967

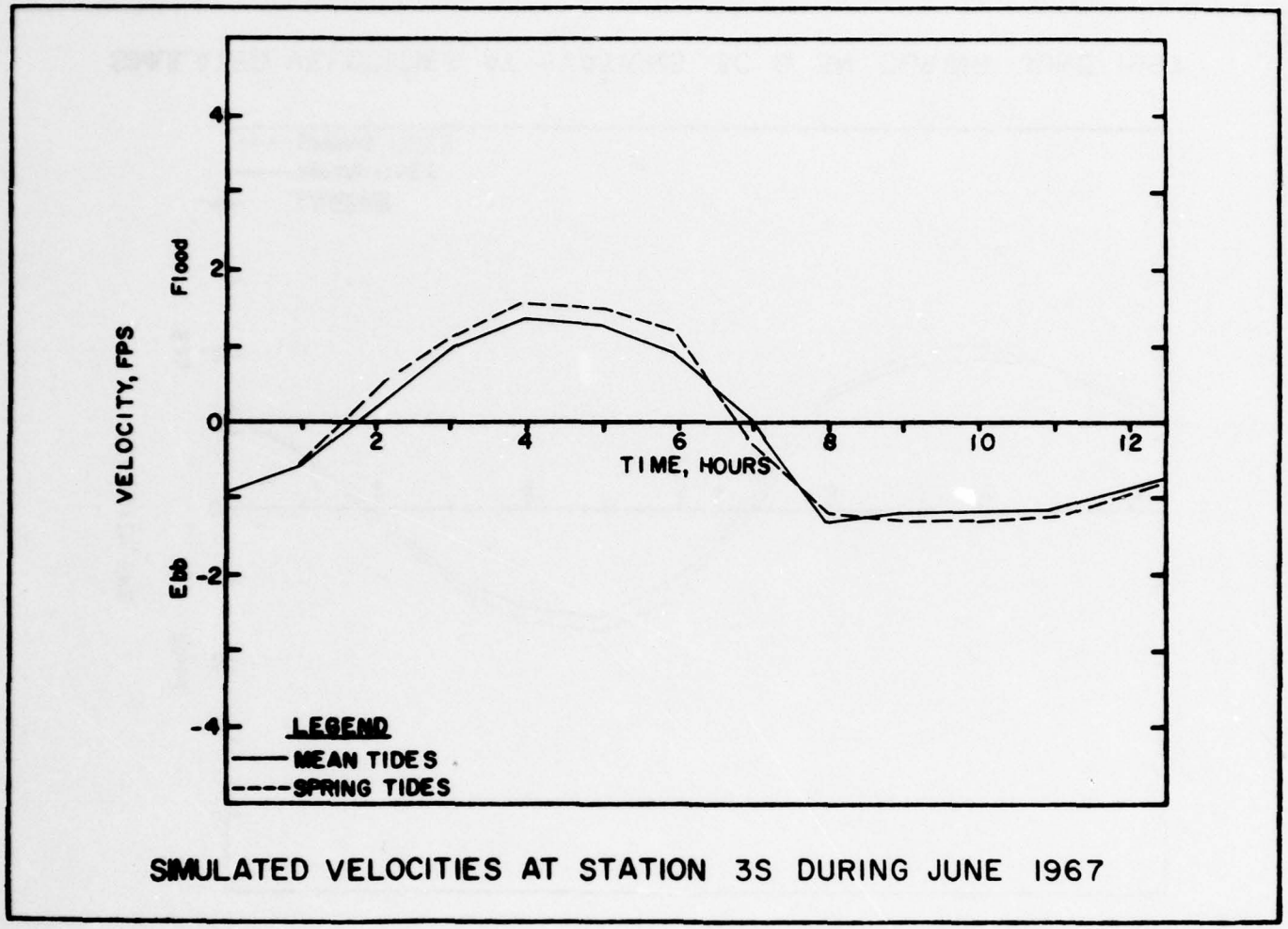

SIMULATED VELOCITIES AT STATION 3S DURING JUNE 1967

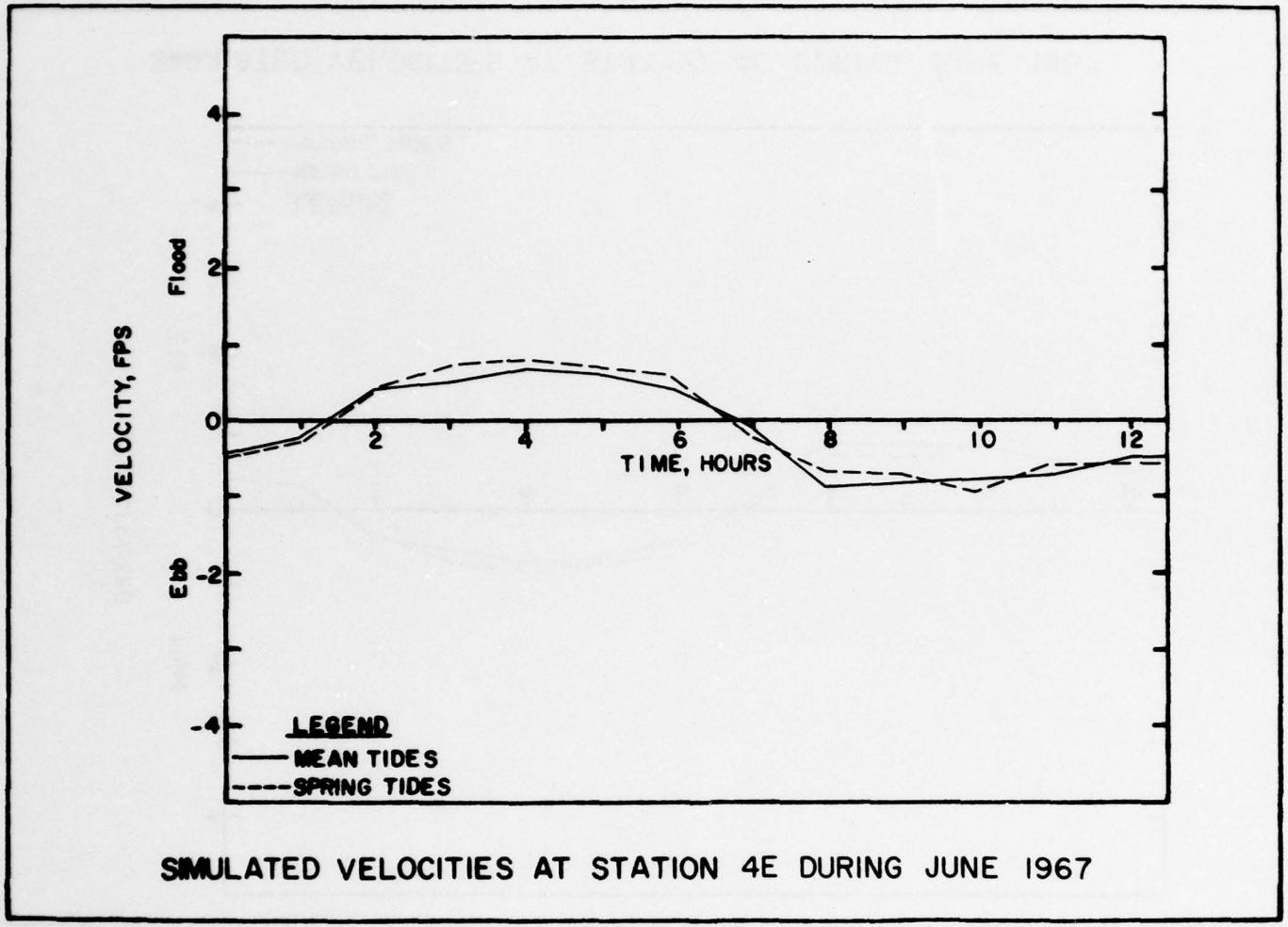

SIMULATED VELOCITIES AT STATION 4E DURING JUNE 1967

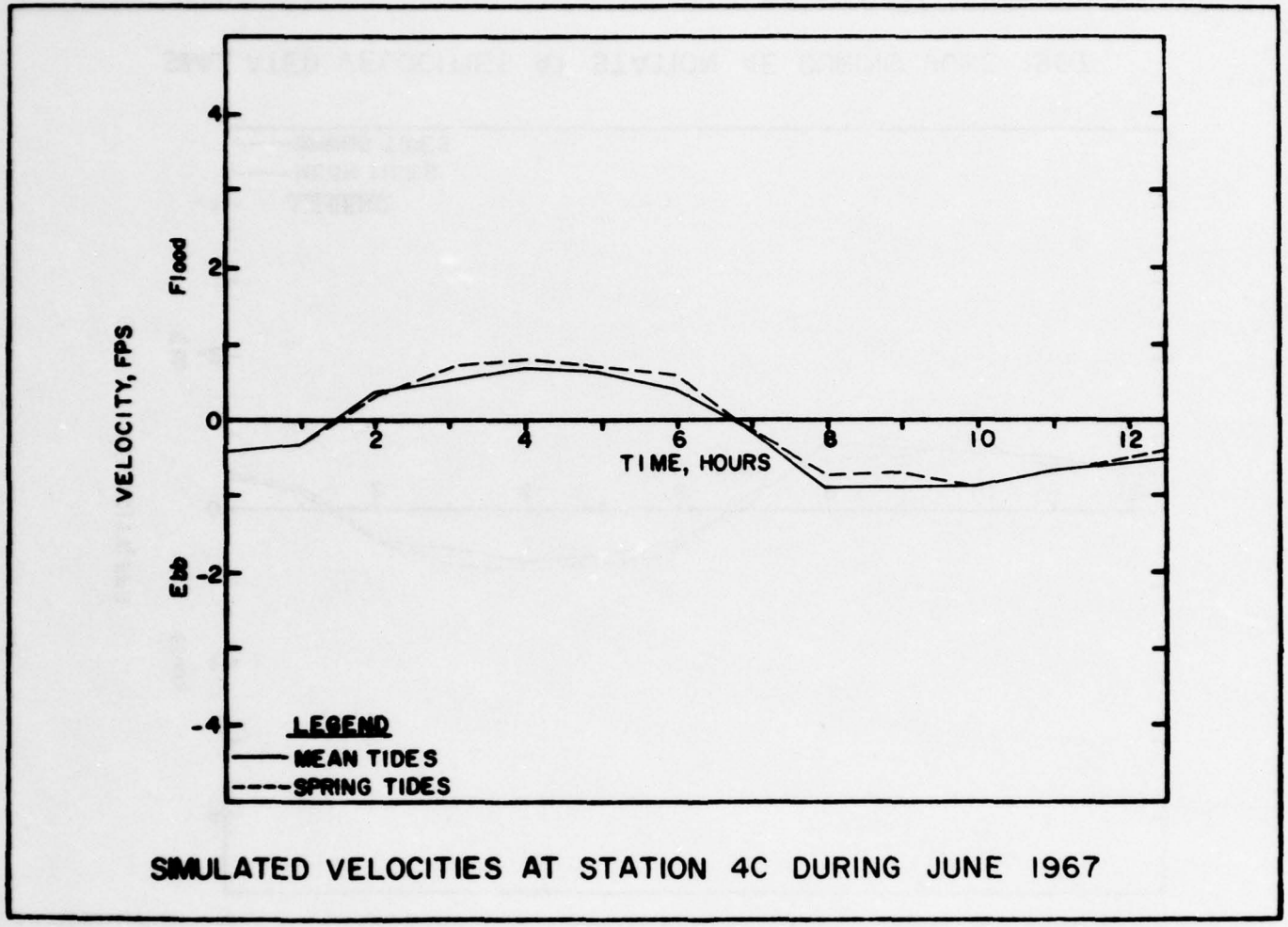

SIMULATED VELOCITIES AT STATION 4C DURING JUNE 1967

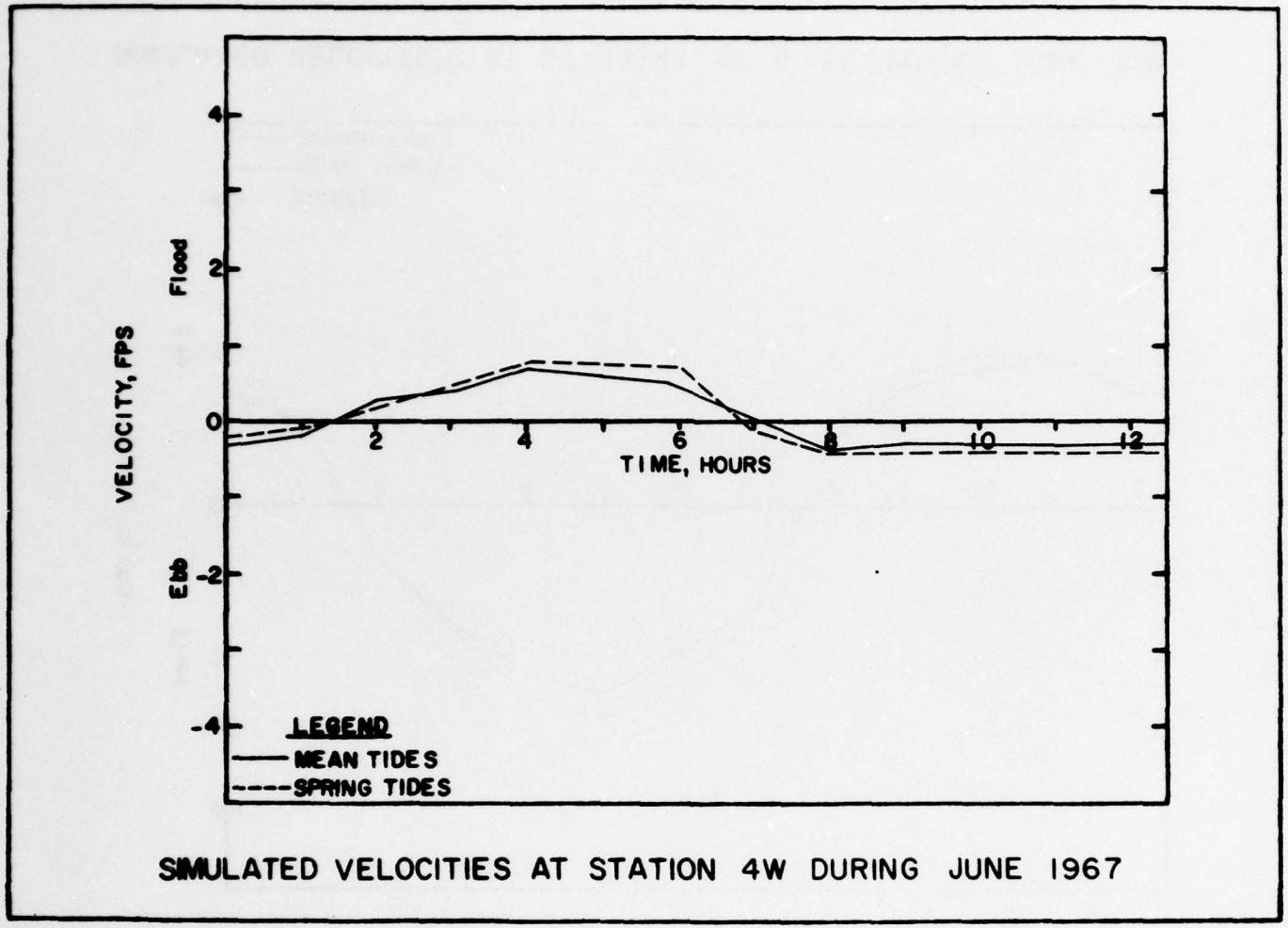

SIMULATED VELOCITIES AT STATION 4W DURING JUNE 1967

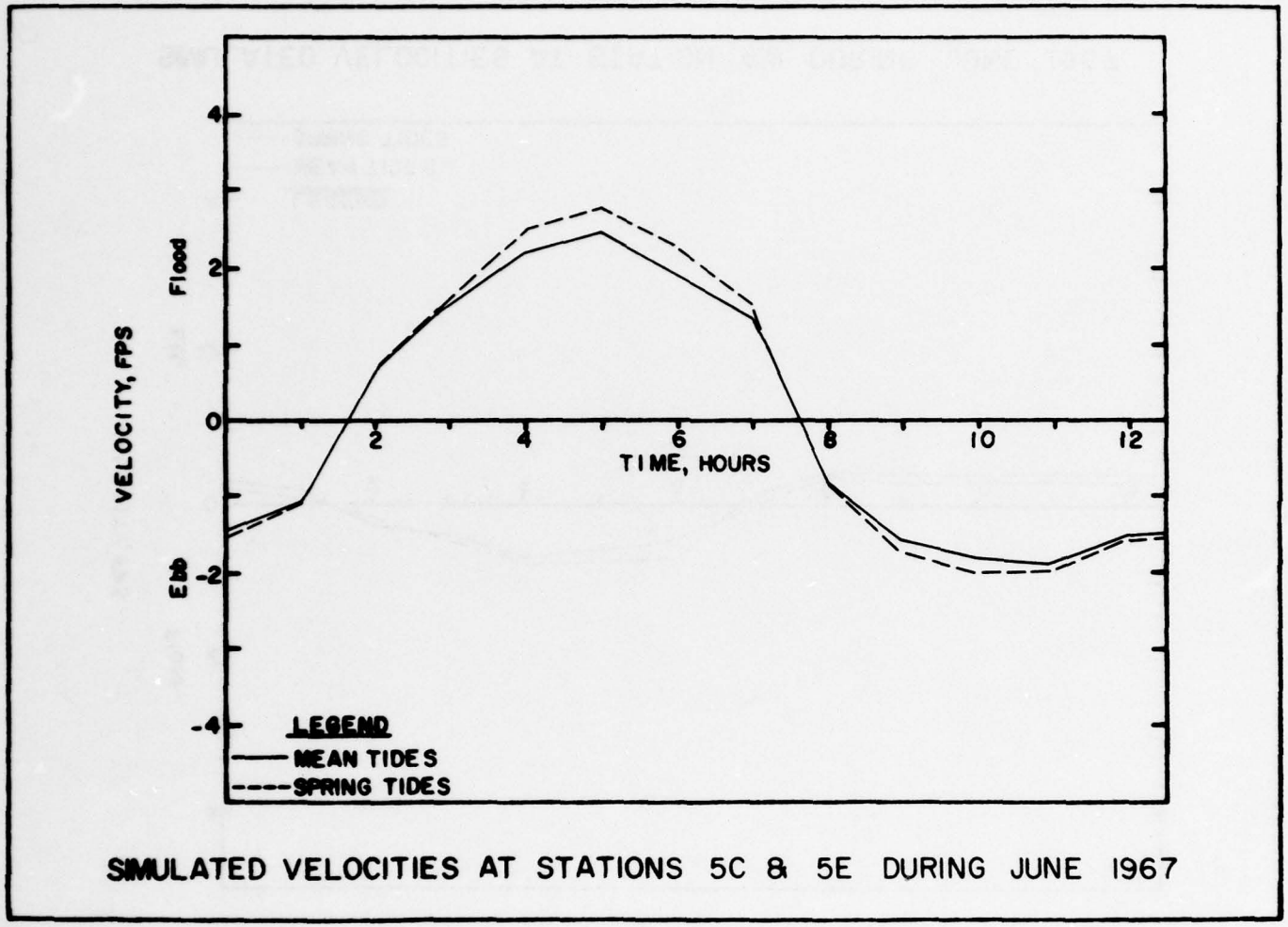

SIMULATED VELOCITIES AT STATIONS 5C & 5E DURING JUNE 1967

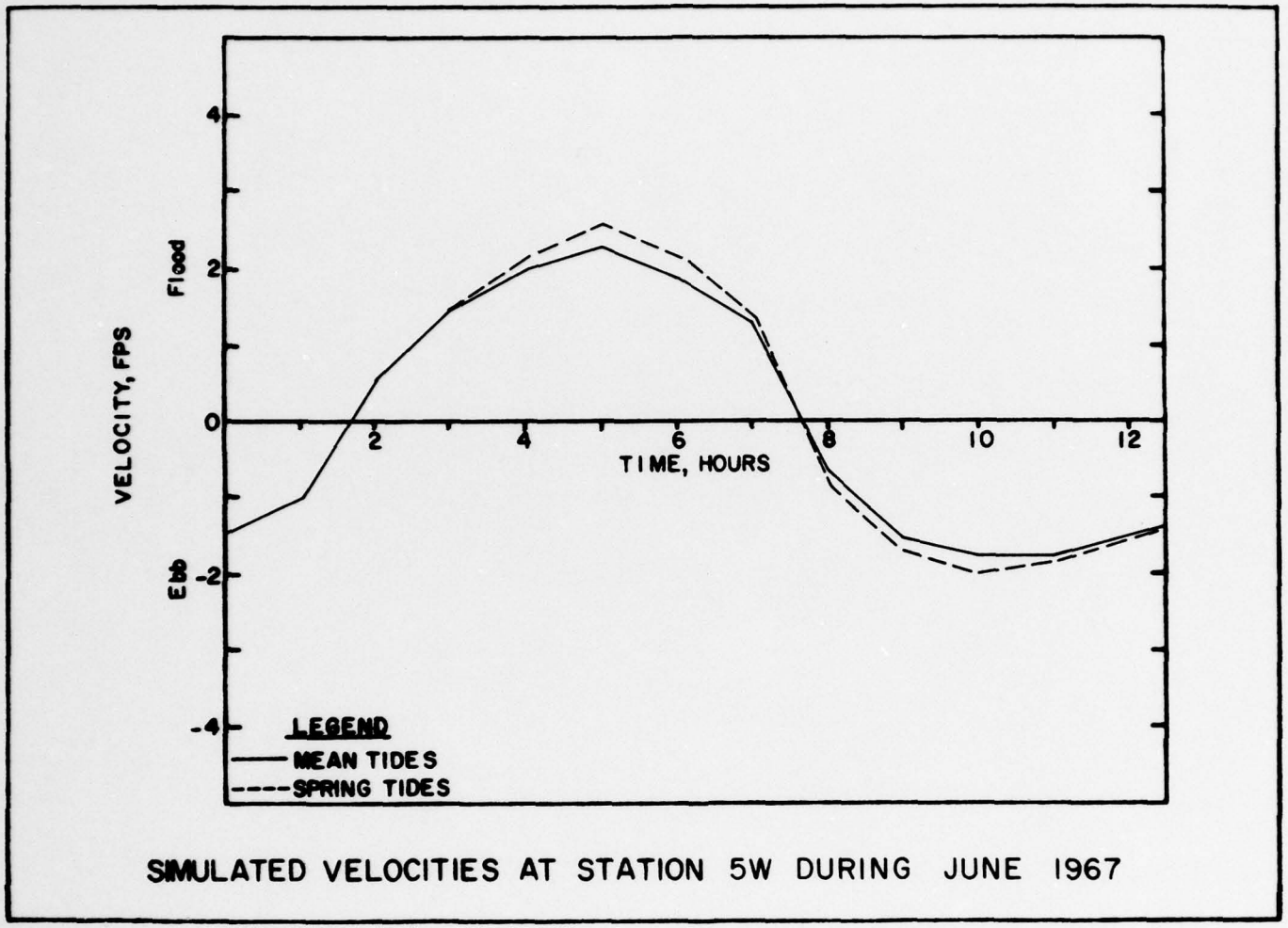

SIMULATED VELOCITIES AT STATION 5W DURING JUNE 1967

In accordance with letter from DAEN-RDC, DAEN-ASI dated 22 July 1977, Subject: Facsimile Catalog Cards for Laboratory Technical Publications, a facsimile catalog card in Library of Congress MARC format is reproduced below.

Masch, Frank D
Comparison of numerical and physical hydraulic models, Masonboro Inlet, North Carolina; Appendix 2: Numerical simulation of hydrodynamics (WRE) / by Frank D. Masch, Robert J. Brandes, and J. Dwight Reagan. Vicksburg, Miss. : U. S. Waterways Experiment Station ; Springfield, Va. : available from the National Technical Information Service, 1977.
2 v. : ill. ; 27 cm. (GITI report - U. S. Army. Corps of Engineers ; 6, Appendix 2)
Prepared for U. S. Army Coastal Engineering Research Center, under Contract DACW72-72-C-0028, by Water Resources Engineers, Inc., Austin, Texas.
General investigation of tidal inlets; a program of research conducted jointly by U. S. Army Coastal Engineering Research Center, Fort Belvoir, Virginia, [and] U. S. Army Engineer Waterways Experiment Station, Vicksburg, Mississippi.
Includes bibliography.

(Continued on next card)

Masch, Frank D
Comparison of numerical and physical hydraulic models, Masonboro Inlet, North Carolina; Appendix 2: Numerical simulation of hydrodynamics (WRE) ... 1977. (Card 2)

1. Finite difference method. 2. Hydraulic models. 3. Hydrodynamics. 4. Masonboro Inlet, N. C. 5. Mathematical models. 6. Numerical simulation. 7. Tidal inlets. I. Brandes, Robert J., joint author. II. Reagan, J. Dwight, joint author. III. United States. Coastal Engineering Research Center. IV. United States. Waterways Experiment Station, Vicksburg, Miss. V. Water Resources Engineers. VI. Series: United States. Army. Corps of Engineers. GITI report ; 6, Appendix 2.
GB454.T5.U5 no.6 Appendix 2